Field Line Resonances in Earth's Magnetosphere: A study of their Observation, Characterization and Wave Sources in the Solar Wind

by

María Laura Patricia Mazzino

A thesis submitted in partial fulfillment of the requirements for the degree of

Doctor of Philosophy

Department of Physics

University of Alberta

Abstract

This thesis is an observational study of Field Line Resonances (FLRs), between 0.5-5 mHz, in the Earth's magnetosphere, and their correlation with Ultra Low Frequency (ULF) waves in the solar wind. The mechanisms for these phenomena are not yet completely understood and there is still great debate on the causes of Field Line Resonances as well as the discrete and repetitive nature reported by some studies. Many studies of FLRs have been reported, in the past decades, and recent work has indicated that discrete, continuous ULF waves in the solar wind may be responsible for driving these FLRs giving rise to particular "magic frequencies" (1.3, 1.9, 2.6 and 3.4 mHz). The premise of this study was that "magic frequencies" existed and the intent was to test the hypothesis that discrete ULF waves in the solar wind directly driving them.

We successfully created an efficient algorithm and computer code to automatically detect ULF coherent waves over a large area within the field of view (FoV) of any Super Dual Auroral Radar Network (SuperDARN)' station that could be later categorized as a "Field Line Resonance". A total of 121 FLRs were identified during 2003 and their primary characteristics were obtained. For the 121 FLRs found in this study, 'magic frequencies' were not predominant in the general distribution. The frequency with more occurrences was the first in the array, 0.6±0.1 mHz. The observation of other frequencies showed a decreasing trend of observation of occurrences for increasing frequency. Results also showed deviations from the classification of FLRs by their azimuthal wavenumber m (high-m vs. low-m) provided by previous studies, in terms of their phase variation vs. magnetic latitude, propagation (sundwards-antisunwards; eastwards-westwards) and location. From the FLRs identified in this study we were not able to classify them into the two distinct groups, based upon the FLR's azimuthal wavenumber m, but rather the classification involved many other variables. Possible alternative classifications that

better adjust the observations in this study include the distinction of FLRs detected during quiet or active geomagnetic times, FLRs located either in or out of the plasmapause region, and classification of FLRs as low-*m*, intermediate-*m*, and high-*m*.

Finally, we applied four different, complementary techniques to evaluate the coherence between ULF waves in the solar wind, detected by the Advanced Composition Explorer (ACE), and the FLRs found in this study. We found that some specific magnetospheric configurations (such as uniform plasma distribution in the flux tubes or previous excitation of the magnetosphere at the driven frequency) might play an important role in the mechanisms driving the FLRs. Additionally, mechanisms other than ULF waves in the solar wind might be involved in driving the FLRs, such as pre-existing wave packets in the solar wind matching the natural frequency of the flux tube with specific magnetospheric configurations that allow the solar wind to drive the FLRs.

Preface

This thesis is an original work by Laura Mazzino, unless otherwise noted throughout the text. No part of this thesis has been previously published.

To the loving memory of my “abuelita” Patricia and my “granny” Daisy

“*Man must rise above the Earth — to the top of the atmosphere and beyond — for only thus will he fully understand the world in which he lives.*”

Socrates

Acknowledgments

Concluding my PhD program and writing this thesis manuscript has been one of the most difficult tasks I have performed. The numerous challenges that I have encountered in the past two years were beyond the ones any PhD physics graduate student might run into in their programs. For that reason, I am doubly grateful to all those people who specially assisted me and believed in me in the past two years of my PhD program.

First, I would like to thank my supervisor, Dr. Rick Sydora, for his professionalism, his continuous support, and his dedication to ensure that I succeeded in completing the PhD program. Rick: "I have no words to thank you enough for your guidance and patience these past 10 months."

Second, I would like to thank my previous supervisor (Dr. Frances Fenrich) for proposing the topic of this thesis and guiding me through the first years of my PhD, and to the past and current members of my committee (Dr. Robert Rankin, Dr. Moritz Heimple, and Dr. Richard Marchand) for assisting me in the development of this research study.

Third, I am very grateful for the advice of UA physics graduate advisers Dr. Sharon Morsink (2008-2011) and Dr. Richard Marchand (2012-Present). Their compassion, patience, and support have been critical in my success to complete this program.

Many thanks to the Center for Space Radiations (Belgium), specially Sylvie Benck and Juan Cabrera, for the scientific collaborations and technical/scientific support. Also, many thanks to Viviane Pierrard and Kris Borremans, from the Belgian Institute for Space Aeronomy, for the plasmaspheric simulations.

I am most grateful to Pasha Ponomarenko (University of Saskatchewan) for meaningful conversations, email exchanges, and scientific/technical support. Acknowledgments to Kevin Sterne (SuperDARN@Virginia Tech), AJ Ribeiro and Ethan Miller (JHU APL) for email exchanges with support on SuperDARN data files. Special thanks to the University of Alberta IST (AICT) support team for helping me in numerous problems with the server, especially to Kyle Dubitz, Jozef Kupnicki, and Ian Chan.

I am very grateful to everyone in the 2008-2015 University of Alberta Space Physics group for providing me with a nurturing and vibrant environment that allowed me to learn more about the field of study and to mature as a researcher. Special thanks to: Professor Ian Mann; former graduate students Maria Usanova, Kyle Murphy, Adrienne Parent, Eun Ah Lee, Hava Turkakin; graduate students Dave Miles, Mauricio Blanco; research associates and staff members Andy Kyle, Dave Milling, Louis Ozeke, Dave Barona, Dmytro Sydorenko; former research associates Zoë Kyle, Alex Degeling, Clare Watts and Jonathan Rae. To all of you, I cherish very much our discussions and common projects for what it has brought to my professional and personal life.

I would like to extend my appreciation for the assistance that the UA department of physics' support staff has given me throughout the years. Thank you to Melanie Faulknor, Sandy Hamilton, Carolyn Steinborn, Linda Jacklin, Suzette Chan, Patty Chu, Nandi Khanna, for your

help and friendship. In particular, I would like to thank Sarah Derr, the UA department of physics' graduate program assistant; since I applied to the UA Physics Graduate Program, Sarah has been a warm human being and a wonderful help in all related to the administrative aspect of my graduate life.

During my graduate studies at University of Alberta, I have met fellow graduate students, research associates, and professors from other physics research areas and even other departments and/or faculties. Rachel McQueen, Piyush Jain, Berta Beltran, Melanie Grob, Holly Freeman, Dunia Blanco, Ross Lockwood, "Henry" Herrera, Lourdes "Lulu" Pelayo, Shalon McFarlane, Nadia Imtiaz, Daniel Foster, Logan Sibley, Nadia Kreimer, Neda Naseri, Janet Couch, Carlos Lange: You all trusted and greatly enriched me with your friendship and I treasure our times together at UA. During my time at UA, I also greatly enjoyed serving with many talented people at the Graduate Physics Student Association, the Graduate Student Association, and the FGSR Outreach program.

I am extremely grateful to my parents (Jorge Mazzino and Carmen Machado) and my four siblings (Lucas, Eugenia, Gabriela and Paula): Throughout their experiences in life and their relationships with me, they all have taught me that the two most important things in life are making good choices and having a good attitude, whatever comes your way. To my best friends Gabriela Alfaro, Mariana Bianchi, and Claudia Cristiani, to my aunt Priscila Mazzino, and to all my extended family: Thank you for your love and words of encouragement.

My deepest gratitude goes to my husband, Brent Villeneuve, and to our son, Connor Villeneuve, for their continuous love and inspiration, for whom everything is possible and worthy. Brent: "Thank you for always being there to encourage me, for doing all the chores around the house these past two years, and for listening to my countless practice speeches even though the topic of my research is foreign and unappealing to you. You are the love of my life and my soulmate". Connor: "I love you very much! I hope one day you will learn from this thesis some interesting physics and, most importantly, that you can achieve everything and anything in life if you set your mind to try your best without giving up. Remember: determination and perseverance will take you far. Always believe in your dreams!"

Lastly, and most importantly, I would like to thank God for the gift of life and His continuous, abundant love to me. Lord: "You surprise me every day with Your blessings!"

This research study was possible through the financial support of the Canadian Space Agengy (CSA)'s Space Science Enhancement Project Funding and the Natural Sciences and Engineering Research Council, and the data contributions from the SuperDARN community and the NASA ACE mission, and their respective financial agencies.

The plasmaspheric simulations have been developed at the Belgian Institute for Space Aeronomy by V. Pierrard and K. Borremans with funding from the European Union's Seventh Programme for Research, Technological Development and Demonstration (www.swiff.eu FP7 SWIFF).

Table of Content

List of Tables

List of Figures or Illustrations

List of Symbols and Abbreviations

γ	ratio of specific heat
β	plasma beta, i.e. thermal to magnetic pressure ratio
ρ	plasma mass density
ε	index related to ionospheric dissipation of energy
σ	plasma conductivity
θ	angle between $\boldsymbol{B_o}$ and wavevector
μ_o	magnetic permittivity of vacuum
ACE	Advanced Composition Explorer
AU	Astronomical Unit
$\boldsymbol{B}$	magnetic field vector
β	plasma beta parameter
C_s	speed of sound
CIR	corotating interaction regions
$\boldsymbol{D}$	electric displacement vector
$\boldsymbol{E}$	electric field vector
E	particle kinetic energy
ELF	extremely low frequency
FLR	Field Line Resonance
HF	High Frequency
IMF	Interplanetary Magnetic Field
$\bar{J}$	electric-current density
$\mathbf{k}$	azimuthal wave vector
l	length of the magnetic field line
L	L-shell or L-value
M_E	magnetic dipole moment

MHD	magnetohydrodynamics
m	mass
m	azimuthal wave number
n	number density
n_e	electron number density
n	fundamental frequency or number of harmonic mode
p	scalar pressure
$R_\odot$	radius of the Sun
R_e	radius of the Earth
SuperDARN	Super Dual Auroral Network
T_e	electron temperature
$\boldsymbol{u}$	plasma flow velocity
ULF	ultra low frequency
UT	universal time
v	particle velocity
v_A	Alfvén speed
v_{ph}	phase velocity
x_r	position near resonance position

Chapter 1

Introduction

1.1 Preliminary remarks

This thesis is an observational study of a particular phenomena occurring in Earth's magnetic field lines called *Field Line Resonances* (FLRs) and the connection between properties in the solar wind that relates to the cause of these phenomena.

This study makes significant contributions to the field of research by:

1) Proposing an automatic methodology to identify FLRs using observations in the upper atmosphere;

2) Describing their observed characteristics and comparing them to current description of characteristics given in the literature;

3) Analyzing the connection between the solar wind and the FLRs.

The sections below are devoted to introduce background information for the general understanding of these phenomena and also of their observation and study using ground and satellite instrumentation.

1.2 The Space Environment

1.2.1 The Sun and the Solar Wind

The Sun is a yellow dwarf star, commonly known as a *main-sequence* star in the nomenclature of astronomy. Nuclear fusion in its interior generates thermal energy that permeates outwards by either radiation or convection. The outward thermal pressure is balanced by the gravitational pressure from the sun's layers so that the Sun is in hydrostatic equilibrium.

The Sun has a *magnetic field* that changes structure during the 11 year *solar cycle*: During quiet times (*solar minimum*), the Sun's magnetic field could be approximated as a magnetic dipole but it changes to more complicated structures during the *solar maximum*. This periodic variation is important in the understanding of variations in the occurrences of field line resonances in Earth's magnetic field, mentioned in chapter 4.

The continuous flux of particles emitted from the Sun, consisting mainly of electrons and protons, is known as the *solar wind*. The solar wind is made of plasma: *Plasma* is defined as a quasi-neutral ionized gas in a stationary state that exhibits collective behavior and constitutes 99% of the observed universe. The solar wind is a highly-conducting plasma that travels at supersonic speeds of approximately 500 km/s [*Baumjohann and Treumann*, 1997]. At 1 AU, the electron density has typical values of $n_e \sim 5$ cm^{-3} and the electron temperature is about $T_e \sim 10^5$ K.

The solar wind's energy density is higher than that of the Sun's magnetic field. Consequently, the magnetic field of the Sun moves with the plasma and is carried outwards into interplanetary space by the solar wind. For this reason, it is known as the *interplanetary magnetic field (IMF)*. Given the rotation of the Sun, the *IMF* describes a spiral [*Parker*, 1958], as shown in Figure 1.1, commonly known as the *Parker Spiral*. The *IMF* magnitude at 1 AU is of the order of 5 nT.

The solar wind has been measured at 1 AU as low as 300-400 km/s, but can rise to values of 700 km/s, as shown in figure 1.2, due to *high-speed streams* emitted from *coronal holes*.

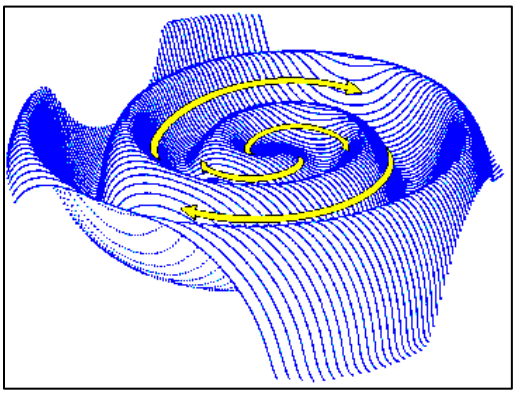

Figure 1.1: Artist conception of the Interplanetary Magnetic Field (blue) and the Parker Spiral (yellow arrows). Credits: J. Jokipii, University of Arizona (from "NASA Cosmicopia", http://helios.gsfc.nasa.gov/solarmag.html).

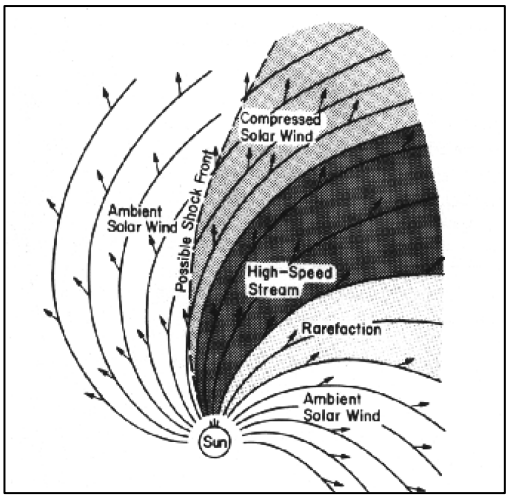

Figure 1.2: Schematic illustration of a fast stream interacting with a slow stream [*Hundhausen*, 1972] (from: http://www.physics.usyd.edu.au/~cairns/teaching/lecture11/node4.html).

Early measurements of solar wind parameters (density, speed, magnitude of the magnetic field) were obtained by the Soviet *Luna* probes (1959-1976) and the American *Mariner 2* mission (1962) [*Kivelson and Russell*, 1995]. Since then, numerous spacecraft missions have been launched by the space agencies of several countries. In particular, the NASA *Advanced Composition Explorer* (ACE) has been operational since 1997 providing valuable data on solar wind parameters. This mission measures and compares the composition of matter samples, such as the solar corona, the solar wind, and other interplanetary particle populations, to name just a few [*Stone et al.*, 1998; *McComas et al.* ,1998; *Smith et al.* , 1998].

Relevant to the studies presented in this thesis are ACE's measurements of solar wind parameters, including the solar wind's proton density, speed flow, components of its magnetic field and its velocity, and plasma dynamic pressure calculated from the proton density and speed flow.

1.2.2 The Magnetosphere

The *Magnetosphere* is the cavity generated by the terrestrial magnetic field inside the '*bow shock*', and its boundary is called the *magnetopause*. Solar wind particle dynamics create the *magnetopause current system* [*Baumjohann and Treumann*, 1997]. The front side of the outer magnetosphere is compressed by the dynamic pressure of the solar wind deforming its dipole configuration (Figure 1.3); that is, the night side of the magnetic field is stretched out in a long tail.

The configuration of the magnetosphere, as shown in figure 1.4, is highly variable and it is determined by the balance of the magnetopause current system given by the dynamic equilibrium between the *solar wind dynamic ram pressure* $p_{dyn} = n_{sw} m_i (v_{sw})^2$ (neglecting the electrons and considering only the ions) and the *plasma pressure of the magnetosphere* $p_B = B^2/2\mu_o$, where $n_{sw,}$ $m_{i,}$ and v_{sw} are the average number density, mass of the ions, and flow speed of the solar wind

respectively, B is the magnetic field of the Earth, and μ_o is the magnetic permittivity of vacuum. The location of the *magnetopause* can be crudely calculated to the location where the solar wind dynamic pressure equals the plasma pressure of the magnetosphere evaluated at the boundery, assuming a dipole configuration of the magnetic field of the Earth [*Schield*, 1969; *Kivelson and Russell*, 1995].

The magnetic field strength is represented by *Magnetic Field Lines*. In the inner part of the magnetosphere, the geomagnetic field can be approximated by a dipole field with a dipole moment M_E=8.05 x 10^{22} Am^2. The geomagnetic field axis is tilted 11° from Earth's axis of rotation. In this dipole configuration, the magnetic field lines are given by the expression $r = r_{eq}\cos^2\lambda$, where λ is the angle from the magnetic equator to the radius crossing the magnetic line (r), given rise to the L-shell parameter or L-value [*McIlwain*, 1969] by the expression:

$$L^{-1} = \cos^2\lambda_E \qquad (1.1)$$

Away from Earth's surface, at approximately around 4 Earth's radii, the deformation of the dipole configuration due to the dynamic pressure of the solar wind, mentioned before, requires a more sophisticated and realistic configuration of the magnetosphere. Such realistic configuration is given by the Tsyganenko Models [*Tsyganenko*, 2002a and 2002b].

Since the magnetic field lines move with the plasma in the magnetosphere, they are said to be '*frozen-in*' and can be thought as *flux tubes*. Standing waves on these flux tubes are called *Field Line Resonances (FLRs)* and are the focus of this study.

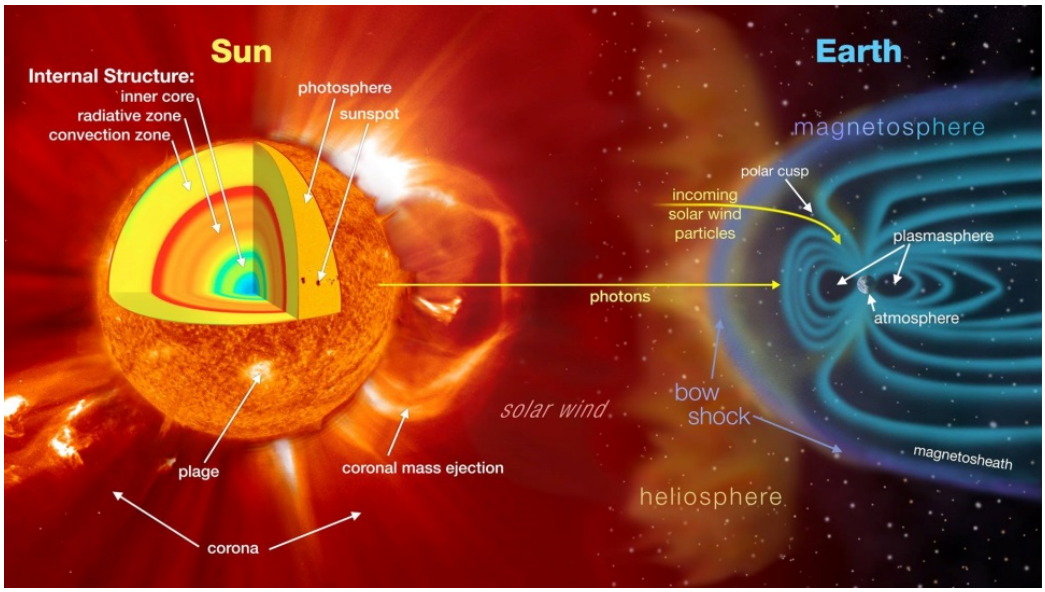

Figure 1.3: Topology of the solar-terrestrial environment. (From: http://svs.gsfc.nasa.gov/vis/a030000/a030400/a030481/).

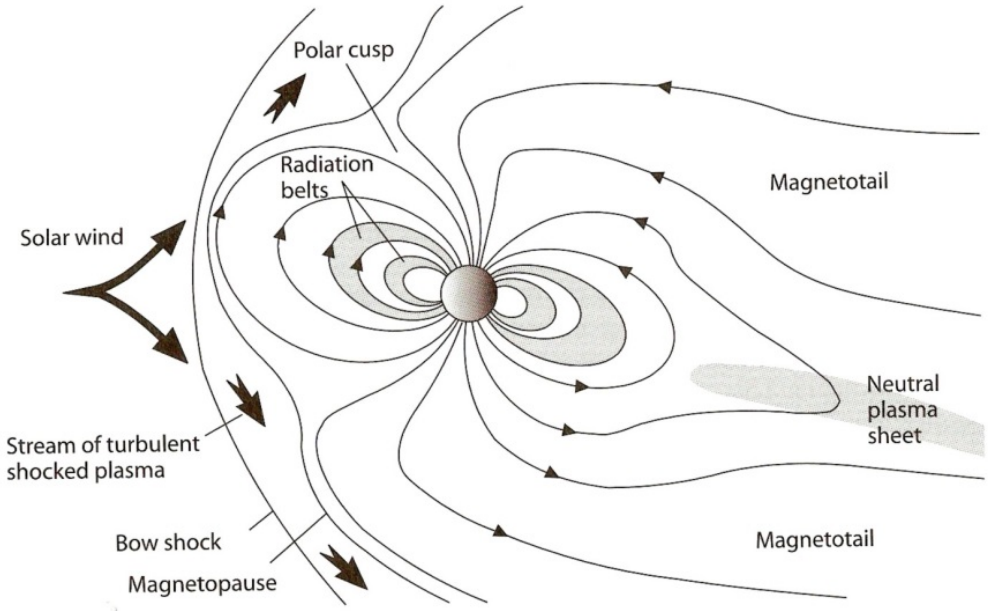

Figure 1.4: Earth's Magnetic Field [*Lanza and Meloni*, 2006].

The solar wind convects open field lines of the magnetosphere. If the right IMF conditions occur, closed field lines in the magnetosphere can be connected to IMF field lines in a process called "*reconnection*" and can be convected to the tail of the magnetosphere as well.

The plasma inside the magnetosphere has very different origins which are beyond the scope of this discussion. The magnetosphere is very dynamic and exhibits multiple plasma regions, as shown in Figure 1.4. These regions are the *Plasmasphere* (a region of cold-dense plasma, $n_e \sim 5 \times 10^2$ cm^{-3}, $T_e \sim 5 \times 10^3$ K), the *Radiation Belts* ($n_e \sim 1$ cm^{-3}, $T_e \sim 5 \times 10^7$ K), the Plasma Sheet ($n_e \sim 0.5$ cm^{-3}, $T_e \sim 5 \times 10^6$ K), and the *Magnetotail* ($n_e \sim 10^{-2}$ cm^{-3}, $T_e \sim 5 \times 10^5$ K). The Radiation Belts, discovered by Van Allen and collaborators in 1958, are doughnut shaped regions populated by energetic electrons and ions ($E_e \sim$ 0.1-10 MeV, $E_p >$50 MeV) [*Baumjohann and Treumann*, 1997].

1.2.3 The Ionosphere

The *Ionosphere* is the outer most region of Earth's atmosphere, composed of a mix of neutral particles and plasma. The plasma in the upper ionosphere is produced by ionization of molecules in the neutral atmosphere by solar ultraviolet light and x-rays, and precipitating particles in the auroral zones.

The region of the Ionosphere between 50-90 km is called the D-region; in this region, ionization is produced by energetic sources, such as solar X-rays, precipitating energetic particles, and cosmic ray particles [*Kivelson and Russell*, 1995], and recombination is high due to high collision frequencies [*Baumjohann and Treumann*, 1997], resulting in attenuation of high-frequency (HF) radio waves, particularly at 10 MHz and below.

The regions above 90 km and 160 km are called the E-region and F-region respectively. In these regions, photo-ionization is high and depends on daytime variations [*Baumjohann and Treumann*, 1997]. Figure 1.5 shows the vertical

profile of mid-latitude electron density during day and night hours. The physical properties of those regions, such as high electron density, and refraction and reflection of radio frequency electromagnetic waves, have not only been utilized for over a century by Amateur Radio enthusiasts, but are critical for the functioning of backscatter radars, such as the *High Frequency* (HF) radars that are part of the *Super Dual Auroral Radar Network* utilized in this study. A picture of one of the Super Dual Auroral Radar Network (SuperDARN) stations is shown in Figure 1.6. Chapter 2 includes a detail description of these physical properties and the operation of the SuperDARN radars.

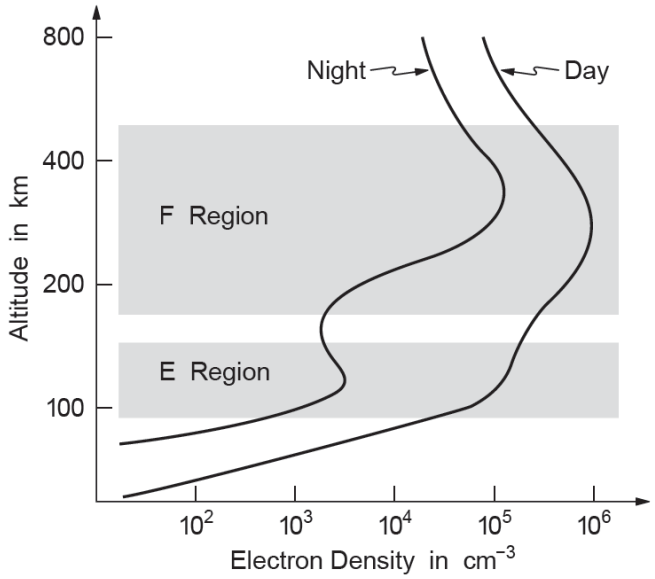

Figure 1.5: Vertical profile of mid-latitude electron density [*Baumjohann and Treumann*, 1997].

The Ionosphere is also highly conductive because ions in the E-region move with the neutral gas due to atmospheric winds and tidal oscillations moving across magnetic field lines but electrons in this region gyrate around those field lines. The relative movement constitute an electric current while charge separation produces an electric field [*Baumjohann and Treumann*, 1997].

Figure 1.6: SuperDARN TIGER Radar with Aurora. Credits: Danny Ratcliffe, La Trobe University, Australia (from: http://www.jhuapl.edu/newscenter/pressreleases/2009/090708_image3.asp).

The magnetic field lines have their footprints on Earth's surface (ground) and extend out into the magnetosphere. SuperDARN detects coherent echoes detected by from plasma irregularities that are aligned with the geomagnetic field [*Greenwald et al.*, 1985]. One of the outcomes of these measurements is the Doppler velocity (line-of-sight irregularity velocity) associated with the ionospheric plasma *ExB* drift, where *E* is ionospheric electric field and *B* is geomagnetic field [*Chisham et al.*, 2007]. The Doppler velocity thus provides excellent information regarding magnetic field line convection and oscillation.

The basics of the operation of the radars that form the SuperDARN network and the development of a code for automatic detection of ULF waves will be described in detail in chapter 2, while the identification and characterization of *Field Line Resonances (FLRs)* using SuperDARN will be explained in chapters 3 and 4.

In the following sections, the theory of FLRs, a summary of the FLRs research studies up to date, the recent studies of possible sources of FLRs, and the goal of this study will be presented.

1.3 ULF Waves and FLR model

The object of this thesis is the study of *Field Line Resonances (FLRs)* in Earth's magnetic field. Basic knowledge of plasma physics can be found in introduction to plasma physics' books and space physics' books, such as *Baumjohann and Treumann* [1997], *Meyer-Vernet* [2007], *Kivelson and Russell* [1995], and *Chen* [1974].

Table 1.1: Properties of space plasma (From *Kivelson and Russell* [1995])

Plasma Type	Density (cm^{-3})	Temp (eV)	Debye Length (m)	Number of particles in Debye Sphere N_D
Solar wind	10	10	10	10^{10}
Solar atmosphere	10^{14}	1	10^{-6}	10^{2}
Magnetosphere	10	10^{3}	10^{2}	10^{13}
Ionosphere	10^{6}	10^{-1}	10^{-3}	10^{4}

The space environment, which is the object of this study, is characterized by low and high energy particle regions and its low density, except for the lowest layer of Earth's ionosphere (where recombination is possible). Table 1.1 summarizes the properties of space plasma. It is worth mentioning that the different regions in the magnetosphere have different plasma parameters.

1.3.1 Theory of Alfvén Waves

The collective behavior of plasma enables the study of plasma as an electromagnetic charged fluid. This is known as *Magnetohydrodynamics (MHD)*. In *ideal MHD,* the fluid has little resistivity and can be treated as a perfect

conductor; therefore, conductivity is large enough ($\sigma \to \infty$) that the displacement current in Maxwell equations can be neglected.

The ideal MHD equations consist of:

Continuity Equation $$\frac{\partial \rho}{\partial t} = \overline{\nabla} \bullet \partial \overline{u} \qquad (1.2)$$

Momentum Conservation $$\rho \frac{\partial \overline{u}}{\partial t} + \rho\left(\overline{u} \bullet \overline{\nabla}\right)\overline{u} = -c_s^2 \overline{\nabla}\rho + \overline{J} \times \overline{B} \qquad (1.3)$$

Faraday's Law $$\frac{\partial \overline{B}}{\partial t} = -\overline{\nabla} \times \overline{E} \qquad (1.4)$$

Ampere's Law $$\mu_0 \overline{J} = \overline{\nabla} \times \overline{B} \qquad (1.5)$$

Divergenceless magnetic field $$\overline{\nabla} \bullet \overline{B} = 0 \qquad (1.6)$$

Ohm's Law (Generalized Ohm's Law)

$$\overline{E} + \overline{u} \times \overline{B} = 0 \qquad \left(\overline{J} = \sigma(\overline{E} + \overline{u} \times \overline{B})\right) \qquad (1.7)$$

Conservation of Specific Entropy $$\left(\frac{\partial}{\partial t} + \overline{u} \bullet \overline{\nabla}\right)\left(\frac{p}{\rho^{\gamma}}\right) = 0 \qquad (1.8)$$

where ρ is the plasma mass density, $\bar{J}$ is the electric-current density, $\boldsymbol{u}$ is the plasma flow velocity, $\boldsymbol{E}$ is the electric field, $\boldsymbol{B}$ is the magnetic field, μ_o is the magnetic permeability of free space, σ is the plasma conductivity, p is the pressure, c_s^2 is the speed of sound and $c_s^2 \approx 0$.

The ideal MHD basic parameters are:

Ratio plasma pressure/magnetic pressure $$\beta = \frac{p}{B^2 / 2\mu_0} << 1 \qquad (1.9)$$

Speed of sound in plasma, C_s $$c_s^2 = \gamma \frac{p}{\rho} \approx 0 \qquad (1.10)$$

Alfvén speed $$V_A = \frac{B}{\sqrt{\mu_0 \rho}} \qquad (1.11)$$

where γ is the ratio of specific heat at constant pressure to the specific heat at a constant volume, p is the plasma pressure, ρ is the plasma mass density, $\boldsymbol{B}$ is the magnetic field, μ_o is the magnetic permeability of free space.

In wave theory, the relationship between the angular frequency ω depends on the wave number k on a wave is given by the *dispersion relations*. The roots of the dispersion relation give the values of the phase velocity:

$$v_{ph} = \frac{\varpi}{k} \qquad (1.12)$$

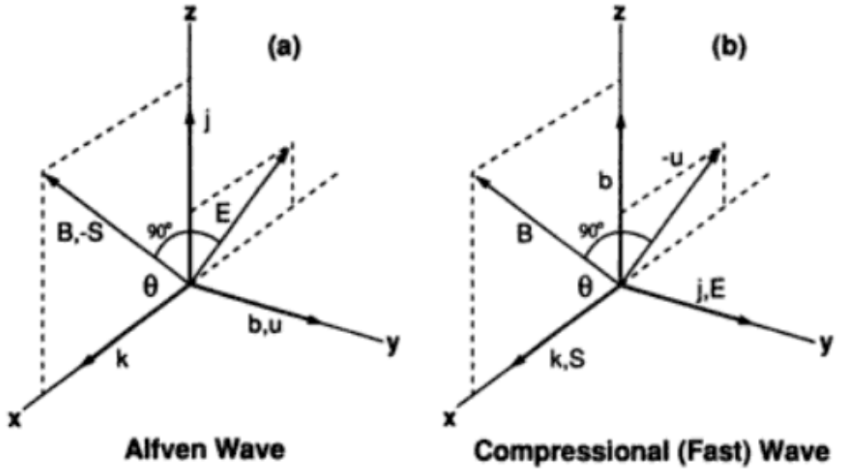

Figure 1.7: Schematic of wave polarizations for the two different types of waves (from *Kivelson and Russell* [1995]).

To derive the dispersion relations of electromagnetic waves in magnetized 'cold plasma' (plasma pressure not important or $\beta<<1$ and $C_s=0$), some assumptions are considered: Assume that the plasma is initially at rest (no background flow), that wave perturbations are small in E, v, density, and B (so small that only linear terms are considered); assume also linear solutions. Then, the dispersion relations of the two types of waves (schematic of wave polarizations shown in Figure 1.7) that are derived from the linearized MHD equation are:

Dispersion Relation for Shear Alfvén Wave $$\varpi^2 = V_A{}^2 k_{\|}{}^2 \qquad (1.13)$$

Dispersion Relation for Compressional Waves (fast magnetosonic waves)

$$\varpi^2 = \bar{k}^2 V_A{}^2 \qquad (1.14)$$

where $\bar{k}$ is the wave-vector, $k_{\|}$ is the component of the wave-vector parallel to the background magnetic field $\boldsymbol{B_o}$.

Field Line Resonances, the object of this study, are shear Alfvén waves on Earth's magnetic field. The following section is devoted to a description of the theory of FLRs.

1.3.2 Field Line Resonance Theory and Profile

Field Line Resonances (FLRs) are standing magnetic field line oscillations on Earth's magnetic field. Theoretical derivations can be found in *Tamao* [1966], *Cummings et al.* [1969], *Southwood* [1974] *Chen and Hasegawa* [1974], *Singer* [1981], *Lee and Lysak* [1989].

FLRs are *Ultra Low Frequency* (ULF) *shear Alfvén waves*, in the Pc5 (2 mHz to 7 mHz) range [*Jacobs et al.*, 1964], and with oscillation periods of the order of several minutes. FLRs (Figure 1.8) are analogous to standing waves in a violin' string: The *E* field would have nodes on the ionosphere if the ionosphere had infinite conductivity. Since the ionosphere is not a perfect reflector to the wave because it has has finite conductance, the energy dissipation results in a finite field line resonance amplitude. In a spatially uniform plasma density and magnetic field strength, the resonant frequency of the FLRs would be inversely proportional to the length of the field line and directly proportional to the Alfvén speed [*Walker et al.,* 1992]. Therefore, the natural resonant frequency would be directly proportional to the strength of the background field and inversely proportional to the square root of the density of the plasma in the flux tube of the field line and it is given by:

$$f = \frac{nv_A}{2l} = \frac{nB}{2l\sqrt{\mu_0 \rho}} \tag{1.16}$$

where l is the length of the field line, n is the fundamental (n=1) or number of harmonic mode (n>1), B is the background field, v_A is the Alfvén speed, μ_0 is the permeability of free space and ρ is the plasma density of the field line (flux tube).

In reality, the field-line's oscillation period represent an integral along the flux tube. Therefore, the FLR frequency decreases with increasing field line length and decreasing Alfvén speed (which it is related to the background magnetic field and plasma density in the flux tube).

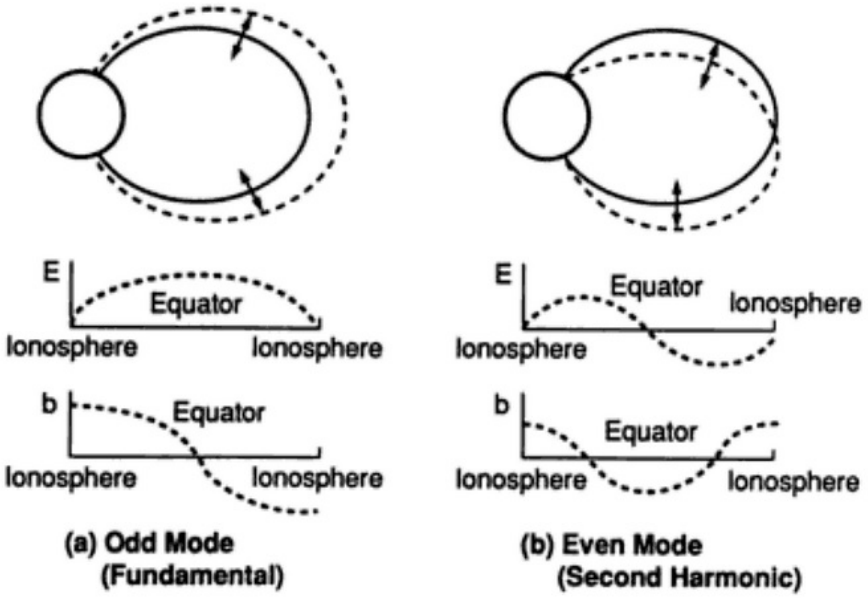

Figure 1.8: Standing oscillations in a dipole magnetic field. "Schematic illustrations of the field displacements in the fundamental and second harmonic of the field line resonances. Dashed lines are the displacement field lines" (From *Kivelson and Russell* [1995]).

FLRs are thought to be the result of the coupling of a monochromatic fast compressional magnetohydrodynamics waves in the outer magnetosphere and shear Alfvén waves in the magnetosphere [*Tamao*, 1966; *Southwood*, 1974; *Chen and Hasegawa*, 1974]. An incoming compressional MHD wave is continuing refracted as it propagates towards the Earth because it encounters a positive gradient in the Alfvén velocity. Beyond the turning point, the wave decays exponentially until a resonance position where a field line resonance Alfvén shear frequency matches the frequency of the fast compressional wave [*Dungey and*

Southwood, 1969; *Southwood*, 1974; *Singer et al.,* 1981; *Walker et al.,* 1992]. From the idealized Ohm's Law, the continuity and the momentum equation and solving Maxwell's equations, assuming the geometry of a 1D box model and assuming infinite, uniform plasma with variation in a single direction and boundary conditions (in the ionosphere and the magnetopause), the solution near the resonance point is given by:

$$E_x = \frac{-E_0\left[\varepsilon + i(x - x_r)\right]}{k_y\left[(x - x_r)^2 + \varepsilon^2\right]} \tag{1.17}$$

where E_x is the radial component of the electric field, k_y is the wave vector in the azimuthal direction in a right-handed coordinate system (z is the direction aligned to the background field B_o, x is the radial direction outwards), x_r is the position near resonance position, and ε is related to the ionospheric dissipation of energy derived in *Fenrich et al.* [1997]. The amplitude and phase profile of E_x as a function of latitude is shown in Figure 1.9.

The standing shear Alfvén wave would grow infinitely without energy dissipation at the resonance position: in reality, the ionosphere has finite conductivity and the perturbations in the magnetic field above the ionosphere drive ionospheric currents that dissipate energy through Joule heating [*Tamao*, 1966; *Southwood*, 1974; *Fenrich and Samson*, 1997; *Rae et al.*, 2008; *Richmond*, 2010]. Figure 1.10 shows schematics of perturbed electric and magnetic fields for a Field Line Resonances in Earth's magnetic field. The polarization patterns mapped down to the ionosphere are very useful to detect FLRs with ground instrumentation. In the next section, a brief discussion of those detection studies will be presented.

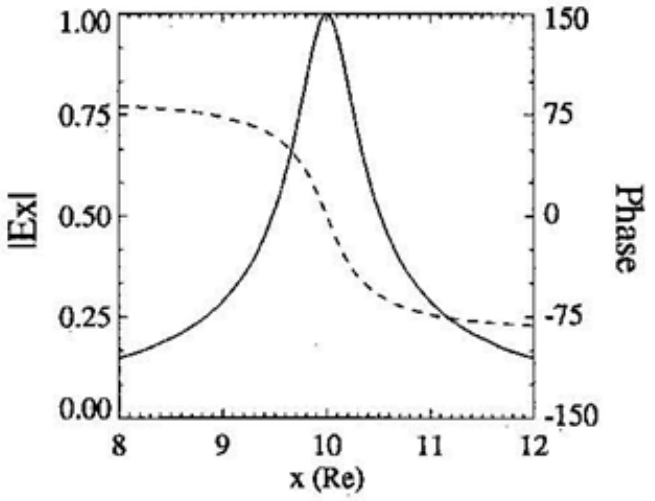

Figure 1.9: Profile of a FLR. Electric Field (x-component) amplitude and phase with resonance at x=10R_e (from *Fenrich and Samson* [1997], figure 5).

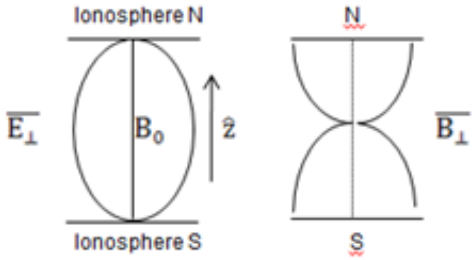

Figure 1.10: Schematics of the electric (left) and magnetic (right) field displacement in a fundamental mode of a field line resonance in Earth's magnetic field, in a box model.

There are two main types of Field Line Resonances: The 'poloidal mode' and the 'toroidal mode'. The 'toroidal mode' corresponds to ULF waves for which E is directed in the radial direction ($\hat{x}$) and the velocity and magnetic field perturbations occur in the azimuthal direction ($\hat{y}$). The 'poloidal mode', on the other hand, corresponds to ULF waves for which E is directed in the azimuthal

direction ($\hat{y}$) and the velocity and magnetic field perturbations occur in the radial direction ($\hat{x}$). Figure 1.11 shows a schematic of the oscillation of a field line in the two lowest frequency field-aligned standing toroidal (left) and poloidal (right) modes, while Figure 1.6 showed the polarization of the poloidal FLRs.

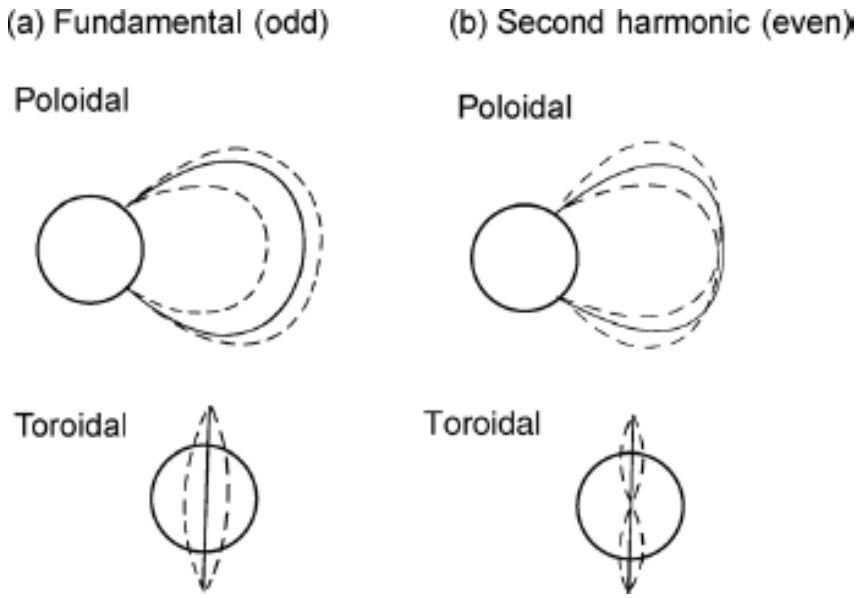

Figure 1.11: Schematic representation of (a) fundamental (odd mode) and (b) second harmonic (even mode) standing oscillations of geomagnetic field lines. Decoupled toroidal and poloidal modes are shown, with dashed lines depicting the displaced field lines (From *Menk and Waters* [2013]).

1.4 Review of Field Line Resonance Literature

1.4.1 Early studies of FLRs

Observations of Ultra Low Frequency waves in the magnetosphere with ground instrumentation were first reported by *Stewart* [1861] and continued throughout the following century. They were called ”*geomagnetic pulsations*”.

Dungey [1954a, b] was the first to suggest that these pulsations were produced by MHD waves in the outer atmosphere and that the period of these "*continuous pulsations*" (Pc-5 pulsations, *Jacobs et al.* [1964]) were the result of a resonant process, that is to say standing waves along magnetic field lines that reflected at the ionosphere at the two ends.

One of the first observational studies of low frequency MHD waves in the magnetosphere was by *Patel* [1964] with magnetometers on board the satellite Explorer XII. He also proposed a method to separate transverse Alfvén waves and magnetosonic waves from the satellite measurements. *Cummings et al.* [1969] investigated standing Alfvén waves in the magnetosphere both observationally (using satellite data) and theoretically, being able to measure 25 separated events that exhibited very nearly monochromatic fluctuations with periods ranging rom 50 to 300 seconds. *Dungey and Southwood* [1969] revised the ground magnetometer and satellite observation of Ultra Low Frequency (ULF) waves in the magnetosphere and revised the concept of resonance modes, earlier introduced by *Dungey* [1954a], and the possibility that a Kevin-Helmholtz instability could be the source of excitation, as well as the energy deposition in the ionosphere by the field line resonances.

Pioneering detection of geomagnetic micropulsations using ground magnetometers were conducted by *Samson et al.* [1971] and *Rostoker et al.* [1972]. They continued their detection of FLRs using magnetometers for decades, thanks to the Canadian Auroral Network for Open Unified Study (CANOPUS). The Canopus Network was expanded with the installation of multiple magnetometer stations across Canada and became the Canadian Array for Realtime Investigations of Magnetic Activity (CARISMA) network [*Mann et al.* 2008], which is still used nowadays for the detection of FLRs and other geomagnetic activity monitoring studies.

The features of Field Line Resonance were theoretically studied by *Southwood* [1974]. *Singer et al.* [1981] introduced a method to numerically determine the *eigenfrequencies* for Field Line Resonances in realistic magnetospheric magnetic field geometry. Significant caracteristics of FLRs related to their azimuthal wave numbers were theoretical studied by *Walker* [1987, 1994], *Taylor and Walker* [1987] and *Walker and Pekrides* [1996]. *Waters et al.* [1994] used magnetometer data to study the resonant frequency, resonance width and damping coefficient of FLRs, and modeled low latitude geomagnetic FLRs; he also proposed a comprehensive ULF resonance structure in the magnetosphere [*Waters*, 2000].

The study of FLRs is also important in the generation of auroral arcs and energy transfer from the outer magnetosphere to ionosphere and ionospheric heating [*Rae et al.,* 2008; *Damiano et al.,* 2007; *Richmond*, 2010]. FLRs are important mechanism for the energization of particles in different regions of the magnetosphere. This idea was introduced by *Lanzerotti and Maclennan* [1987]. The interaction of ULF waves' fields and electron's drift orbits accelerates electrons in the magnetosphere to MeV energies [*Elkington et al.,* 1999; *Mathie and Mann*, 2000; *Elkington et al.,* 2003; *Mann et al.,* 2003; *Rae et al.,* 2006; *Zong et al., 2009*].

1.4.2 FLRs research studies using SuperDARN

For the past three decades, the SuperDARN network has proven to be an excellent instrument for detection of FLRs. Walker and Greendward, among others, were pioneers of detection of FLRs using SuperDARN [*Greenwald et al.* 1978; *Walker et al,* 1979; *Walker,* 1980 and *Walker,* 1995]. Fenrich and Samson performed systematic detection of FLRs utilizing radar data from the early SuperDARN network [*Fenrich et al.,* 1995]. Fenrich, in her PhD Thesis [1997] extensively studied FLRs using SuperDARN and identified and classified the two

FLR modes, 'poloidial mode' and 'toroidial mode', by their azimuthal wavenumber.

A comparison study between SuperDARN and CANOPUS observations of FLRs was conducted by *Ziesolleck et al.* [1998], which showed agreement in the measured resonance frequency and azimuthal wave numbers (m-number) for some cases but not for others. *Ponomarenko et al.* [2001] conducted similar comparison studies and was able to determine the limitations of both radars and ground magnetometers in the measurement of m-numbers of FLRs, which it is important when comparing measurements done by each instrumentation.

An automated method for detection of FLRs using ground magnetometers was developed by *Berube et al.* [2003]. Ponomarenko [2003] published a comprehensive technique for visualization of ULF waves in SuperDARN data, which is very useful for this thesis. Furthermore, the techniques for FLR identification using SuperDARN used in this thesis have been extensively developed by *Fenrich et al.* [2006]. The results of that study showed the discrete and repetitive nature of FLRs and gave rise to the concept of '*magic frequencies*', also known as "*Samson's magic frequencies*". These frequencies are 1.3, 1.9, 2.6 and 3.4 mHz.

1.4.3 Studies on FLR characteristics

The two types, toroidal and poloidal mode, of Field Line Resonances have been successfully observed and their properties studied by many researchers: *Chen and Hasegawa* [1974], *Walker* [1994], *Walker and Pekrides* [1996], *Allan and Wright* [1997], *Ziesolleck et al.* [1998], Yeoman et al. [2000], just to name a few.

Some of the extensive studies were conducted by *Fenrich et al.* [1995], *Fenrich* [PhD Thesis, 1997], and *Fenrich and Samson* [1997]: In those studies, the FLRs were categorized as 'poloidal mode' if they exhibit a large ($m \geq 17$)

azimuthal wave number (*high-m*) and as 'toroidal mode' FLRs if they had a small azimuthal wave number (*low-m*). In those studies, low-*m* FLRs exhibited a standard decrease in the latitudinal phase shift throughout the resonance peak, while high-*m* were characterized by a phase increase with latitude [*Fenrich et al.*, 1995].

Fenrich and Samson [1997] postulated that the 180 phase decrease (a known driven resonance effect) found for the FLR low-*m* case is attributed to the latitudinal/radial gradient in the standing Alfven wave frequency. They also suggested that the increase in phase variation with latitude for the high-*m* could be explained as the wave-particle coupling acting as an internal driver. In that study, *Fenrich and Samson* [1997] used a heuristic model driving term suggested by *Southwood* [1974] for the high-*m* waves, within an MHD formulation, to try to theoretically explain their observations. However, *Mann* [1998] pointed out problems in that study, citing unphysical results, and offered an alternative heuristic MHD model to better described the observations of high-*m* FLRs.

Some studies have proposed complementary and/or alternative classification for FLRs. *Allan and Wright* [1997] defined small-*m* modes as those FLRs with m <10 and large-*m* events for FLRs with $10 < m < 50$. *Wright and Yeoman et al.* [1999] stated that FLRs "*exhibit small effective azimuthal wave numbers (m) typically in the range 0-20 (…)". Yeoman et al.* [2010; 2012] proposed that ULF waves are classified as "*high-m*" if $m > 15$. Alternatively, *Wright and Yeoman et al.* [1999] and *Yeoman et al.* [2000] explained that particle-driven ULF waves are high-*m* pulsations and they can be categorized into "storm time Pc5's" and 'Pg' (giant) pulsations observed when geomagnetic conditions are quiet, with average $m \sim -26$ (negative sign means westward propagation) and as high as $m \sim 100$.

Mager et al. [2010] postulated that the increase in phase variation with latitude profile of high-*m* FLRs could be explained "in terms of a model of wave excitation by an azimuthally drifting particle inhomogeneity injected during

substorm activity": the increase in phase variation would be caused by fact that the radial component of the phase velocity (directed toward Earth) was led by the cloud stretched into spiral in the equatorial plane when the drift velocity increases with the radial coordinate, given that the azimuthal direction of the phase velocity coincided with that of the particle cloud.

This mechanism was supported by observations by *Yeoman et al.* [2010]: They offered a case study of an intermediate-*m* (*m*=13) case of a FLR with increase phase variation with latitude, occurred on 21 March 2002, detected by SuperDARN radars at Hankasalmi, Finland and Þykkvibær, after a substorm interval detected by the IMAGE (International Monitor for Auroral Geomagnetic Effects) magnetometer array. It is worth to mention that *Yeoman et al.* [2012] presented a case of a high-*m* case detected by SuperDARN on October 15, 1998 with neither "poleward" nor "equatorward" latitudinal phase propagation, but rather curve phase fronts.

Observed with radars, FLRs that exhibit a standard decrease in the latitudinal phase shift throughout the resonance peak show a "*poleward phase propagation*" (in the time plots of the analytic signal) or "*poleward moving bands*" (in the range-time plots), while FLRs that exhibit a standard decrease in the latitudinal phase shift throughout the resonance peak show a "*equatorward phase propagation*" or "*equatorward moving bands*" [*Waldock et al.*, 1983; *Tian et al.*, 1991; *Yeoman et al.*, 1992; *Fenrich et al.,* 1995; *Yeoman et al.,* 2012]. This terminology will be used throughout this manuscript.

The study of the latitude phase variation (standard/reverse) that is the same to say the latitude phase propagation (poleward/equatorward) and the longitudinal phase propagation (eastward/westward, sunwards/anti-sunwards) of FLRs using SuperDARN radars was also studied by *Fenrich et al.* [1995], *Fenrich* [PhD Thesis, 1997] and *Fenrich and Samson*[1997]. However, the

classifications contradict some of the results obtained by *Yeoman and Lester* [1990], *Tian et al.* [1991], *Yeoman et al.* [1992], and *Yeoman et al.* [2010].

1.4.4 Recent studies of possible sources of FLRs

The complex interactions of the solar wind with the Earth's magnetosphere have been studied for the past five decades but the cause of Field Line Resonances is still under debate. The difficulties with proposed sources has been discussed by *Fenrich et al.* [1995], *Waters* [2000], *Stephenson and Walker* [2002], *Walker* [2005] and *Menk* [2011], among many others.

Kevin-Helmholtz instability was the earliest mechanism proposed (*Dungey* [1954a]), but failed to explain the discrete nature of FLRs observed at different latitudes. Another explanation proposed was the cavity or waveguide modes but they fail to explain the low frequency FLRs observed and the repetitiveness nature of the 'magic frequencies' since the magnetosphere is a very active region and its size varies continually under different solar wind conditions.

Several FLR case studies have been conducted using SuperDARN, magnetometers, and other instruments, which reported a repetitive nature of discrete frequencies observed over others. These 'magic frequencies' were found by *Samson et al.* [1991], *Fenrich et al.* [1995], *Francia and Villante* [1997], *Villante et al.* [2001], *Francia et al.* [2005], *Thomson et al.* [2007], to name a few. *Vial et al.* [2009] and *Archer and Plaschke* [2014] presented a historical compilation of the detection of these 'magic frequencies', detected by different ground and spacecraft instrumentation between 1991 and 2009. A theory that intends to explain the repetitive nature of discrete FLRs is that they are directly driven by ULF waves in the solar wind with matching frequency.

The dependence of solar activity and FLRs has been studied by numerous scientists. *Ziesolleck and McDiarmid* [1995] conducted a statistical study and they found ULF pulsations occurring with the same frequency at all latitudes but

the frequencies detected in the study were different than the so called "magic frequencies". *Vellante and Förster* [2005] investigated the relationship between solar irradiance's dependence of FLRs, showing the dependency of solar irradiance and plasma density in the flux tubes.

Rae et al. [2005] made a comprehensive investigation of an FLR event using ground magnetometers, satellite instrumentation, and SuperDARN radars. In this case, the event showed no relationship to dynamic pressure variations in the solar wind, and the authors suggested that the event was excited by the Kevin-Helmoltz instability in the magnetopause. *Rae et al.* [2012] analyzed 15 years of ground-based magnetometer data and found no enhancement at discrete frequencies in the power spectrum. That paper presented an excellent historical review and compelling discussion on the topic. Similarly, *Baker et al.* [2003] analyzed 10 years of magnetometer data and found no evidence of stable, recurring, discrete frequencies in the Pc5 range.

Furthermore, *Archer and Plaschke* [2014] well pointed out that the existence, significance, and stability of the so called "magic frequencies" is disputed. They utilized an entire solar cycle's worth of solar wind data (from OMNI database) to investigate the distribution of magnetopause surface waves, using realistic models of the magnetosphere and the magnetosheath. These magnetopause surface waves, also called Kruskal-Schwartzschild (KS) modes, "had been suggested as a possible source of 'magic' frequencies". The study revealed that the most likely fundamental frequency, under non-storm conditions was 0.64±0.06 mHz. They also found that the distribution exhibited a significant spread (±0.3mHz), much larger than suggested by proponents of discrete, stable 'magic' frequencies.

All these studies enumerated contradict the idea that FLRs are directly driven by ULF waves in the solar wind with the same frequency.

On the other hand, some studies claim to provide observational evidence to confirm the theory that ULF waves are direct drivers of FLRs. *Viall et al.* [2009] conducted an analysis of the occurrence distribution of statistically significance correspondence between solar wind number density structures and FLR events, using 11 years (1995-2005) of solar wind data and discrete oscillations identified during a 10 year period (1996-2005), which they found in 54% of the cases. *Fenrich and Waters* [2008] developed a new technique of "cross-power and cross-phase" and demonstrated phase coherence of a field line resonance and solar wind oscillation for an event in Nov 21, 2003, with 95% confidence level. An independent study by *Stephenson and Walker* [2010] of another event using a different technique provided the same result.

This study intended to systematically study the characteristics of Field Line Resonances in Earth's magnetic field and to study the correlation between ULF waves in the solar wind and FLRs.

1.5 Objective and Main Goals

The main goal of this study was to statistically determine which portion of Field Line Resonances (FLRs) in Earth's Magnetic Field (Magnetosphere) between 0.5 mHz and 5mHz has their origin in the solar wind Ultra Low Frequency (ULF) waves.

Another important goal of this study was to produce an automated algorithm to identify ULF waves using SuperDARN, and to create and validate a large database of FLRs from which to determine FLR statistics on classification of their characteristics, such as frequency, latitude, local time, m-value, etc. It is worth mentioning that there have been recent attempts (simultaneous to, but independent from, this study) by *Mangus* [2009] and *Bland et al.* [2014] to develop computer algoritms to automatically detect Pc5 using SuperDARN. The autor of this manuscript did not have knowledge of these efforts until the final

edits performed in this manuscript. Comparisons of the methodology used in this study and the other studies will be described at the end of Chapter 2.

The methodology of systematic detection of ULF waves using SuperDARN will be explained in Chapter 2. In this chapter, an overview of the technical specifications of the SuperDARN radars will be given, as well as the signal processing techniques applied. Chapter 3 will present the methodology for the identification and classification of field line resonances from the ULF waves detected. An extensive analysis of the results, including the study of the latitude phase variation (standard/reverse; poleward/equatorward) and the longitudinal phase propagation, as well as the azimuthal wave numbers, will be presented in chapter 4. A detailed description of the signal processing techniques applied towards the study of coherence between FLRs and solar wind will be presented in Chapter 5 and the technical specifications of NASA ACE mission (that provides the solar wind measurements) will be given in that chapter. A summary of these results will be given at the end of the chapter. The general conclusion in chapter 6 will close this manuscript.

Chapter 2

Systematic Detection of ULF Waves Using the Super Dual Auroral Network

One of the main goals of this thesis research was to create a large database of FLRs that provided statistics on their characteristics (e.g. resonant frequency distribution, latitude, magnetic local time, m-value, etc.) and would allow for the statistical analysis of their wave sources. Sections 1.3.3 and 1.3.4 summarized the discrepancies among results presented by several studies that contradict each other. The creation of a large library of FLRs systematically detected was crucial to conduct a methodic analysis of FLRs and their characteristics that could provide further information of these discrepancies.

Past and current detection techniques that identify ULF waves using SuperDARN, which can later be tested for FLRs criteria, rely on visual inspection of Doppler velocity backscatter patterns. The visualization of these waves using SuperDARN requires a very well trained eye and might introduce some bias in the final FLR sample group. To eliminate that visual bias, the motivation for this study was to produce an automated code to identify ULF waves from SuperDARN data that were good candidates for FLR events. The automatization, which processed a large amount of data corresponding to an extended period of time (a year or longer), provided 'blind detection' of ULF waves, i.e. the events were not

identified *a priori* by eye nor the data was inspected before applying the identification process.

The sections below describe in detail the concept behind the "ULF wave *blind detection* code", while the processes of identification, classification, and characterization of FLRs are extensively described in the next chapter.

2.1 General Information regarding SuperDARN

The Super Dual Auroral Radar Network (SuperDARN) has successfully been used over the past 20 years to detect ULF waves that can be later identified as FLRs, due to its large coverage over the polar cap and auroral region. The radar network has proven to be more efficient than magnetometers in the detection of FLRs, since magnetometers do not detect very high-*m* waves [*Wright et al.,* 1999; *Wright and Yeoman*, 1999; *Yeoman et al.*, 2000; *Baddeley et al.*, 2005]: Radars have better spatial resolution, wider coverage and measure time delay, and/or amplitude of returned signal of ionosospheric processes related to ULF waves while magnetometers measure currents that are subject to the transition at the boundary between the ionosphere and the neutral atmosphere. However, radars measurements are limited to periods of times with good backscatter, depending on electron density fluctuations from day and geomagnetic variability [*Ballatore et al.,* 2001], for which some FLR occurrences cannot be detected by the radars if they occur in times of poor backscatter conditions.

SuperDARN is an international radar network that has been operational for over 20 years. A comprehensive description of the radars' hardware, software, and capabilities can be found at *Greenwald et al.* [1985; 1993]. More information about the SuperDARN network, its capabilities and operation can be found in *Chisham et al.* [2007] and *Lester* [2013]. The sections below describe the location

of the stations, their principles of operation, and the availability of the data used in this study.

2.1.1 The SuperDARN Network

SuperDARN currently consists of over 30 backscatter radars, operating on frequencies between 8 and 30 MHz and observing processes in mid latitude and Polar Regions of the Earth. Figure 2.1 shows the location of all SuperDARN stations, operational and out of service.

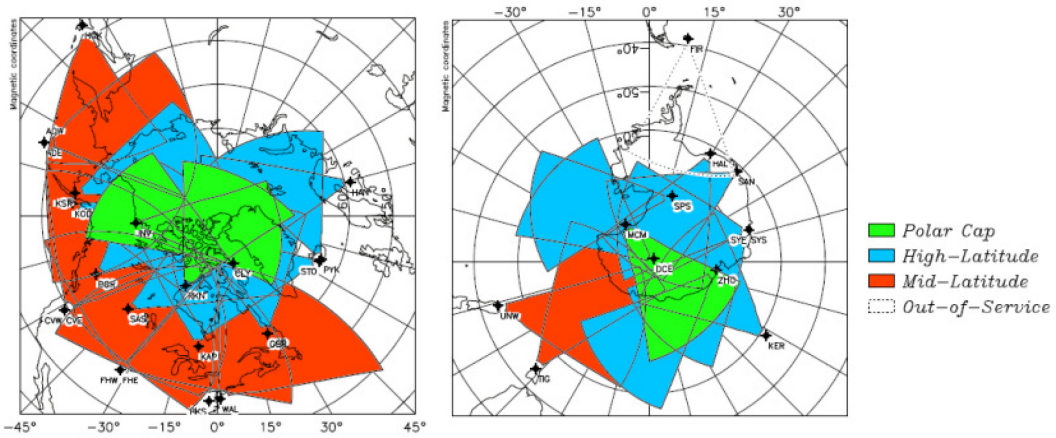

Figure 2.1: SuperDARN radars field of views for the northern hemisphere (left) and southern hemisphere (right). High-Latitude stations are show in blue, Mid-latitude stations in red and radars covering the polar cap in green. The Falkland Island station, currently out of service, is show in gray (from http://superdarn.org/tiki-index.php?page=Radar+Overview).

The first SuperDARN station, Goose Bay, was developed and deployed in 1985 by The John Hopkins University Applied Physics Laboratory and served as the prototype for the current SuperDARN Radars. By 1995, the SuperDARN collaboration constituted 9 stations, 5 in the northern hemisphere and 3 in the southern hemisphere. Each station is operated and maintained by a research institution/university and has a Principal Investigator assigned to it. Some institutions/PIs run few stations. Table 2.1 and Table 2.2 (courtesy of the

SuperDARN Virginia Tech team) shows the geographical location of each station (geographic latitude, longitude and boresite), the station code, the PI/Institution in charge of operations, the magnetic coordinates (geomagnetic latitude, longitude and boresite), and other useful information. Currently, SuperDARN is formed by more than 30 radar stations in both northern and southern hemisphere.

Table 2.1: Information regarding SuperDARN stations in the Southern Hemisphere (from SuperDARN Virginia Tech team, http://superdarn.org/tiki-index.php?page=Radar+Overview)

Southern Hemisphere SuperDARN Radars													
Radar Name (Clickable)	PI Institution (Clickable)	Geographic			**Geomagnetic			Beams	Gates	Start Year	New Code	Station ID	Scan Direction
		Lat. [°]	Lon. [°]	Boresite [°]	Lat. [°]	Lon. [°]	Boresite [°]						
Dome C Show Hdw Table	Institute for Space Astrophysics and Planetology *Dr. Ermanno Amata*	-75.090	123.350	115.0	-88.9	54.6	-105.5	16	75	2013	**dce**	96	
Falkland Islands Show Hdw Table	British Antarctic Survey *Dr. Mervyn Freeman*	-51.83	-58.98	178.2	-39.0	9.9	172.4	16	75	2010	fir	21	E
Halley Show Hdw Table	British Antarctic Survey *Dr. Mervyn Freeman*	-75.52	-26.63	165.0	-62.1	29.3	174.1	16	75	1988	**hal**	4	E
Kerguelen Show Hdw Table	CNRS/LPCE *Dr. AurÃ©lie Marchaudon*	-49.22	70.14	168.0	-58.7	122.7	-163.0	16	75	2000	**ker**	15	W
McMurdo Show Hdw Table	University of Alaska, Fairbanks *Dr. Bill Bristow*	-77.88	166.73	300.0	-80.0	-33.3	-148.2	16	75	2010	**mcm**	20	E
SANAE Show Hdw Table	South African National Space Agency *Dr. Jon P.S. Rash*	-71.68	-2.85	173.2	-61.8	43.7	-162.4	16	75	1997	**san**	11	W
South Pole Station Show Hdw Table	University of Alaska, Fairbanks *Dr. Bill Bristow*	-89.995	118.291	75.7	-74.3	18.5	-20.3	16	75	2013	**sps**	22	
Syowa East Show Hdw Table	National Institute of Polar Research *Dr. Akira Sessai Yukimatu*	-69.00	39.58	106.5	-66.5	72.2	143.0	16	75	1997	**sye**	13	E
Syowa South Show Hdw Table	National Institute of Polar Research *Dr. Akira Sessai Yukimatu*	-69.00	39.58	159.0	-66.5	72.2	-157.7	16	75	1997	**sys**	12	W
Tiger Show Hdw Table	La Trobe University *Dr. John Devlin*	-43.40	147.20	180.0	-54.8	-133.2	169.4	16	75	1999	**tig**	14	W
Unwin Show Hdw Table	La Trobe University *Dr. John Devlin*	-46.51	168.38	227.9	-54.4	-106.2	-152.2	16	75	2004	**unw**	18	W
Zhongshan Show Hdw Table	Polar Research Institute of China *Dr. Hongqiao Hu*	-69.38	76.38	72.5	-74.9	97.2	123.5	16	75	2010	**zho**	19	E

Table 2.2: Information regarding SuperDARN stations in the Northern Hemisphere (from http://superdarn.org/tiki-index.php?page=Radar+Overview)

Northern Hemisphere SuperDARN Radars													
Radar Name (Clickable)	PI Institution (Clickable)	Geographic			**Geomagnetic			Beams	Gates	Start Year	New Code (Clickable)	Station ID	Scan Direction
		Lat. [°]	Lon. [°]	Boresite [°]	Lat. [°]	Lon. [°]	Boresite [°]						
Adak Island East Show Hdw Table	University of Alaska, Fairbanks *Dr. Bill Bristow*	51.88	-176.62	46.0	47.6	-113.0	31.6	24	675	2012	**ade**	209	E
Adak Island West Show Hdw Table	University of Alaska, Fairbanks *Dr. Bill Bristow*	51.88	-176.62	-28.0	47.6	-113.0	-34.2	24	675	2012	**adw**	208	W
Blackstone Show Hdw Table	Virginia Tech *Dr. J. Michael Ruohoniemi*	37.10	-77.95	-40.0	48.2	-2.7	-41.5	24	110	2008	**bks**	33	W
Christmas Valley East Show Hdw Table	Dartmouth College *Dr. Simon Shepherd*	43.27	-120.36	54.0	49.5	-58.3	40.2	24	75	2011	**cve**	207	E
Christmas Valley West Show Hdw Table	Dartmouth College *Dr. Simon Shepherd*	43.27	-120.36	-20.0	49.5	-58.3	-31.2	24	75	2011	**cvw**	206	W
Clyde River Show Hdw Table	University of Saskatchewan *Dr. Jean-Pierre St.-Maurice*	70.49	-68.50	-55.6	78.8	18.1	-42.5	16	100	2012	**cly**	66	W
Fort Hays East Show Hdw Table	Virginia Tech *Dr. J. Michael Ruohoniemi*	38.86	-99.39	45.0	48.9	-32.2	41.3	22	110	2009	**fhe**	205	E
Fort Hays West Show Hdw Table	Virginia Tech *Dr. J. Michael Ruohoniemi*	38.86	-99.39	-25.0	48.9	-32.2	-32.3	22	110	2009	**fhw**	204	W
Goose Bay Show Hdw Table	Virginia Tech *Dr. J. Michael Ruohoniemi*	53.32	-60.46	5.0	61.1	22.9	11.0	16	100	1983	**gbr**	1	E
Hankasalmi Show Hdw Table	University of Leicester *Dr. Mark Lester*	62.32	26.61	-12.0	59.1	104.5	1.5	16	75	1995	**han**	10	W
Hokkaido Show Hdw Table	Nagoya University *Dr. Nozomu Nishitani*	43.53	143.61	25.0	37.3	-144.9	23.9	16	110	2008	**hok**	40	W
Inuvik Show Hdw Table	University of Saskatchewan *Dr. Jean-Pierre St.-Maurice*	68.42	-133.5	26.4	71.5	-85.1	4.4	16	100	2008	**inv**	64	E
Kapuskasing Show Hdw Table	Virginia Tech *Dr. J. Michael Ruohoniemi*	49.39	-82.32	12.0	60.2	-8.3	15.3	16	100	1993	**kap**	3	W
King Salmon Show Hdw Table	National Institute of Information and Communications Technology *Dr. Tsutomu Nagatsuma*	58.68	-156.65	-20.0	57.5	-99.1	-31.3	16	75	2001	**ksr**	16	W
Kodiak Show Hdw Table	University of Alaska, Fairbanks *Dr. Bill Bristow*	57.62	-152.19	30.0	57.2	-94.9	11.9	16	75	2000	**kod**	7	E
Pykkvibaer Show Hdw Table	University of Leicester *Dr. Mark Lester*	63.77	-20.54	30.0	64.6	67.3	40.2	16	75	1995	**pyk**	9	E
Prince George Show Hdw Table	University of Saskatchewan *Dr. Kathryn McWilliams*	53.98	-122.59	-5.0	59.6	-64.3	-16.2	16	75	2000	**pgr**	6	W
Rankin Inlet Show Hdw Table	University of Saskatchewan *Dr. Jean-Pierre St.-Maurice*	62.82	-93.11	5.7	72.6	-26.4	1.8	16	100	2007	**rkn**	65	W
Saskatoon Show Hdw Table	University of Saskatchewan *Dr. Kathryn McWilliams*	52.16	-106.53	23.1	60.9	-43.8	16.9	16	75	1993	**sas**	5	E
Schefferville Show Hdw Table	CNRS/LPCE *Dr. Christian Hanuise*	54.80	-66.80	15.0	63.7	14.9	21.9	16	75	1986	sch	2	W
Stokkseyri Show Hdw Table	Lancaster University *Dr. Jim Wild*	63.86	-22.02	-59.0	64.9	66.1	-33.0	16	75	1994	**sto**	8	W
Wallops Island Show Hdw Table	JHU Applied Physics Laboratory *Dr. Ethan Miller*	37.93	-75.47	35.9	48.7	0.8	46.7	24	110	2005	**wal**	32	E

2.1.2 Main characteristics of the SuperDARN radar operations: Principles of Coherent scattering

The general principles of radar coherent backscatter from ionospheric E-region plasma irregularity is described in detail by *Schlegel* [1995]. This section gives a brief description of the operation of SuperDARN radars. For a more in depth and comprehensive description of SuperDARN radar operation, beam steering, and processing of the signals collected, refer to *Greenwald et al.* [1985] , *Ponomarenko et al.* [2003], *Danskin* [2003], *Hannah* [2004], *Healey* [2005], *Lointier et al.*[2008], *Ribeiro et al.* [2013].

Plasma irregularities (electron density irregularities) in the ionosphere are magnetic field aligned. Following the Bragg condition, in order for a radar to detect a backscatter signal from a plasma irregularities, the wave transmitted by the radar must be directed normal to the irregularities in the region of interest, as shown in Figure 2.2, and the wavelength of the irregularity must be half of the wavelength of the radar [*Schlegel*, 1995]. In the high-latitude ionosphere, the normality condition can only be achieved if the ray path is refracted toward the horizontal as the wave enters the ionosphere. The refraction needed, obeying Snell's law, is sufficiently large that the radar must be operated at High Frequency (HF 3-30MHZ). It is important to mention that the high latitude ionosphere is affected by geomagnetic activity and diurnal variations and geomagnetic activity, for which different amounts of refraction in the course of a day would be expected for an HF wave of a given emission frequency [*Greenwald et al.*, 1985]. Therefore, the SuperDARN radars utilize a range of HF waves (between 8 and 30 MHz) to ensure good backscatter, although some disturbances in the ionosphere related to severe geomagnetic activity might occasionally result in poor backscatter.

Each SuperDARN radar is composed of an electronically steerable phased array of 16 log periodic antennas used both for transmission and reception

[*Villain et al.*, 1987]. The antennas form a beam of half-power width of about 3.24 degrees of azimuth that can be steered rapidaly in 16 directions. Therefore, each radar *Field of View (FoV)* generally comprises 16 "Beams" (0 being the most westwards and 15 the most eastwards) covering 52 degrees of azimuth. The beams are distributed in azimuth symmetrically about the scanning boresite direction. SuperDARN stations Christmas Valley East and West operate describing 24 beams; Adak Island East and West operate describing 22 beams. The Wallops Island Station used to operate describing 16 beams until March 12, 2006 and now it describes 24. Fort Hays East and West stations used to operate describing 16 beams but after June 27 2010 they describe 22 beams. More details on beam steering can be found in *Healey* [2005].

The radars send multiple transmission (7 to 8 pulses over a 100 milliseconds time period, each transmitted pulse with a duration of 300 μs) and multiple sequence repeated 30 to 70 times for a given beam position, to partially suppress the contributions from pulses that encounter other scattering regions at the same sampling times, maximizing the number of unique lags between the pulses. The detected backscatter signal is processed by on-site computers in real time 17-lag complex autocorrelation functions (ACFs), with a basic unit of lag of 2400 μs. The ACFs calculated from all sequences are integrated to minimize interference and increase gain [*Ribeiro et al.*, 2013]. ACFs provide measurements of the backscattered power, the spectral width, and the Doppler velocity (line-of-sight velocity) associated with the ionospheric plasma drift speeds. Details of the signal processing techniques related to ACFs and measurements of spectral width and Doppler velocity (from the Doppler frequency measured) can be found in *Villain et al.* [1987] *Danskin* [2003], *Hannah* [2004], *Lointier et al.*[2008], and *Ribeiro et al.* [2013].

The Doppler shift measurements generally reflect plasma motion, which usually represents $\boldsymbol{E}x\boldsymbol{B}$ drift, where $\boldsymbol{E}$ is ionospheric electric field and $\boldsymbol{B}$ is geomagnetic field. Since plasma irregularities in the ionosphere are aligned to the

magnetic field lines of Earth's magnetic field, the echoes of the signal that return to the radar are normal to the plasma irregularities and hence normal to the magnetic field lines. These measurements give insight on the properties of the standing waves that occur on the magnetosphere.

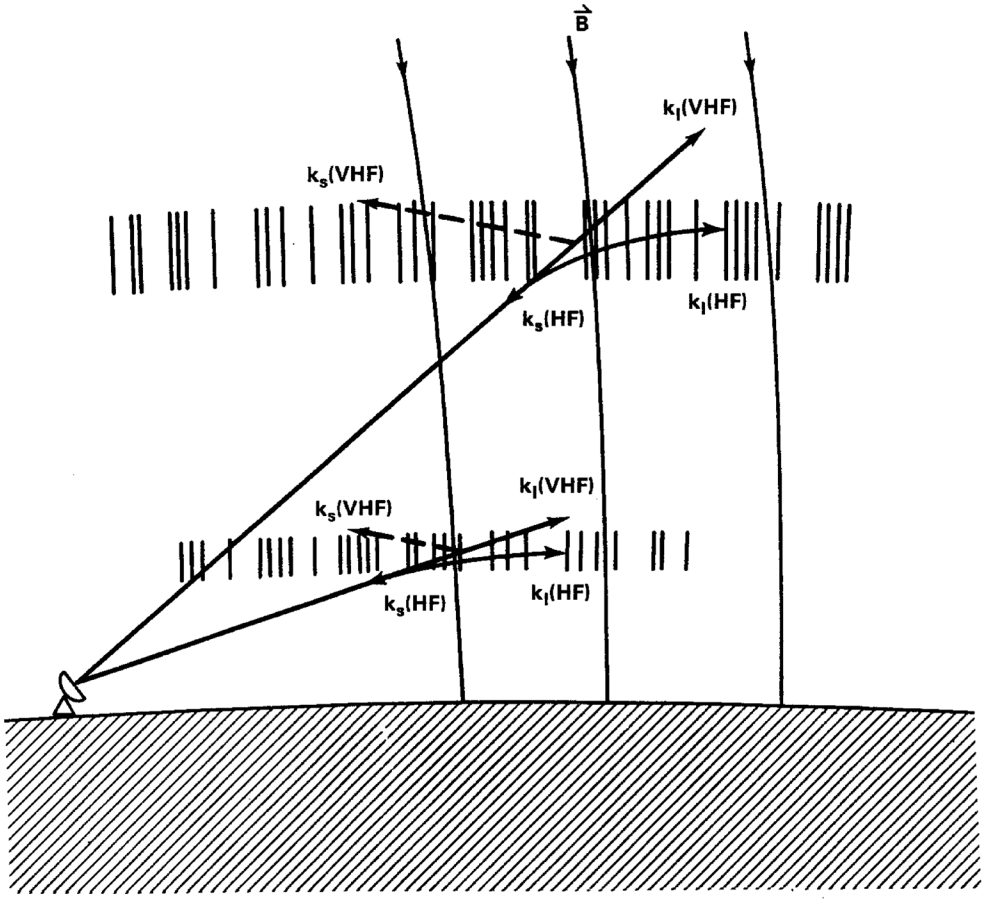

Figure 2.2: Illustration of the path followed by HF and VHF radar signals as they enter the E and F regions of the ionosphere. The radar signals are scattered into space by ionospheric irregularities if the angle of incidence of the signal is not normal to the plasma irregularity. High frequency radar signals are refracted toward the horizontal as they enter the two ionospheric layers and if the angle of incidence to the plasma irregularity is 90°, the backscatter signal returns to the radar (From *Greenwald et al.*, [1993]).

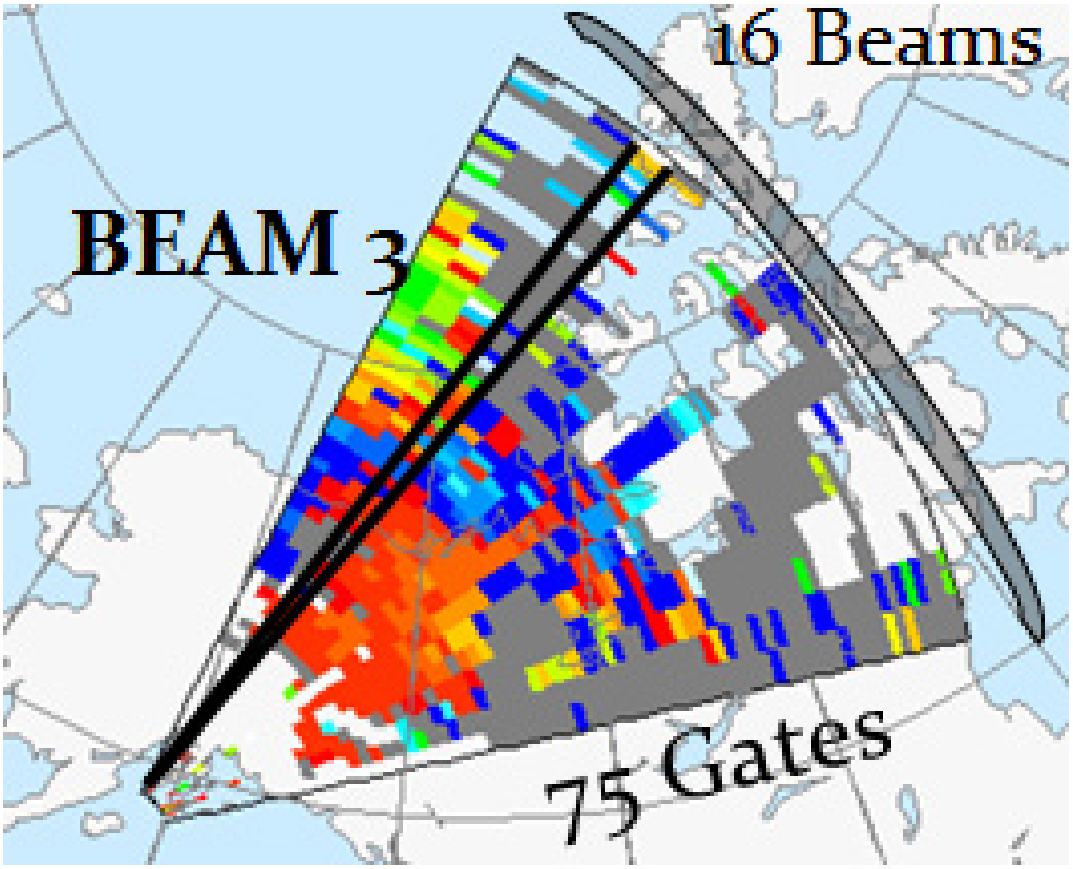

Figure 2.3: Field of View of the Kodiak station. The 16 beams described, which cover 52 degrees azimuth are outline, with beam 3 highlighted with black lines. The radar describes 75 range gates separated by 45 km, the first one located at 180 km in height (from http://superdarn.jhuapl.edu/, old website 2008).

The radars operate in a number of special modes, whose parameters (number of beams, sampling rate, frequencies etc.) are tuned to study a particular phenomenon, or generally in 'normal mode'. During normal mode, the radars utilize a schedule of predefined operating times and frequencies, for which each radar describes 75 range gates, the first range gate located at 180 km, with a range gate separation of 45 km. Figure 2.3 shows the FoV of the Kodiak station, with beam #3 outlined with black lines. The orientation of the range gates and beams described are also shown in that figure.

2.1.3 Availability of Data and general format of data available

The data used in this study were acquired during 2003 by 15 SuperDARN stations located both in the Southern and Northern hemispheres, as shown in Table 2.3. The raw data, facilitated by the SuperDARN collaboration, was formatted in the old "*fitacf*" files. The Barnes' *OldFitOpen* and *OldFitRead* IDL procedures were used to read the files and extract information needed from them. Table 2.4 summarizes the list of parameters and data extracted from the "*fitacf*" files for this study.

Table 2.3: SuperDARN stations used in this study. The third column shows the data availability in which the code for identification was used

Station Name (abbreviation)	Station ID	Hemisphere	Months in 2003 of data analyzed
Goose Bay (GBR)	1	Northern	Jan-Nov
Kapuskasing (KAP)	3	Northern	Jan-Dec
Halley Station (HAL)	4	Southern	Jan-Dec
Saskatoon (SAS)	5	Northern	Jan-Dec
Prince George (PGR)	6	Northern	Jan-Dec
Kodiak (KOD)	7	Northern	Jan-Dec
Stokkseri (STO)	8	Northern	Jan-Dec
Pykkvibaer (PYK)	9	Northern	Jan-Dec
Hankasalmi (HAN)	10	Northern	Jan-Dec
Sanae (SAN)	11	Southern	Jan-Dec
Syowa South (SYS)	12	Southern	Jan-Dec
Syowa East (SYE)	13	Southern	Jan-Dec
Tiger (TIG)	14	Southern	Jan-Dec
Kerguelen (KER)	15	Southern	Jan-Dec
King Salomon (KSR)	16	Northern	Jan-Dec

Table 2.4: Parameters and data loaded from the SuperDARN '*.fit*' files

Parameter/Variable	Description
prm.time.yr	Year
prm.time.mo	Month
prm.time.dy	Date
prm.time.hr	Hour (UT)
prm.time.mt	Minute (UT)
prm.time.sc	Second (UT)
prm.scan	Scan mode
prm.time.bmnum	Beam number
prm.time.intt.sc	Integration time
fit.qflg	Quality Flag
fit.v	Velocity (m/s)
fit.p_l	SNR (Power from lambda fit)
fit.w_l	Width from lambda fit
fit.gflg	Ground Scatter Quality Flag

2.2 Methodology for systematic detection of ULF waves using SuperDARN: Development of a new technique

2.2.1 Current Methods for ULF detection using SuperDARN

ULF pulsations in the *E* and *F* regions associated with field line resonances are observable in the range-time plots of the line-of-sight Doppler velocities. *Fenrich et al.* [1995], *Fenrich* [PhD Thesis, 1997], *Ponomarenko et al.* [2003] and *Fenrich et al.* [2006] have comprehensive descriptions of these methodologies. Figure 2.4 shows the Doppler velocity corresponding to the SuperDARN Kodiak for December 20th, 2003 which shows at 18:45-20:00 UT a visible ULF pattern for gates between 15 and 22, characterized by the alternative pattern of Doppler velocity, in this case between 100 m/s and -300 m/s. These ULF pulsations were

later confirmed to be an FLR of 1.1±0.3 mHz observed by the radar (see next chapter). These types of plots are commonly known in the SuperDARN community with the name of range- time plots. Current detection techniques to identify FLRs using SuperDARN include visual inspection of Doppler velocity backscatter patterns and visualization of the ULF signature in the time series requires a very well trained eye, which might introduce bias in the detection of events related to the individual capabilities of each person in identifying the visual patters.

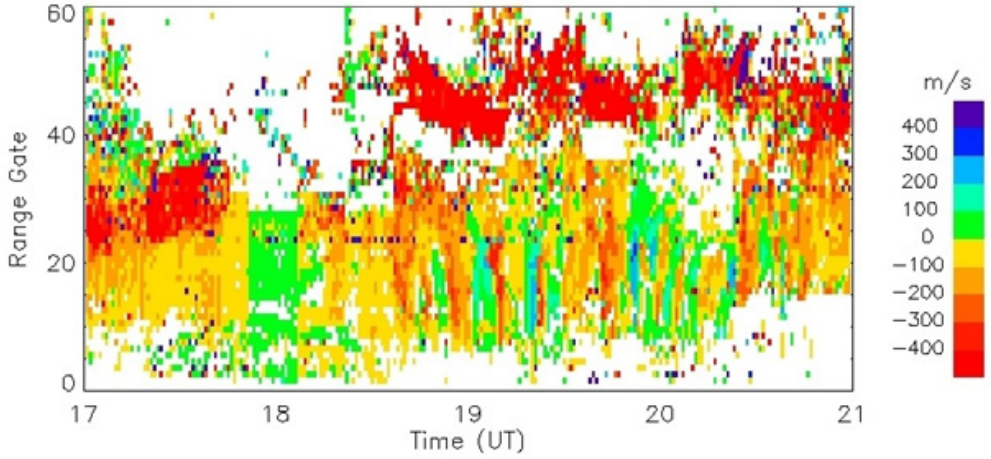

Figure 2.4: Doppler velocity time series for the SuperDARN Kodiak Station for December 20th, 2003, Beam 8. An ULF was also automatically detected by our technique at 18:45-20:00UT on that day. It was later determined that this ULF wave detected corresponded to an FLR at 1.1 mHz, by additional criteria. Current detection techniques to identify ULF waves using SuperDARN include visual inspection of Doppler velocity backscatter patterns like this one.

2.2.2 Proposed methodology for FLR systematic detection, identification, and characterization

A computer program was created in order to automatically detect a ULF **coherent wave over a large area** within the field of view (FoV) of a SuperDARN Radar Station that can be later categorized as a "Field Line Resonance". This code is based on the "Cross-power-Cross-phase Technique"

developed by *Fenrich and Waters* [2008] to find coherence between ULF solar wind waves and ULF waves detected by SuperDARN. In that publication, they also applied the methodology to SuperDARN signals corresponding to two beams significantly separated in the FoV. They found that there was high cross-power and low variance in phase for the Doppler velocity signals of those beams. Therefore, this methodology takes that technique and systematically extends it to be generalized as a ULF detection methodology using SuperDARN signals.

The computer program was developed in *Interactive Data Language (IDL)*, a popular programming language in areas of science such as astrophysics, space science, and medical imaging. IDL shares a similar FORTRAN-like syntax, as well as many common commands, functions, and subroutines. IDL has the advantage to be very fast at doing vector operations and numerically heavy computations. Also, IDL gives great freedom in the creation of plots to visualize the results. The computer program is composed of three nested, independent codes. The first code reads the raw data and loads it into a hyper-matrix, the second code makes the calculations, and the third code applies the threshold of final selection of events, for a given station and year. By launching the third code, the other two are automatically called and launched. Currently, the computer program takes up to 2 weeks to analyze, in an Intel Xeon CPU @2.8GHz and RAM memory of 23.5 GB, about 500 GB of data from all 15 stations for a given year, with an average time of less than 1 day per year of data for a given station. Appendix A contains full texts of the codes.

The following paragraphs explain the computer program in detail.

2.2.3 Automatic Algorithm

The ULF detection computer program has been designed to analyze multi-year data from multiple SuperDARN radars. The code outputs 'flagged ULF candidates' that could then be further examined and established as a FLR with

additional characterization criteria. The code runs a loop for the year 2003 for the 15 stations. To provide continuity of the analysis, the data from consecutive days were concatenated. The "*fitacf*" files were read using the old Barnes' procedures and to increase the efficiency of the algorithm only selected data was loaded in a hyper-matrix: In order to ensure uniformity of the spectral analysis band, selected data corresponded to "normal mode" operations (scan=0, 1) and beam integration time corresponding to sampling rate of 60 seconds with Nyquist frequency 8.33 mHz (prm.intt=3). Data corresponding to "special" mode operations and/or to sampling rate other than 60 seconds (e.g. 120 seconds) were not considered in this study. Table 2.5 enumerates the list of requirements to ensure the data quality and uniformity.

Table 2.5: List of requirements to ensure the data quality and uniformity

Condition #	Criteria
Condition 1	Normal mode (scan=0,1)
Condition 2	Integration time (prm.intt=3), sampling rate ~ 1 min
Condition 3	Ground scatter removed (Blanchard and Baker criteria)
Condition 4	Spikes removed (v > 700m/s)
Condition 5	46 good data points on 60 data point window for 1 hr.

SuperDARN radars detect backscatter echoes from ground-scatter, *E* and *F* regions. The SuperDARN "*fitacf*" contain a quality flag (fit.qflg=0 is bad, fit.qflg=1 is good), and a ground-scatter flag (fit.gflg≥1 for ground-scatter, fit.gflg=0 for ionospheric scatter). However, these flags might discard some useful data (K. Sterne, AJ Ribeiro, E. Miller, private communication). A more comprehensive approached to remove ground-scatter was presented by *Ponomarenko et al.* [2007]: Figure 2.5 shows the relationship between velocity and spectral width, given by the autocorrelation functions, for each of the echoes of each region. *Ponomarenko et al.* [2007] explains that ground-scatter follows the Blanchard and Baker criteria (private communication with Ponomarenko)

given by equations 2.1 and 2.2, where $G \leq 0$ corresponds to ground scatter echoes, V_D is the ling-of-sight Doppler velocities and W is the spectral width. *Ponomarenko et al.* [2007] explain that echoes with $|V_D| \geq 200$ m/s represent the F-region scatter, the low-velocity enhancement across W = 100-200 m/s describes E-region scatter and the section corresponding to $W \leq 100$ m/s and $V_D \leq 200$ m/s consist of sea and mixed scatter echoes applying different thresholds to remove ground scatter for that particular study.

$$G = |V_D| - V_D^{\max}\left(1 - \frac{|W|}{W^{\max}}\right) \tag{2.1}$$

Blanchard and Baker criteria:

$$V_d^{\max} = 30\,m/\sec \qquad W^{\max} = 90\,m/\sec \tag{2.2}$$

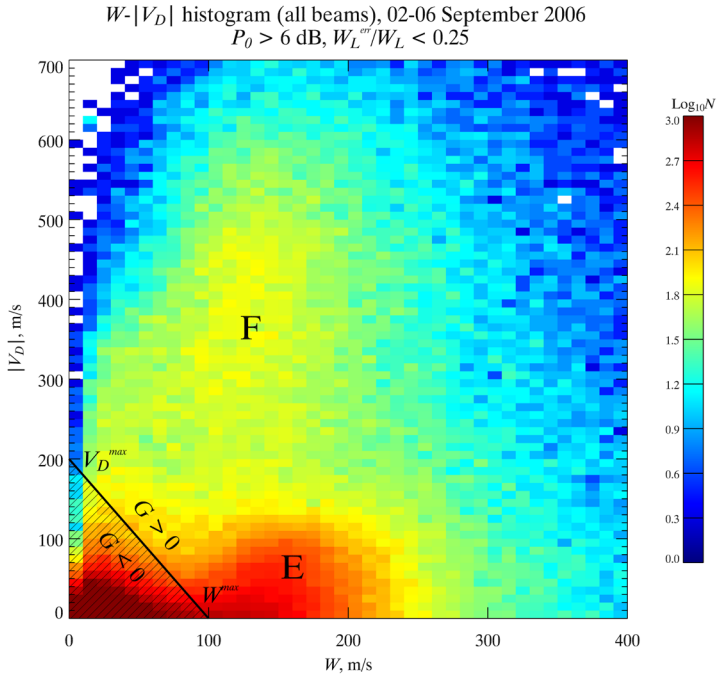

Figure 2.5: Plot of Doppler velocity vs width. The ground-scatter and scatter from the *E* and *F* regions is shown (From: *Ponomarenko et al.* [2007]).

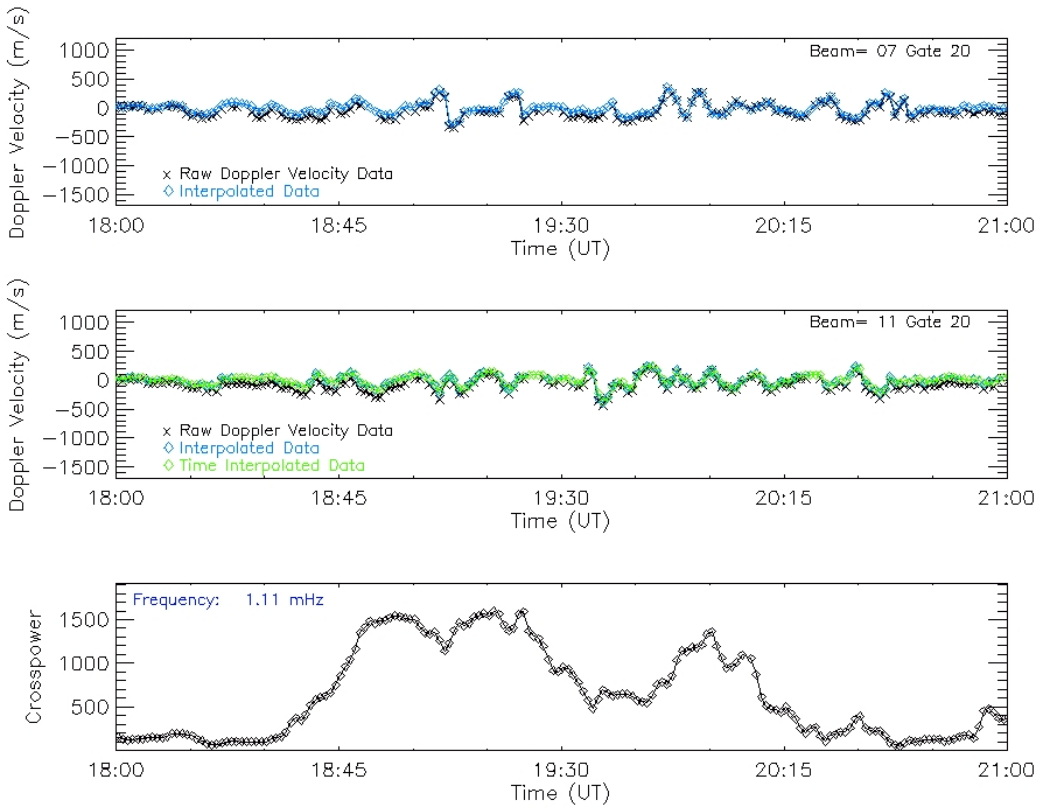

Figure 2.6: Doppler velocity raw data (top 2 panels) corresponding to Beams 7 (top) and 11 (middle) both at gate 20 and cross-power (bottom) between beams 7 and 11 for gate 20 for the Kodiak station on December 20th, 2003. The code automatically flagged the event as a 'candidate' given established criteria.

In this study, data identified as ground-scatter was removed, following the Blanchard and Baker criteria removing backscatter where $G \leq 0$ (equation 2.1) with values $|V_D| = 30$ m/s and W =90 m/s (equation 2.2). Data points with speeds greater than 700 m/s were classified as spikes and removed from data-set. The Doppler velocity data were linearly interpolated to eliminate original gaps of few data-points existing in the data (due to poor backscatter) or gaps created by the removal of ground scatter and single data-point spikes, with the conditions that at least 46 valid data points were available on the original data any given 1-hour period (e.g. 14 or less data points had to be linearly interpolated to eliminate

gaps) and that there were less than 5 consecutive missing datapoints in any gap. The time series was de-trended by subtracting a 30-min sliding average, to remove low frequency trends corresponding to frequencies below 0.5 mHz, since the range of frequency of interest in this study was 0.5-5 mHz. Figure 2.6 shows the raw data and the data after being processed: data in black corresponds to the raw data, while data in blue corresponds to the data in which the ground-scatter and spikes were removed, and data were interpolated and de-trended.

We applied cross-spectral analysis to the data separated by four beam widths: data for beam pairs that were separated by 4 (e.g. beam 4 gate 10 and beam 8 gate 10, etc.) were selected and the time series of the second beam (beam=n+4) was interpolated to the times of the first beam (beam=n). The Fast Fourier Transform of the two time series was calculated. The analysis was performed using a one hour sliding window for 1-hour periods of times with at least 46 valid data points on the original data. The frequency array, the frequency step, and Nyquist frequency determined by the FFT for 60 data-points in one hour are given by a frequency array of $0.55\hat{6} \pm n$ x $0.27\hat{7}$ mHz (where n=0, 1, 2, …, 15), with a frequency step of $\Delta f = \frac{1}{N\Delta t} = 0.27\hat{7}$ (N=60 data-points, Δt=60 seconds) and a Nyquist frequency of $\frac{1}{2\Delta t} = 8.33\hat{3}$ mHz.

The one hour dynamic power and dynamic phase were then calculated for the beam pair for the time interval on the sliding window, as follows:

$$\mathrm{Im} = FFT_{real}(Beam_n) \times FFT_{\mathrm{Im}}(Beam_{n+4}) - FFT_{\mathrm{Im}}(Beam_n) \times FFT_{real}(Beam_{n+4}) \quad (2.3)$$

$$\mathrm{Re} = FFT_{real}(Beam_n) \times FFT_{real}(Beam_{n+4}) + FFT_{\mathrm{Im}}(Beam_n) \times FFT_{\mathrm{Im}}(Beam_{n+4}) \quad (2.4)$$

$$CrossPower = \sqrt{(\mathrm{Im})^2 + (\mathrm{Re})^2} \tag{2.5}$$

$$CrossPhase = TAN^{-1}\left(\frac{\mathrm{Im}}{\mathrm{Re}}\right) \tag{2.6}$$

The cross-phase was *unwrapped*: When computer programs calculate the phase using the arctangent (ATAN) routine, values might exceed the common phase range of $-\pi$ to $+\pi$, and the plot of phase vs. time or frequency would show a *phase wrapping*, a sharp change from $+\pi$ to $-\pi$; to correct that, any change exceeding 2π has been corrected (*Ramirez*, 1985), following standard signal processing techniques. The dynamic variance in the '*unwrapped cross-phase*' was obtained by the calculation of the variance across one hour sliding window centered at the data point.

Te code calculated the mean daily dynamic cross-power, cross-phase and variance in cross-phase for each frequency component and for each beam-pair. To detect a coherent ULF waves over a large area in the FoV of the radar, the code "flagged" the dynamic cross-power that corresponded to values above the daily mean+2σ and cross-phase variance that corresponded to values below mean-2σ, since these 'unusual' events respond to a threshold unlikely to be produced by random processes (such as random noise in the radar). Table 2.6 gives a full description of the selection criteria implemented for automatic detection of ULF waves using SuperDARN.

Figure 2.7 shows plots of the daily dynamic cross-power and daily dynamic variance in the cross-phase between beams 7 and 11, both at gate 20, for the Kodiak station on December 20, 2003, for the frequency spectrum between 0.5-5 mHz. Notice the area inside the red circle that shows the high cross-power and low variance in cross-phase with respect of the daily values.

Table 2.6: List of conditions included in the code criteria for automatic detection of ULF waves

Condition #	Criteria
Condition 6	Dynamic Cross-power > Daily Mean + 2σ
Condition 7	Dynamic Variance in Cross-phase > Daily Mean - 2σ
Condition 8	3 adjacent beam-gate pairs and their respective conjugates that meet conditions 6 and 7

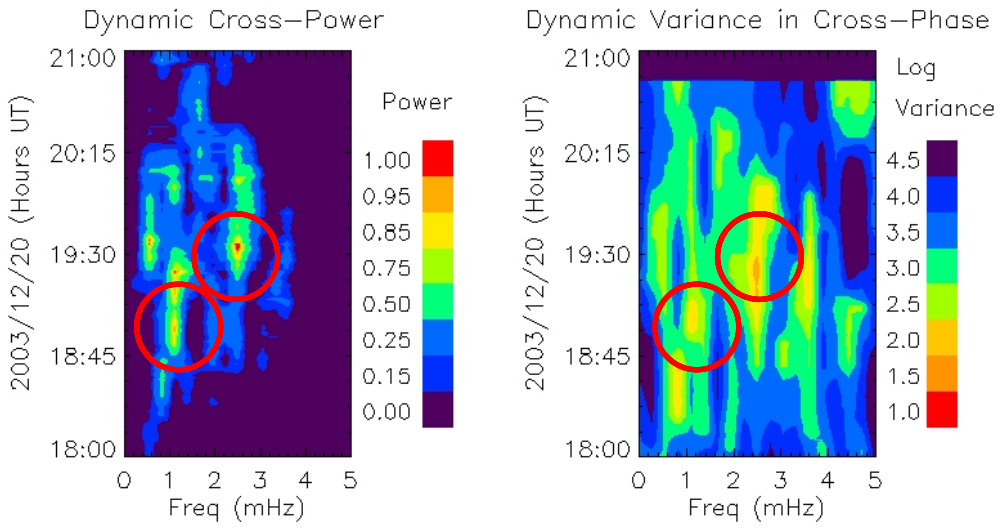

Figure 2.7: Plots of crosspower and crossphase for beams 7 and 11 for gate 20 corresponding to the Kodiak station on December 20, 2003 at 17:00-21:00 UT. We see that candidates for the 1.1 mHz and 2.5 have been found at 18:45-19:45 UT and 19-20 UT respectively.

2.2.4 Trials

The successful rate of the code was defined as the ratio of the FLR classified over the 'flagged occurences'. Early versions of parts of the code were tested, in the development phase, for two known FLR events: These two trials were run for the Prince George station data for November 20, 2003 and the Kodiak station

data for November 21, 2003, since these two events were extensively studied by *Fenrich and Waters* [2008].

An early version of the code "*flagged*" occurrences in frequencies for which the dynamic cross-power was greater than the daily mean cross-power plus 2 standard deviations and dynamic variance in cross-phase was less than the daily mean variance in cross-phase minus 2 standard deviations (as shown in figures 2.6 and 2.7) for a beam-pair for one gate only, as seen in figure 2.8 (a). This early version was run for stations Kodiak and Prince George for the year 2003 in unknown data (e.g. not known events in that period). Even though the early version of the code produced some clear FLR events, the successful rate (# of FLRs/# of flags) was mediocre (<50%).

The code was then refined by extending the criteria such that the conditions of cross-power and variance in cross-phase were met by beams pairs (beam separated by 4) simultaneously at 3 adjacent gates, as seen in figure 2.8 (b). This later version of the code was applied to all available data for the 14 stations and had better success rate (66.50% of the flags were FLRs). However, some FLR events identified with the first version of the code did not pass the new criteria: with more requirements, a new bias was introduced in the selection of 'successful flags'. This limitation of the code is explained in detail in section 3.3. The list of results in the next chapter includes a list of FLRs found in the process of developing the criteria for the code, which did not make the final list produced by the latest version of the code. Therefore, it is important to emphasize that this methodology is successful to systematically 'blind detect' FLRs, without using visual techniques of inspection of backscatter patterns, since a high ratio of flags produce FLRs but it does not detect "all" FLR events in a particular year.

It is worth mentioning that the outcome text file with flags would return numerous entries for the same event corresponding to multiple flags for different beam/gate pairs. Since FLRs have been reported in the past 20 years to last for

about one hour, a 'unique flag' was defined as a flag for a station, date, and frequency that has at least an hour difference with another 'unique flag'. Flags with the same station, date and frequency within a 60 minute interval were considered to be part of the same ULF event, since FLRs have been reported in the past 20 years to last for about one hour.

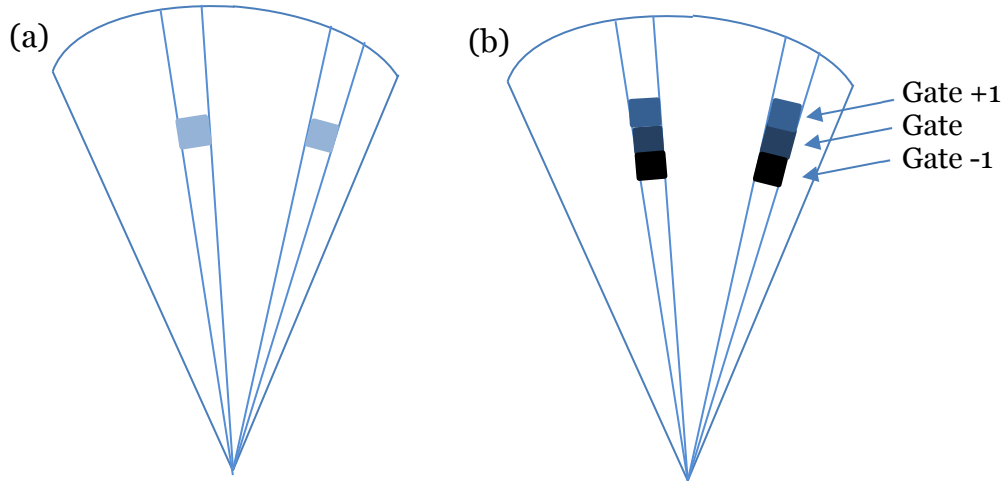

Figure 2.8: Schematics of the FoV of a SuperDARN radar and the condition used for early versions of the code (a) and the latest version of the code (b): Selection criteria was applied for a beam-pair for one gate only in early versions (a), while criteria had to be met simultaneously by beams pairs (beam separated by 4) at 3 adjacent gates in the latest version of the code (b).

Figure 2.9 shows plots of the daily dynamic cross-power and daily dynamic variance in the cross-phase between beams 7 and 11, both at gate 20, corresponding a ULF wave 1.1±0.1 mHz detected by the code by the Kodiak Station on December 20, 2003. Between 18:45 UT and 19:30 UT, high dynamic cross-power was observed above the daily mean=371 (red line) and the mean+2σ = 1292 (blue line). At that same interval of time, the dynamic variance in cross-phase is less than the daily mean variance in cross-phase=3.2 (red line) and the daily mean variance in cross-phase minus 2 standard deviations (2.2). The code automatically flagged the event (green lines) as a 'candidate' because the

selection conditions were met in both beams for gates 19 to 21. Notice that at around that time, several data points also meet the threshold criteria for gate 20, but they were not flagged as candidates because they fail to meet the adjacency condition (gates 19 and 21).

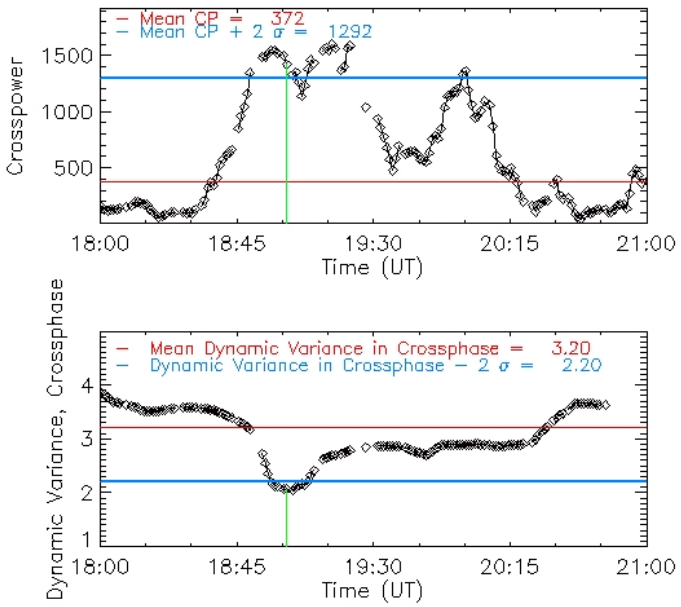

Figure 2.9: Plots of the dynamic cross-power (top) and dynamic variance in the cross-phase (bottom) for beams 7 and 11, at gate 20, from Kodiak on December 20, 2003 for 1.1±0.1 mHz frequency component. Between 18:45UT and 19:30, high cross-power (top) and low cross-phase variance were observed. The code automatically flagged the event (green lines) as a 'candidate' given that the same threshold criteria were met for beams 7 and 11 for gates 19 to 21.

A total of 161 flags were recorded using the methodology described in this chapter. Information on the 'flagged candidates' (station, date, time, frequency, beam, gate, magnetic latitude, magnetic longitude) was recorded automatically by the code (old and new version) in the output files. These 'flagged ULF waves' were individually analyzed to see if they met the "FLR criteria". The procedure to analyze the FLR profile is the topic of the next chapter. The list of 'flagged ULF

wave', FLR candidates, are included in the next chapter, where successful events were analyzed and characterized.

2.3. Summary

In this chapter, the methodology for systematic detection of ULF wave with the SuperDARN radar network was explained in detail. The major achievement in the development of this methodology is the systematic detection of ULF waves without using the visual identification techniques utilized by *Fenrich et al.* [1995], *Fenrich* [PhD Thesis, 1997], *Ponomarenko et al.* [2003] and *Fenrich et al.* [2006].

In the past decade, significant advances in the deployment and operations of the SuperDARN radars have occurred. The number of SuperDARN Radars increased from 6 operational radars in 1995 to 15 stations in 2003. Availability of a larger number of stations for this project provided a more comprehensive study, both in the northern and southern hemisphere. Moreover, computational capabilities have largely improved in the recent years, allowing advancing in data analysis, such as the development of this new technique: The processing of larger amounts of data made a systematic study possible and eliminated the need of visual techniques for identification of ULF waves that were good candidates to be tested for the FLR criteria.

It is worth mentioning that the methodology explained in this chapter is not the only effort to systematically detect ULF waves: *Bland et al.* [2014] has recently published an effort for systematic detection of ULF waves using an alternative data processing technique with SuperDARN. However, that study does not target the detection of FLRs, a very small and specific subset of ULF waves in the magnetosphere, and it does not include any other further selection of data that might be useful in the detection of FLRs. *Mangus* [2009], in his PhD

thesis, developed an automatic algorithm to systematically detect ULF waves using SuperDARN. The algorithm found significant peaks in the power spectrum of a single beam-gate, instead of calculating the cross-power and variance in cross-phase for beam pairs significantely separated in the FoV of the radar, with a threshold of 3 standard deviations, instead of 2. The pulsation finder tagged beams with significant peaks in power spectrum for 3 contiguous range gates; events with significant peaks in non contiguous range gates were ignored. The study claimed that single records did not allow for the determination of special characteristics of the driver to identify a pulsation as field line resonance. This study reported over 10,000 pulsation events detected for the year of 2014 using 15 SuperDARN stations but confirmed the typical profile of FLRs for only one of the events but does not extend the characterization to any of the other pulsations. It is also unclear in that study if each of the pulsation found correspond to unique events in a 1-hour period of time, or if multiple flags for a radar station for a 1-hour period of time are counted as individual pulsations. Furthermore, the study did not exclude ground or sea scatter.

Overall, the methodology developed in this study yielded very good results: 161 ULF waves were automatically detected, with a success rate of 66.50% for ULF waves resulting in FLRs: the analysis of results of ULF waves automatically detected and the criteria for FLR identification and characterization of each event is the main topic of the next chapter.

Chapter 3

Observation of Field Line Resonances

Field Line Resonances are Ultra Low Frequency waves in the magnetosphere that meet additional criteria. As explained in section 1.3.3, FLRs exhibit a maximum in power at the latitudinal location of resonance and a 180 degrees decrease (low azimuthal wave number, *m*) or increase (high azimuthal wave number) in the latitudinal phase shift throughout the resonance maximum (see Figure 1.8). In the previous chapter, a technique for systematic detection of ULF waves using SuperDARN was presented. In this chapter, the techniques explained in *Walker et al.* [1992] and *Fenrich et al.* [1995] for identification of FLR profiles, using the SuperDARN Doppler velocity data, have been applied to the 161 ULF waves pre-selected to be further analyzed if they met the FLR criteria and to obtain their spectral characteristics and spatial variations.

Each ULF wave 'flagged candidate' was carefully evaluated, using the cross-spectral and analytic signal to determine if they corresponded to a FLR occurrence. For the cross-spectral technique, plots of the Doppler velocity as a function of range gates and time, in a time interval of two hours prior and after the flag (as shown in Figure 2.4), were produced for all beams of the radar and ULF wave patterns were visually inspected. The Doppler velocity time series and the power spectrum, around the time of the event, were examined for each flagged candidate. Figure 3.1 shows the power spectrum for the Kodiak station on December 20th, 2003, Beam 7 at gate 20, for the hourly window corresponding to

18:28-19:28 UT. A maximum in power is found at the 1.1±0.1 mHz frequency at that time interval.

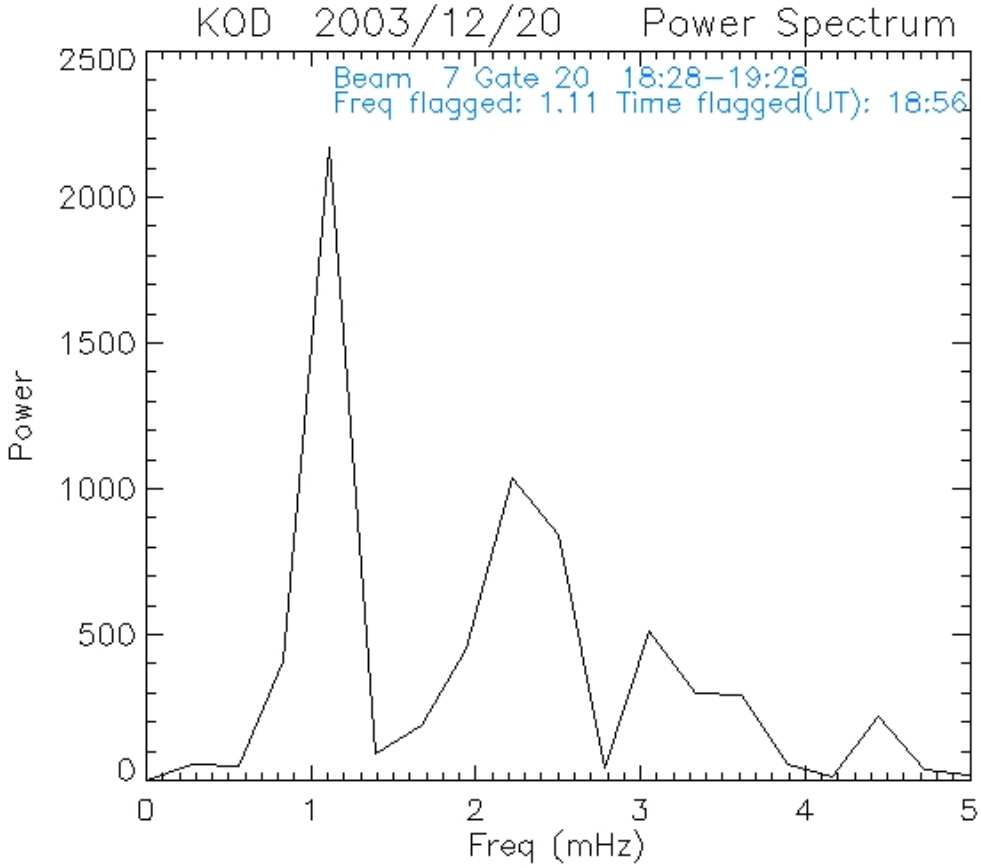

Figure 3.1: Plot of power spectrum corresponding to Beam 7 at gate 20 for the Kodiak station on December 20th, 2003, for the hourly window 18:28-19:28UT. A maximum of high power is found at the 1.1±0.1 mHz frequency.

The sections below describe in detail the processes of identification of FLRs from the ULF wave database.

3.1 Profile of FLRs [1]

3.1.1 Basic profile criteria for FLRs

For each flagged ULF wave, the Doppler velocity signal was bandpass filtered in the time domain, with a bandwidth of Δf (0.3 mHz) centered at the frequency of interest, to isolate the flagged frequency component. Figure 3.2 shows a plot of the Doppler velocity (black) linearly interpolated, de-trended, de-spiked, for beam 7 gate 11 corresponding to Kodiak on December 20, 2003 between 16 UT and 22 UT. A bandpass filter (red) of 1.0 mHz < f < 1.3 mHz was applied to the signal to isolate the 1.1±0.1 mHz frequency component, which was the frequency flagged by the ULF identification code. A coherent wave around the time of the flags (18:56-19:01UT) is observed. A plot of the same filtered oscillation and its envelope, calculated as the amplitude of the analytic signal is shown in Figure 3.3.

The analytic signal was calculated because "they are useful in the interpretation of signals which are quasi-monochromatic [...] providing an objective estimate of the instantaneous amplitude and phase of them" *Walker et al.* [1992]. For a real time series $f_{(t)}$, the associated analytic signal is defined as $F_{(t)} = f_{(t)} - iHi_{(t)}$, where $Hi_{(t)}$ is the Hilbert transform of $f_{(t)}$ [*Walker et al.*, 1992; *Bracewell*, 1986]. The Hilbert transform, commonly used in mathematics and in signal processing, is a linear operator which takes a function $f_{(t)}$ and produces a function $Hi_{(t)}$ with the same domain; it extends the real signal $f_{(t)}$ into the complex plane such that "*the Fourier transform of* $Hi_{(t)}$ *is the Fourier transform of* $f_{(t)}$ *with positive frequency components multiplied by* i *and negative frequency components multiplied by* $-i$ *(...)"* [*Walker et al.*, 1992].

[1] All codes in this section are largely modified versions of the original codes developed by F. Fenrich (IDL based)

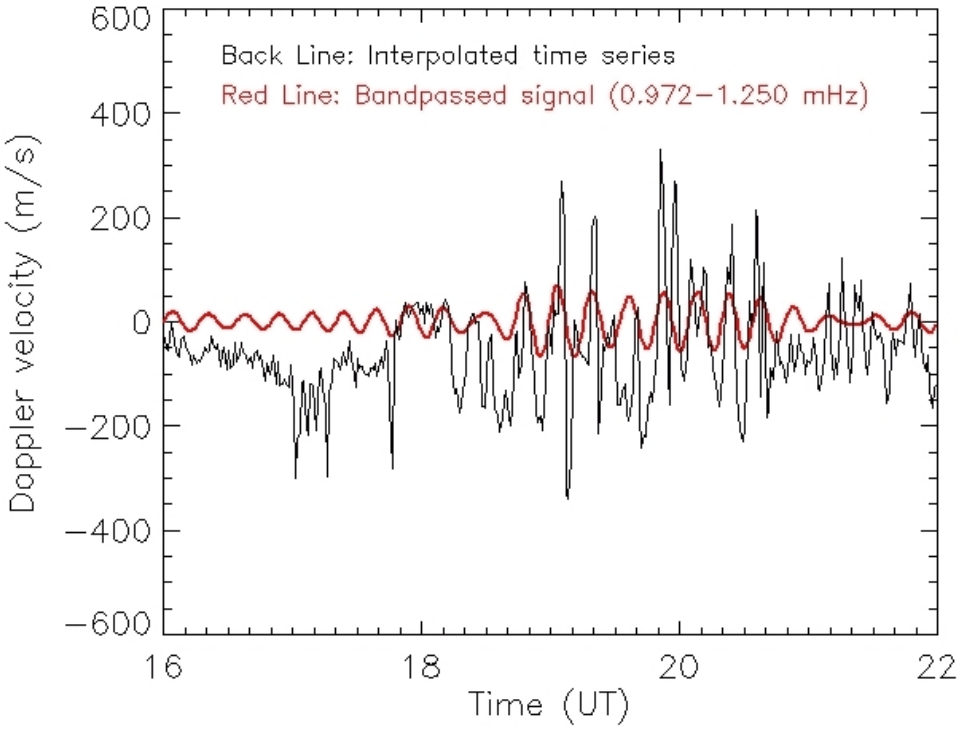

Figure 3.2: Interpolated Doppler velocity (black) and the band-passed (1.0 mHz < f < 1.3 mHz) signal (in red), for beam 7 gate 20 corresponding to the at 1.1 ±0.1 mHz ULF wave detected by Kodiak on December 20, 2003.

The instantaneous amplitude and instantaneous phase given by the analytic signal were examined as a function of magnetic latitude and longitude for the field of view of the radar. Figure 3.4 shows the FoV of the analytic signal bandpass filtered for frequency 1.1 ±0.1 mHz corresponding to Kodiak on December 20, 2003 at 18:49UT, around the time that the event started. Each beam/gate pair of a SuperDARN radar station has a tabulated AACGM magnetic latitude and longitude. To develop visualization of the analytic signal on the FoV of the radar, each beam-gate pair for the FoV was mapped to magnetic latitude and magnetic longitude and the analytic signal interpolated; a contour function was used to produce the plot. For magnetic latitudes between 64 and 70 degrees azimuth, the high amplitude (left panel) and wave front in phase (right panel) are observed. Plots corresponding to cross-sections for a fix magnetic longitude of

the analytic signal amplitude and phase as a function of latitude were carefully evaluated, as detailed in Fenrich *et al.* [2006]. An example of those cross-section plots are exemplified in Figure 3.5, which corresponds to the event shown in figures 3.1-3.4.

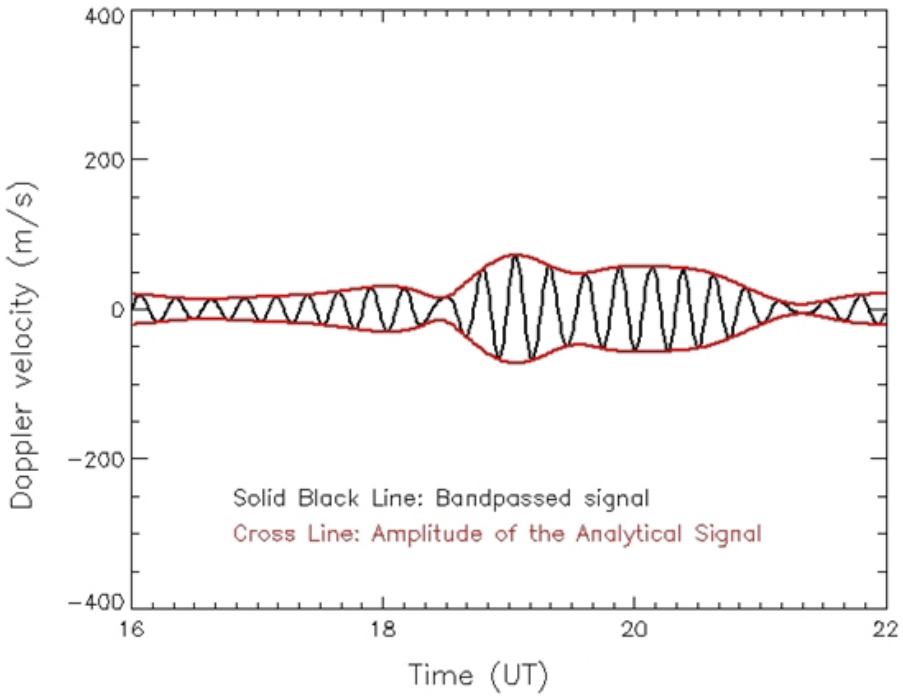

Figure 3.3: Plot of the band passed signal (1.0 mHz < f < 1.3 mHz) and analytic signal, for beam 7 gate 20 corresponding to Kodiak on December 20, 2003. Filtered oscillation is shown in black and the envelope corresponding to the instantaneous analytic signal is shown in red.

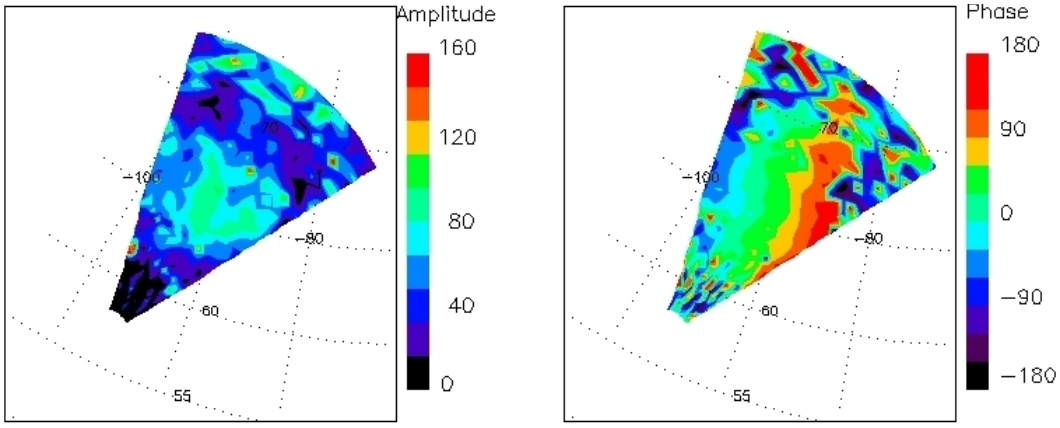

Figure 3.4: Plot of the analytic signal amplitude (left) and phase (right) as a function of magnetic latitude and magnetic longitude for the field of view (range gates 0-35) of Kodiak on December 20th, 2003 corresponding to 18:49 UT for the bandpass analytic signal for 1.1 ±0.1 mHz. For magnetic latitudes between 64 and 70 degrees azimuth, the high amplitude (left panel) and wave front in phase (right panel) are observed. The event lasted for one hour.

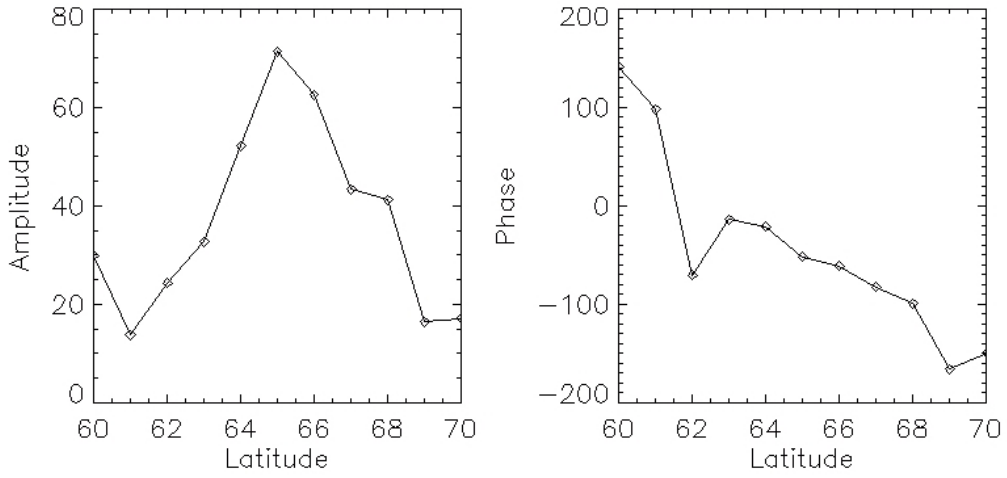

Figure 3.5: Latitude profile of the spectral power (left) and phase (right) at 1.1 ±0.1 mHz corresponding to the Kodiak station on December 20, 2003
(Along -89 degrees magnetic longitude) at 19:49 UT. The maximum peak is observed at magnetic latitude 65 degrees.

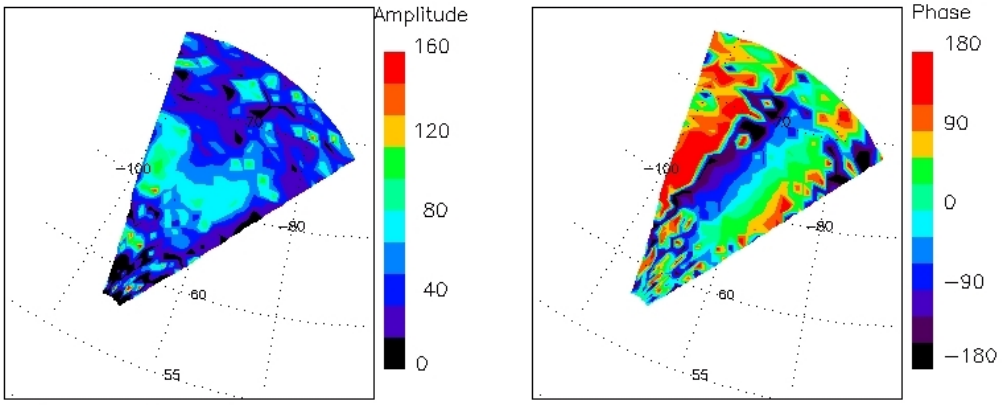

Figure 3.6: Plot of the analytic signal amplitude (left) and phase (right) as a function of magnetic latitude and magnetic longitude for the field of view (range gates 0-35) of Kodiak on December 20th, 2003 corresponding to 19:49 UT for the bandpass analytic signal for 1.1 ±0.1 mHz. For magnetic latitudes between 64 and 70 degrees azimuth, the high amplitude (left panel) and wave front in phase (right panel) are observed. The event lasted for one hour.

In order for a pre-selected ULF wave to be characterized as "Field Line Resonance", it has to meet the basic ***"FLR Profile Criteria"***, explained in *Fenrich et al.* [1995]:

i) There should be a maximum in the wave analytic signal amplitude as a function of latitude (Figure 3.5, left panel)

ii) There should be an analytic signal phase increase or decrease across the maximum latitude location corresponding to a minimum of 90 degrees, and an optimal of 180 degrees or more (Figure 3.5, right panel)

The flagged ULF wave was successfully characterized as an FLR occurrence because a clear FLR profile was obtained from the analytic signal cross-sections, as shown in Figure 3.5. From the phase decrease across the maximum latitude location it can be seen that lower latitudes (corresponding to shorter field lines) "lead" in phase while higher latitude (corresponding to longer field lines) "lag" in

phase; we can then infer that the FLR is propagating polewards in the ionosphere and therefore radially outwards in the magnetosphere to increasing L-shells. Figure 3.6 shows the same FoV of the event at 19:49UT, from which the FLR profile was obtained. The event lasted for one hour.

Each pre-selected ULF wave was cautiously evaluated if it met the "FLR Profile Criteria" by obtaining cross-sections of the analytic signal that showed an FLR profile at the time of the event. Plots of the analytic signal as a function of AACGM magnetic latitude and longitude, band-passed at the frequency component flagged by the ULF identification code, for the FoV of the radars were generated for a two hour span, centered at the time of the flagged ULF wave. Information produced by the flags was use to explore the magnetic location and its vicinity for the FLR profile. Cross-sectional plots of the analytic signal amplitude and phase as a function of latitude were generated for the flagged ULFs and the exact magnetic latitude/longitude location of the FLR occurrence was successfully obtained for a large majority of them.

Figure 3.7 shows a compilation of plots corresponding to the FoV of Kodiak on December 20th 2003 from 19:30UT to 19:45 UT: The westward propagation and poleward phase variation of the FLR is noticeable in the phase plots (left panels). Please notice that the right color bars and magnetic latitude and longitude grids are identical to those on figure 3.4.

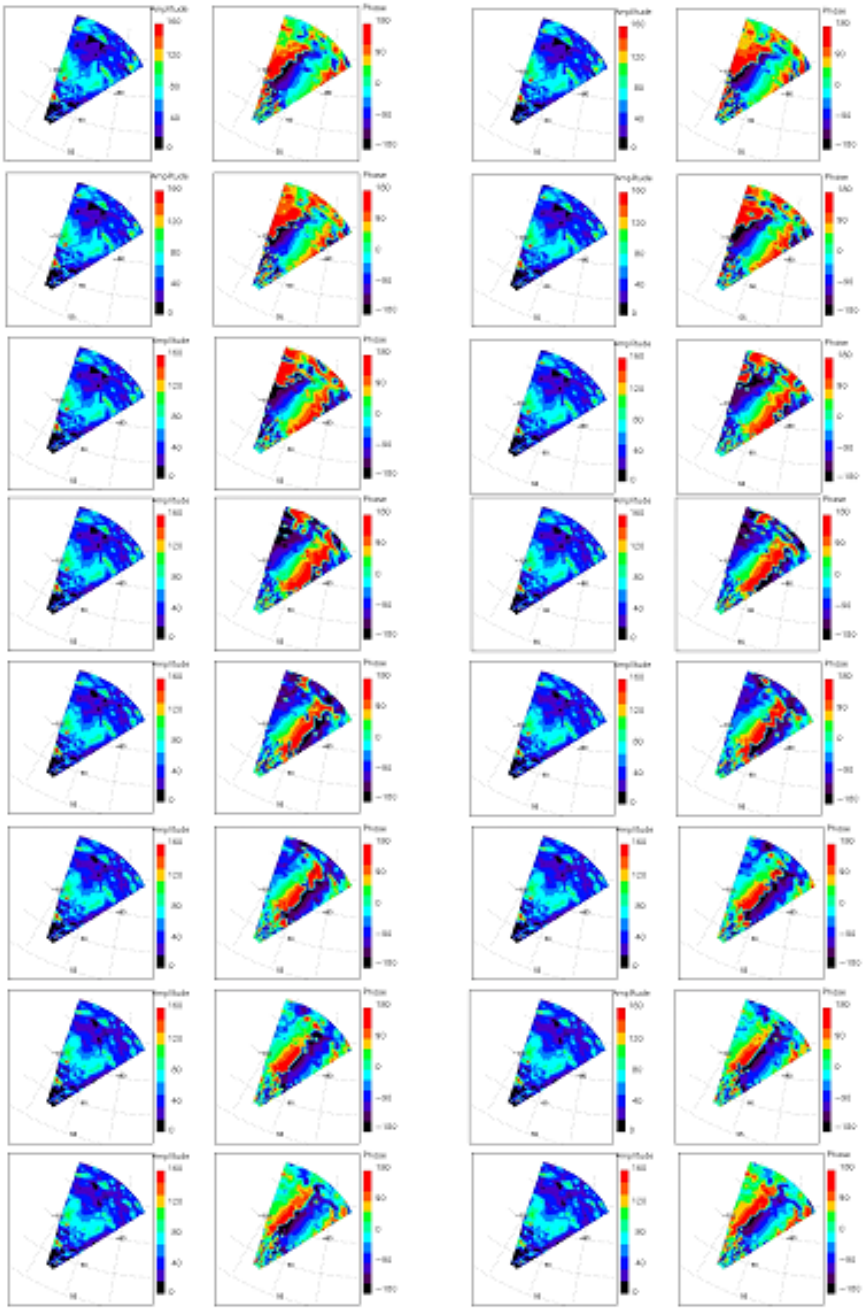

Figure 3.7: Series of plot of the analytic signal amplitude (left) and phase (right) for 19:30 UT to 19:45 UT similar to figures 3.4 and 3.6 (sidebards and magnetic grid identical to those plots) for the bandpass signal for 1.1 ±0.1 mHz. The westward propagation and poleward phase variation of the FLR is noticeable in the phase plots (left panels).

FLRs with a phase decrease across the maximum latitude location were characterized to have a 'standard phase' variation and for those with a phase increase across the maximum latitude location to have a 'reverse phase' variation, as tabulated in *Fenrich and Samson* [1995]. For the latest, lower latitudes (corresponding to shorter field lines) "lag" in phase while higher latitude (corresponding to longer field lines) "lead" in phase, and corresponds to FLR propagating equatorwards in the ionosphere and therefore radially inwards in the magnetosphere to lower L-shells.

For the identified FLRs, propagation of the wave polewards or equatorwards, given the phase increase or decrease as a function of latitude was recorded and the Magnetic Local Time (MLT) of the events was calculated using the SuperDARN AACGM codes, from the information (date, time, magnetic longitude) of the occurrence wave.

In future work, now that the ULF wave pre-selection technique was successfully implemented, the process for obtaining the FLR profile from a ULF wave flagged could be automatized as well.

3.1.2 Properties of FLRs: Azimuthal wavenumber *m*

Field Line Resonances (FLRs) are standing wave oscillations on the plasma tubes in the Earth's magnetosphere, each with its own eigenfrequency; the waves' electric field is given by $E_{(t)} = |E|e^{i(-\omega_x t + m\varphi)}$, where ω_x is the resonant eigenfrequency and x is the radial coordinate [*Yeoman et al.,* 2010].

FLRs are sometimes characterized by an azimuthal wavenumber *m* (which it is determined by the exciting source) since it gives important information related to the scale lengths of the FLRs in the azimuthal direction: The azimuthal wavenumber provides the number of complete wave cycles that would fit around the Earth in the azimuthal direction by quantifying the phase change of the wave per degree of magnetic longitude. [*Yeoman et al.* 2000]. ULFs and FLRs with

large azimuthal scale lengths are called "*Toroidal modes*' while "*Poloidial modes*" are waves with short azimuthal scale lengths. A mixture of the two is often found in the magnetosphere, as will be shown in the next chapter.

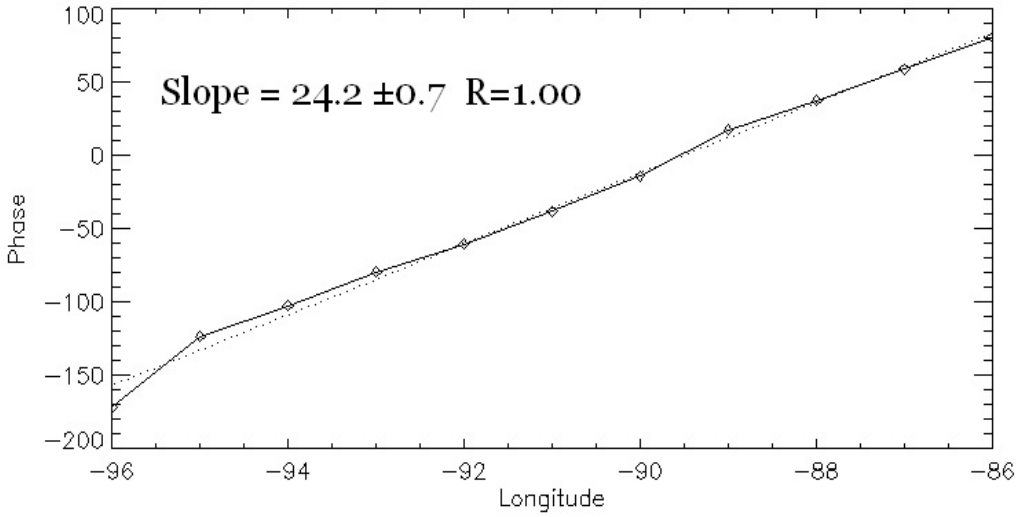

Figure 3.8: Spectral Phase as a function of longitude gives the m-value of the wave at 1.1 ±0.1 mHz corresponding to the Kodiak station on December 20, 2003 (along 66 degrees magnetic latitude) at 19:49UT. The slope of this plot gives the azimuthal wavenumber *m* of the FLRs, and for this event it was determined to be m=24.2±0.7.

From the measurements of FLRs using SuperDARN, the slope of the instantaneous phase of the resonance versus the AACMG magnetic longitude gives a reliable measurement of the azimuthal wavenumber, *m* [*Fenrich et al.* 1995]. For this study, a **reliable azimuthal m-number measurement** was **determined from the slope of a plot of phase vs longitude,** with **r>0.80 for all cases**. It is important to mention that small slope values, and therefore small *m* values, generally have a larger percentage error associated with them due to the rounding to one significant figure for the uncertainty in the slope that results in an uncertainty comparible to the linear fit used to obtain the value of the slope. Figure 3.8 shows that the azimuthal wavenumber for the event exemplified throughout this thesis was m=24.2±0.7.

In the past 20 years, there have been several efforts to characterize FLRs by the azimuthal wavenumber *m* [*Yeoman et al*, 1990; *Grant et al*, 1992; *Fenrich et al.*, 1995; *Fenrich and Samson*, 1997; *Wright et al.*, 1997; *Mann*, 1998; *Wright and Yeoman.,* 1999; *Yeoman et al*, 2000; *Yeoman et al*, 2010; *Yeoman et al*, 2012]. The extensive characterization of FLRs in the database and their properties, including their *m* wavenumbers, is the topic of the next chapter.

3.1.3 Results

In this study, from the 161 automatically detected ULF waves that were recorded, we found that 66.50% of those flags were successfully confirmed to be FLRs. It is important to remark that the rest of the flags could correspond to either FLRs for which a profile could not be successfully retrieved or ULF propagating waves that are not FLRs. The next section is devoted to explain the challenges presented in obtaining the FLR profiles for some FLRs.

Table 3.1 shows a list of the 107 ULF waves, pre-selected by the ULF identification code, for which the FLR profile was successfully obtained. The phase variation (standard/reverse) as a function of latitude, the azimuthal wavenumber *m*, the MLT and the propagation (towards the east or west, and towards the sun or away from the sun) of each FLR are also included in that table. Table 3.2 contains a list of the ULF waves for which the FLR profile was not obtained. That table outlines the visually identified FLRs for which profiles could not be obtained and flags that do not correspond to FLRs but rather to ULF wave activity. Flags in both tables are first arranged in chronological order (date, time) and then sorted in ascending frequency.

Table 3.1: Flags produced by the ULF identification code for which a FLR profile was obtained for the year 2003

EVENT #	Station	Month	Day	Fq (mHz)	Flag Hr	Flag Min	Beam	Gate	Event Time (UT)	AACGM Longitude	AACGM Latitude	Phase variation vs latitude	*m*[a]	δm	% Err	R	MLT	e/ w[b]	sun/ anti[c]
1	7	1	3	0.83	8	14	8	30	7:48-8:48	-83	70	standard	14	2	13	0.93	22	1	0
2a	7	1	3	0.56	12	23	6	20	11:53-12:53	-86	67	standard	10	1	10	0.96	2	0	0
2b	7	1	3	0.83	12	35	3	21	12:4-13:4	-94	70	standard	1	0.6	46	0.58	1	0	0
3	7	1	3	4.17	16	41	2	19	16:40-17:40	-97	67	reverse	37	5	14	0.92	5	0	0
04a	7	1	3	2.50	19	2	0	16	18:26-19:26	-89	66	standard	54	2	4	0.99	8	1	1
4b	7	1	3	3.61	19	47	8	18	19:3-20:3	-89	68	standard	11	1	6	0.98	8	1	1
4c	7	1	3	3.89	19	49	8	18	19:41-20:41	-90	66	standard	12	1	20	0.96	8	1	1
4d	7	1	3	4.44	19	49	8	18	19:27-20:27	-90	66	standard	12	1	12	0.94	8	1	1
5a	10	1	7	0.56	20	54	0	21	20:29-21:29	100	68	reverse	18	2	13	0.93	22	1	0
5b	10	1	7	0.83	20	38	5	19	20:7-21:7	101	68	reverse	21	2	11	0.95	22	1	0
5c	10	1	7	3.06	20	54	2	23	20:20-21:20	100	68	reverse	17	2	9	0.97	22	1	0
5d	10	1	7	3.61	20	59	3	20	20:41-21:41	102	66	standard	51	6	12	0.94	22	1	0
6	9	1	7	1.94	21	24	5	7	22:7-23:7	76	68.5	reverse	18	2	11	0.95	21	1	0
7	8	1	7	1.11	23	7	8	7	22:52-23:52	62	70	reverse	13	1	4	0.99	22	1	0
8	10	1	16	1.67	20	59	9	28	20:32-21:32	116	71.5	reverse	8	1	14	0.92	23	1	0
9a	10	1	16	0.83	23	24	11	26	22:45-23:45	116	69	reverse	16	2	11	0.95	1	1	1
9b	10	1	16	1.39	23	20	8	20	23:12-24:12	112	67.5	reverse	36	5	14	0.92	1	0	0
9c	10	1	16	2.78	23	18	10	23	22:39-23:39	112	68	reverse	25	3	14	0.93	1	1	1
10	8	1	19	2.78	17	48	4	13	17:29-18:29	59	70	standard	26	3	12	0.94	16	1	0
11	14	1	21	1.11	11	41	3	26	11:13-12:13	-130	69	reverse	25	3	12	0.94	22	1	0
12	13	1	26	1.11	2	46	9	3	2:32-3:32	76	-68	standard	39	3	7	0.98	2	0	0

[a]Azimuthal wave number. The errors correspond to the linear square fit

[b]Propagation: 0-eastwards; 1-westwards

[c]Propagation: 0-sunwards; 1-antisunwards

Table 3.1: Flags produced by the ULF identification code for which a FLR profile was obtained for the year 2003 (cont.)

EVENT #	Station	Month	Day	Fq (mHz)	Flag Hr	Flag Min	Beam	Gate	Event Time (UT)	AACGM Longitude	AACGM Latitude	Phase variation vs latitude	*m*[a]	δm	% Err	R	MLT	e/ w[b]	sun/ anti[c]
13a	3	1	29	0.83	23	57	1	5	23:56-24:56	-12.50	63.25	reverse	19	4	19	0.87	17	1	0
13b	3	1	29	1.39	23	59	2	4	23:50-24:50	-12.00	63.00	reverse	28	3	12	0.94	17	1	0
14	13	2	7	1.11	3	6	5	19	2:48-3:48	86	-72.5	standard	5	1	19	0.86	3	1	1
15	10	2	19	0.56	0	0	0	25	0:40-1:40	100	67	reverse	16	1	9	0.96	1	1	1
16a	13	2	19	0.56	21	7	4	13	20:42-21:42	80	-71	standard	9	1	17	0.89	21	0	1
16b	13	2	19	0.83	21	4	6	15	21:28-22:28	83	-70.5	reverse	55	4	6	0.98	21	0?	1
16c	13	2	19	2.22	21	25	5	11	21:12-22:12	82	-70	reverse	59	8	13	0.93	21	1	0
16d	13	2	19	2.78	21	25	3	11	20:41-21:41	77	-71.25	reverse	22	5	23	0.83	21	1	0
17	13	2	20	0.56	1	43	6	15	1:2-2:2	82	-72	standard	3	0.6	22	0.83	2	1	1
18	11	2	23	0.83	1	21	3	18	1:5-2:5	35	-68	reverse	7	1	14	0.92	22	1	0
19	13	3	3	1.94	1	7	6	17	0:43-1:43	82	-72.5	reverse	11	2	18	0.88	1	0	0
20	13	3	3	0.56	2	47	6	17	2:8-3:8	82	-72	standard	6	1	21	0.85	3	0	0
23	5	3	6	1.94	5	48	9	4	6:10-7:10	-41	64.5	reverse	67	5	8	0.97	22	1	0
24	9	3	8	1.94	1	50	6	24	1:32-2:32	72	89	standard	7	1	21	0.85	2	1	1
25	9	3	8	1.39	18	55	6	6	18:21-19:21	76	67.5	standard	14	2	13	0.96	19	1	0
26	9	3	10	3.33	19	11	7	7	18:41-19:41	76	66.5	reverse	36	6	17	0.89	19	1	0
27a	13	3	12	3.06	22	1	0	20	21:44-22:44	80	-74	reverse	18	5	21	0.79	22	0	1
27b	13	3	12	0.56	23	3	4	17	22:18-23:18	82	-72.5	standard	6	1	15	0.91	23	1	0
28	9	3	15	0.56	1	49	7	2	1:5-2:5	75	68	standard	52	6	12	0.94	1	0	0
29	14	3	15	0.83	11	52	2	19	11:25-12:25	-133	-64	standard	16	1	5	0.99	22	1	0
30a	13	3	17	1.11	2	55	3	16	2:55-3:55	83	-72.5	standard	10	1	13	0.93	3	0	0

[a]Azimuthal wave number. The errors correspond to the linear square fit

[b]Propagation: 0-eastwards; 1-westwards

[c]Propagation: 0-sunwards; 1-antisunwards

Table 3.1: Flags produced by the ULF identification code for which a FLR profile was obtained for the year 2003 (cont.)

EVENT #	Station	Month	Day	Fq (mHz)	Flag Hr	Flag Min	Beam	Gate	Event Time (UT)	AACGM Longitude	AACGM Latitude	Phase variation vs latitude	*m*[a]	δm	% Err	R	MLT	e/ w[b]	sun/ anti[c]
30b	13	3	24	0.56	1	47	2	16	1:28-2:28	78	-71.5	standard	9	1	16	0.90	2	0	1
32	9	3	29	0.56	18	56	0	6	18:22-19:22	73	67.5	reverse	23	3	13	0.94	19	0	1
33a	8	3	29	1.39	19	2	8	4	18:35-19:35	64	68	reverse	35	5	14	0.92	18	1	0
33b	8	3	29	4.17	19	3	8	7	18:30-19:30	62	68.5	reverse	47	8	17	0.89	18	1	0
34b	6	4	1	3.33	2	1	8	7	2:1-3:1	-64	64	reverse	24	2	7	0.98	16	1	0
35a	6	4	8	1.11	9	22	4	7	8:56-9:56	-71	63.5	reverse	21	2	11	0.95	23	1	0
39	8	4	26	1.39	23	15	8	7	22:55-23:55	60	70	reverse	20	3	17	0.89	22	1	0
42a	13	5	6	2.22	7	45	5	15	7:9-8:9	84	-72	standard	3	1	28	0.76	8	1	1
42b	13	5	6	3.33	7	49	4	13	7:44-8:44	79	-71	standard	2	0.5	23	0.83	8	1	1
42c	13	5	6	2.50	7	52	5	15	7:34-8:34	83	-72	standard	2	0.4	16	0.90	8	1	1
42d	13	5	6	4.44	7	54	5	15	7:45-8:45	82	-72	standard	11	2	15	0.92	8	1	1
44	6	5	18	1.11	6	49	4	20	6:23-7:23	-73	68.5	reverse	35	3	10	0.96	21	1	0
47	7	5	31	0.83	12	49	3	25	12:12-13:12	-92	69	reverse	21	0.6	3	1	1	0	0
49	9	6	3	1.11	2	44	8	7	2:3-3:3	76	67.25	standard	1	2	-	0.1	3	1	1
50	6	6	8	0.83	5	18	2	5	4:35-5:35	-69	62.5	reverse	7	1	20	0.86	19	1	0
51a	8	6	8	0.83	22	43	8	6	22:15-23:15	61.5	68.5	reverse	11	2	14	0.92	22	1	0
51b	8	6	8	0.56	23	42	4	6	23:57-24:57	62	68.25	reverse	16	3	20	0.86	23	1	0
52	8	6	15	0.56	2	49	3	6	2:36-3:36	60	67.5	reverse	13	3	20	0.86	2	0	0
53a	5	6	15	1.39	9	12	4	9	8:40-9:40	-42	65.75	standard	9	1	14	0.92	2	2	2
54	13	6	16	0.56	0	0	7	10	0:-42-0:18	78.00	-70.00	reverse	7	1	16	0.90	0	1	1
57	8	7	1	1.11	4	43	2	6	4:25-5:25	62.00	67.75	reverse	26	2	9	0.97	4	1	1

[a]Azimuthal wave number. The errors correspond to the linear square fit

[b]Propagation: 0-eastwards; 1-westwards

[c]Propagation: 0-sunwards; 1-antisunwards

Table 3.1: Flags produced by the ULF identification code for which a FLR profile was obtained for the year 2003 (cont.)

EVENT #	Station	Month	Day	Fq (mHz)	Flag Hr	Flag Min	Beam	Gate	Event Time (UT)	AACGM Longitude	AACGM Latitude	Phase variation vs latitude	*m*[a]	δm	% Err	R	MLT	e/ w[b]	sun/ anti[c]
60	6	7	9	3.61	9	43	8	23	9:10-10:10	-78	70.5	reverse	19	2	13	0.94	23	1	0
61	13	7	26	4.17	3	20	4	15	2:52-3:52	82	-72	standard	55	6	11	0.95	3	1	1
62	8	7	26	0.56	21	8	1	8	20:49-21:49	60.00	68.00	reverse	1	1	121	0.26	20	1	0
65	6	7	31	1.67	5	48	0	6	5:8-6:8	-70.50	62.75	reverse	40	5	12	0.94	20	1	0
68a	6	8	8	0.83	7	44	8	7	7:6-8:6	-66.00	64.00	standard	3	1	33	0.56	22	0	1
69	8	8	8	0.83	23	49	3	9	23:12-24:12	57.00	67.50	reverse	39	6	16	0.90	22	0	1
70	13	8	15	0.56	0	43	2	11	1:26-2:26	80	-71.5	reverse	8	1	8	0.97	1	0	0
72a	8	8	22	0.83	2	27	8	9	1:42-2:42	58.00	68.50	reverse	26	5	19	0.87	1	0	0
73	13	9	8	1.39	0	50	2	11	0:21-1:21	80.00	-72.00	reverse	5	0.7	14	0.92	1	0	0
75	14	9	21	1.39	10	49	2	25	10:16-11:16	-136	-66.5	reverse	9	1	11	0.95	21	1	0
76a	13	9	29	0.56	0	52	3	14	0:13-1:13	81	-72	reverse	3	0.6	23	0.82	2	0	0
76b	13	9	29	1.11	1	14	2	14	0:44-1:44	79	-73	standard	23	2	8	0.97	1	0	0
76c	13	9	29	2.50	1	39	10	13	0:57-1:57	82	-70.5	standard	30	2	7	0.98	2	0	0
77	13	9	29	0.56	22	5	3	10	22:47-23:47	82	-70.5	standard	3	2	49	0.56	22	1	0
78	13	9	29	0.56	23	5	3	17	22:47-23:47	87	-72	reverse	6	0.6	10	0.96	0	1	1
80a	7	10	8	1.67	12	9	8	35	11:51-12:51	-80	74	standard	8	1	13	0.93	2	1	1
81a	10	10	11	0.56	0	53	4	27	0:33-1:33	105	72	reverse	62	9	15	0.92	3	0	0
81c	9	10	11	1.11	1	12	7	20	0:54-1:54	87	69	reverse	7	1	14	0.93	3	0	0
83b	5	10	13	1.39	23	41	8	10	23:28-24:28	-37	66	reverse	4	3	73	0.41	16	0	1
84	7	10	13	1.11	10	9	0	27	9:42-10:42	-94	69.5	reverse	17	1	5	0.99	23	1	0
85a	5	10	14	1.39	11	45	3	8	11:35-12:35	-46.00	65.50	standard	20	2	11	0.95	4	0	0

[a]Azimuthal wave number. The errors correspond to the linear square fit

[b]Propagation: 0-eastwards; 1-westwards

[c]Propagation: 0-sunwards; 1-antisunwards

Table 3.1: Flags produced by the ULF identification code for which a FLR profile was obtained for the year 2003 (cont.)

EVENT #	Station	Month	Day	Fq (mHz)	Flag Hr	Flag Min	Beam	Gate	Event Time (UT)	AACGM Longitude	AACGM Latitude	Phase variation vs latitude	*m*[a]	δm	% Err	R	MLT	e/ w[b]	sun/ anti[c]
85b	5	10	14	2.22	12	6	2	6	11:35-12:35	-44.00	66.00	reverse	37	2	6	0.99	4	0	0
86a	5	10	16	1.94	23	57	6	10	23:44-24:44	-45	66.5	reverse	22	5	21	0.85	16	0	1
86b	5	10	16	2.22	23	56	4	9	23:11-24:11	-40.00	66.50	standard	6	1	24	0.81	16	0	1
89	7	10	27	3.61	7	4	7	11	6:27-7:27	-92	63	standard	31	3	9	0.96	20	1	0
91a	6	11	7	0.83	2	5	4	19	1:24-2:24	-72	67	reverse	11	1	12	0.94	16	1	0
91b	6	11	7	1.11	2	6	4	15	1:36-2:36	-72	66	reverse	8	2	20	0.86	16	1	0
92	6	11	7	2.78	4	17	4	18	3:56-4:56	-78	68	standard	7	1	13	0.93	18	0	1
93	10	11	7	4.44	5	40	4	23	5:11-6:11	103	68.5	reverse	7	0.6	9	0.97	8	0	0
94	13	11	7	1.67	21	6	4	14	20:58-21:58	82	-71	reverse	6	0.8	13	0.93	21	0	1
95	13	11	8	0.56	20	18	5	16	19:38-20:38	79	-73	standard	11	1	9	0.96	20	1	0
96	5	11	20	1.67	11	45	7	6	11:10-12:10	-43.00	66.00	standard	24	2	9	0.96	4	0	0
97	5	11	20	3.33	15	17	3	6	14:49-15:49	-44.00	64.50	standard	45	5	11	0.95	7	1	1
99a	9	12	4	0.83	22	42	11	9	22:27-23:27	78.00	67.00	reverse	20	3	13	0.93	22	1	0
99b	9	12	4	1.11	22	53	9	8	22:21-23:21	78.00	67.00	reverse	21	2	8	0.97	23	1	0
100	5	12	5	0.83	0	0	7	30	0:-44-0:16	-24	72	reverse	25	4	15	0.91	17	1	0
101	5	12	5	2.78	11	17	5	5	10:43-11:43	-43.00	64.25	standard	33	4	12	0.94	4	0	0
102	8	12	11	0.56	21	17	4	9	21:14-22:14	60.5	67	reverse	9	1	15	0.91	20	1	0
105	16	12	20	1.67	18	46	0	16	18:13-19:13	-113	64	reverse	17	1	7	0.98	6	1	1
106a	7	12	20	1.11	18	56	7	20	18:28-19:28	-91	66	standard	18	0.5	3	1	7	1	1
106b	7	12	20	2.78	19	56	7	19	20:37-21:37	-91	67	standard	61	2	3	0.99	8	1	1
106c	7	12	20	1.67	20	5	7	18	20:36-21:36	-91	65.5	standard	34	2	6	0.99	9	1	1

[a]Azimuthal wave number. The errors correspond to the linear square fit

[b]Propagation: 0-eastwards; 1-westwards

[c]Propagation: 0-sunwards; 1-antisunwards

Table 3.2: Flags produced by the ULF identification code for which a valid FLR profile could not be retrieved

EVENT #	Station	Year	Month	Day	Fq (mHz)	Flag Hr	Flag Min	Beam	Gate
13c	3	2003	1	29	3.61	23	59	9	5
13d	3	2003	1	29	3.89	23	59	11	6
13e	3	2003	1	29	4.72	23	58	9	4
21	5	2003	3	5	0.56	1	33	8	12
22*	9	2003	3	6	0.56	4	53	4	5
31	5	2003	3	28	0.56	1	38	10	8
33c*	8	2003	3	29	2.5	19	6	8	10
34a*	6	2003	4	1	0.56	1	48	0	9
35b	6	2003	4	8	0.56	10	25	2	4
36*	6	2003	4	10	0.56	9	52	2	10
37	8	2003	4	17	1.11	2	5	1	5
38	5	2003	4	23	3.06	3	47	8	23
40	8	2003	5	1	0.56	7	20	4	10
41a	3	2003	5	4	1.39	6	19	2	20
41b	3	2003	5	4	0.83	6	40	0	23
43*	5	2003	5	10	1.67	3	38	8	5
45	6	2003	5	18	1.67	12	19	5	23
46	5	2003	5	30	3.61	11	49	3	6
48	5	2003	6	2	1.94	9	31	3	3
37	8	2003	4	17	1.11	2	5	1	5
40	8	2003	5	1	0.56	7	20	4	10

* Visually confirmed FLRs with no available profile

Table 3.2: Flags produced by the ULF identification code for which a valid FLR profile could not be retrieved **(cont.)**

EVENT #	Station	Year	Month	Day	Fq (mHz)	Flag Hr	Flag Min	Beam	Gate
41a	3	2003	5	4	1.39	6	19	2	20
41b	3	2003	5	4	0.83	6	40	0	23
43	5	2003	5	10	1.67	3	38	8	5
45	6	2003	5	18	1.67	12	19	5	23
46	5	2003	5	30	3.61	11	49	3	6
48	5	2003	6	2	1.94	9	31	3	3
53b	5	2003	6	15	3.06	9	47	9	6
55a	12	2003	6	22	0.56	18	4	6	5
55b	8	2003	6	22	2.22	18	5	11	6
56	12	2003	6	22	3.06	18	22	4	4
58	12	2003	7	3	1.39	18	52	8	2
59	6	2003	7	8	1.39	8	9	8	27
63*	5	2003	7	29	1.67	9	25	8	4
64*	8	2003	7	29	1.39	17	57	2	4
66a	8	2003	8	1	2.22	4	20	0	7
66b	8	2003	8	1	4.72	4	20	0	6
67*	5	2003	8	8	2.5	10	36	7	6
68b	6	2003	8	8	1.39	7	46	7	7
68c	6	2003	8	8	0.56	7	52	8	8
71*	10	2003	8	16	0.83	23	5	6	23
72b*	9	2003	8	22	1.39	2	37	8	7

* Visually confirmed FLRs with no available profile

Table 3.2: Flags produced by the ULF identification code for which a valid FLR profile could not be retrieved (cont.)

EVENT #	Station	Year	Month	Day	Fq (mHz)	Flag Hr	Flag Min	Beam	Gate
74a	8	2003	9	16	1.94	21	46	4	11
74b	8	2003	9	16	4.17	22	14	6	7
79*	9	2003	10	6	2.22	5	16	3	18
80b	7	2003	10	8	2.78	13	7	9	34
81b	10	2003	10	11	3.61	1	5	7	26
82	9	2003	10	11	0.83	22	43	4	22
83a	5	2003	10	13	1.11	23	34	10	11
86c*	5	2003	10	16	2.5	23	59	5	9
86d*	5	2003	10	16	5	23	57	6	10
87a*	5	2003	10	17	0.56	0	1	5	11
87b	5	2003	10	17	3.89	0	0	4	10
88*	8	2003	10	18	4.44	1	36	3	9
90*	9	2003	11	6	0.83	1	29	3	16
98*	3	2003	11	20	4.72	23	56	5	7
103	8	2003	12	12	1.94	17	31	4	11
104	9	2003	12	20	0.83	17	11	7	6
107a*	9	2003	12	21	1.94	0	50	2	7
107b*	9	2003	12	21	2.22	1	9	0	8
108	13	2003	12	30	0.56	23	3	2	7

* Visually confirmed FLRs with no available profile

For simplicity, given that the outcome text file with ULF flags would often return numerous entries for the same event corresponding to multiple flags for different beam/gate pairs and that a 'unique flag' is defined as a flag for a station, date, and frequency that has at least an hour difference with another 'unique flag', tables 3.1 and 3.2 contain only the first entry flagged if corresponding to multiple flags for the same ULF wave event. Therefore, the beam/gate recorded in that table might not correspond to the center location of the FLR within the FoV of the radar. The AACGM magnetic latitude and longitude, reported in Table 3.1, correspond to the location in which the profile exhibits the best match to the "FLR Profile Criteria". Harmonics of the same event (different frequencies detected at the same time for the same radar) are identified in Tables 3.1 and 3.2 by the same number and consecutive letters.

Table 3.3: Results of flags, confirmed FLRs

Flags	161	Flags, Low Gates (0-14)	70	Flags, High gates (15-70)	91
FLRs	107	FLRs, Low Gate	24	FLRs, High gates	83
No FLR profiled obtained	54	No FLR profiled obtained	46	Not profile obtained	8
% Effic.	66	% Effic.	34	% Effic.	91

Table 3.3 summarizes the total number of flags, the number of FLRs successfully found with the further analysis and the number of flags for which a FLR profile was not obtained. Further inspection showed that a large number of flags for which the FLR profile could not be obtained corresponded to lower gates (0-14), where backscatter from the E-region is predominant. Taking into account only those flags detected at the low gates, the efficiency of this code when applied to those low gates was as low as 34%. If the lower gate flags were removed from the dataset, the efficiency of the code to pre-select ULF waves that can be further analyzed and characterized as FLRs improves to 91%, as shown in Table 3. Therefore, this methodology would be very efficient to find ULF waves corresponding to FLRs in the F-region at mid and high gates (15-60) of SuperDARN radars, but not efficient for lower gates.

3.2 Challenges in the identification of FLRs

From a total of 161 ULF waves pre-selected by the code 33.50% flags did not return a valid FLR profile and therefore, they were not classified as such. Reasons for the unavailability of obtaining an FLR profile include:

i) Problems in obtaining the FLR profile due to one beam working on a special mode near the location of the FLR;
ii) Problems in obtaining the FLR profile due to the FLR event occurring too close to the edge of the FoV of the radar;
iii) Detection by the code of an ULF wave activity on the radar signal that did not correspond to FLR activity but might correspond to ULF propagating waves or other interesting phenomena (26 % of the flags).
iv) Problems in obtaining an azimuthal wave number for pure global toroidal mode FLRs, with polarward phase variation as a function of latitude was observed across the FoV of the radar (6 cases with FLR profile)

As stated in the previous section, events corresponding to i) and ii) can be visually recognized as FLRs from their series of plots of the analytic signal amplitude and phase (as the one shown in Figure 3.7) but FLR profiles were not able to be retrieved.

An example of an ULF wave pre-selected for which its FLR profile could not be obtained, as described in item i), is the ULF wave detected by the SuperDARN Pykkvibaer station on March 6th, 2003 corresponding to 4:48 UT at the resonant frequency of 0.6±0.1 mHz. The code flagged an ULF wave 'candidate for FLR further analysis' from beams 4 through 14 (except beam 5), range gates 4 to 8 corresponding to a possible FLR centered at magnetic latitude 67 degrees, and 73

degrees azimuth for magnetic longitude. Figure 3.9 shows plots of the amplitude (left) and phase (right) as a function of magnetic latitude and magnetic longitude for the analytic signal, bandpass at 0.6±0.1 mHz, for FoV of the radar corresponding to beams 0 through 15 and range gates 0-20 at 4:48UT: At the time, beam 5 was working on a special mode (sample rate: 3 seconds) and all the other beams were working on normal mode. The white patch observed on the amplitude plot shows the location of Beam 5. Visual inspection of the plots in Figure 3.9 reveals a phase jump and amplitude maximum in latitude at the magnetic latitude and longitude corresponding to the beam-gates flagged, but in this particular case an FLR profile could not be obtained. It is worth mentioning that few ULF waves pre-selected corresponding to similar situations were able to return an FLR profile if the beam working in a different mode was located further from the FLR location. SuperDARN radar stations have the ability to run 'special modes (all beams in a sampling period different than 60 seconds) and 'stereo modes', that is to say a beam has a different sampling period from the others; this is done to address specific scientific topics (such as rocket launches, ULF pulsations, E-region measurements, satellite conjunctions), directed by Principal Investigators requesting it [*Baker*, 2011].

Figure 3.10 shows an example of a flagged candidate that occurred too close to the edge of the FoV of the radar, for which the profile of the FLR could not be obtained, as described in item ii). The code flagged an ULF wave as an 'FLR candidate' multiple times, at Pykkvibaer on March 28th, 2003 occuring between 1:38 and 1:44 UT at beams pairs 10 and 14 and 11 and 15, rage gates 7-9 (around magnetic latitude 65.5 degrees for magnetic longitude around -39.8 degrees azimuth). The plots in Figure 3.10 correspond to the analytic signal amplitude (left) and phases (right), bandpass at 0.6 mHz, as a function of magnetic latitude and magnetic longitude for beams 0-15 and range gates 5-15 of the field of view of the SuperDARN Pykkvibaer station on March 28th, 2003 corresponding to 1:38 UT.

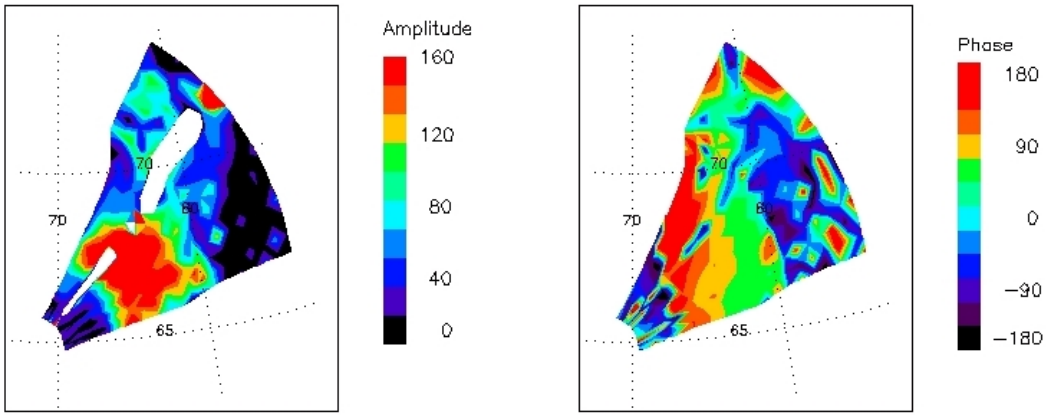

Figure 3.9: Plot of the analytic signal amplitude (left) and phase (right) as a function of magnetic latitude and magnetic longitude for the field of view (Beams: 0-15; Gates: 0-20) of the SuperDARN Pykkvibaer station on March 6th, 2003 corresponding to 4:48 UT for the bandpass analytic signal for 0.6±0.1 mHz. Beam 5 was working on a special mode (white patch on the amplitude plot) and all the other beams were working on normal mode.

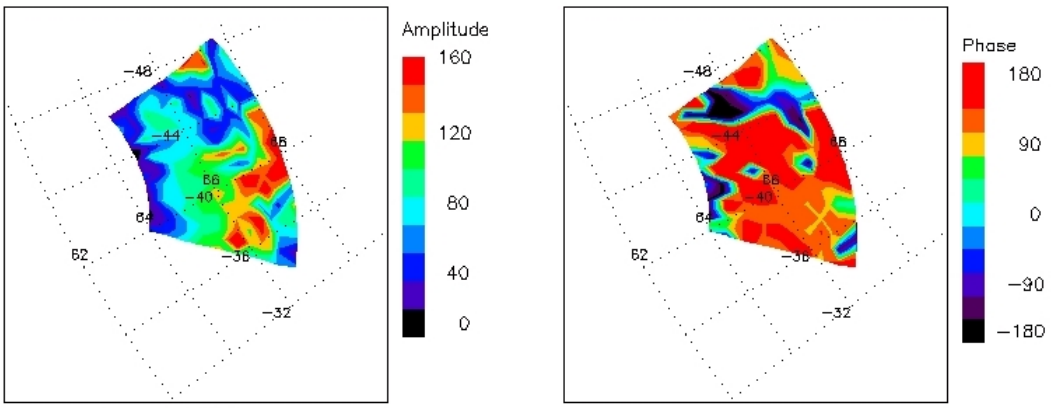

Figure 3.10: Plot of the analytic signal amplitude (left) and phase (right) as a function of magnetic latitude and magnetic longitude for beams 0-15 and range gates 5-15 of the field of view of the SuperDARN Pykkvibaer station on March 28th, 2003 corresponding to 1:38 UT, bandpass at 0.6±0.1 mHz. The code flagged a 'candidate' at magnetic latitude 65.5 degrees for magnetic longitude around -39.8 degrees azimuth (beams pairs 10-14 and 11-15, both at rage gates 8). The event occurred too close to the edge of the radar and a profile could not be obtained.

3.3 Limitation of this technique

In the previous chapter, it was explained that the new criteria for the code was made stricter to increase the success rate of the code for producing ULF flags that corresponded to FLRs and there were some good FLR events characterized from ULF flags (found while developing the early stages of the code) that did not meet the latest threshold criteria (e.g. they met the criteria for one gate but not for three adjacent gates).

Additionally, the code flagged ULF events with values for cross-power and cross-phase variance above daily mean values. These daily mean values were arbitrarily calculated from 0 UT to 24 UT for each day with selected data (as explained in section 2.2) and this introduced another bias. Some FLRs occurred on days with poor backscatter echoes, for which the only good backscatter was observed by SuperDARN around the time of the event. Therefore, mean daily values on those days are close to the values of the events.

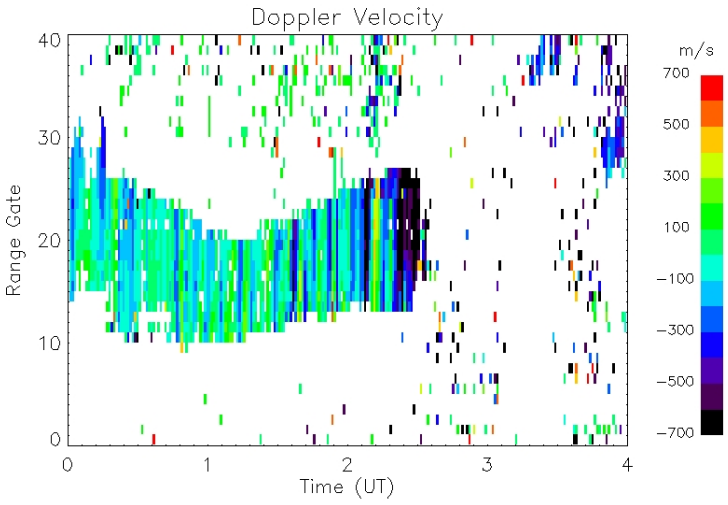

Figure 3.11: Doppler velocity range-time plot for Prince George for October 25th, 2003, Beam 2. A ULF wave patter is noticeable between 1UT and 2:30UT. An FLR of 2.2±0.1 mHz was later confirmed at 1:15-2:30UT for that day.

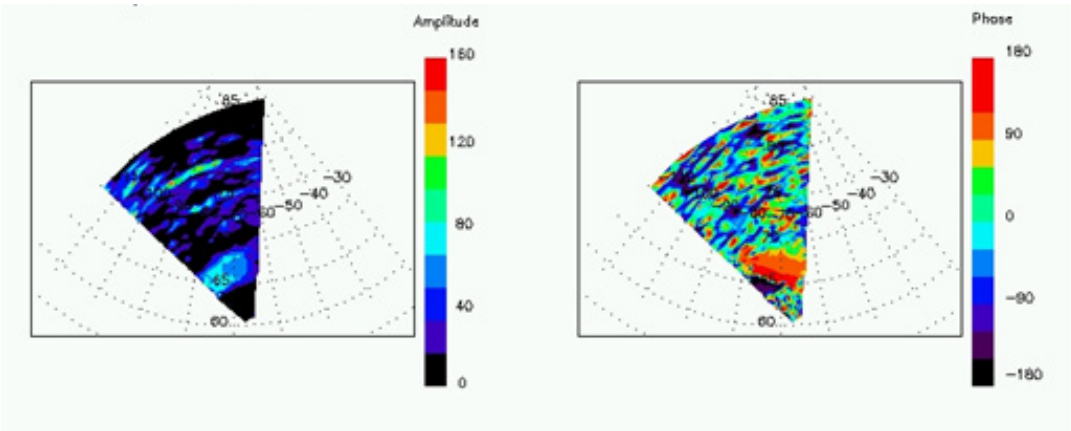

Figure 3.12: Plot of amplitude and phase as a function of magnetic latitude and magnetic longitude for the field of view of the SuperDARN Prince George station on October 25th, 2003 corresponding to 1:21UT for the bandpass analytic signal for 2.2±0.1 mHz. For magnetic latitudes between 63 and 67 degrees azimuth, the high amplitude (left panel) and wave front in phase (right panel) are observed. The event lasted one hour.

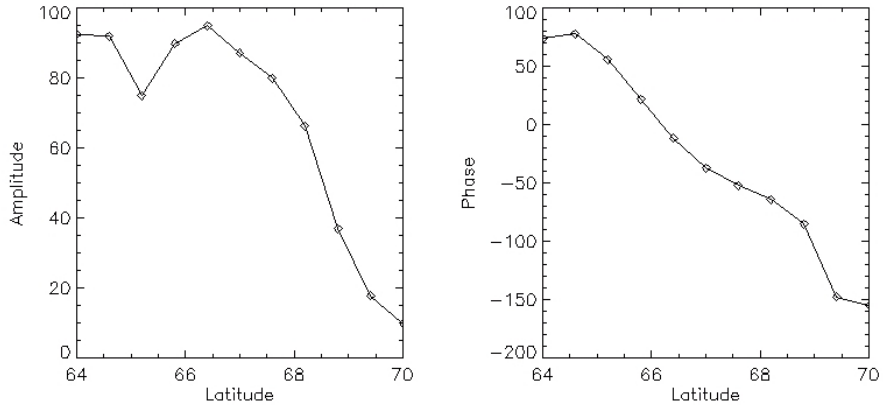

Figure 3.13: Latitude profile of the amplitude and phase of the v signal at 2.2±0.1 mHz corresponding to the Prince George station on October 25, 2003 (along -74 degrees magnetic longitude) at 1:43UT. The maximum peak is observed at magnetic latitude 66.5 degrees.

A good example of this is a 2.2±0.1 mHz FLR occurrence detected on Beam 2 at 1:15-2:30UT on Oct 25th 2013 by the SuperDARN Prince George Station. The backscatter Doppler velocity pattern, the FoV of the radar with the analytic signal at the time of the event, the cross-section plots with the latitude of the amplitude and phase of the analytic signal with the FLR profile, and the phase versus longitude (which gives the *m* azimuthal wavenumber) are shown in figures 3.11, 3.12, 3.13 and 3.14.

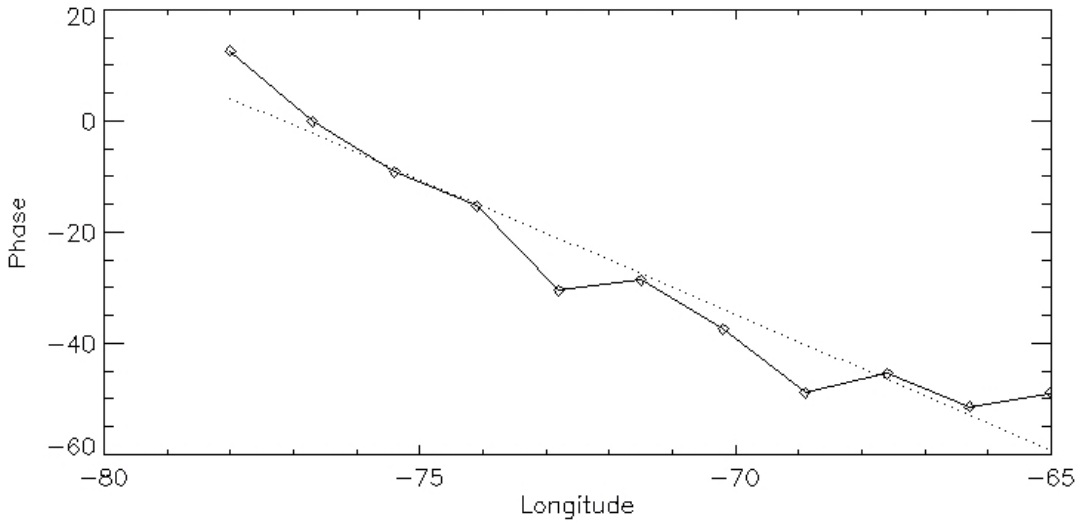

Figure 3.14: Spectral Phase as a function of longitude gives the m-value of the wave at 2.2±0.1 mHz corresponding to the Prince George on October 25, 2003 (along 66.5 degrees magnetic latitude) at 1:43UT with m=4±1.

Table 3.4 contains a summary of 15 FLRs that have been found during the developing of the code through early versions but that did not match the final threshold established for automatic detection of ULF wave candidates for FLRs.

Table 3.4: FLRs found during the development of the ULF identification code that did not met the final threshold established

EVENT #	Station	Month	Day	Fq (mHz)	Flag Hr	Flag Min	Beam	Gate	Event Time (UT)	AACGM Longitude	AACGM Latitude	Phase variation vs latitude	*m*[a]	δm	% Err	R	MLT	e/ w[b]	sun/ anti[c]
109a	7	1	14	2.22	15	51	7	29	14:40-16:40	-77	71	standard	6	1	16	0.91	6	1	1
109b	7	1	14	2.50	16	31	8	28	15:45-16:45	-75	71	standard	6	1	7	0.98	6.7	1	1
110	11	1	17	2.22	6	31	2	24	6:15-7:0	38	-69	standard	31	2	7	0.98	4.3	0	0
111	7	1	21	3.33	17	48	6	30	17:45-18:45	-80	71	standard	3	1	17	0.89	7.5	1	1
112	14	2	19	1.39	13	9	2	27	12:45-13:20	-135	-69	standard	24	2	7	0.98	23.3	0	1
113	11	2	23	2.22	4	23	6	13	4:0-5:0	37	-66	reverse	51	4	8	0.97	1.9	0	0
114	13	3	3	1.39	3	5	3	10	2:45-3:30	88	-71	standard	7	1	12	0.94	4	1	1
115	5	3	6	1.11	6	1	0	14	6:0-7:0	-49	68	reverse	8	1	8	0.98	21.8	1	0
116	13	3	17	0.83	2	44	3	20	2:15-3:14	79	-70	standard	8	1	16	0.90	3.1	1	1
117a	14	3	19	0.56	12	12	1	29	12:0-12:45	-137	-70	reverse	8	1	12	0.95	22.2	1	0
117b	14	3	19	1.11	12	6	3	28	12:0-12:46	-137	-64	reverse	33	3	9	0.97	22.1	1	0
118a	13	3	29	0.56	22	47	6	22	22:37-23:30	89	-74	standard	9	2	19	0.87	23.9	0	1
118b	13	3	29	0.83	22	20	4	17	22:15-23:0	90	-73	reverse	9	1	8	0.97	23.5	0	1
119	5	7	8	1.11	6	20	4	28	6:15-7:30	-41	74.5	standard	52	8	16	0.91	22.7	0	1
120	6	10	25	2.22	1	54	2	17	1:0-2:40	-74	66.50	standard	4	1	12	0.94	16.3	0	1

[a]Azimuthal wave number. The errors correspond to the linear square fit

[b]Propagation: 0-eastwards; 1-westwards

[c]Propagation: 0-sunwards; 1-antisunwards

3.4 Summary

In this chapter, the basic criteria for identification of FLRs, from the ULF waves identified by the code, has been explained in detail. The major achievement of this study is the development of a 'non visual' technique that efficiently allows, in an automatic way, the identification of a large number ULF waves that result in FLRs, once the criteria is applied to the flags.

The procedures by *Bland et al.* [2014] for systematic detection of ULF waves using an alternative data processing technique with SuperDARN does not target the detection of FLRs and it is not successful to identify specifically that phenomena. *Mangus* [2009] did target the identification of continuous pulsations, using SuperDARN, that are FLRs. However, the study does not confirm the typical profile of FLRs for the events did not exclude ground or sea scatter. For this reason, the efficiency of the code (# of FLRs/# continuous pulsations detected) cannot be evaluated for comparison reasons.

The efficiency of the methodology, defined as the number of events characterized as FLRs over the number of ULF waves flagged, is 66.50%. Efficiency improves to 91% when applied to gates higher than 14. Therefore, this study proves that this methodology is very useful to find a large number of FLRs using SuperDARN.

A total of 121 FLRs have been identified during 2003 and their primary characteristics (MLT, frequency, propagation, phase variation with latitude, azimuthal wavenumber m) have been recorded and tabulated. A large database has been created to analyze the characteristics of FLRs and to study the coherence of solar wind ULF waves with the FLRs to establish their wave sources.

The sample FLR event presented throughout these two chapters present an interesting result: In their study, *Fenrich and Samson* [1995] characterized FLRs

with azimuthal wavenumber $m > 17$ as "High-m" FLRs; all these events presented a reverse phase variation (increase latitudinal phase shift). Furthermore, FLRs with azimuthal wavenumbers $m < 17$ were called "Low-m" FLRs, characterized with a standard phase variation (decrease latitudinal phase shift). The event exemplified in this chapter has a standard phase variation and an azimuthal wavenumber m=24.2±0.7. This is not the only case in the database that presents this type of discrepancy. Furthermore, events in the database presented in this study show deviations for the characterizations proposed in *Fenrich et al.* [1995] in terms of the FLR propagations (sundwards-antisunwards; eastwards-westwards) and location. It is clear that the FLRs identified in this study cannot be classified into the two distinct groups defined by *Fenrich et al.* [1995] and *Fenrich and Samson* [1997] based upon the size of the FLR azimuthal wavenumber m.

In the next chapter, the characterization of FLRs will be explored and some case studies will be presented. Some studies [*Yeoman et al*, 1990; *Grant et al*, 1992; *Wright et al.*, 1997; 1999; *Mann*, 1998; *Wright and Yeoman.; Yeoman et al*, 2000; *Yeoman et al*, 2010; *Yeoman et al*, 2012] have presented alternatives to the classification suggested by *Fenrich et al.*, [1995] and *Fenrich and Samson* [1997], and they proposed mechanisms for the excitation and growth of FLRs that suggests that more than two groups of FLRs coexists.

Chapter 4

Classification and Characterization of Field Line Resonances

The second main goal of this thesis research was to systematically analyze the characteristics of FLRs and the statistics of their occurrences. Some of the interesting aspects of FLRs are for example:

- their frequency distribution (Are some frequencies occurring more often than others?),
- latitude of occurrences (How often is the same frequency observed at different latitudes?),
- *m*-value (What are the differences between low-*m* FLRs and high-*m* FLRs?),
- magnetic local time (Do low and high-*m* FLRs occur in the same MLT sector?), etc.

The sections below describe the processes of characterization of the FLRs in the database and the statistical results on these properties. Comparison with the results on the studies described in the literature review in section 1.3.2 will be presented.

4.1 Statistical Analysis of Field Line Resonances Detected

4.1.1 Statistical Analysis of Occurrence vs Frequency

Figure 4.1 shows the 121 FLRs occurrences, found in this study, as a function of frequency. The plot presents a 1/*f* frequency distribution. This result agrees with the results found by *Mangus* [2009] with his pulsation finder to detect ULF waves using SuperDARN, and the results found in *Archer and Plaschke* [2014]. It is also worth to remark that 'magic frequencies' (1.3, 1.9, 2.6 and 3.4 mHz) were not particularly observed in the results of this study, in agreement with results reported by *Mangus* [2009] and *Archer and Plaschke* [2014].

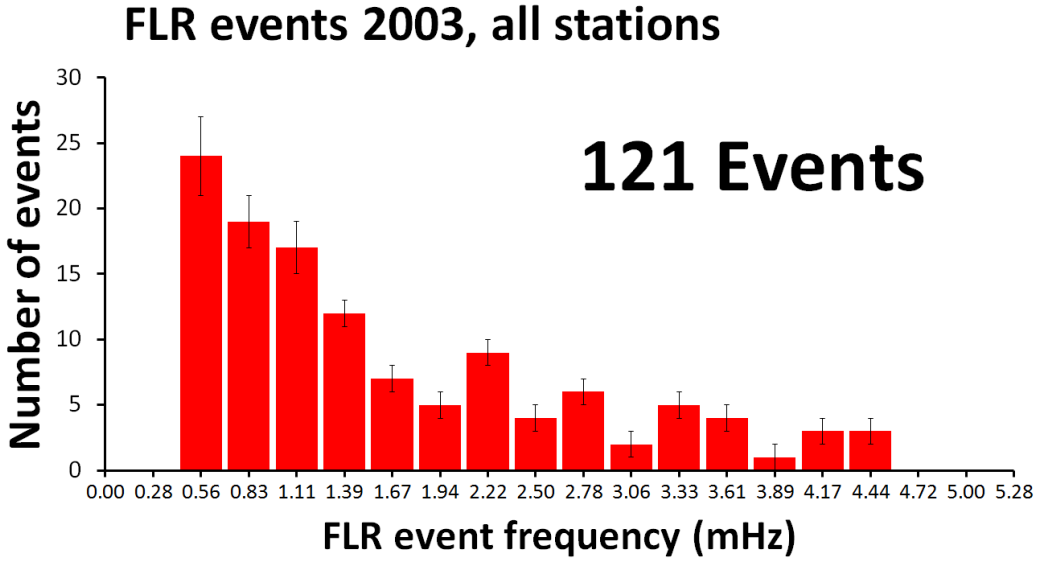

Figure 4.1: Event occurrence as a function of frequency of the event.

Significantly, the distribution reported in *Fenrich et al.* [1995] corresponded to a small sample, only 31 FLR events. Some might argue that study covered most of the solar cycle 22 (1988-1994), and that "*the events were found to occur both the dayside and nightside of the magnetosphere during predominantly quiet days with most events occurring when Kp ≤ 3*" [*Fenrich et al.*, 1995] and that the magic frequencies would be noticeable in a distribution that follows those caracteristics.

The year 2003, the object of this study, was a very geomagnetically active year, with 34 geomagnetic storms [*Mazzino et al.*, 2008], for which some might argue that many mechanisms could affect the final distribution of the number of events vs. frequency. This year occurred during the declining phase of the solar cycle: a) the number of geomagnetic storms during this phase in a solar cycle is more than the number of geomagnetic storms in the minimum and inclining phase of the solar cycle; b) moreover, the number of geomagnetic storms during the declining phase is the same or more than the number of geomagnetic storms occur during solar maximum [*Mazzino et al.*, 2008]. Therefore, FLRs observed in this study were indeed observed during both geomagnetic active times (Kp > 3) and in quiet times (Kp ≤ 3).

Figure 4.2 shows the distribution of number of events vs. frequency separated by geomagnetic activity: 40% were observed during active times (Kp > 3) and 60% during quiet times (Kp ≤ 3). The number of events found during quiet times (Kp ≤ 3), shown in blue, was double the amount reported in *Fenrich et al.* [1995]. In this distribution, 'magic frequencies' (1.3, 1.9, 2.6 and 3.4 mHz) were not particularly observed, and it is more likely to be a Poisson distribution (proper for the observation of 'rare events). The distribution of events observed during active times (Kp > 3), shown in red, shows a power law.

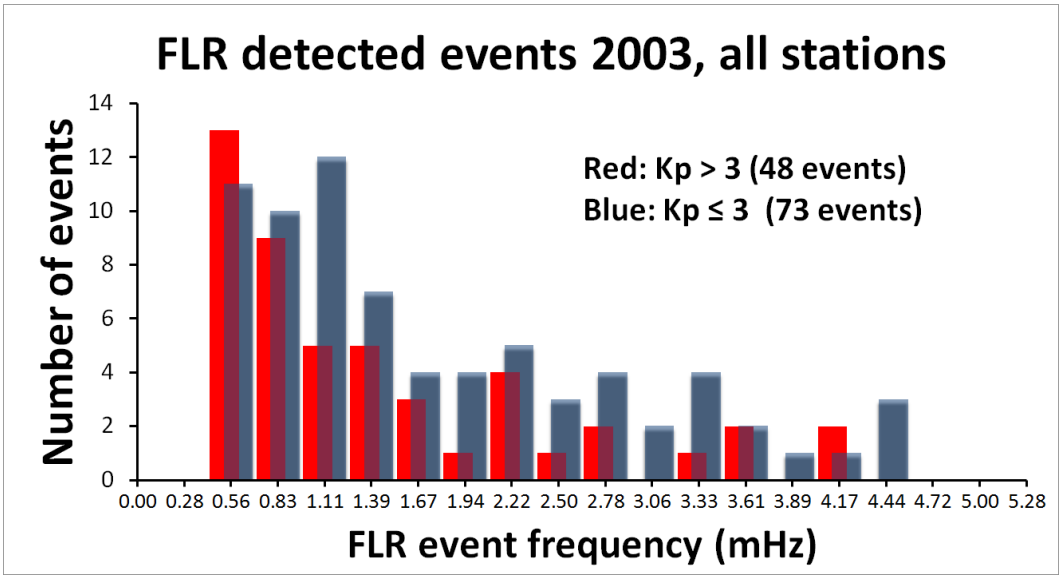

Figure 4.2: Distribution of number of events vs. frequency separaded by geomagnetic activity. (red: active times; blue: quiet times).

A direct comparison between the dataset from *Archer and Plaschke* [2014], *Mangus* [2009] and our study could provide further information on this topic. The extension of this methodology to all other years of the solar cycle 23 is the goal of future work.

In the past decade, significant advances in the deployment and operations of the SuperDARN radars have occurred. The number of SuperDARN Radars increased from 6 operational radars in 1995 to 15 stations in 2003. The study conducted by *Fenrich et al.* [1995] used only three radars (Goose Bay, Kapuskasing and Saskatoon) all located on the east coast of North America. Availability of a larger number of stations for this project provided a more comprehensive study, both in the northern and southern hemisphere. A larger database compiled by a systematic and automatic detection system provides a more precise result than events identified by eye.

4.1.2 Phase variation across the localized position of resonance

The phase shift as a function of latitude throughout the resonance maximum was computed for all FLRs in the database. Following the definition established by *Fenrich et al.* [1995], a decrease in the latitudinal phase shift throughout the resonance peak with latitude is defined as "*standard*", while a phase increase with latitude is defined as "*reverse*". *Fenrich et al.* [1995] and *Fenrich* [PhD Thesis, 1997] reported that all low-m ($m < 17$) FLRs in that study exhibited "*standard*" phase variation while all high-m ($m \geq 17$) exhibited a "*reverse*" phase variation. Table 4.1 summarizes the results of all FLRs in the database following the classification by *Fenrich et al.* [1995].

In this study, we observed that a little over one third of the high-m ($m \geq 17$) presented "*standard*" phase variation while almost half of the low-m ($m < 17$) exhibited "*reverse*" phase variation. These results were puzzling. Further examinations of the phase shift, following the classification proposed by *Yeoman et al.* [2010; 2012], and revealed that most of the FLRs with azimuthal wavenumbers less than 4 had standard phase variation while about half of events with azimuthal wavenumbers between $4 \leq m \leq 14$ had a reverse phase variation, as shown in Table 4.2. One third of the FLRs with azimuthal wavenumber $m > 14$ exhibited "*standard*" phase. Changing the threshold produced deviation from these results, as seen in Table 4.3.

The cause of these discrepancies might lay in the fact that the events found in *Fenrich et al.* [1995] occurred during quiet times with low Kp. Geomagnetic disturbances in Earth's magnetic field, measured on variation of Kp, modifies the localization of the plasmapause. The sharp decrease in density in the plasmapause results in a sharp increase of the eigenfrequency of the field line,

since the frequency of the FLRs is inversely proportional to the field line plasma density, as shown in equation 1.18.

Table 4.1: FLRs' phase variation given their azimuthal wavenumber following classification by *Fenrich et al.* [1995]

Phase shift	$m \leq 17$	$m > 17$
Standard	36 (58 %)	26 (42 %)
Reverse	19 (42 %)	40 (68 %)

Table 4.2: FLRs' phase variation given their azimuthal wavenumber following classification by *Yeoman et al.* [2010]

Phase shift	$m < 4$	$4 \leq m \leq 14$	$m > 14$
Standard	9 (82%)	26 (55%)	20 (32%)
Reverse	2 (18%)	21 (45%)	43 (68%)

Table 4.3: FLRs' phase variation given their azimuthal wavenumber

Phase shift	$m < 7$	$7 \leq m \leq 14$	$m > 14$
Standard	16 (73 %)	19 (31 %)	20 (53 %)
Reverse	6 (27 %)	42 (69 %)	43 (68%)

Table 4.4: Location of the events with respect of the plasmasphere

Phase shift	Inside Plasmasphere	At plasmapause	Beyond plasmapause
Standard	0 (0 %)	0 (0 %)	55 (51 %)
Reverse	0 (0 %)	13 (100 %)	53 (49 %)

In the plasmasphere, before the plasmapause is reached, where the plasma density is uniform, eigenfrequency decreases monotonically with latitude due to the decrease of B for larger L-shells. In the plasmapause, the eigenfrequency increases sharply in response to the sharp decrease in density. Beyond that, in the plasmathrough, the eigenfrequency decreases monotonically with latitude. This characteristic variation of eigenfrequency with latitude is known as the eigenfrequency continuum and was first introduced by *Orr and Hanson* [1981]. Figure 4.3, taken from *Orr and Hanson* [1981], represents the eigenfrequency continuum and illustrates how the sharp decrease in density found in the plasmapause would produce a '*reverse*' phase variation in the FLR profile. The dashed horizontal lines show a particular driving frequency (ω_f). As a result, three separate geomagnetic field lines may be resonantly excited at locations A (Plasmasphere), B (Plasmaspause) and C (Plasmathrough). Observations of the continuum of eigenfrequencies are used to determine equatorial plane plasma mass densities, and thus to study large scale cold plasma dynamics within the magnetosphere [*Dent*, 2003].

Experimental evidence of this eigenfrequency continuum has been presented using data 53 recorded using ground-based magnetometers [*Obayashi and Jacobs*, 1958; *Glassmeier et al.*, 1984], and satellites [*Takahashi and McPherron*, 1982; *Takahashi et al.*, 1984]. First radar observations by the Sweden and Britain auroral Radar Experiment (SABRE) where reported and discussed in *Waldock et al.* [1983] and *Poulter et al.,* [1984].

In the study by *Waldock et al.* [1983], the occurrence probability of polewards and equatorward moving bands found in the beams backscatter profiles was investigated as a function of UT time. The conclusion of that study was that the reversal phase variation might be linked to the movements of the plasmapause.

Titan et al. [1991] also analyzed 157 Pc 5 pulsations detected by SABRE during a 5-year period (1985-1989) and concluded that that events with poleward propagation corresponded to field lines resonances within the plasmatrough while equatorward propagating events corresponded to resonant structures at the plasmapause.

It is clear that it would be possible to find FLRs for the natural resonant frequencies for cases A, B, and C if available detection instrumentation is available for those latitudes, such as the recently deployed mid-latitude SuperDARN radars. More importantly, significant changes in the plasmasphere structure, due to geomagnetic disturbances in Earth's magnetic field, would signify that the latitude location of the natural resonant frequencies for cases A, B, and C would increase if the location of the magnetopause is extended to higher L-shells.

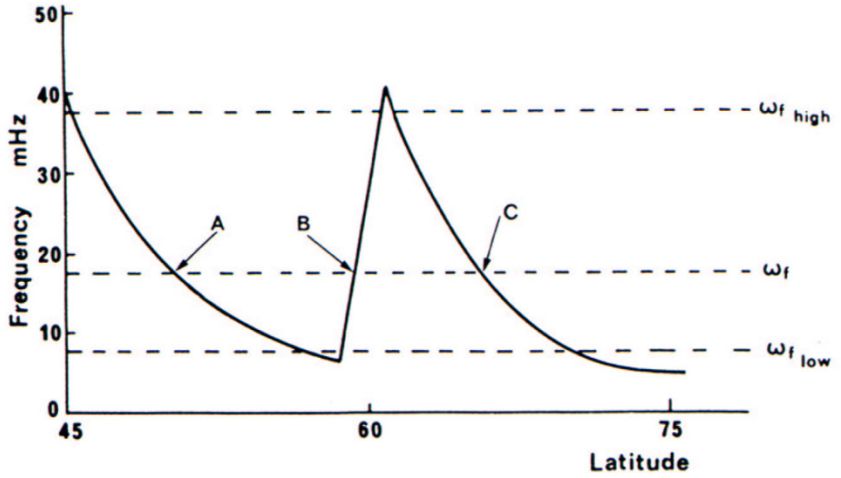

Figure 4.3: Schematic representation, by *Orr and Hanson* [1981], of the eigenfrequency continuum: the variation of field line resonance frequency with latitude.

Pierrard and Stegen [2008], developed a three-dimensional physical dynamic model of the plasmasphere[2], constrained by realistic data, which takes into account both the rotation of the plasmasphere and the geomagnetic activity's level that defines the plasmapause region's position and width. The kinetic models used in their plasmasphere's model also feature the erosion of the plasmasphere during geomagnetic storms and substorms, based on work by *Pierrard and Lemaire* [1996; 2001; 2004], *Pierrard and Cabrera* [2005; 2006], among others. The dynamic code that calculates the position of the plasmapause versus MLT, every hour UT using values of Kp, can be run in the European Space Weather Portal, where simulations for the whole day can be downloaded.

In this study, we explored this idea in all FLRs in the database, looking for the location of the plasmaspause at the MLT of occurrence, to explain discrepancies regarding some of the FLR's phase variations. For each FLR, their corresponding L-shell location was obtained by introducing the height (obtained from the slant range calculated from the gate number) and the magnetic coordinates (calculated by the SuperDARN software) into the NASA OMNIweb interface for the "Corrected geomagnetic coordinates IGRF/DGRF model parameters". Simulations from the European Space Weather Portal (ESWP) on the localization of the plasmasphere and plasmapause were downloaded for the date of each event. The location of the plasmapause at the UT time, L-shell and MLT location of the event was obtained by observing the animations and 1-hour snap shots produced by the simulations created by *Pierrard and Stegen* [2008].

---

[2] The plasmaspheric simulations shown in this chapter have been developed at the Belgian Institute for Space Aeronomy by V. Pierrard and K. Borremans with funding from the European Union's Seventh Programme for Research, Technological Development and Demonstration (www.swiff.eu FP7 SWIFF).

The above information was used in this study to test the theory by *Orr and Hanson* [1981] that the '*reverse*' phase variation in an FLR profile is due to the sudden decrease of plasma density corresponding to the magnetopause, and that the "*standard*" phase variation corresponds to regions with smooth decrease in the field line's eigenfrequency, such as the plasmasphere or the plasmatrough or beyond. Table 4.4 summarizes these findings.

None of the events in the FLR database occurred inside of the plasmasphere; for the 13 FLRs that occurred in the magnetopause, all showed a reverse phase variation, despite that 4 of them featured azimuthal wave numbers $m < 17$.

The rest of the events occurred in the plasmathrough, with half of the events showing a "*standard*" phase variation and the other half showing a "*reverse*".

The 1.1±0.1 mHz FLR event detected by Kodiak on December 20, 2003 at 18:50 UT, featured throughout this thesis, agrees with this theory: in the previous chapter, the phase variation for this event was presented as "*standard*" due to the decrease of phase change as a function of latitude (Figure 3.7); however, the event was classified as a high-m since m=24.2±0.7 (Figure 3.8). Figure 4.4, downloaded from the European Space Weather Portal (ESWP) and courtesy of *Pierrard and Stegen* [2008], shows Kp=5 at around that time (top) and the simulation of the location of the plasmasphere (blue, green, yellow, see electron density scale on figure), plasmapause (purple diamonds) and plasmatrough (red) for the time of the event from a polar view (bottom, left) and from the equator view (bottom, right). The event was localized in the L =7.07 at MLT=7. For MLT=7, the plasmapause is located at around L=5 R_e, for which the event's phase variation is compatible to a phase variation of an event located beyond the plasmatrough.

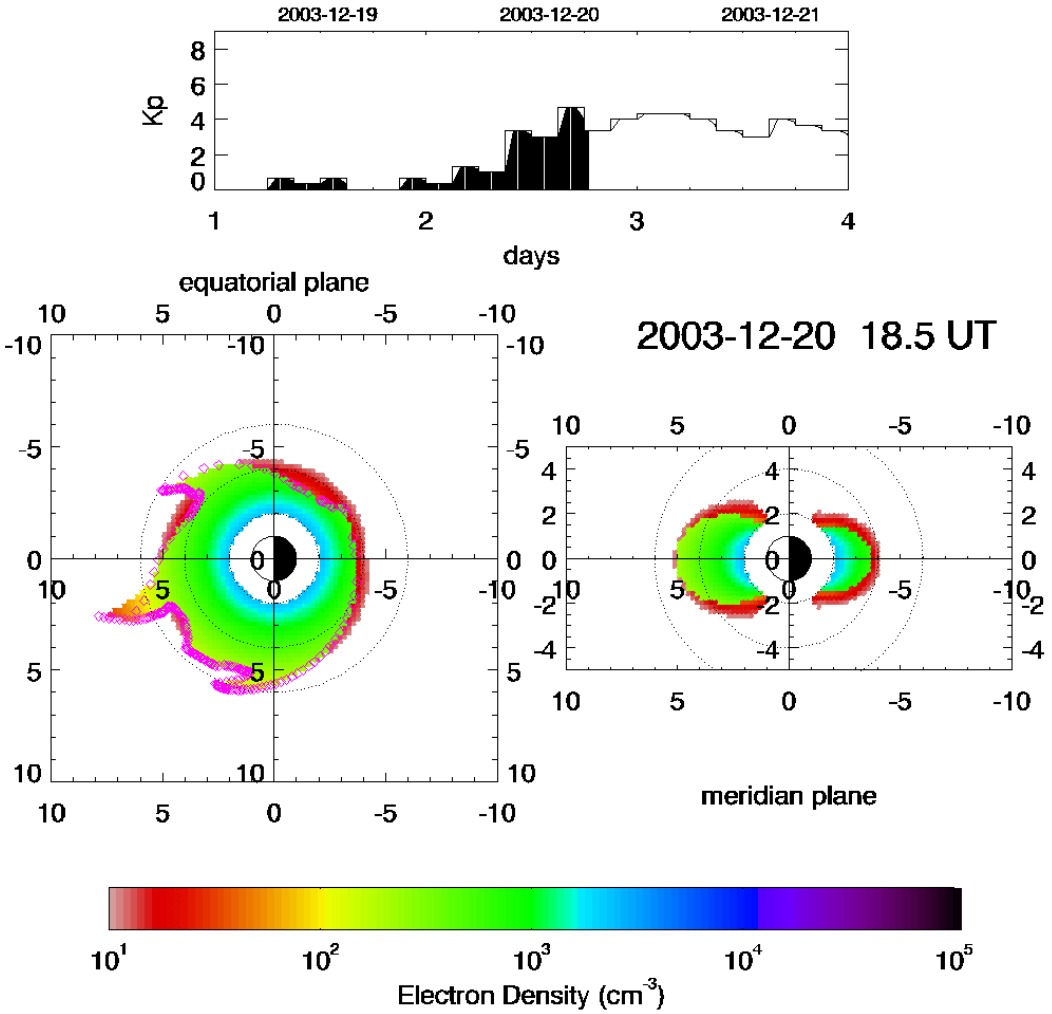

Figure 4.4: (Top) Plot of Kp variation and (bottom) location of the plasmasphere, in R_e scale, as view from a pole (left) and equator (right) corresponding to the 1.11 mHz event detected by Kodiak on December 20, 2003 at 18:50 UT, L-shell=7.07 and MLT=7. Purple diamonds mark the plasmapause. Low plasma density regions (in red) show the position of the plasmathrough. (Picture courtesy of *Pierrard and Stegen* [2008], downloaded from the European Space Weather Portal, ESA)

Another example that agrees with the theory by *Orr and Hanson* [1981] is the 1.1±0.1 mHz FLR event detected by Prince George on November 7, 2003 at 2:06 UT, L-shell=6.86 and MLT=16. Figure 4.5 shows the FLR profile, along -72 degrees magnetic longitude for the amplitude (left) and the phase variation (right) as a function of latitude: The maximum peak is observed at the magnetic latitude 66 degrees and this event presented as "*reverse*" due to the increase of phase variation as a function of latitude. The event was classified as a low-*m* since *m*=8±2 (Figure 4.6). The event was localized in the L-shell=6.86 at MLT=16. Figure 4.7, also downloaded from the ESWP and courtesy of *Pierrard and Stegen* [2008], shows Kp=6 at around that time (top) and the simulation shows that the plasmapause location (purple diamonds) is at L ~ 7 due to a plume around MLT=16. This explains why the FLR event was classified as low-*m*, yet presents a "*reverse*" phase variation due to the sharp density decrease at the plasmapause.

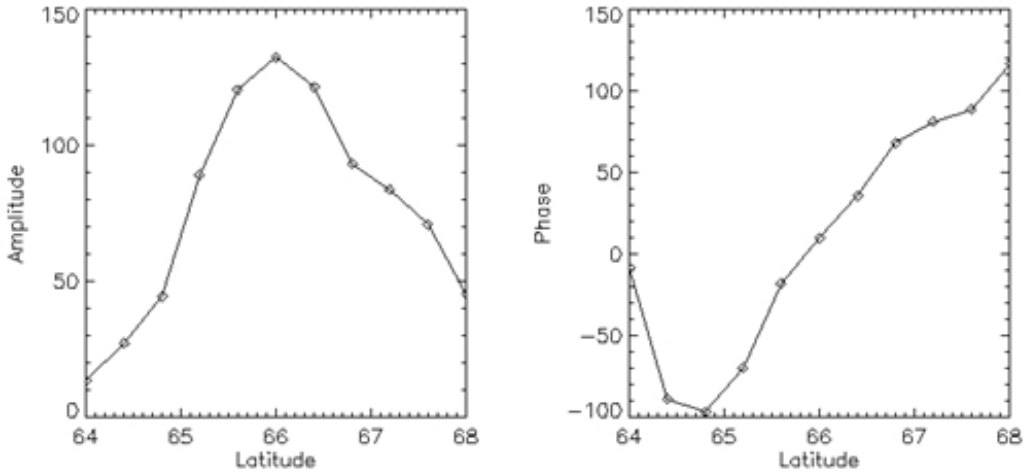

Figure 4.5: Latitude profile of the spectral power (left) and phase (right) at 1.1±0.1 mHz corresponding to the Prince George station on November 7, 2003 (Along -72 degrees magnetic longitude) at 2:06 UT, L-shell=6.86 and MLT=16. The maximum peak is observed at magnetic latitude 66 degrees.

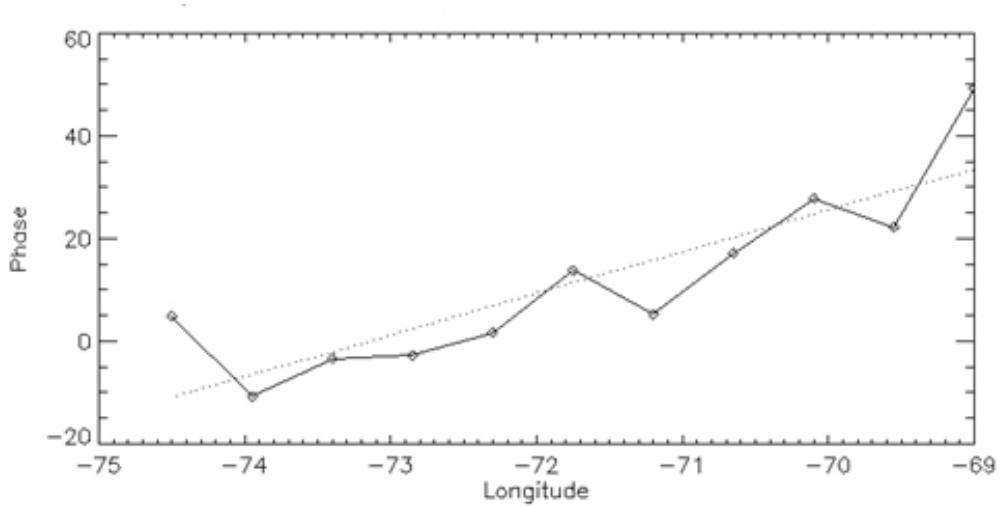

Figure 4.6: Spectral Phase as a function of longitude gives the m-value of the wave at 1.1 (±0.1) mHz corresponding to Prince George on November 7, 2003 (along 66 degrees magnetic latitude) at 2:06 UT, L-shell=6.86 and MLT=16. The slope of this plot gives the azimuthal wavenumber m of the FLRs, and for this event it was determined to be m=8±2.

For the 55 events in this region featuring "*standard*" phase change, 35 of them had $m < 17$, but the rest were events with $m \geq 17$, believed to be driven by particle enhancement that could couple with the waves. Inspection of these events revealed depletion of the plasmasphere and plumes, as well as high Kp, indicating some sort of storm-substorm conditions present at that time, which agrees with that scenario. The puzzling matter is why they all showed "*standard*" phase change profile and that all but 2 occurred in the flanks (characteristics of low-m events), if these events were driven by wave-particle interactions (characteristics of high-m events). Those events should be the object of a more carefully and throughout study.

Finally, for the 53 events, occurring in this region, with "*reverse*" phase change, 31 of them had $m \geq 17$, which agrees with explanation given for high-m events by previous studies; the rest, 22 events, had $m < 17$ with all but one event occurring in the night sector also suggesting that substorm activity might be

responsible for their occurrence and they should each be further examined as 'case studies'.

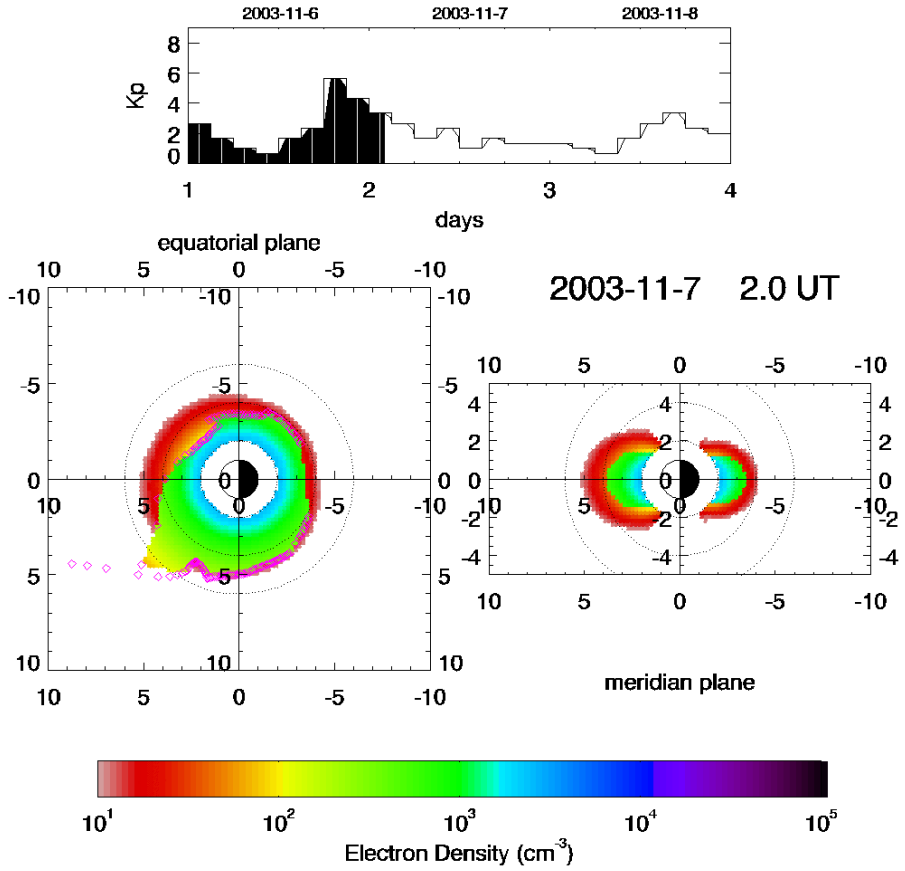

Figure 4.7: (Top) Plot of Kp variation and (bottom) location of the plasmasphere, in R_e, as view from a pole (left) and side (right) corresponding to the 1.11 mHz event detected by Prince George on November 7, 2003 at 2:06 UT, L-shell=6.86 and MLT=16. Purple diamonds mark the plasmapause. Observe the plume at the MLT=16 Low plasma density regions (in red) show the position of the plasmathrough. (Picture courtesy of *Pierrard and Stegen* [2008] for the global plasmasphere. Belgian Institute for Space Aeronomy).

Plot of a distribution of FLRs (Figure 4.8, top) by magnetic latitude vs. frequency, given that ground scattering was substracted from the data, shows that the frequencies, including the most low ones, occurred in a wide range of magnetic latitude (with only one event occurring in an open field line). Considering only FLR events with "*standard*" phase change, low-*m* FLRs are localized in higher latitudes and high-*m* FLRs are localized in lower latitudes (Figure 4.8, right); on the other hand, FLRs with "*reverse*" phase variation, both low-*m* and high-*m*, are evenly distributed across all latitudes. Finding a frequency at different latitudes is compatible with the changes in the length of the field lines (compression/elongation) due to deformities of the magnetospheric cavity produced by the solar wind dynamic pressure, as well as dynamic changes in $\boldsymbol{B}$ strength and plasma density inside the magnetosphere due to geomagnetic activity.

In terms of the theory suggested by *Manger et al.* [2009] that intends to explain the *reverse* phase variations on FLRs due to an alternating currents associated with substorm-injected proton clouds drifting in the magnetosphere in the azimuthal direction, the analysis of particle analysis and substorm activity for the events in the current database is beyond the scope of this thesis, but it would be interesting to be considered in future studies.

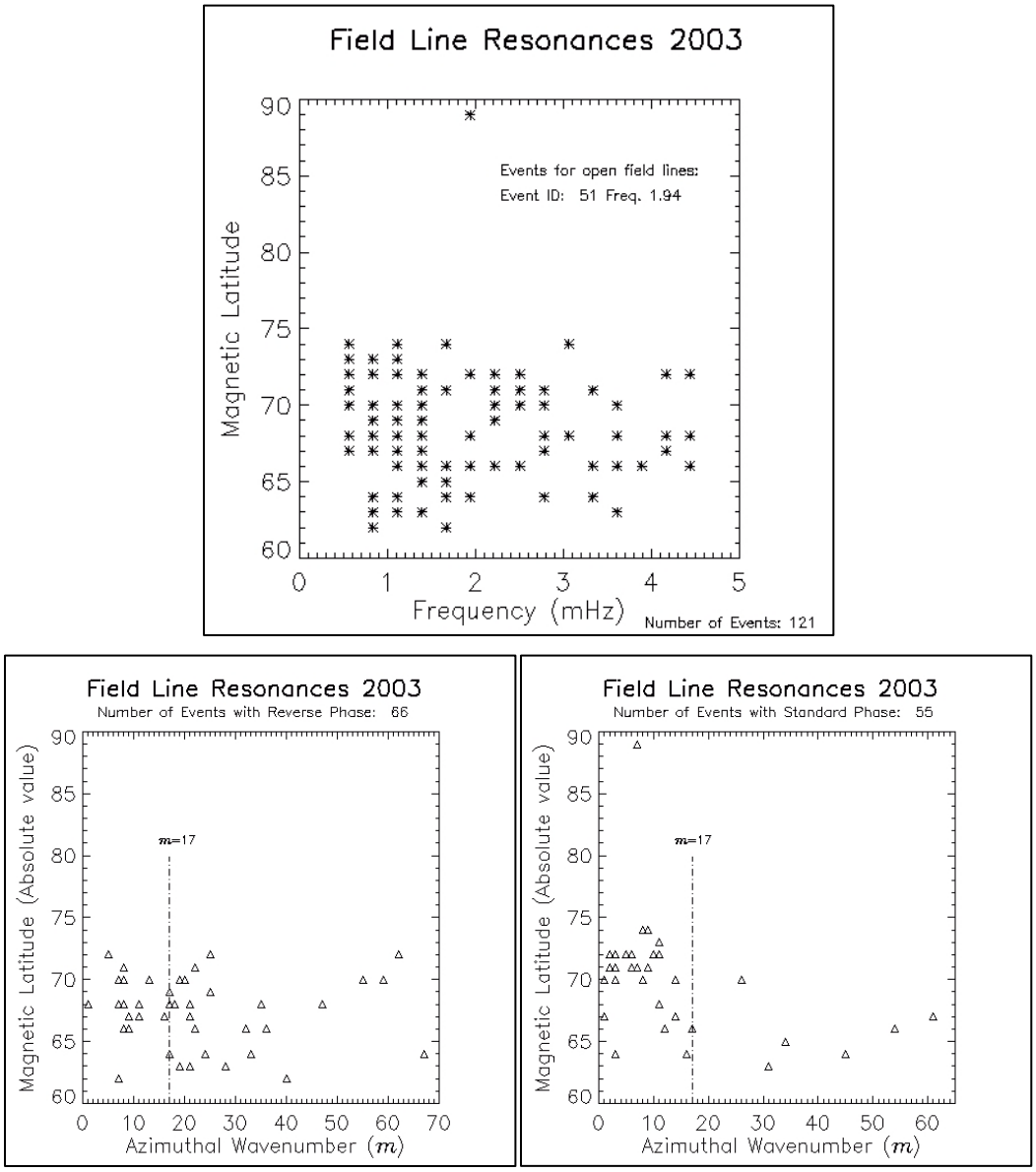

Figure 4.8: (Top) Distribution of FLRs by magnetic latitude vs frequency. (Bottom, left) FLRs with "*reverse*" phase change; (Bottom, right) FLRs with "*standard*" phase change.

To summarize, it is clear that all 13 events located in the plasmapause exhibit a "*reverse*" phase change, regardless of their azimuthal wavenumber *m*, and that further in-depth study is needed for the 108 events that occurred in the plasmatrough, to examine that '*anomalies*' found with respect of the classification given by previous literature that showed that events with low azimuthal wavenumbers located in the plasmatrough should exhibit a "*standard*" phase variation with latitude.

4.1.3 Statistical Analysis of Occurrence vs MLT

Previous studies [*Fenrich et al.,* 1995; *Fenrich,* PhD Thesis, 1997; *Fenrich and Samson*, 1997] have reported that all the FLRs with azimuthal wavenumbers $m < 17$ occurred in the dusk/dawn 'flanks' of the magnetosphere, while most of the FLRs with azimuthal wavenumbers $m \geq 17$ occurred in the dusk-midnight sector an day sector.

In this study, FLRs were not observed at the noon sector since density variations in the ionosphere at MLT noon result in poor backscatter. We found that FLR events are evenly distributed in all other MLT sectors, regardless the value of their azimuthal wavenumber *m*. Figures 4.9 and 4.10 show a representation of the MLT occurrences of the events: high-*m* events correspond to FLRs with azimuthal wavenumbers $m \geq 17$ and low-*m* events to those with $m < 17$. In those figures, the radial position is proportional to their magnetic latitude (outer signifies lower latitude; inwards signifies higher latitudes). This distribution raises the question of the significance of the geomagnetic activity and its role in the transformation of the magnetospheric environment (plasma density, background magnetic field strength, compression of the magnestosphere), added to the effects of wave-particle interaction, and the importance of a case study, in the future, for each of the FLR events found in this study.

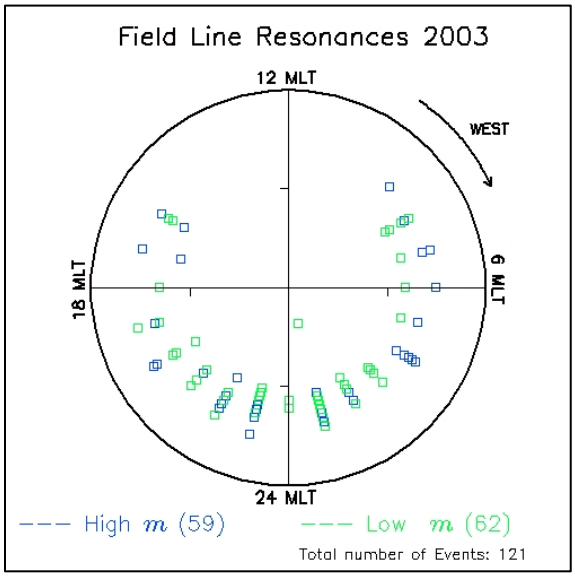

Figure 4.9: Distribution of events as a function of the Magnetic Local Time. The radial position is proportional to their magnetic latitude (outer signifies lower latitude, closer to the equator; inwards signifies higher latitudes, closer to the pole).

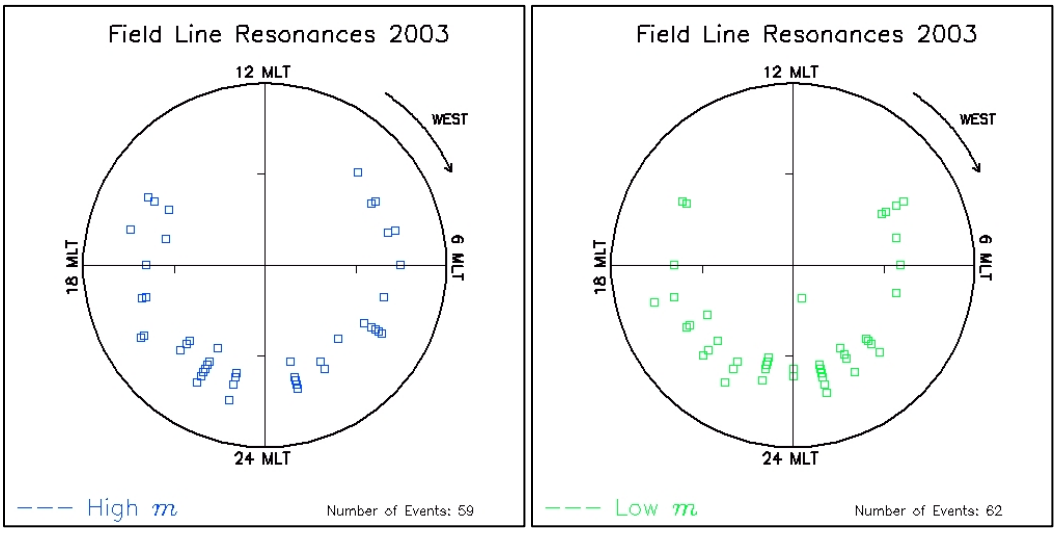

Figure 4.10: Distribution of events as a function of the Magnetic Local Time. Left: high-*m* FLRs; right: low-*m* FLRs.

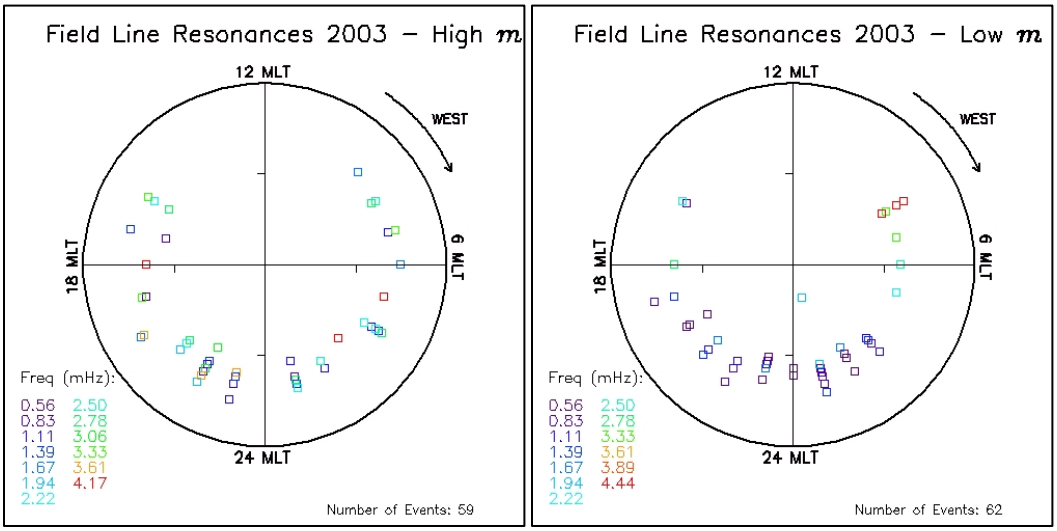

Figure 4.11: Distribution of FLRs as a function of the Magnetic Local Time by frequency (left: high-*m*, right: low-*m*).

Lastly, the distribution of FLRs as a function of the Magnetic Local Time by frequency (Figure 4.11) shows that the majority of low frequency events occurred at midnight, which agrees with the fact that field lines in the night sector are stretched.

4.1.4 Statistical Analysis of occurrences vs. Frequency depending on azimuthal wavenumber

The distribution of FLR occurrences as a function of frequency for FLRs with azimuthal wavenumbers $m < 17$ (Figure 4.12) is similar to the general distribution of events in the database: The frequency with more occurrences in this study is the first frequency of the array, 0.6±0.1 mHz. This result shows good agreement with ground magnetometer observations as presented by *Murphy et al.* [2011]. In that study, 14 years of magnetometer data during solar cycle 23 were analyzed to produce hourly power spectral density (PSD); plots of PSD vs. frequency, for each of the solar cycle phases, all show monotonous decrease, which agrees with

results shown in Figure 4.12. It is worth mentioning that ground magnetometers successfully detect low-*m* ULF waves but they do not detect high-*m* ULF waves due to, for example, the screening in the ionosphere, for which the comparison of these results cannot be extended to the distribution of FLR occurrences for high-*m* FLRs.

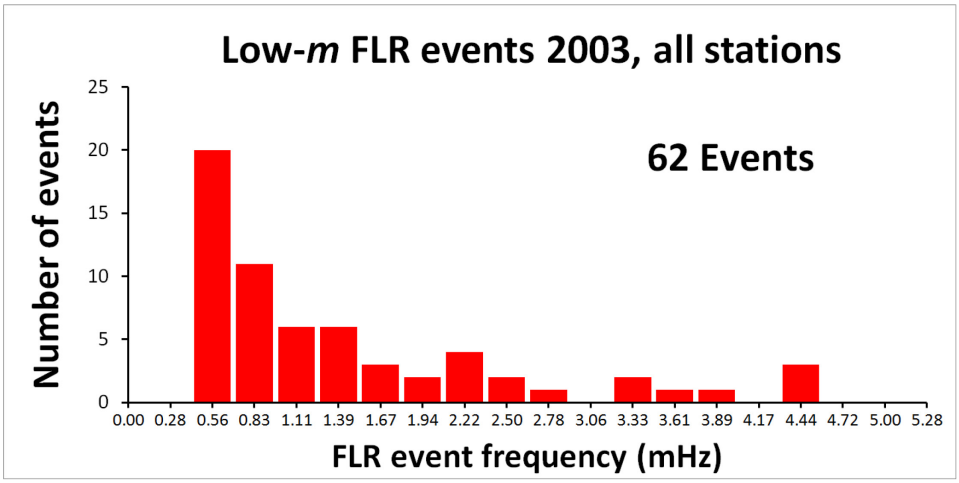

Figure 4.12: Low-*m* (62 events) FLRs occurrence as a function of frequency of the event.

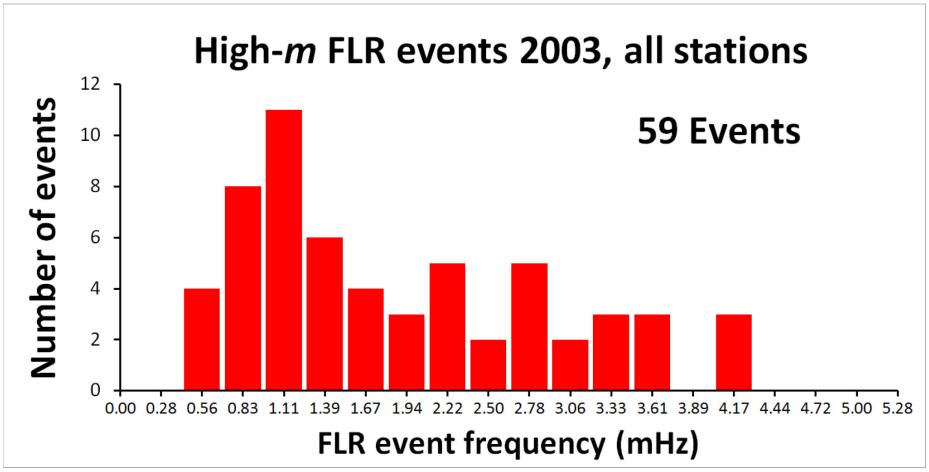

Figure 4.13: High- *m* (59 events) FLRs occurrence as a function of frequency of the event.

Interestingly, the distribution for FLRs with azimuthal wavenumbers $m \geq 17$ (Figure 4.13) shows a maximum around the frequency 1.1 ±0.1 mHz FLR. These events should be the focus of future work that will include particle analysis and substorm activity, since a case-to-case study of the events in the database is beyond the scope of this thesis work.

4.1.5 Propagation of FLRs

Another interesting result of this study is the analysis of the propagation (westward/eastwards, sunwards/antisunwards) of FLRs in the database.

In their studies, *Fenrich et al.* [1995] and *Fenrich* [PhD Thesis, 1997] reported that all observed low-*m* ($m < 17$) FLRs propagated antisunwards. This propagation of low-*m* FLRs was attributed to the fact that they were believed to be originated by surface waves in the flanks, propagating in the same direction that convecting open-field lines. The studies also reported that all observed high-*m* ($m \geq 17$) but one propagated westwards and were believed to be originated by west-drifting ions in the ring current.

In this study, we found that half of the low-*m* FLRs propagated antisunwards, while the other half propagates towards the sun (Figure 4.14, left). Further inspection revealed that most of those events (26 out of 29) exhibited a "*reverse*" phase variation (Figure 4.14, right). On the other hand, two-thirds of the high-*m* FLRs propagated westwards (Figure 4.15, left), with the high-*m* FLRs propagated eastwards mostly located in the night-to-dawn sector (a large number of those latest events, 10 out of 21, displaying a "*standard*" phase variation). However, there were numerous occurrences (9 out of 37) of westward propagating high-*m* FLRs that exhibited a "*standard*" phase variation as well.

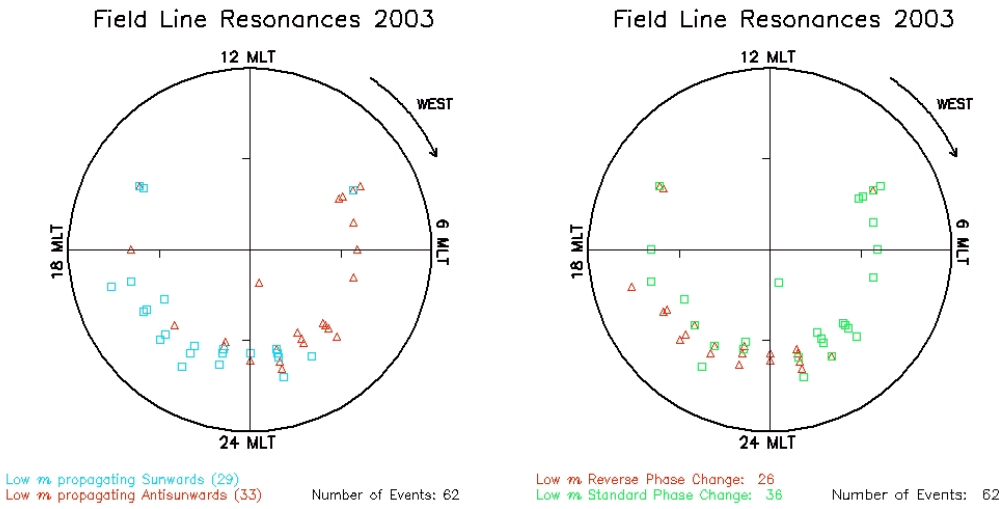

Figure 4.14: Distribution of FLRs with low-*m* as a function of the Magnetic Local Time. Left: FLRs propagating eastwards or westwards; Right: FLRs with reverse or standard phase change

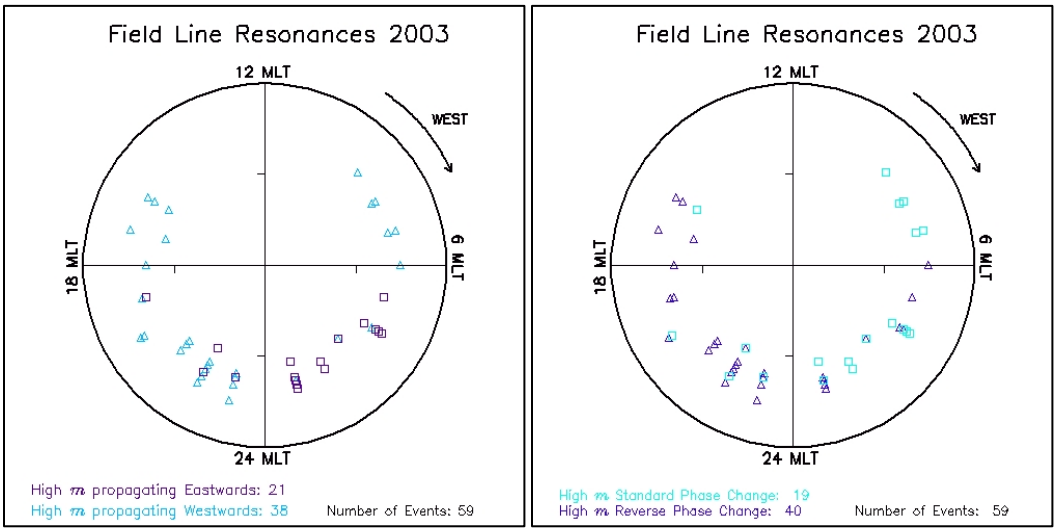

Figure 4.15: Distribution of FLRs with high-*m* as a function of the Magnetic Local Time. Left: FLRs propagating eastwards or westwards; Right: FLRs with reverse or standard phase change.

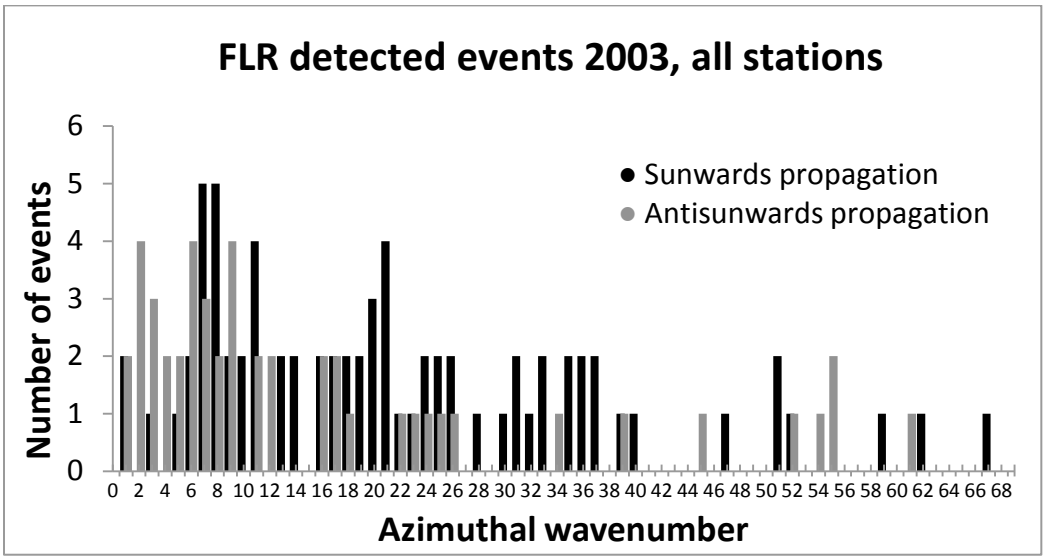

Figure 4.16: Distribution of FLRs as a function of azimuthal wavenumber *m*. Black: FLRs propagating sunwards. Gray: FLR propagating antisunwards.

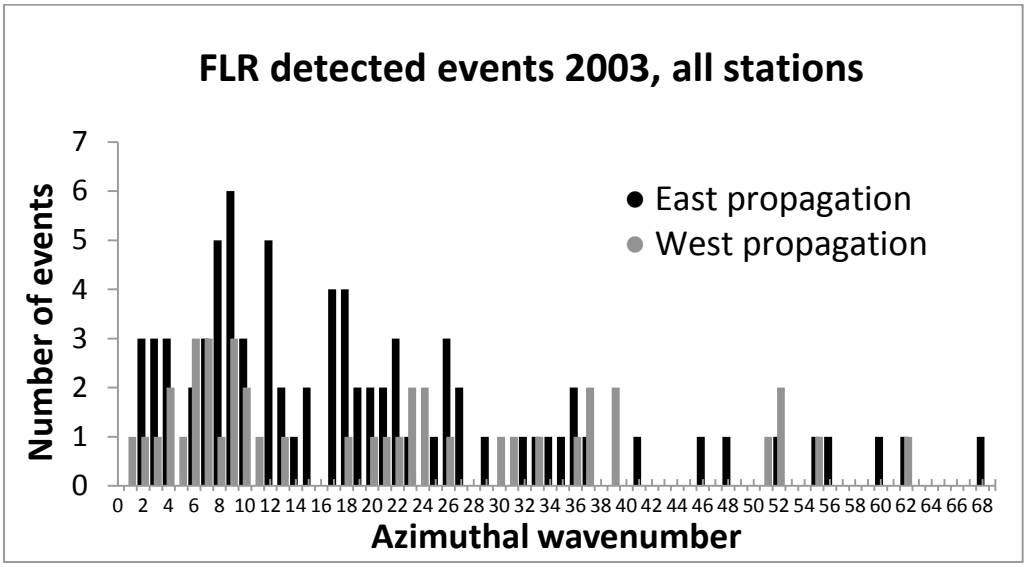

Figure 4.17: Distribution of FLRs as a function of azimuthal wavenumber *m*. Black: FLRs propagating eastwards. Gray: FLR propagating westwards.

Also among the results, we observed that both sunward and antisunward low-*m* are concentrated around *m*=8 (Figure 4.16). FLRs propagating eastward also peaked around *m*=8, while FLRs propagating westward ranged from a wide range of azimuthal wavenumbers (Figure 4.17).

4.2 Summary

In this chapter, we described the process of characterization of the FLRs in the database, as well as the statistical results on these properties. We also provided comparisons with previous characterization studies, presented in the introduction. Interesting aspects of FLRs, which were found in this study, included frequency distribution, latitude of occurrences, *m*-value, magnetic local time.

In terms of frequency distribution, we particularly study if some frequency occurred more often than others. This is an important question, since the repetitive observation of the so called "magic frequencies" are the argument that one uses to find sources of both high-*m* and low-*m* in ULF waves in the solar wind, but their repetitive, discrete nature is not undisputed.

For the 121 FLRs found in this study, 'magic frequencies' (1.3, 1.9, 2.6 and 3.4 mHz) were not particularly observed. The frequency with more occurrences in this study is the first frequency of the array, 0.6±0.1 mHz, with a decreasing trend for increasing frequency. This is compatible with the recent study by *Archer and Plaschke* [2014] on distribution of magnetopause surface waves observed throughout an entire solar cycle.

For FLRs with $m < 17$ we saw a decreasing trend for increasing frequency, which agrees with ground magnetometer observations reported by *Murphy et al.* [2011]. The distribution for FLRs with azimuthal wavenumbers $m \geq 17$ presented

a maximum around the frequency 1.1 ±0.1 mHz FLR. These events should be the focus of future work, since a case-to-case study of the events in the database is beyond the scope of this thesis work, because it would involve studies of particle injection due to substorm activity.

With respect to their magnetic local time for their occurrence, we saw that all FLRs are evenly scattered in all MLT locations, with exception of the noon sector. For the FLRs presented in our database, there was no preference for events to be localized in a specific MLT sector depending on their azimuthal wavenumbers m. We did find that low-m events with low frequencies are localized in the night sector.

We also examined the classification of FLRs given their m-values and the phase variations as a function of latitude, since this is a topic that presents controversy in the field. For the events in our database, results showed that all the events occurring in the magnetopause, as located using the simulations by *Pierrard and Stegen* [2008], exhibited '*reverse*' phase variation regardless of their azimuthal wavenumber m. We also saw that for events in the plasmatrough, two-thirds of the FLRs with "*reverse*" phase change had $m \geq 17$, while the rest with < 17 (exhibited "*standard*" phase change), most of them located between magnetic latitude 65 and 72 degrees; likewise, two-thirds of the FLRs with "*standard*" phase change, most of them located at lower magnetic latitude (62-66 degree), had $m < 17$, while the rest with $m \geq 17$ (exhibited *"reverse*" phase change).

We also studied how often the same frequency is observed at different latitudes and in our results we found the same frequency extended throughout a wide range of latitudes. We infered that variation of plasma density in the tubes, as well as MLT location of the events (due to dynamics in the plasmasphere and

convection of field lines due to solar wind dynamic pressure) might play an important role in finding the same frequency in different latitudes.

In terms of the FLRs' propagation, we found that a half of the low-*m* FLRs propagated antisunwards; the other half propagates towards the sun and most of the events exhibited a "*reverse*" phase variation. On the other hand, two-thirds of the high-*m* FLRs propagated westwards, with the high-*m* FLRs propagated eastwards mostly located in the night-to-dawn sector, a large number of those latest events displaying a "*standard*" phase variation. However, there were numerous occurrences of westward propagating high-*m* FLRs that exhibited a "*standard*" phase variation as well, which it is puzzling.

There are several questions arising from this study. Previous studies might generalize certain characteristics of FLRs, but a large database shows that discrepancies with these generalizations stress the importance of a case-to-case study of all events, which, given the amount of FLRs currently in the database, will extend for a long period of time and it is beyond the time allocated to this thesis research.

Most importantly, significant advances in the deployment and operations of the SuperDARN radars in the past decade as well as improvements in the computational capabilities in the recent years, allow advance data analysis, such the development of the new technique for identification of ULF waves pre-selected for further FLR characterization. A large database compiled by a systematic and automatic detection system provides more precise results than events identified by eye (which might be prone to visual bias in terms of how the group sample is selected) and reveals the urgent need of further in-depth studies of FLRs.

4.3 Conclusions

The new findings in this chapter include:

1) FLRs occurring in the magnetopause (located using the simulations by *Pierrard and Stegen* [2008]), exhibited 'reverse' phase variation regardless of their azimuthal wavenumber m. These results are an important observational validation of the theory proposed by *Orr and Hanson* [1981] and the early radar observations by *Waldock et al.* [1983].

2) 'Magic frequencies' (1.3, 1.9, 2.6 and 3.4 mHz) reported in previous studies corresponded to periods of low geomagnetic activity (low Kp), being a special subset of the larger spectrum of FLRs occurring during quiet and active geomagnetic times. Our study corresponded to a broader range of geomagnetic activity, both with low and high Kp values. The frequency distribution did not depict magic frequency preferences but rather showed a decreasing trend of occurrences for increasing frequency, compatible with the recent study by *Archer and Plaschke* [2014] on the distribution of magnetopause surface waves observed throughout an entire solar cycle and with the study by *Mangus* [2009]. The distribution of FLRs for different geomagnetic activity (measured by the Kp index) did not reveal magic frequencies either but rather showed a poisson distribution for events detected during quiet geomagnetic activity and a power law for events occurring during geomagnetic active times.

Chapter 5

ULF waves in the solar wind as possible sources of Field Line Resonances

The third and final main goal of this thesis research was to test what percentage of FLRs in the database were driven directly by ULF waves in the solar wind. Several case studies have been conducted in the past 20 years which showed that the ULF waves in the magnetosphere appeared to be directly driven by ULF waves in the solar wind [*Stephenson and Walker*, 2002*; Kepko et al.*, 2002*; Kepko and Spence,* 2003*; Fenrich and Waters*, 2008; *Viall et al.*, 2009; *Mthembu et al.*, 2009; *Stephenson and Walker*, 2010]. The motivation of this hypothesis was initially based on the claim that discrete, stable FLRs were often observed in Earth's magnetosphere [*Fenrich and Waters*, 2008*; Fenrich and Samson*, 1997]. It is disputed that these 'magic frequencies' occurred more often than others. The results presented in the previous chapter made a strong case for the contrary. However, the large FLR database collected in this study was the perfect tool to systematically test the hypothesis that FLRs are directly driven by ULF waves in the solar wind.

The FLRs' wave sources have been under debate for over 15 years and numerous authors have proposed possible mechanisms. *Dungey* [1954] proposed Kelvin-Helmholtz vortices, excited by solar wind, travel along the magnetosphere. Surface waves can be created by the flow of the solar wind

around the magnetopause. Compressional coupling of field lines at the magnetopause and field lines inside the magnetosphere would set the latter into oscillations, while receiving energy from the former. The theoretical studies of these processes were conducted by *Southwood* [1974] as well as *Chen and Hasegawa* [1974]. Successful observations of this mechanism were reported using ground observations [*Samson and Rostoker*, 1972] and spacecraft observations [*Perraut et al.*, 1978; *Takahashi and McPherron*, 1982; *Takahashi, McPherron and Hugues*, 1984]. Kelvin-Helmholtz instabilities in the magnetic field of the Earth fails to explain, however, the reproducibility of the observed discrete frequencies of ULF pulsations [*Provan and Yeoman*, 1997; *Fenrich and Samson*, 1997].

Kivelson and Southwood [1985] and *Allan and Poulter* [1989] suggested a cavity mode responsible for discrete FLRs. In this scenario, the magnetosphere is a cavity that can resonate at its discrete frequencies as the magnetosphere responds to abrupt changes in solar wind dynamic pressure. This theory failed to explain stable, discrete FLRs claimed by some studies: The magnetosphere changes size continuously, due to solar wind variability and a continuum of frequencies should be observed.

Given the lack of observational evidence [*Mthembu et al.*, 2009] for the cavity mode theory in mid-80's and early 90's, *Walker* [1992] proposed that the magnetosphere was not a closed cavity but rather an open-ended waveguide with boundaries in the magnetopause and turning points where the Alfven waves are reflected. This new theory of the open-ended waveguide was supported by observations [*Mathie and Mann*, 2001; *Engebretson et al*, 1992].

The sections below describe the methodology used to evaluate the coherence between ULF waves in the solar wind and FLRs in four steps: First, the correlation of the times series was evaluated (section 5.1.1.); second, the power

spectra of the series was inspected (section 5.1.2.); third, an evaluation of the band-pass signal and analytic signal was conducted (section 5.1.3); finally, the cross-power and cross-phase of both series were calculated and assessed to establish the level of coherence (section 5.1.4). Results are discussed in section 5.2 and the chapter is closed with a summary in section 5.3.

5.1 Methodology

In this thesis, solar wind properties were studied using measurements taken on board the Advanced Composition Explorer (ACE), a mission launched by NASA in 1997. ACE is located in the Sun-Earth Lagrangian Point 1 (L-1) about 1.5 million km (0.1 AU; 235 R_e) from Earth and 148.5 million km from the Sun. ACE carries three instruments: the "Solar Wind Electron Proton Alpha Monitor" (SWEPAM), the "Energetic, Proton and Alpha particle Monitor" (EPAM), and two magnetometers (MAG). Further details of the ACE spacecraft and the instruments on board can be found in *Stone et al.* [1998], *McComas et al.* [1998], and *Smith et al.* [1998].

Table 5.1: Solar wind parameters as recorded by spacecraft ACE

Solar Parameter	Units	Instrument
Proton Density	cm^{-3}	SWEPAM
Proton Speed	km/s	SWEPAM
Vx	km/s	SWEPAM
Vy	km/s	SWEPAM
Vz	km/s	SWEPAM
Magnetic Field	nT	MAG
Bx	nT	MAG
By	nT	MAG
Bz	nT	MAG

Table 5.1 shows a list of solar parameters used, in this project, to study solar wind coherence with FLR events. SWEPAM gives 64-second Average Solar Wind Ion Parameters, while MAG gives 16-second Averaged Interplanetary Magnetic Field Data. Level 2 raw data, in binary form, was directly downloaded from the ACE website and processed using IDL procedures.

In the study of correlation and coherence of the solar wind time series and the SuperDARN Doppler velocity time series, delay-times corresponding to solar wind travel times from the satellite to the magnetopause, plus propagation times of the compressional waves throughout the magnetosphere, should be taken into account.

Solar wind travel times from the location of ACE to the magnetopause vary with solar wind speeds [*Weimer et al.* 2004]. Usually, travel times range from 30 minutes to 80 minutes. Table 5.2 shows some travel time's estimates for typical solar wind speeds, calculated from ACE's location to an average magnetopause location of 10 R_e, following the study in *Weimer et al.* [2004]. These are only estimates, since magnetopause location varies with solar wind dynamic pressure which depends not only on solar wind speeds but also on solar wind ion density.

Table 5.2: Estimate of travel times from ACE to magnetopause

Solar Wind Speed (km/s)	Travel time (Minutes)
300	80
400	60
400	60
500	48
600	40
700	34
800	30

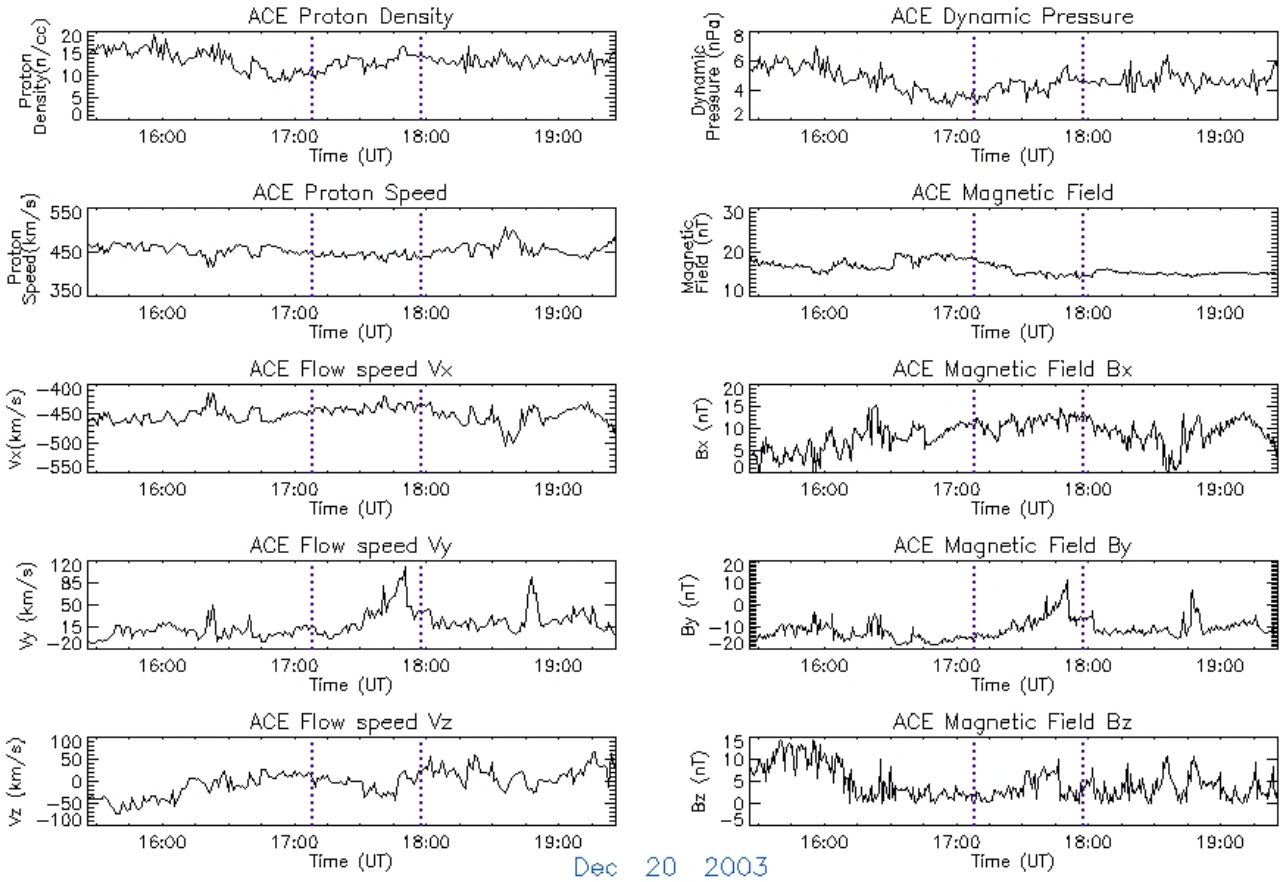

Figure 5.1: From top to bottom and from left to right, plots of the solar wind proton density, proton speed, V_x, V_y, V_z, Dynamic Pressure, Magnetic field, B_x, B_y, B_z, corresponding to December 20th 2003. Dotted lines correspond to intervals between 30-80 minutes prior the beginning of the one hour 1.1 mHz FLR event detected by Kodiak.

When comparing ACE solar wind measurements with observations from SuperDARN, there should also be an extra time delay, added to the travel time, to account for propagation times of compressional waves through the magnetosphere to resonant field lines. Propagation times from the bow shock nose through the magnetosheath and through the magnetopause to the ground depend on local Alfvén speeds and they have been reported in similar correlation and/or coherence studies to range between few minutes (2 minutes for *Mthembu et al.* [2009], 5 minutes for *Kepko et al.* [2002]) to several minutes (15 minutes for *Fenrich and Waters* [2008]). For their study, *Fenrich and Waters* [2008] stated that changing the propagation time, throughout the magnetosphere, from 1 minute to 30 minutes did not change their result of coherence.

In this study, solar wind data were interpolated to fill in gaps corresponding to bad or missing data-points flagged in the dataset. Figure 5.1 shows plots of the proton density, proton speed, V_x, V_y, V_z, Magnetic Field, B_x, B_y, and B_z, corresponding to the Dec 20th 2003 event. Dotted lines in the solar parameter plots correspond to interval of times 30-80 minutes prior the FLR event. The following sections explain the methodology used to study the possible coherence between ULF waves in the solar wind with FLRs.

5.1.1 Step 1: Correlation of the time series in the time domain

The first step in the study of the coherence between solar wind ULF waves and FLRs in the magnetosphere was to evaluate the correlation among the time series.

Kepko et al. [2002] studied the correlation between the time-series of solar wind number density and dynamic pressure measured by the Wind spacecraft with the ULF pulsations detected by the geosynchronous GOES satellite. In their study, they presented two events in which both solar wind time-series (number

density and dynamic pressure) exhibited high correlation coefficients, of the order of R~0.9, with the ULF measurements inside the magnetosphere, when appropriately time-shifted. These results, added to the excellent agreement they found on the power spectral peaks, led them to the conclusion that the solar wind is, at least in some cases, a direct source for discrete ULF pulsations in the magnetosphere.

In general, correlation coefficients below 0.5 correspond to 'poor correlation', correlation coefficients between 0.5-0.7 correspond to 'good correlation' and correlation coefficients above 0.7 are considered 'excellent correlation'. For each FLR event, the raw solar wind time-series of each solar wind parameters were interpolated to the times for the SuperDARN Doppler velocity corresponding to the event, given that the time resolution for some solar parameters was either 64 minutes or 16 minutes. A one-hour Doppler velocity sliding window corresponding to the FLR event was overlap to a one-hour segment of the solar wind parameter and the correlation was calculated. Records of the correlation coefficients were collected as the Doppler velocity window slid through the solar parameter dataset.

The maximum correlation corresponding to lags between 80 minutes and 30 minutes prior the beginning of the event (defined as '*default time interval*') was automatically detected and registered. Additionally, the maximum correlation coefficient within the time interval centered at the *delay-time* (defined as the time elapse between lags corresponding to travel time and the lags corresponding to the addition of the travel time and the propagation time) was automatically found. The travel time from ACE to the magnetopause for each of the events was calculated following the minimum variance method of *Weimer et al.* [2003]. For this procedure, a one-hour solar wind average calculated with the data between two hours to one hour prior the beginning of the FLR event was used. The propagation time was estimated to be half hour. Therefore, to account

for varying propagation times within the magnetosphere, an interval of half hour was added to the travel time to obtain the *delay-time*.

Figure 5.2 shows a plot of the solar wind proton density as measured by ACE-SWEPAM (top panel) and the SuperDARN Doppler velocity time series (second panel). The bottom panel on this figure shows the cross-correlation of the one-hour moving window with the time signal. The correlation coefficient corresponding to lags between -80 and -30 (80 minutes to 30 minutes prior the occurrence of the FLR event) was found at lag -58 minutes and the correlation coefficient corresponding to that lag was to be R=0.23, which shows no correlation between the proton density and the Doppler velocity time series.

For this FLR event, the travel time was calculated to be 55 minutes and therefore the *delay-time interval* was set in the interval 70±15 minutes (between 85 minutes and 55 minutes) prior the event, to account for propagation of the wave inside the magnetosphere. The lag that corresponds to the largest value of correlation in that delay-time interval and the corresponding correlation coefficient were coincidentally 58 minutes prior the event and R=0.23 respectively, given that the delay-time interval mostly overlaps with the default time interval. Notice that there is another relative maximum peak in the interval between -30 and 0 minutes, but was not considered because it falls outside of the delay-time interval.

For this event, similar poor-correlation was exhibited for all the other solar parameters. The correlation coefficients within the delay-time calculated for the event were: for proton speed, R= 0.47 (at lag -76); for V_x, R =0.38 (at lag -84); for V_y, R = 0.25 (at lag -76); for V_z, R =0.33 (at lag -58); for B_x, R =0.35 (at lag -83); for B_y, R = 0.28 (at lag -76) ; for B_z, R =0.5 (at lag -80); for magnetic field magnitude R =0.22 (at lag -56); lastly for the dynamic pressure was R = 0.29 (at lag -55).

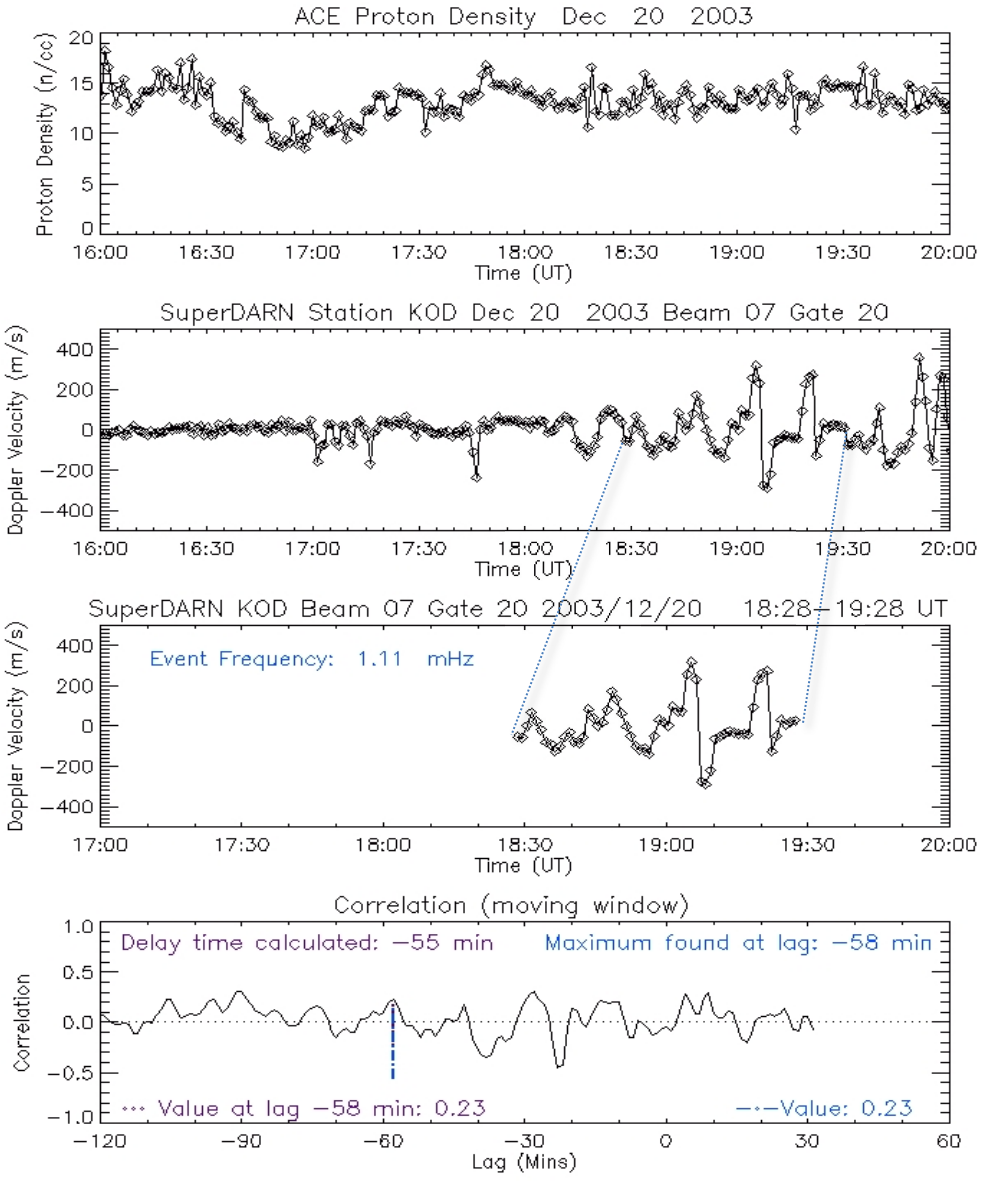

Figure 5.2: Plot of the solar wind proton density component (top panel), the Kodiak Doppler velocity backscatter (second panel), one-hour window used for the correlation (third panel) and the correlation plot (bottom panel). Poor correlation (R=0.23) was found between the solar wind proton density signal and the one-hour window corresponding to the FLR event with a delay of 58 minutes between the 1.1 mHz solar wind proton density wave and the FLR.

The maximum correlation coefficients found for the default time interval (absolute-maximum correlation coefficient found any time between 80 and 30 minutes prior the event) were: proton speed, R= 0.47 (coincidentally at lag -76); for V_x, R =0.24 (at lag -32); for V_y, R =0.44 (at lag -31); for V_z, R =0.33 (coincidentally at lag -58); for B_x, R =0.26 (at lag -32); for B_y, R = 0.41 (at lag -31); for B_z, R =0.5 (coincidentally at lag -80); for magnetic field magnitude R =0.27 (at lag -40); lastly for the dynamic pressure was R =0.34 (at lag -43).

The procedure was systematically applied to all FLR events. Results and discussions of this methodology will be presented in the results' section, section 5.2.

5.1.2 Step 2: Power spectra evaluation

The second step in the study of the coherence between solar wind ULF waves and FLRs in the magnetosphere was to evaluate the power spectra of the two time series.

Step 1 was conducted just to compare the results of *Kepko et al.* [2002] with the implementation of that methodology in the large database of FLRs. However, correlation between two times-series is often not a good indicator of the similarities between two signals and does not indicate causality: Spectral analysis could produce good agreement at a specific frequency, while in the time-domain poor correlation is found.

In the case of Field Line Resonances, the hypothesis to be tested is if solar wind ULF waves 'drive' the FLRs, which implies that the driven frequency found in the solar wind should match the natural eigenfrequency of the field line. If the eigenfrequency of the field line is not found in solar wind ULF waves, within some physical-reasonable *delay-time* (travel + propagation), then the cause of the FLR is other than ULF waves in the solar wind, or at least other mechanisms are necessary to complement the process of excitation of FLRs. This technique

was conducted to compare results with the studies conducted by *Viall et al.* [2009]. The study referred to statistical analysis of spectral distributions for long periods of times in the solar wind and the FLR occurrences (such as the ones conducted by *Mann et al.*, 2004; *Pahud et al.*, 2009; *Murphy et al.*, 2011) and stated that similarity in enhancement in the occurrence distribution of spectral peaks suggested a physical relationship between frequencies observed in the solar wind number density and those observed in the magnetosphere did not demonstrate causality . *Viall et al.* [2009] pointed out that to make an important connection between solar wind waves and FLRs, an estimate of how often the solar wind drives discrete oscillations in the magnetosphere was needed. The authors asserted they found significant spectral peaks both in the solar wind and in the magnetosphere for 54% of the cases for 11 cases analyzed in that study.

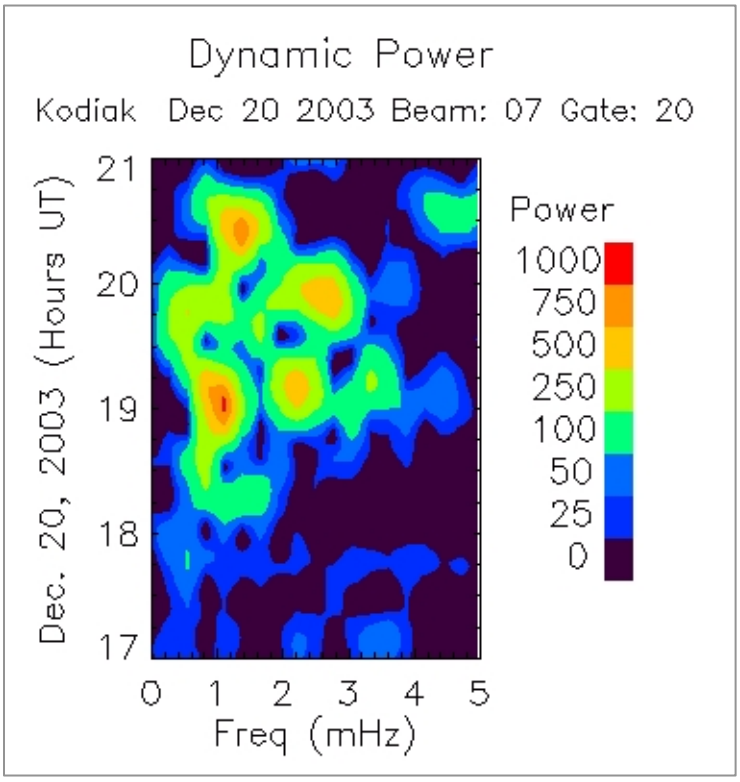

Figure 5.3: Spectrogram of Kodiak Doppler velocity backscatter.

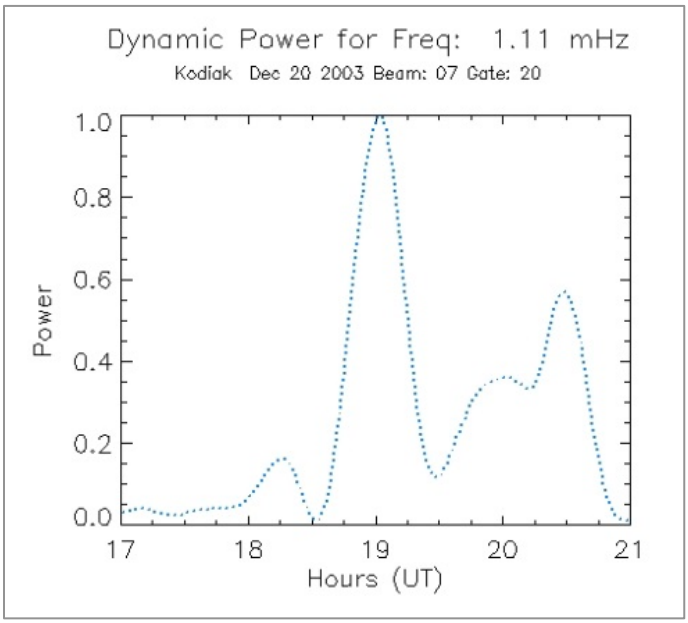

Figure 5.4: Kodiak Doppler velocity backscatter power spectrum corresponding to December 20, 2013 for frequency 1.1 mHz, between 17-21 UT.

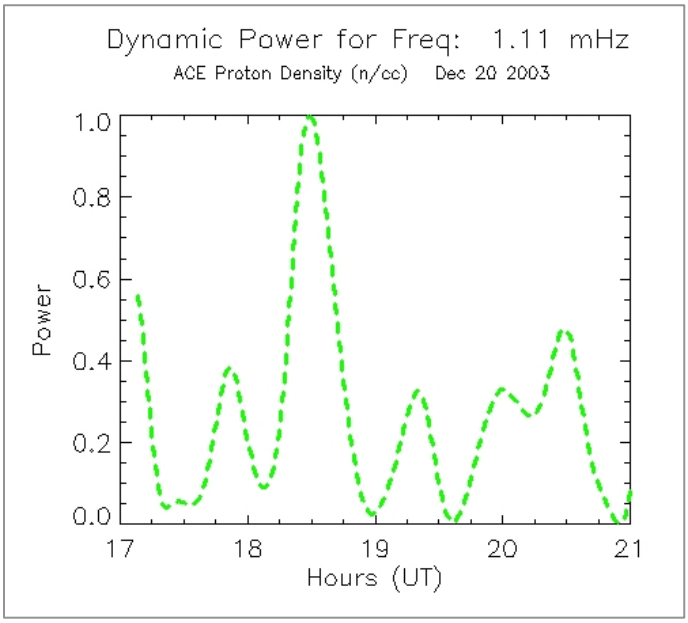

Figure 5.5: Power spectrum of the solar wind proton density corresponding to December 20, 2013 for frequency 1.1 mHz, between 17-21 UT.

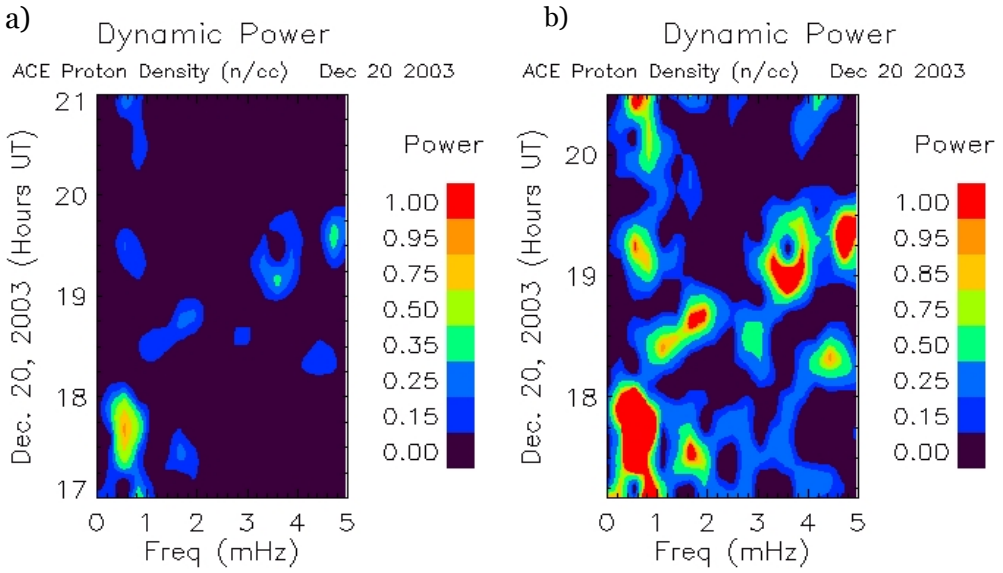

Figure 5.6: Spectrogram of the solar wind proton density corresponding to proton density a) normalized to the power for 0.6 mHz local maximum at approximately 17:30 UT and b) normalized to the power for the 1.1 mHz local maximum at around 18:29 UT

For the spectral evaluation, the data series for both the solar wind and SuperDARN were linearly interpolated to eliminate gaps; the data were also detrended, to eliminate low frequency trends, by subtracting a half-hour running average. The dynamic power was obtained by calculating the discrete-time short-term fast Fourier transform with a Hanning weighting and a 1 point shift (to reduce the spectral leakage created by the one hour sliding window utilized to calculate the dynamic power).

Figure 5.3 shows a plot of the spectrogram for Kodiak Doppler velocity backscatter corresponding to beam 7, gate 20 on December 20, 2003 between 17UT and 22UT. Around this time, four FLRs were identified and classified, as detailed in chapters 3 and 4, corresponding to events 105 and 106a-c. The FLRs had frequencies of 1.7 mHz (18:13-19:13 UT), 1.1 mHz (18:28-19:28 UT), 2.8 mHz (20:37-21:37 UT), and 1.7 mHz (20:36-21:36 UT), respectively. Dominant frequencies for all 4 FLRs are visible in the spectrogram for Kodiak Doppler

velocity backscatter, although event 105 (f=1.7 mHz starting at at 18:13 UT) is less prominent in the spectrogram than the other three FLRs because of normalization of the power within the period plotted. The maximum power observed in this 4-hour interval is found for event 106b corresponding to the 1.1 mHz FLR occurring between 18:28-19:28 UT.

The cross-section of the power spectrum at 1.1 mHz for the Kodiak Doppler velocity backscatter normalized power, corresponding to event 106b, is shown in figure 5.4: The maximum power for the 1.1 mHz frequency in this 4-hour interval is found at 19:02 UT.

Similar normalized power spectrum was obtained for the proton density for 1.1 mHz in that time interval: figure 5.5 shows that the proton density dynamic power exhibits a prominent local maximum at 18:29 UT. Even though these two power spectra seem to agree at first sight, the *time delay* (time difference) between both maxima is below the travel time of the ULF wave from ACE to the magnetopause, calculated to be at least 55 minutes. Furthermore, the spectrogram for the proton density shows that the 1.1 mHz local maximum at around that time only lasts for a short period of time and is not the dominant frequency in the solar wind in this 4-hour time interval; rather, the dominant frequency in this 4-hour time interval is 0.6 mHz at around 17:15-18 UT, as shown in figure 5.6 (a). A possible candidate to drive the FLR at 1.1 mHz is an enhancement of power found in the proton density spectrogram at the 1.1 mHz frequency at around 17:50 UT, with a value of 0.25 in the normalized scale shown on the figure 5.6 (b). Notice that the power enhancement at that time for that frequency is not a local maximum. It is puzzling that a 0.6 mHz solar wind ULF wave with strong power between 17-18 UT excites no FLR in the magnetosphere, while, an hour later, a 1.1 mHz solar wind ULF wave with less power would be able to drive a discrete FLR. These results might suggest that some specific magnetospheric configurations (such as uniform plasma distribution in the flux tubes or previous excitation of the magnetosphere at the driven frequency) would

need to be met to drive FLRs and/or that additional mechanisms (such as surface waves), other than ULF waves in the solar wind, should be involved in driving the FLRs.

5.1.3 Step 3 : Examination of the Band-pass signal and Analytic signal

The third step in the study of the coherence between solar wind ULF waves and FLRs in the magnetosphere was to examine the band-pass and analytic signals for both ACE and SuperDARN at around the time of the event.

When a *modulating signal* (in this case the time series for ACE and SuperDARN) is bandpass with some *passband* concentrated about a *Carrier frequency* f_c, the modulated signal has a spectral magnitude that is nonzero for frequencies corresponding to that *passband*. The narrowband signal, then, will describe wave-packets corresponding to f_c if there is a wave of this frequency in the period considered. The calculation of the analytic signal of the narrowband signal describes the envelop enclosing the wave-packets; the amplitude and phase of the analytic signal represent the instantaneous amplitude and instantaneous phase of the signal, respectively. The packet structure grows and decays in time with the analytic signal's amplitude, and the frequency is remarkably constant when the amplitude is large [*Walker et al.*, 1992].

Chapter 3 of this thesis focused on the application of these properties to find FLRs in the magnetosphere. Moreover, these properties have been utilized in the study of ULF waves in the solar wind and in the magnetosphere around the frequency of interest. *Stephenson and Walker* [2002] used this technique to calculate the instantaneous energy flux in the solar wind, as measured by WIND, in bands corresponding to frequencies of four FLRs detected by the SuperDARN SHARE radar on April 1997. By finding the same frequencies in the solar wind, with a compatible delay time of 70 minutes, they concluded that there was

"*evidence that, at least on this occasion, the field line resonances were directly driven by oscillatory power incident on the solar wind*". Years later, *Stephenson and Walker* [2010] repeated their studies with another FLR detected by SHARE in June 2000, with similar results. In this study, the correlation on two signals with a very narrow band passed filter was utilized to study the delay times between wave packets in the solar wind and those in the magnetosphere that correspond to FLRs.

The time series for both ACE and SuperDARN were bandpass around the FLR's frequency, with a passband corresponding to frequencies in the interval defined as f_{FLR}-0.14< f_{FLR}< f_{FLR}+0.14. The analytic signal was obtained as described in chapter 3. Figure 5.7 shows a plot of the band-pass signal corresponding to the proton density (top panel, a), the Kodiak Doppler velocity backscatter (middle panel), and the correlation plot (bottom panel) for the 18:28-19:28 UT sliding window of the SuperDARN signal over the solar wind signal. The highest correlation (R=0.96) is found at a time difference of 45 minutes between wave packets, outside of the delay time interval (lag: -70±15) while correlation seems to be in its minimum for the throughout the delay time interval.

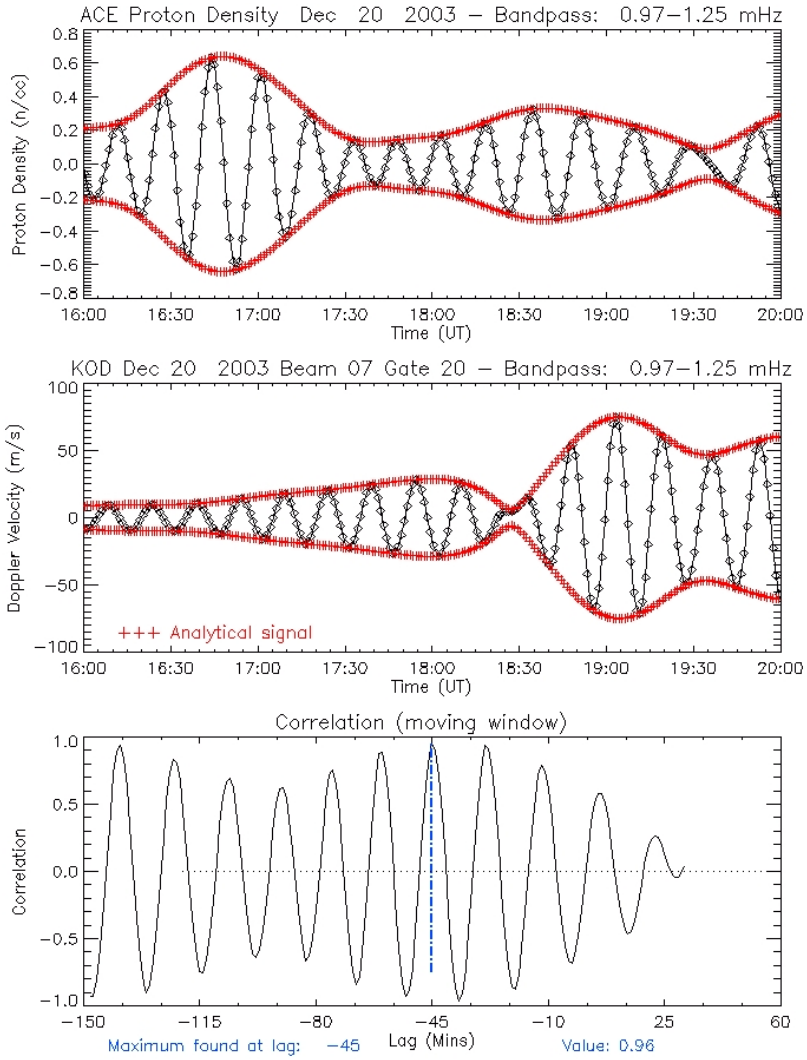

Figure 5.7: Plot of the band-pass signal corresponding to the proton density (top panel), the Kodiak Doppler velocity backscatter (middle panel), and the correlation plot (bottom panel) for the 18:28-19:28 UT sliding window of the SuperDARN signal over the solar wind signal. The highest correlation (0.9) is found at a time difference of 45 minutes in the wave packets, while correlation seems to be in its minimum throughout the delay time interval (lag: -70±15).

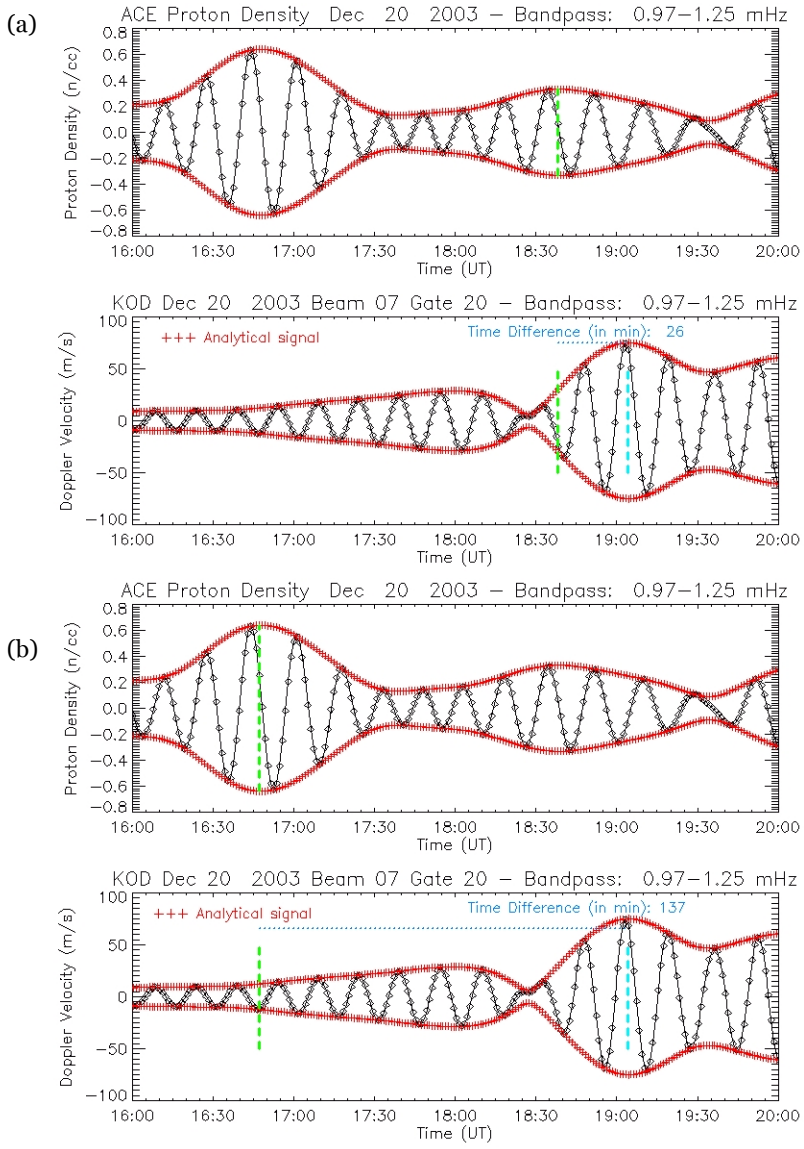

Figure 5.8: (a) Plot of the proton density band-pass signal (top panel, a) and the Kodiak Doppler velocity backscatter band-pass signal (bottom panel, a), centered at f_{FLR} =1.1 mHz, between 16 UT and 20UT on December 20, 2003. Time difference between wave packets is 26 minutes, less than the travel time. (b) Same plot as (a). Time difference between the event and the large wave package in the solar wind is 137 minutes, much larger than the calculated delay time interval (70±15 min).

Figure 5.7 (a) shows the same band-pass signals, corresponding to the proton density (top panel, a), the Kodiak Doppler velocity backscatter (bottom panel, a), with a time difference of 26 minutes between the maximum amplitude of both wave packets. Please notice the large wave package corresponding to f_{sw}= 1.1 mHz for the solar wind is found at approximately 16:50 UT, 137 minutes prior the FLR event (Figure 5.7, b). If ULF waves in the solar wind drive FLRs in the magnetosphere, wave packets in the solar wind corresponding to a driving frequency matching the natural frequency of the FLR would be found in a physically compatible time interval. If that is to be true, this event shows that the calculation of the travel time is not accurate and longer or shorter time travels should occur.

5.1.4 Step 4: Cross-power and Cross-phase evaluation[3]

The fourth and final step in the study of the coherence between solar wind ULF waves and FLRs in the magnetosphere was to evaluate the cross-power and cross-phase of the two signals, a technique developed by *Fenrich and Waters* [2008]. In their study, *Fenrich and Waters* [2008] showed a 1.7 mHz FLR detected by the SuperDARN station Kodiak on November 21, 2003 that exhibited phase coherence with a 1.7 mHz ULF proton density wave, as detected by ACE SWE. The authors explained that *'if two data sets are correlated and exhibit a high degree of phase coherence as a specific frequency then the cross-phase measurements will be approximately constant with time'*, since *'the cross-power spectrum of two time series is the discrete Fourier transform of their cross-correlation and the cross-phase yields the phase difference between the two time series at each frequency [Ramirez, 1985]'*.

[3] All codes in this section are largely modified versions of the original codes developed by F. Fenrich (IDL based)

For their event, *Fenrich and Waters* [2008] calculated a travel time of the solar wind proton density as approximated 50 minutes and they added a 15 minutes to account for propagation time within the magnetosphere. After shifting the proton density signal by the 65 minute time-lag, they observed high dynamic cross-power and low dynamic variance in cross-phase among the two signals at the time and frequency of the event, compared to simulated proton density and Doppler velocity red noise. Red noise was used in the study to show the 5% significance levels because it is characterized by a $\frac{1}{f^2}$ power law, similar to solar wind, as shown in *Goldstein and Roberts* [1999]. *Fenrich and Waters* [2008] stated that 'delay-times between 51 minutes and 80 minutes yielded similar results'.

In their studies, *Fenrich and Waters* [2008] found that not only the proton density exhibited coherence with the FLR but also ACE total magnetic field measurements showed coherence as well. The total magnetic field was 180° out of phase, which was an indication of a slow mode type compressional MD wave possibly responsible to drive the FLR. The IMF B_y was dominant, indicating reconnection in the flanks; the FLR had westward phase propagation from dusk which was '*consistent with a source such as solar wind MHD compressional wave transmission through a dusk flank reconnection region*' [*Fenrich and Waters*, 2008].

In this current study, we followed, step-by-step, the procedure detailed in *Fenrich and Waters* [2008], with the addition that the cross-power and cross-phase technique was systematically implemented, for comparison reasons, using three different time-lags, illustrated in the schematics shown in figure 5.9:

a) The solar wind time-lag was determined by 15 minutes added to the travel time calculated using the minimum variance method of *Weimer et al.* [2003] (to replicate the study by *Fenrich and Waters* [2008]),

b) The time lag was determined as the time difference between the FLR occurrence and the maximum power in the solar wind found within the period of time corresponding to the delay-time interval (travel time + 30 minutes for propagation time) and the travel time.

c) The time lag was determined as the time difference between the signals' dynamic power maxima, for which the maximum power in solar wind was detected between the FLR occurrence (maximum power) and the lag corresponding to the delay-time (travel time + 30 minutes for propagation time). The reason that this item was included in the study was that local maximum in the solar wind there were observed in periods inferior to the calculated travel time using the minimum variance method of *Weimer et al.* [2003].

The methodology was as follows: The time signals were individually interpolated to avoid data gaps and the normalized dynamic power was calculated as detailed in section 5.1.2. Maxima in power for solar wind parameters were found for lags described in the previous paragraph. The time signals were detrended by subtracting a half-hour running average, as specified in section 5.1.1 and the solar wind data was then interpolated to match the times corresponding to the SuperDARN time-series. The solar wind data was shifted by the time lag specified in the previous paragraph, and the dynamic Fast Fourier Transform (FFT) cross-power and cross-phase between ACE and SuperDARN was calculated using a one hour FFT window with a Hanning weighting and a 1 point shift. The variance in cross-phase over one hour intervals

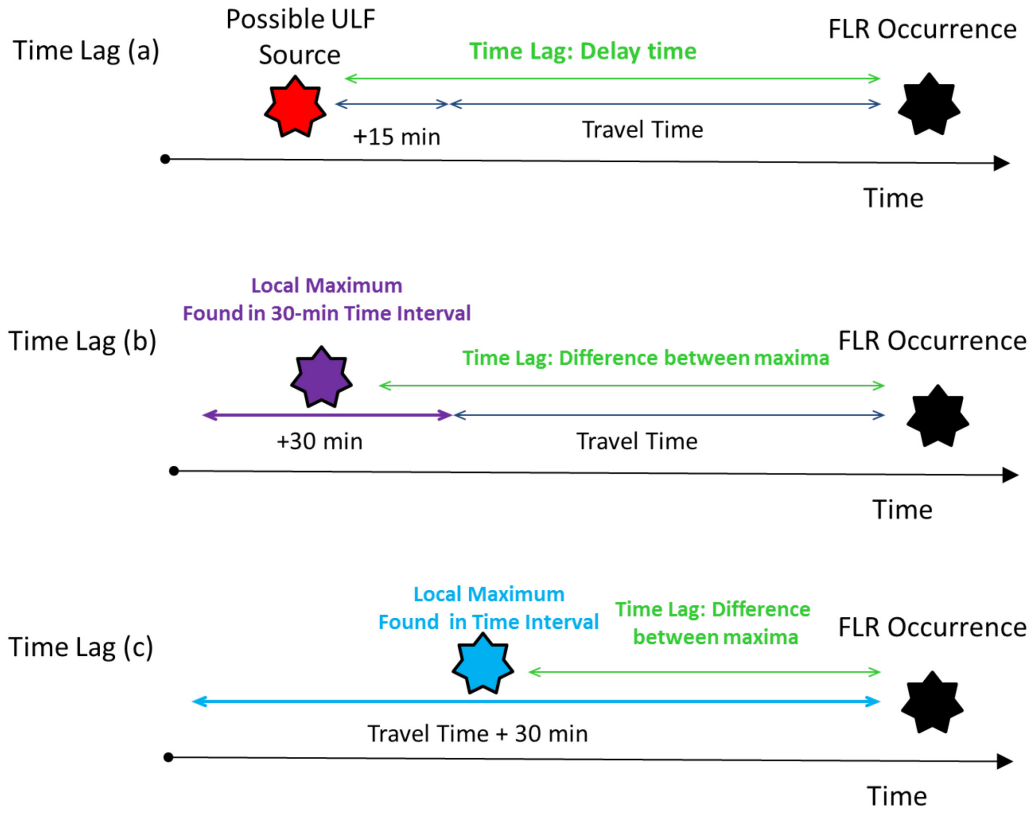

Figure 5.9: Schematics of the three time lags used to shift the solar wind dataset prior to calculating of the cross-power and cross-phase among ACE and SuperDARN datasets.

at each frequency and time was calculated to quantify the degree of phase coherence. Given that random noise might generate low cross-phase variance with the sliding FFT window method 5000 four-hour, red noise data sets were simulated for the solar wind and SuperDARN using the equation $x_i = x_{i-1} + random(seed) \times \sigma \times 0.65$, where σ is the standard deviation of the detrended four-hour ACE dataset, reproducing the study in *Fenrich and Waters* [2008]. Values for local maximum in cross-power and local minimum in dynamic cross-phase variance at the time of the event were recorded for the frequency of the event, and the results were compared to the values of red noise.

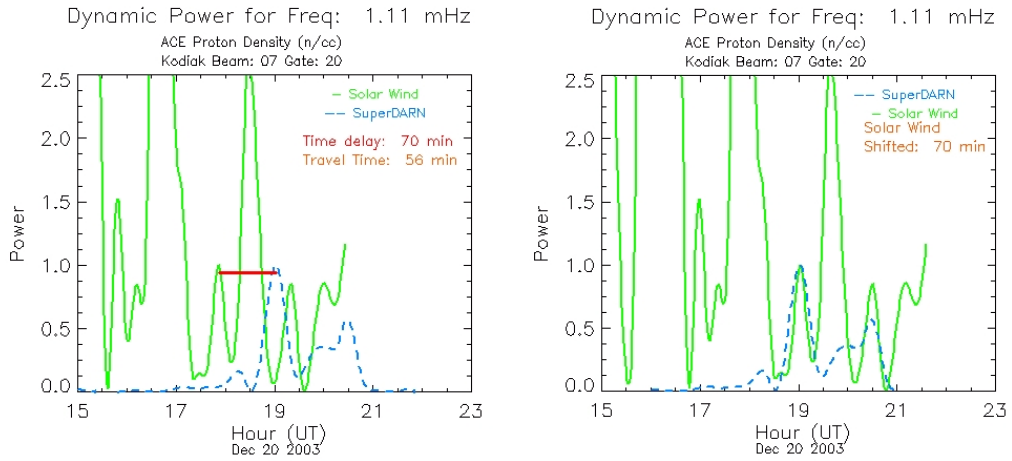

Figure 5.10: (Left) Plot of the dynamic power corresponding to the proton density (solid-green line) and Kodiak Doppler velocity backscatter (dash-blue line), normalized to the power of the local maximum occurred at 17:52 UT on December 20, 2003. The local maximum corresponds to the delay-time calculated for this event. (Right) proton density dynamic power (solid-green line) shifted 70 minutes corresponding to the delay-time and Kodiak Doppler velocity backscatter (dash-blue line): The solar wind and SuperDARN signals aligned when shifted. Notice the other higher power local maxima in solar wind prior and after.

Figure 5.10 (left) shows the normalized dynamic power of Kodiak in dashed-blue line, with a maximum observed around the center of the event at 19:02 UT. In this example, the delay-time was 70 minutes (55 minutes for the travel time plus 15 minutes for propagation inside the magnetosphere). Coincidentally, the normalized dynamic power of proton density, shown in solid-green line, exhibits a local maximum precisely at the time considered for the delay-time, at around 17:52 UT. Notice that this dynamic power local maximum is lower than the adjacent local maxima observed an hour prior (16:30 UT) and an hour after (at 18:29 UT).

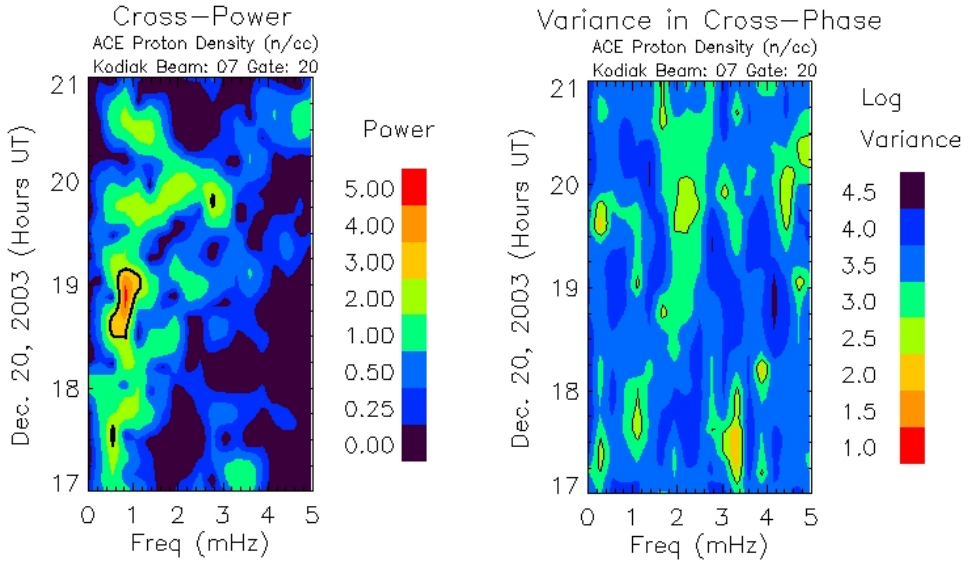

Figure 5.11: Plot of the cross-power (left) and variance in cross-phase (right) corresponding to the proton density (shifted by 70 minutes) and Kodiak Doppler velocity backscatter for the 1.1 mHz FLR event. Black lines correspond to the 5% significant level curves.

The proton density time-series was shifted by 70 minutes (shift shown in Figure 5.10, right). The calculation of dynamic cross-power and dynamic cross-phase variance among the delayed proton density signal and the Kodiak signal, as well as the simulated red noise, was performed as explained earlier in this section. High cross-power (6.07) above the 5 % confidence level to red noise (3.74) and low variance (2.15) above the 5 % confidence level to red noise (4.52) for 1.1 mHz are observed at around 18:45-19:00 UT (Figure 5.11). The other FLRs found in this 4-hour time interval, 1.7 mHz (18:13-19:13 UT), 2.8 mHz (20:37-21:37 UT), and 1.7 mHz (20:36-21:36 UT) also exhibit some enhancement in cross-power and cross-phase in low variance, even though there are not as prominent as the 1.1 mHz maximum at 18:45 UT due to the normalization scale.

Dynamic pressure was also examined for this case study. The dynamic pressure is a very important solar wind parameter because sudden increase in it

produces compressional waves that get transmitted internally and give "*a strong kick to the magnetic field lines which then oscillate with different frequencies at different latitudes*" [*Mthembu et al.*, 2009]. On the other hand, the dynamic pressure ULF oscillatory changes slowly affect the size of the magnetospheric cavity. "*The magnetospheric field increases or decreases as needed to balance the internal magnetic pressure against the external dynamic pressure. In this manner, oscillatory variations of the dynamic pressure lead directly to oscillatory changes in the magnetospheric magnetic field strength*" [*Kepko et al.*, 2002].

The normalized dynamic power of dynamic power, shown in solid-green line in figure 5.12 (top: non-shifted, bottom: shifted), exhibits a local maximum also at the time considered for the delay-time, at around 17:52 UT. The dynamic cross-power among the 70-minutes delayed dynamic pressure signal and the Kodiak signal shows (Figure 5.13) high cross-power (1.77) above the 5 % confidence level to red noise (1.07), while and dynamic cross-phase variance exhibits low variance (2.42) compared to the 5 % confidence level to red noise (4.52) for 1.1 mHz are observed at around 18:45-19:00 UT.

Equally important, the dynamic cross-power for both the 70-minutes delayed magnetic field B_z and magnetic field B_y signal with the Kodiak signal (Figure 5.14 and Figure 5.15 respectively) shows high cross-power (12.93 and 20.50 respectively) above the 5 % confidence level to red noise (5.70 and 7.99, respectively), while and dynamic cross-phase variance exhibits low variance (2.53 and 2.49, respectively) compared to the 5 % confidence level to red noise (4.52 for both) for 1.1 mHz are observed at around 18:45-19:00 UT. In this event, B_z is first dominant, suggesting that reconnection mechanisms at the nose of the magnetosphere were important half hour prior the event. Furthermore, B_y becomes later dominant: As discussed in the previous chapter (Chapter 4), the 1.1 mHz FLR detected on December 20, 2003 at around 19 UT occurred at the dawn sector, at 7 MLT and L=7, exhibits a westward (anti-sunward) propagation which

is consistent with a source as solar wind MHD compressional wave transmission through flank reconnection.

The local maximum with most significant dynamic power for solar wind proton density in the interval of 90 minutes prior the time of the occurrence of the FLR event occurs at 18:29 UT. Figure 5.16 shows the normalized dynamic power of Kodiak in dashed-blue line, with a maximum observed around the center of the event at 19:02 UT. The delay time is 33 minutes, less than the time travel calculated.

Figure 5.17 shows a plot of cross-power (left) and variance in cross-phase (right) corresponding to a time shift of 33 minutes for the proton density: High cross-power (6.07) above the 5 % confidence level to red noise (3.74) and low variance (2.15) above the 5 % confidence level to red noise (4.52) is observed at around 19 UT for f_{FLR}=1.1 mHz (18:28-19:28 UT). Interestingly enough, high power is observed at nearby 18:30UT for f=0.6 mHz, at around 19:20 UT for f=1.9 mHz, and at nearby 19:50UT for f=0.6 mHz, matching the other FLRs occurring in this 4-hr time interval. Notice that local minima exhibits stronger relative normalized power than in the plot corresponding to the delay time.

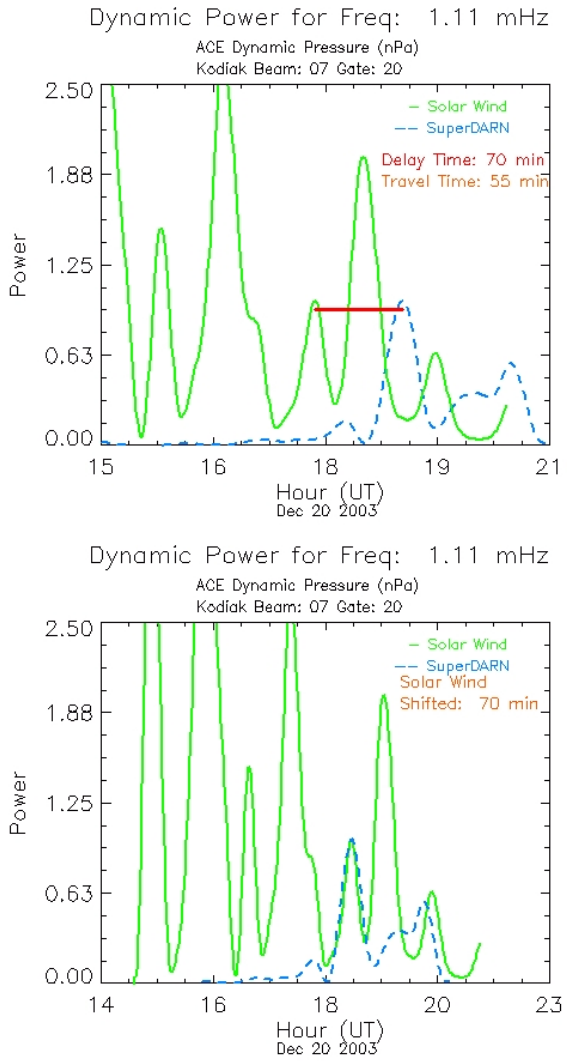

Figure 5.12: (Top) Plot of the dynamic power corresponding to solar wind dynamic pressure (solid-green line) and Kodiak Doppler velocity backscatter (dash-blue line) normalized to the power of the local maximum occurred at 17:52 UT on December 20, 2003. A local maximum is found at a time corresponding to the delay-time calculated for this event. (Bottom) Solar wind dynamic pressure dynamic power (solid-green line) shifted 70 minutes corresponding to the delay-time and Kodiak Doppler velocity backscatter (dash-blue line): The solar wind and SuperDARN signals aligned when shifted. Notice the other local maxima in solar wind with higher power prior and after the local maximum chosen for the delay-time.

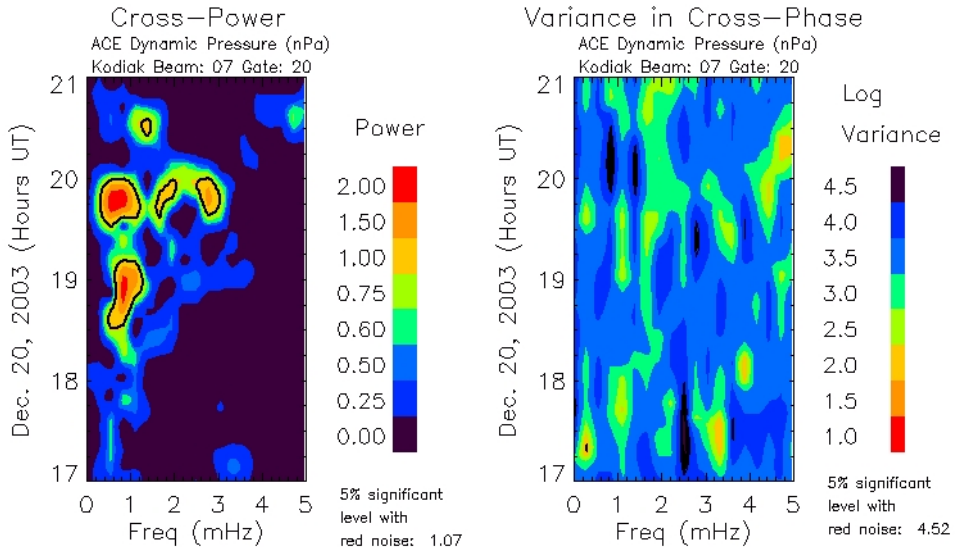

Figure 5.13: Plot of the cross-power (left) and variance in cross-phase (right) corresponding to the dynamic pressure (shifted by 70 minutes) and Kodiak Doppler velocity backscatter for the 1.1 mHz FLR event. Black lines correspond to the 5% significant level curves.

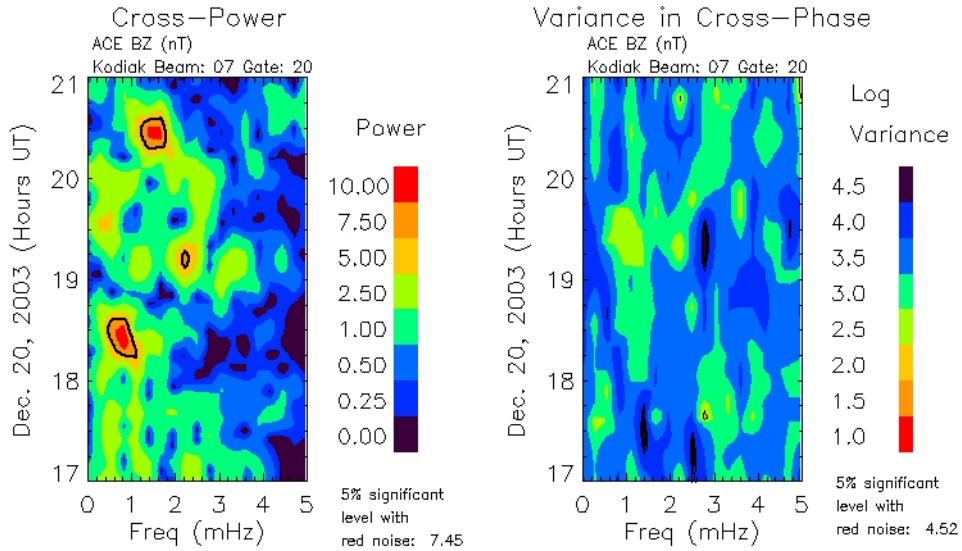

Figure 5.14: Plot of the cross-power (left) and variance in cross-phase (right) corresponding to the magnetic field B_z (shifted by 70 minutes) and Kodiak Doppler velocity backscatter for the 1.1 mHz FLR event. Black lines correspond to the 5% significant level curves.

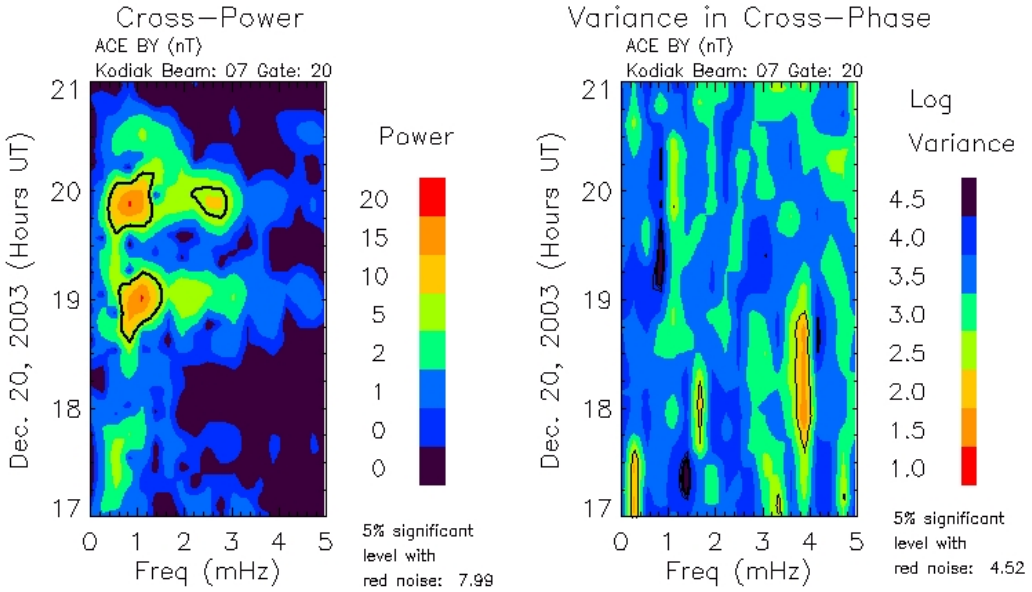

Figure 5.15: Plot of the cross-power (left) and variance in cross-phase (right) corresponding to the magnetic field B_y (shifted by 70 minutes) and Kodiak Doppler velocity backscatter for the 1.1 mHz FLR event. Black lines correspond to the 5% significant level curves.

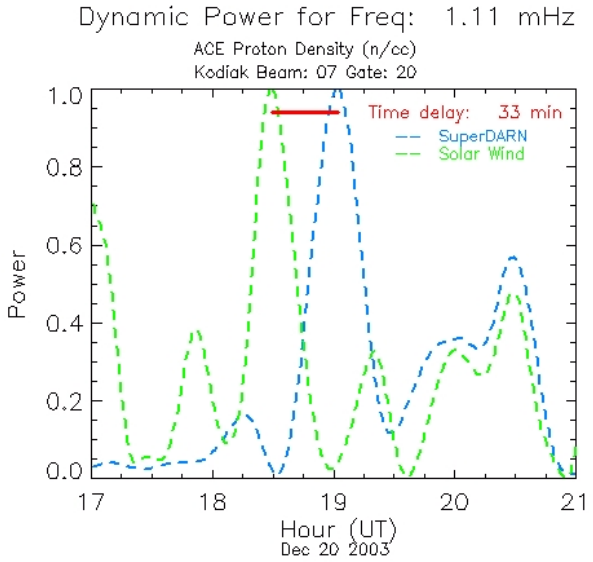

Figure 5.16: Plot of the dynamic power corresponding to the proton density (green) and Kodiak Doppler velocity backscatter (blue).

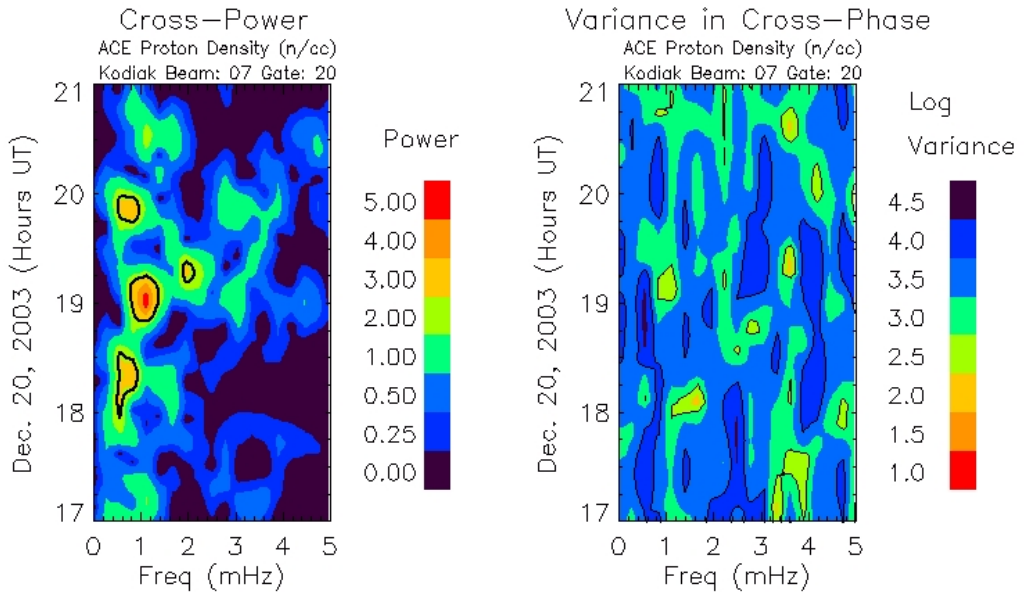

Figure 5.17: Plot of the cross-power (left) and variance in cross-phase (right) corresponding to the proton density and Kodiak Doppler velocity backscatter for the 1.1 mHz FLR event. Black lines correspond to the 5% significant level curves.

5.2 Discussion of Results

The methodology outlined in the previous section was systematically applied to all the events. From the 122 FLRs in the database, solar wind available data was found for analysis for only 116 events. The rest of the events corresponded to periods of time where solar wind data was either bad or missing and data from other spacecraft should be used to analyze those FLRs. For time constrains, we only analyzed the events for which ACE data was good. For each of the steps described in section 5.1, additional requirements on number of valid data-points were needed; therefore, results for fewer than 116 events were available for each step of the methodology. The subsections below detail the results found in them.

5.2.1. Results for correlation of the time series in the time domain

The first step in the methodology, delineated in the previous section, consisted in the study of the correlation of the time series corresponding to solar wind and SuperDARN around the time period of the FLRs in the database, as described in section 5.1.1. This step intended to apply the methodology detailed in the study of *Kepko et al.* [2002] and compare our results to those on that study.

Correlation coefficient corresponding to two different time intervals, between -80 and -30 minutes prior the occurrence of the FLR event, denoted as LAG-A, and within the *delay-time interval* (delay-time ± 15 minutes), called LAG-B, were found. The maximum correlation coefficients of each period were recorded. Appendix B contains a complete list of those results.

Figure 5.18 shows plots of the maximum correlation coefficients corresponding to the study of correlation between Proton density and SuperDARN found in two time intervals: On the left, the correlation coefficients correspond to maximum found in time interval noted as LAG-A, between -80 and -30 minutes prior the occurrence of the FLR event; on the right, the correlation coefficients correspond to maximum found in time interval noted as LAG-B, within the *delay-time interval* (delay-time ± 15 minutes). In both plots, the blue vertical dotted-line corresponds to R=0.5 while the green vertical dotted-line corresponds to R=0.7. The red crosses in the left plot show agreement of times for maximum correlation found for Lag-A and Lag-B, while the red crosses in the plots in to right plot show times for maximum found in the Lag-B interval that coincide with the travel-time calculated for the event.

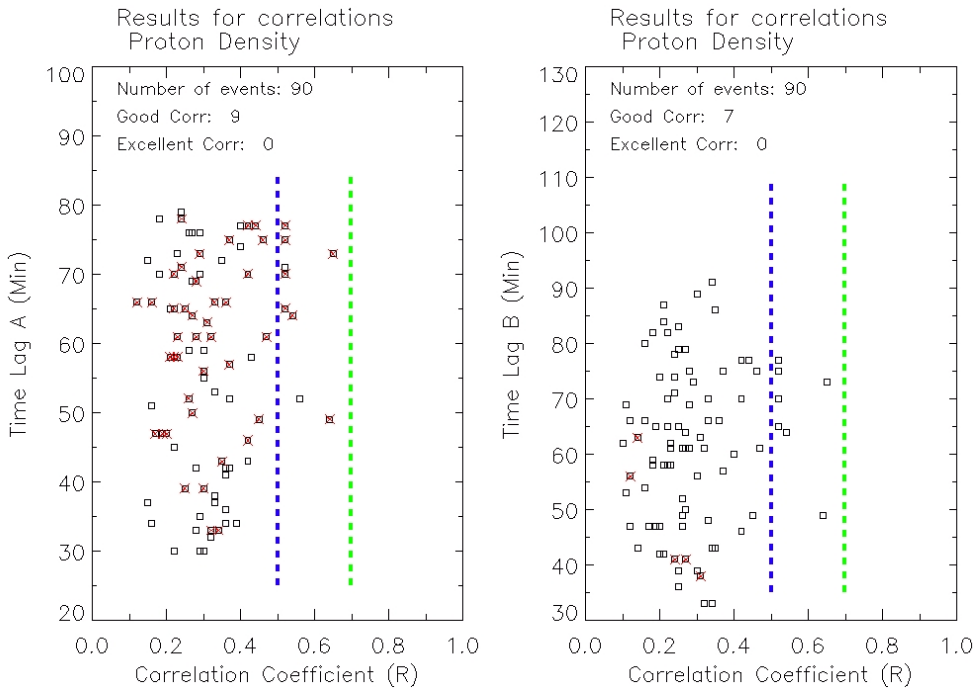

Figure 5.18: Plot of the correlation coefficients corresponding to the study of correlation between Proton density and SuperDARN, for time intervals LAG-A (Left), between -80 and -30 minutes prior the occurrence of the FLR event, and LAG-B (right), within the *delay-time interval* (delay-time ± 15 minutes). Blue vertical dotted-line corresponds to R=0.5 while green vertical dotted-line corresponds to R=0.7. Red crosses in the left plot show agreement of Lag-A and Lag B times for maximum correlation coefficients, while red crosses in right plots show agreement between travel time and time for maximum found in the Lag B interval.

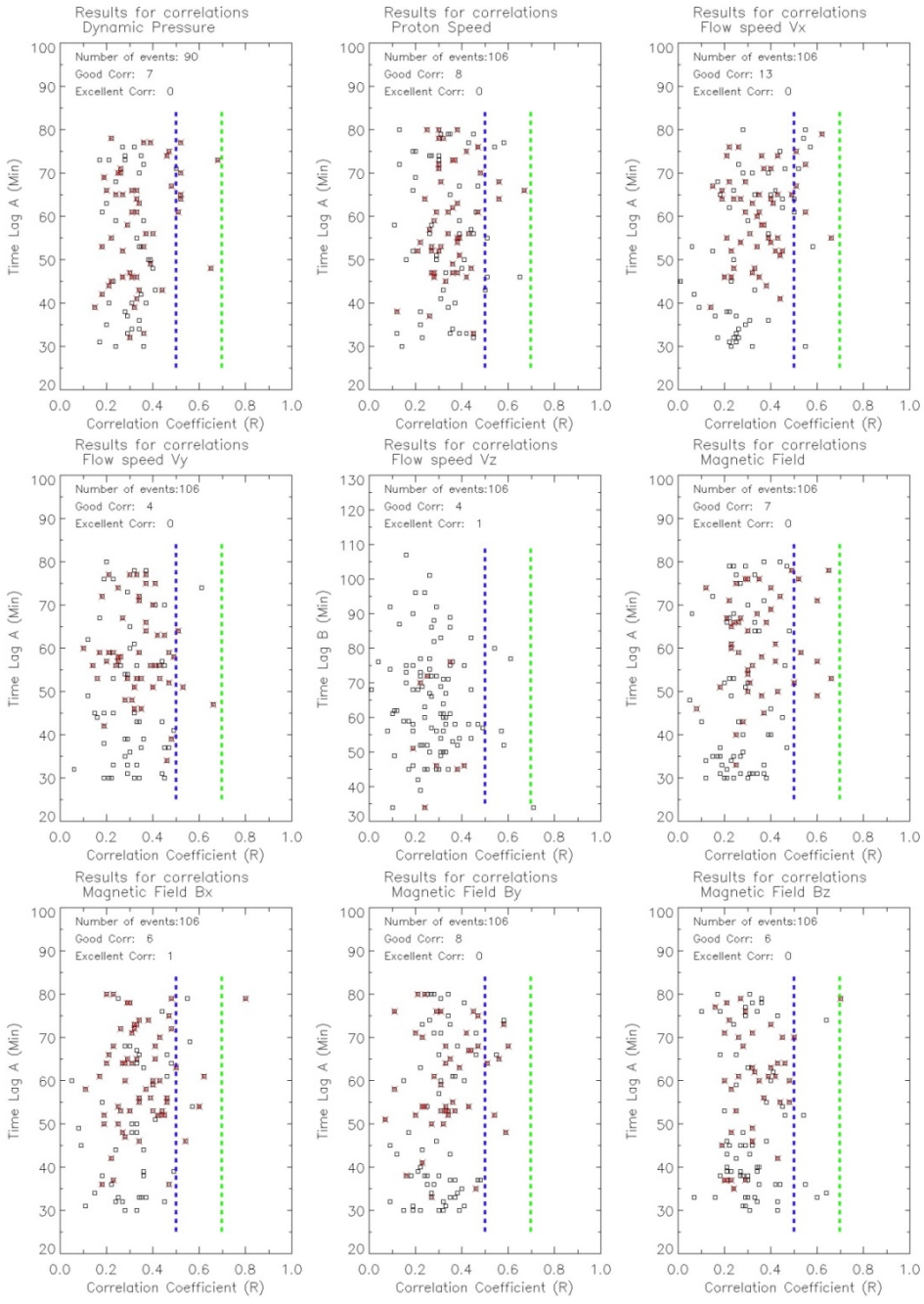

Figure 5.19: Plot of the correlation coefficients corresponding to the study of correlation between solar parameters and SuperDARN, for time intervals LAG-A, between -80 and -30 minutes prior the occurrence of the FLR event.

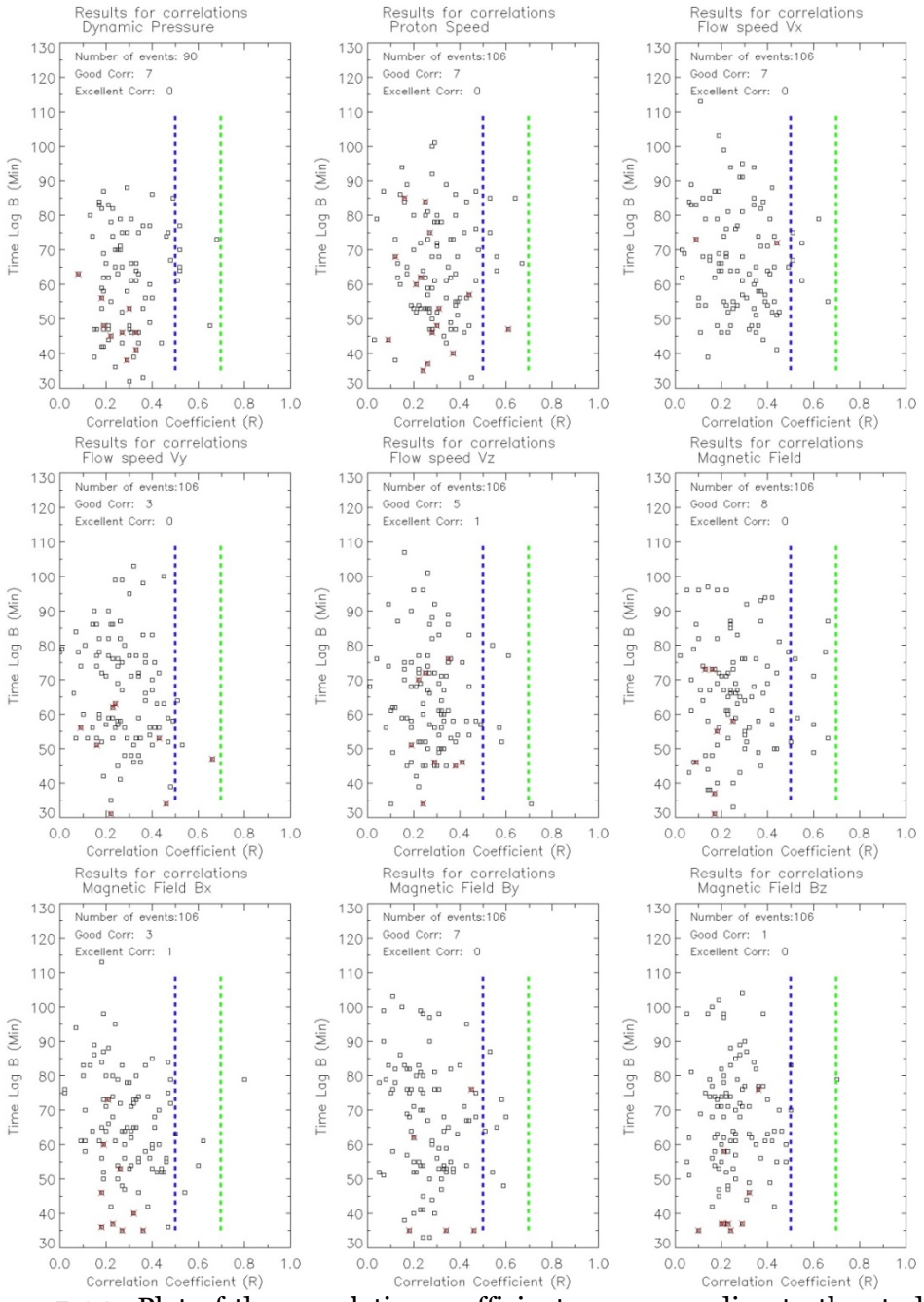

Figure 5.20: Plot of the correlation coefficients corresponding to the study of correlation between solar parameters and SuperDARN, for time interval LAG-B, within the *delay-time interval* (delay-time ± 15 minutes).

For the proton density and dynamic pressure, solar wind data were available for time periods corresponding to 90 FLRs, while for the rest of the solar parameters, there was data available for 106 FLRs. In this analysis, we found that 9 out of 90 (10%) FLRs show good correlation with solar wind proton density in an interval of 80 to 30 minutes prior the FLR occurrence (figure 5.18, left), while good correlation found inside the delay-time interval (figure 5.18 right) is less than 10% (7 out of 90 FLRs). We can infer, then, that the successful rate of correlation of solar wind proton density with FLR events, as detected with SuperDARN, is very low.

Table 5.3: Results for correlation analysis

Solar Parameter	Events with good correlation, Lag-A	Events with good correlation, Lag-B
Proton Density	9	7
Proton Speed	8	7
Vx	13	7
Vy	4	3
Vz	5	4
Magnetic Field	7	8
Bx	6	3
By	8	7
Bz	6	1
Dynamic Pressure	7	8

Similar results were found for all the other solar parameters: correlation between FLR wave structure and solar wind v_x time series turned out to be excellent for only for one event in an interval of 80 to 30 minutes prior the FLR occurrence, while none of the other solar parameters reported a correlation coefficient above R=0.7. Moreover, in the delay-time interval prior the FLR, correlation turned out to be excellent for only for one event occurrence between FLR wave structure and solar wind v_x and for another event occurrence between FLR wave structure and solar wind B_x, while none of the other solar parameters

reported a correlation coefficient above R=0.7. Good correlation was found for less than 13% in all solar parameters within both lags of time intervals. For all solar parameters, the times for maximum found in Lag A and Lag B match approximately 2/3 of the times (Figure 5.19, red cruces), while the times for maximum found in Lag B rarely match the travel-time (Figure 5.20, red cruces)

Table 5.3 summarizes the number of FLR events which exhibit good correlation with solar wind parameters. It is fair, then, to infer from this results that that either:

a) Solar wind might drive FLRs in the magnetosphere in rare cases, or
b) The correlation analysis is not a good method to establish coherence between solar wind and FLRs.

5.2.2. Results for examination of the Band-pass signal and analytic signal

The second step in the methodology, delineated in the previous section, involved the examination of the band-pass and analytic signals. Appendix C contains a complete list of those results. This evaluation permits the examination of wave packets in the solar wind of the same frequency as the natural frequency of the FLRs.

For the proton density and the radar bandpass signals, as expected, over 70% show agreement at the FLR frequency: good correlation coefficients were found in 32% while excellent correlation coefficients were found in 38% of the cases (figure 5.21, left). The reminding 29% showed poor correlation, which implies that the wave packets corresponding to the detected FLRs did not good agreement with the wave packets found in the solar wind within the interval time. In a similar token, the proton density wave packets maximum values found between the two hours prior to the event agreed only in 2 occasions with the

maximum values found in the delay time interval. Furthermore, for a majority of the events the maximum was found outside of the delay time interval (figure 5.21, right): most of the events showed a maximum value corresponding for time intervals between proton density and radar maxima shorter than the *delay time*, while few showed time intervals longer than the *delay time*.

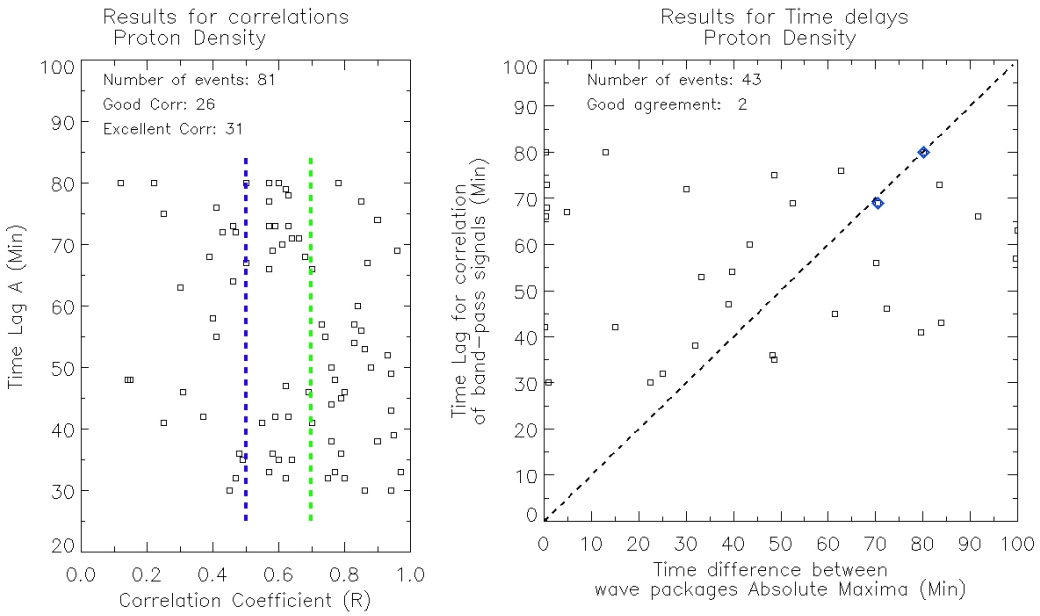

Figure 5.21: (Left) Plot of the correlation coefficients corresponding to the study of correlation between the analytic signal Proton density and analytic signal SuperDARN, for time intervals LAG-A, between -80 and -30 minutes prior the occurrence of the FLR event. Blue vertical dotted-line corresponds to R=0.5 while green vertical dotted-line corresponds to R=0.7. (Right) Time intervals LAG-A vs time difference between absolute Maxima between wave packets. Dotted slope shows good agreement.

The other solar parameters revealed similar results. Figure 5.22 shows the plot of the correlation coefficients corresponding to the study of correlation between the analytic signal of the other solar parameters and the analytic signal SuperDARN, for time intervals LAG-A, between -80 and -30 minutes prior the occurrence of the FLR event, while the blue vertical dotted-line and green

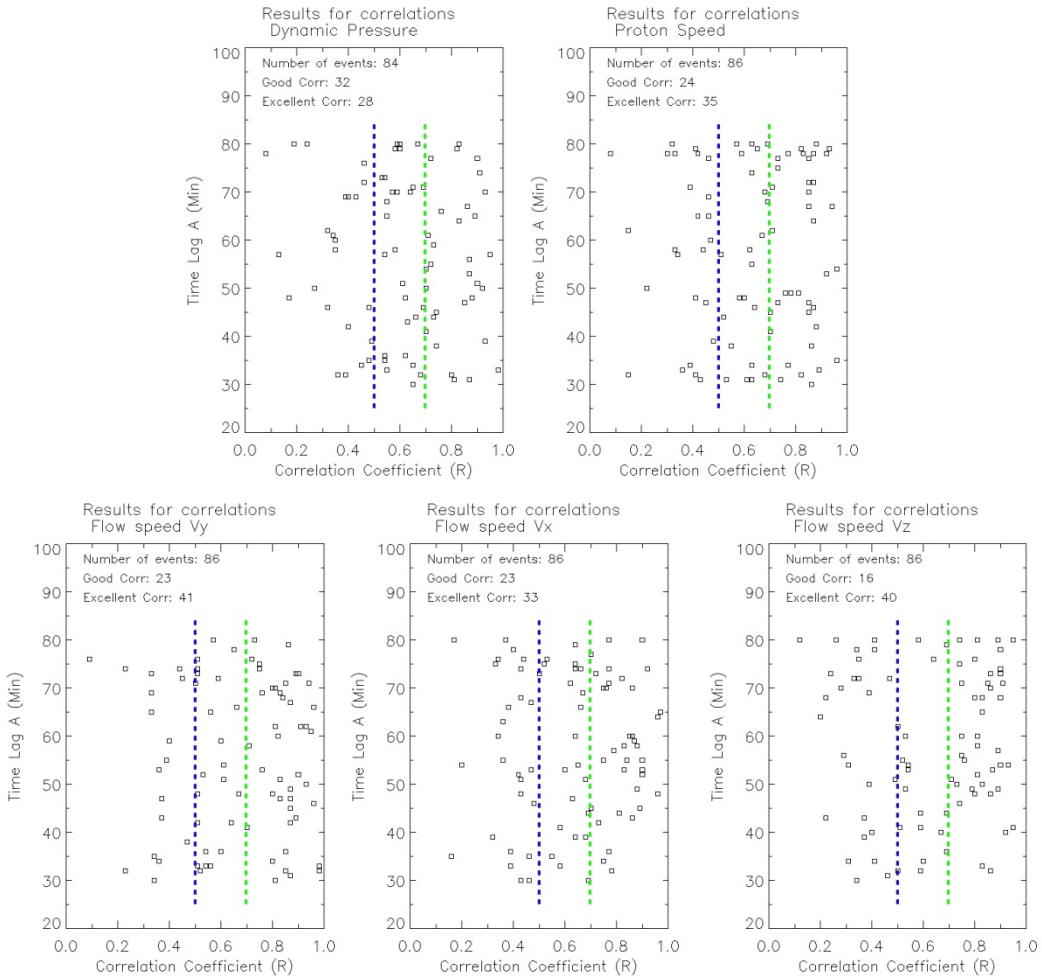

Figure 5.22: Plot of the correlation coefficients corresponding to the study of correlation between the analytic signal of other solar parameters and analytic signal SuperDARN, for time intervals LAG-A, between -80 and -30 minutes prior the occurrence of the FLR event. Blue vertical dotted-line corresponds to R=0.5 while green vertical dotted-line corresponds to R=0.7.

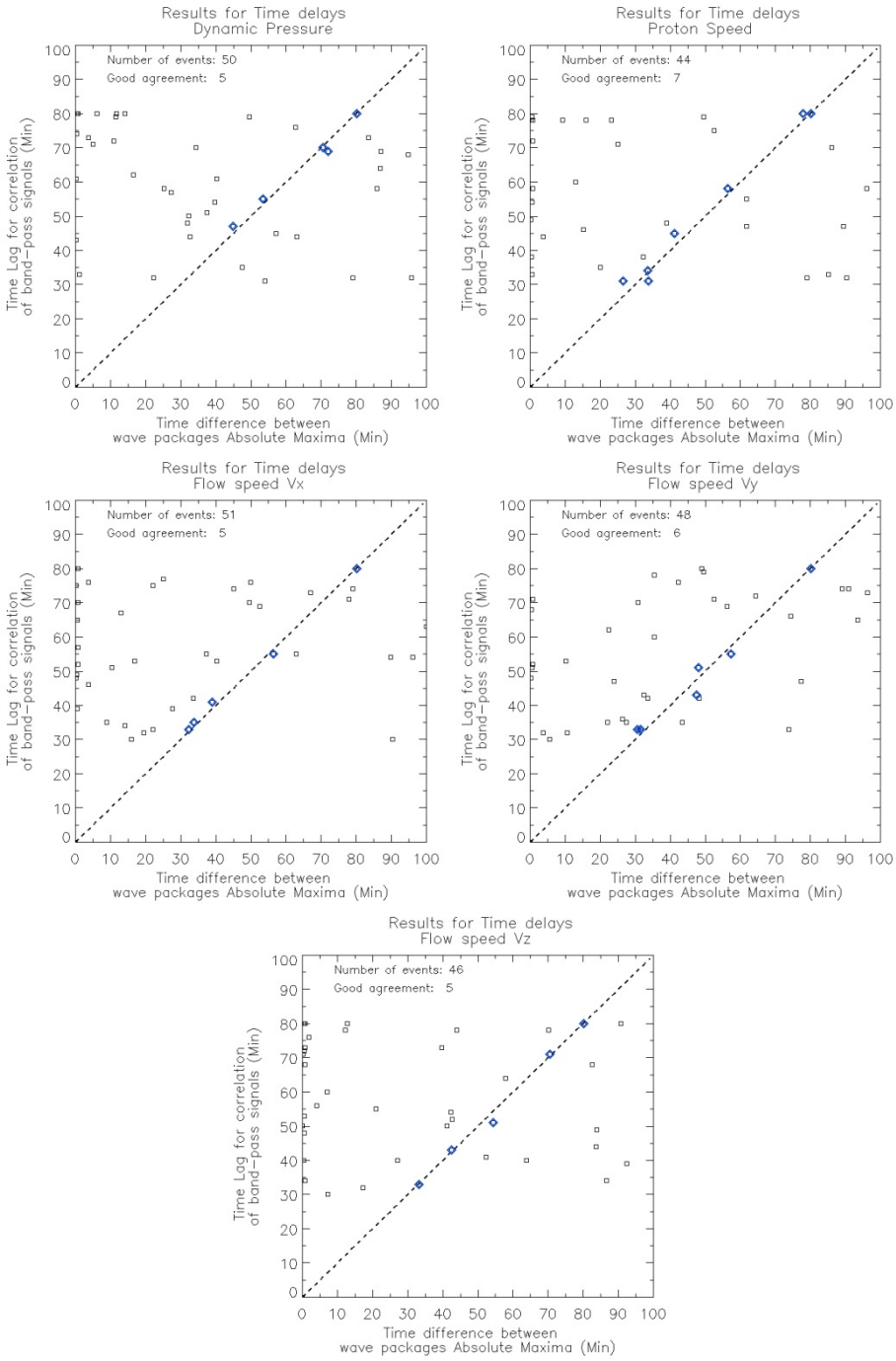

Figure 5.23: Time intervals LAG-A vs time difference between the analytic signal of the other solar parameters and analytic signal SuperDARN wave packets absolute maxima for the other solar parameters.

vertical dotted-line correspond to correlation values above R=0.5 and R=0.7, respectively. It is important to remark that for all other solar parameters, similar percentages of poor correlation among wave packets are found. Figure 5.23: shows the time interval LAG-A vs time difference between the analytic signal of the other solar parameters and analytic signal SuperDARN wave packets absolute maxima for the other solar parameters. These plots show similar percentages as the proton density results.

5.2.3. Results for power spectra examination, evaluation of the cross-power and the cross-phase variance

The last step in the methodology, detailed in the previous section, comprised the examination of the power spectra and the evaluation of the cross-power and cross-phase variance. The main goal of this step was to study the correlation and degree of phase coherence between the two data sets.

Table 5.4: Available solar wind data for cross-power/cross-phase analysis

Solar Parameter	Events with good solar wind data Lag-A	Events with good solar wind data Lag-B	Events with good solar wind data Lag-C
Proton Density	104	120	120
Proton Speed	104	120	120
Vx	104	120	120
Vy	104	120	120
Vz	103	118	118
Magnetic Field	110	118	118
Bx	110	118	118
By	110	118	118
Bz	110	118	118
Dynamic Pressure	103	118	118

The methodology was extended to the 120 FLR occurrences where solar wind data were available (there was not solar wind available data for all solar parameters event 34b). For the three different lags and for some individual solar parameters, the calculated values of cross-power and cross-phase variance were not able to be returned due to bad or missing data for that particular period of time and solar parameter. Table 5.4 summarizes the number of events with good solar wind data for each solar parameter for each individual lag.

For all three lags, the majority of FLRs exhibited values of high cross-power and a low cross-phase variance compared to the red noise 5% confidence level randomly generated. A summary of the number of events that exhibit coherence are shown in table 5.5 for each of the solar parameters, with their respective percentages. Two thirds of the events exhibited good coherence with solar parameters for most of the solar parameters for all lags. As expected, percentages are slightly higher for results corresponding to LAG B compared to LAG A: Lag A corresponds to calculations with the solar wind parameter shifted by the *delay time* while calculations using Lag B corresponds the solar wind parameter shifted by the time difference between the event and the maximum found in the solar wind power in the *delay-time interval*. These results confirm that the statement by *Fenrich and Waters* [2008] that 'delay-times between 51 minutes and 80 minutes yielded similar results' can be generalized for all the events. It is worth mentioning that in general, only one third of the power spectral maximum time of occurrence corresponding to time shifts for LAG B are coincidental with the time of occurrence corresponding to time shifts LAG A, as demonstrated in figures 5.24, 5.26, 5.27 and 5.28, which indicates that the methodology to study coherence with LAG B is more refined and exhibits slightly better results.

Table 5.5: Summary of the number of events that exhibit coherence

Solar Parameter	LAG A Number of Events (and %) compared to red noise	LAG B Number of Events (and %) compared to red noise	LAG C Number of Events (and %) compared to red noise
Proton Density	71 (68%)	88 (73%)	91 (76%)
Proton Speed	73 (70%)	88 (73%)	89 (74%)
Vx	74 (71%)	91 (76%)	90 (75%)
Vy	74 (71%)	88 (73%)	94 (78%)
Vz	67 (65%)	86 (73%)	94 (80%)
Magnetic Field	73 (66%)	81 (69%)	92 (78%)
Bx	80 (73%)	87 (74%)	89 (75%)
By	70 (64%)	83 (70%)	93 (79%)
Bz	72 (65%)	81 (69%)	85 (72%)
Dynamic Pressure	70 (68%)	87 (74%)	90 (76%)

Results of good coherence percentages yielded from LAG C are slightly higher than those found with LAG B (and therefore significantly higher than those found for LAG A) with approximately only half of the cases having both lags to agree in the shifted time, as seen in figures 5.25, 5.29, 5.30 and 5.31. This result is puzzling since for a large number of events the times found in LAG C yielded a time shift less than the 15 minutes needed for propagation from the magnetopause to Earth, which might infer that there might be an unforeseen bias in the methodology that needs to be addressed.

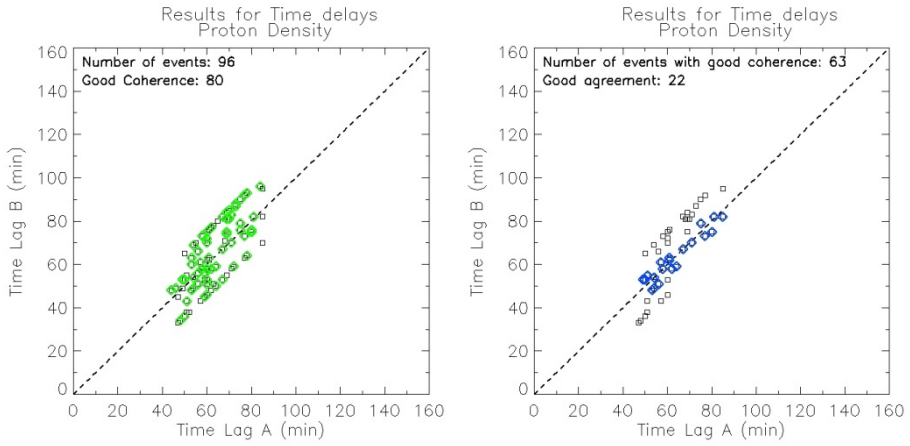

Figure 5.24: (Left) Plot of the power spectral maxima found in the study of time intervals LAG-B vs LAG-A; results of good coherence between solar parameter and SuperDARN are shown in green. (Right) Plot of good coherence results corresponding to LAG-B vs LAG-A; lags within a 5-min interval are shown in blue.

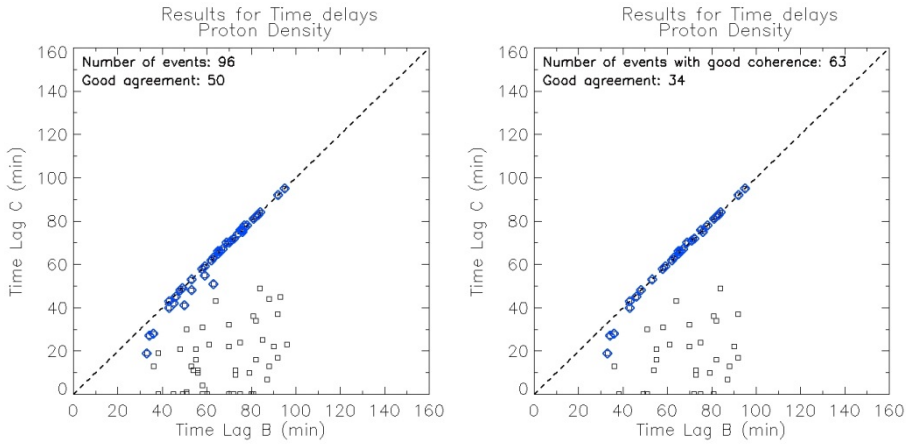

Figure 5.25: (Left) Plot of the power spectral maxima found in the study of time intervals LAG-C vs LAG-B. (Right). Plot of good coherence results corresponding to LAG-A vs LAG-B. For both plots, lags within a 15-min interval are shown in blue.

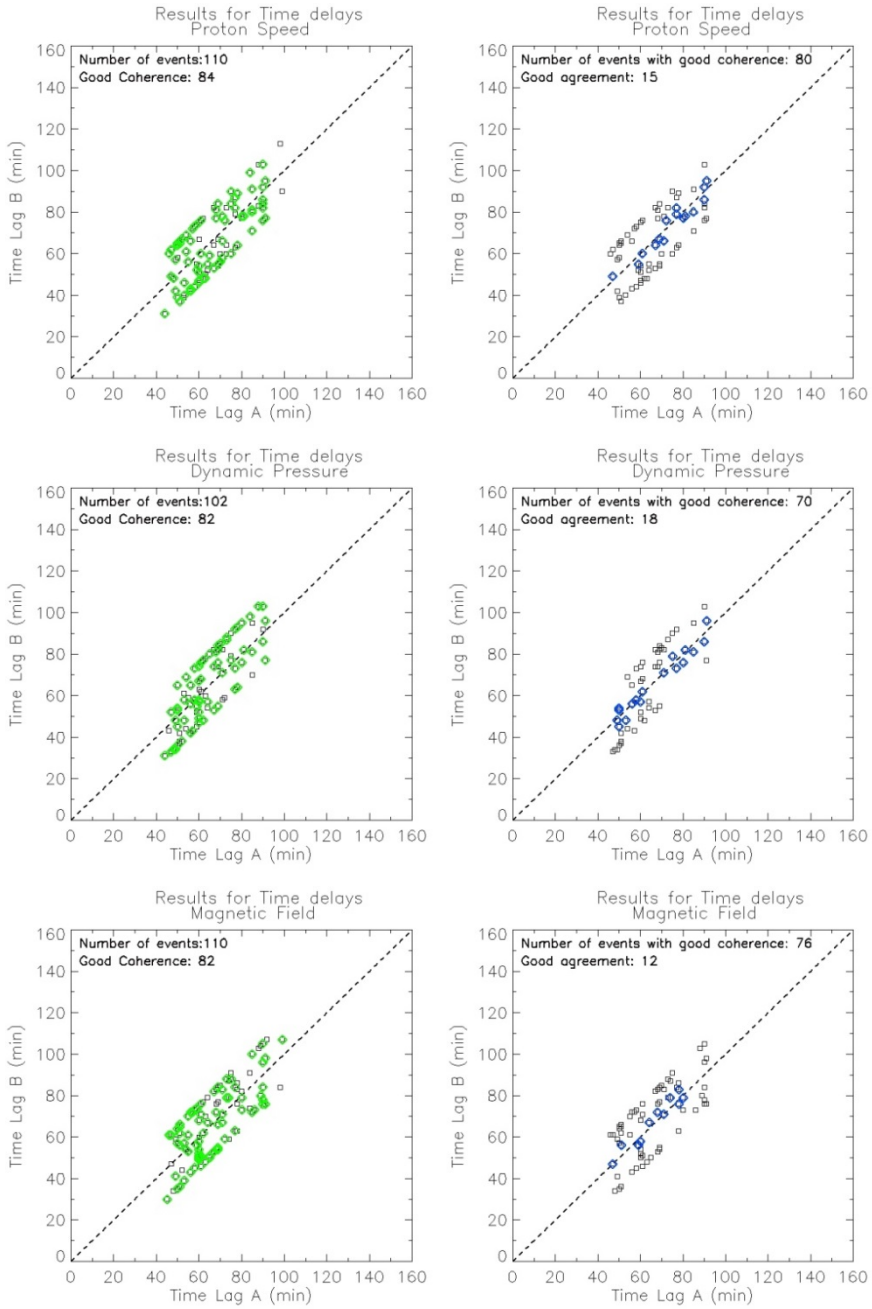

Figure 5.26: (Left panels) Plot of the power spectral maxima for LAG-B vs LAG-A for proton speed (top), dynamic pressure (middle) and magnetic field (bottom); good coherence is shown in green. (Right panels) Good coherence results corresponding to LAG-A vs LAG-B; lags within a 5-min interval are shown in blue.

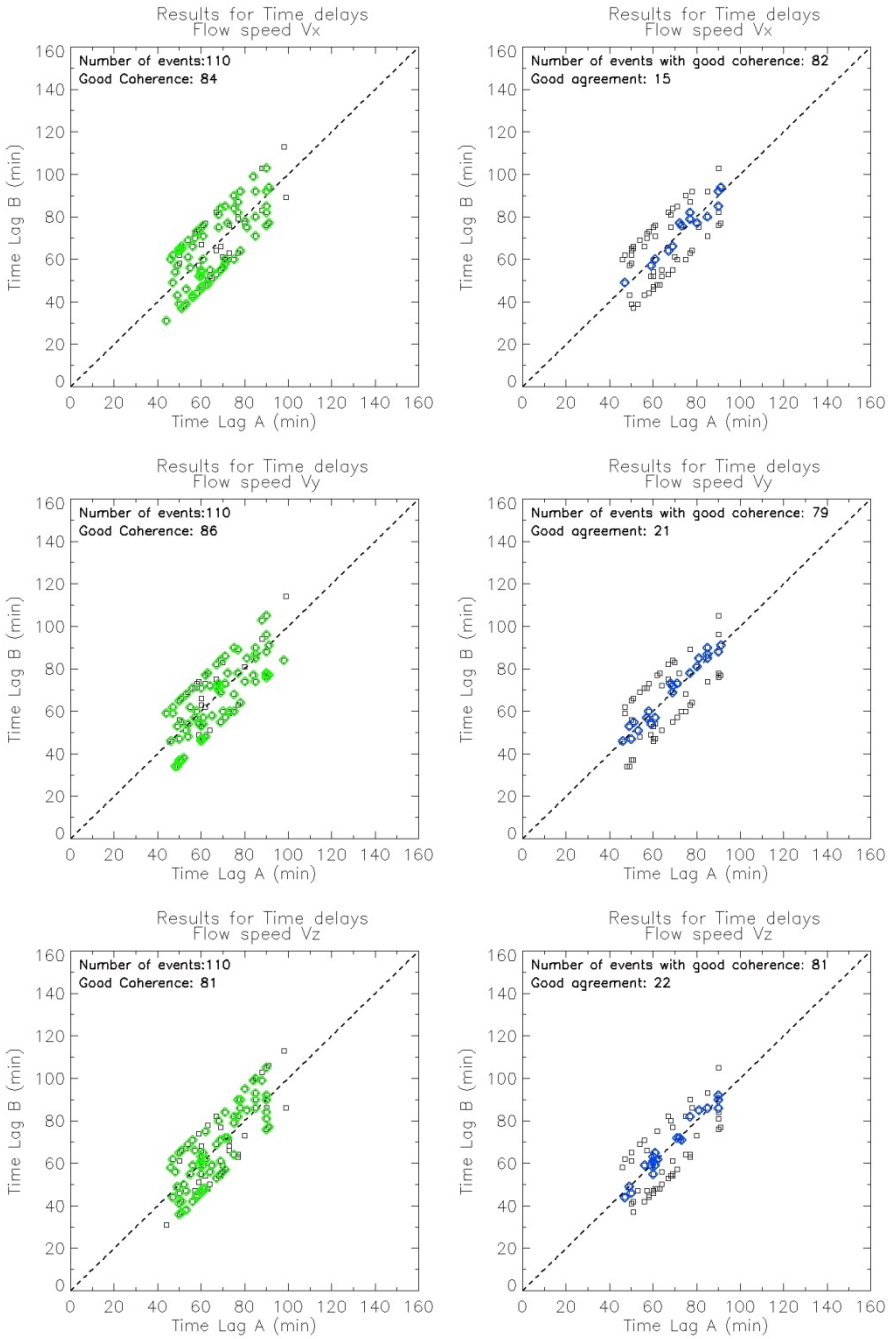

Figure 5.27: (Left panels) Plot of the power spectral maxima for LAG-B vs LAG-A for flow speed v_x (top), v_y (middle) and v_z (bottom); good coherence is shown in green. (Right panels) Good coherence results corresponding to LAG-A vs LAG-B; lags within a 5-min interval are shown in blue.

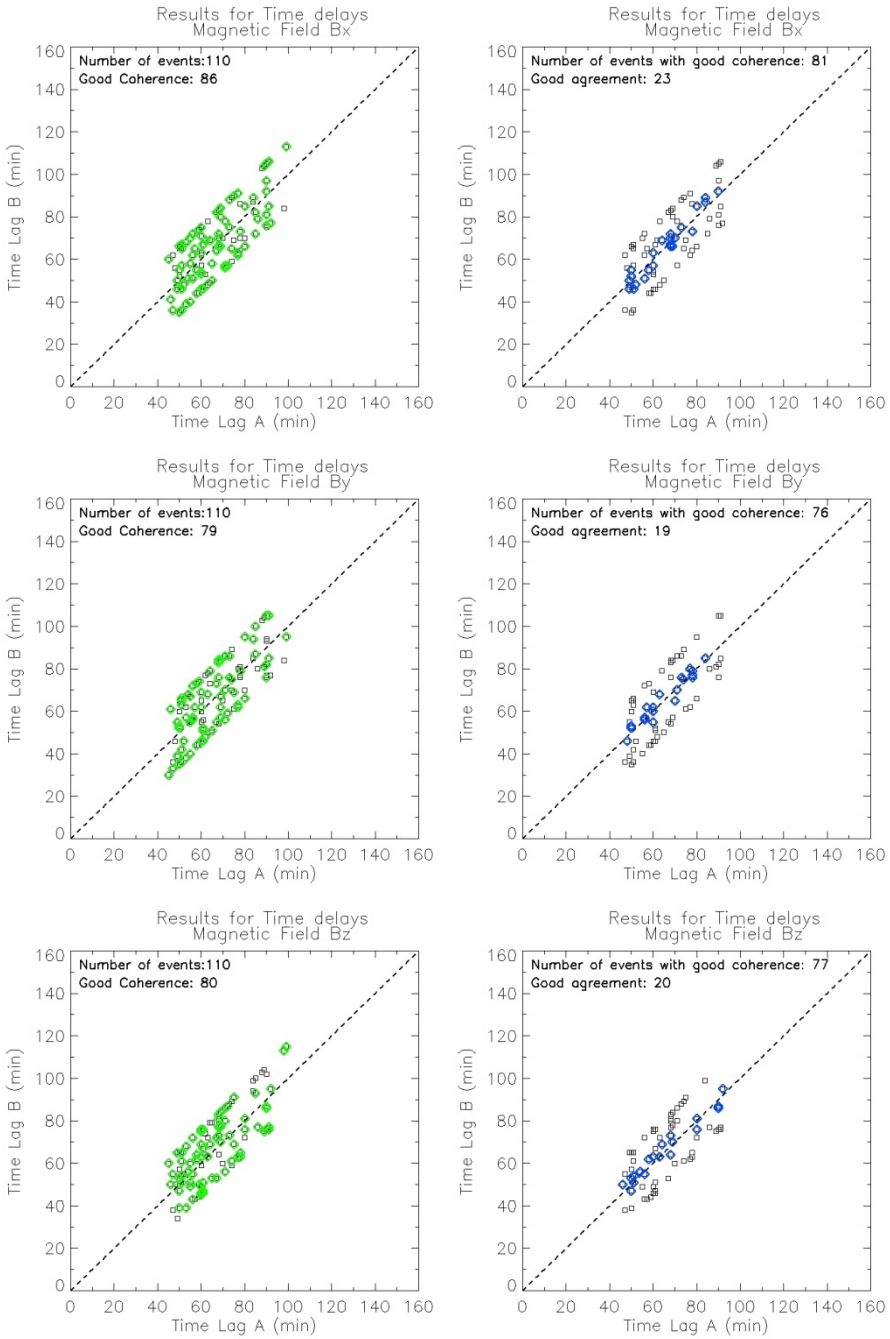

Figure 5.28: (Left panels) Plot of the power spectral maxima for LAG-B vs LAG-A for B_x (top), B_y (middle), B_z (bottom); good coherence is shown in green. (Right panels) Good coherence results corresponding to LAG-A vs LAG-B; lags within a 5-min interval are shown in blue.

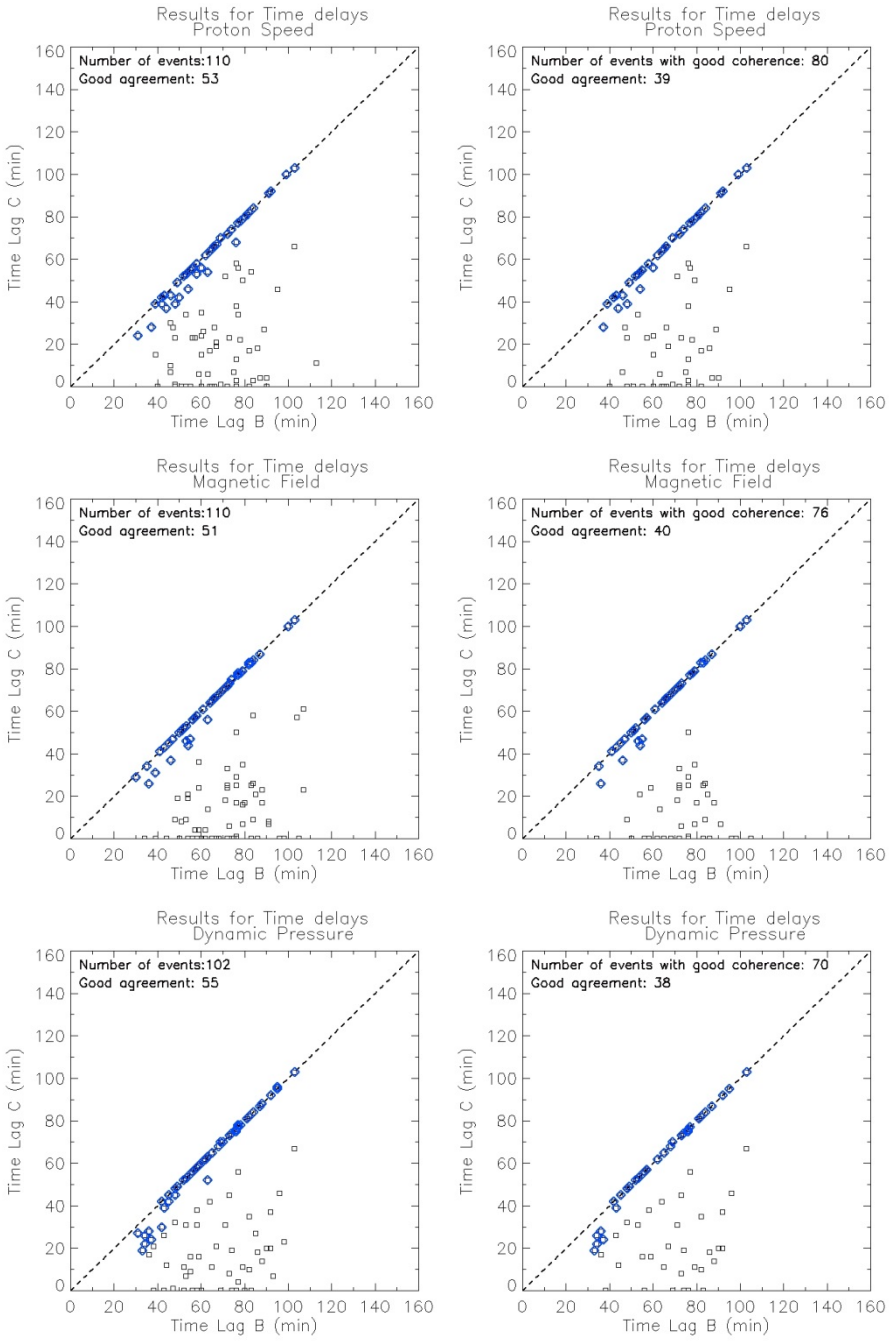

Figure 5.29: (Left) Plot of the power spectral maxima found in the study of time intervals LAG-C vs LAG-B for proton speed (top), magnetic field (middle) and dynamic pressure (bottom). (Right) Plot of good coherence results corresponding to LAG-A vs LAG-B. For all plots, lags within a 15-min interval are shown in blue.

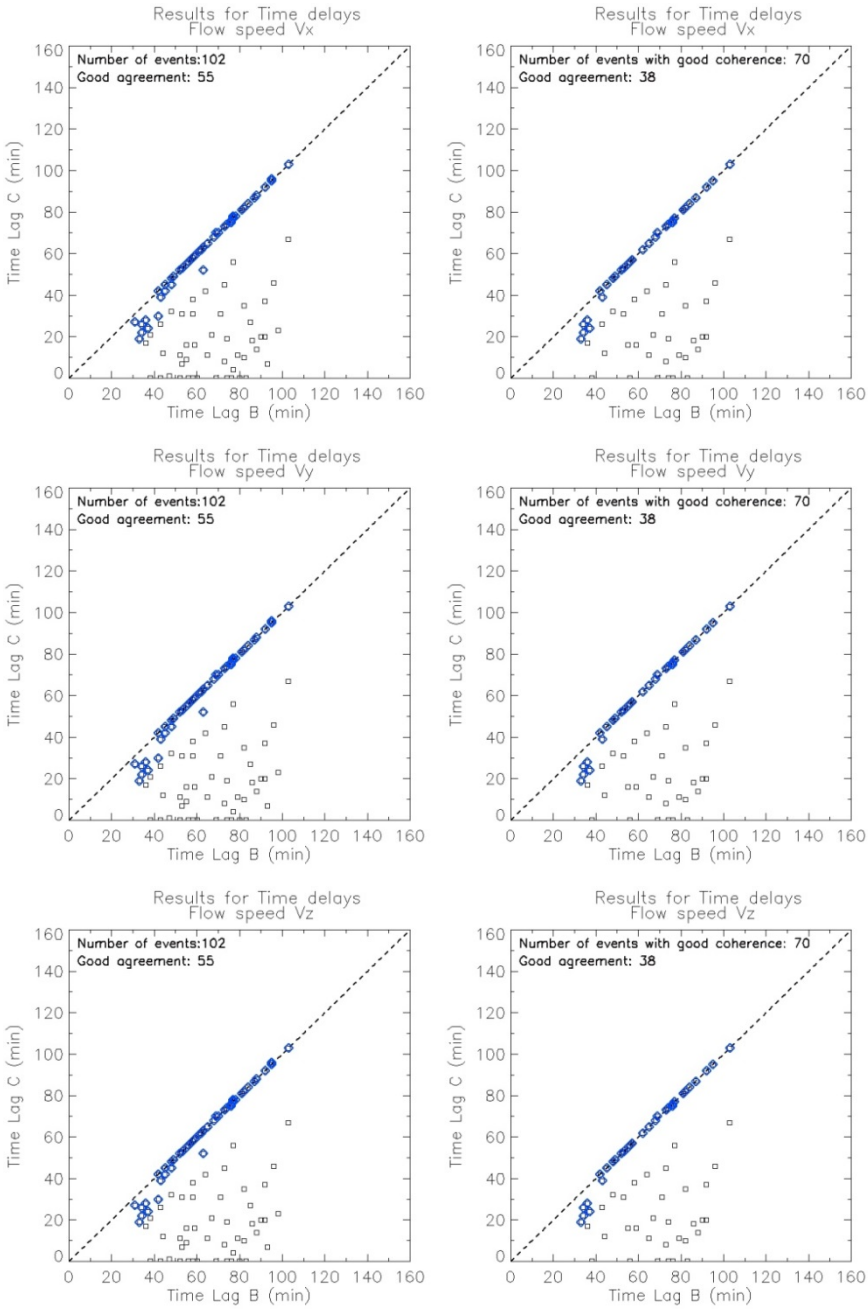

Figure 5.30: (Left) Plot of the power spectral maxima found in the study of time intervals LAG-C vs LAG-B v_x (top), v_y (middle) and v_z (bottom). (Right) Plot of good coherence results corresponding to LAG-A vs LAG-B. For all plots, lags within a 15-min interval are shown in blue.

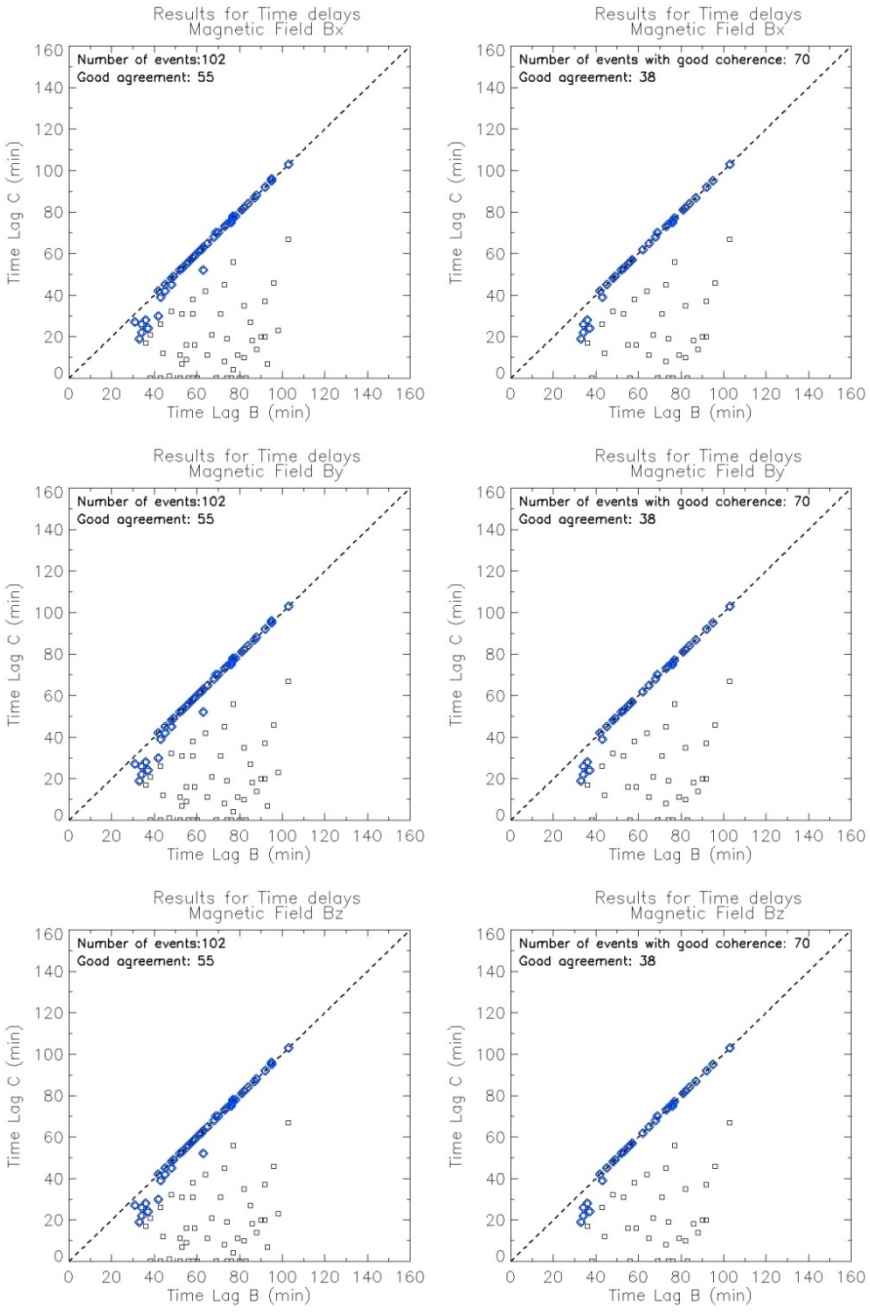

Figure 5.31: (Left) Plot of the power spectral maxima found in the study of time intervals LAG-C vs LAG-B for B_x (top), B_y (middle), B_z (bottom). (Right) Plot of good coherence results corresponding to LAG-A vs LAG-B. For all plots, lags within a 15-min interval are shown in blue.

Results yielded from LAG C might also suggest that sudden increase in dynamic pressure [*Mthembu et al.*, 2009] and/or surface waves [*Southwood*, 1974; *Archer and Plaschke*, 2014] in the magnetopause might play, after all, an important role in preparing the magnetospheric conditions needed for the solar wind to directly drive FLRs in the magnetosphere.

5.3 Summary

In this chapter, we used four different techniques as methodology to evaluate the coherence between ULF waves in the solar wind and FLRs in four steps.

The methodology outlined in the previous sections was systematically applied to all 120 events for which solar wind data was available. The rest of the events corresponded to periods of time where solar wind data was either bad or missing and data from other spacecraft should be used to analyze those FLRs. For the first technique, explained in section 5.1, additional requirements on number of valid data-points were needed; therefore, results for fewer than 116 events were available for each step of this technique. For time constrains, we only analyzed systematically the events for which ACE data was good. In future work, a deep and through study of each of the FLRs in the database would provide further insight in the particular physical characteristics of each of the events.

Solar wind properties were studied using measurements taken on board of the Advanced Composition Explorer (ACE). When comparing ACE solar wind measurements with observations done by SuperDARN, we accounted for solar wind travel times from the location of ACE to the magnetopause calculated following the minimum variance method of *Weimer et al.* [2003] and added an

extra time delay of 15 minutes to account for propagation times of compressional waves through the magnetosphere to resonant field lines.

First, we evaluated the correlation of the times series (section 5.1.1.). For this section, we followed the technique presented in the studies of correlation between the time-series of solar wind conducted by *Kepko et al.* [2002]. Correlation coefficient were found for two different time intervals, the first corresponding to the times between -80 and -30 minutes prior the occurrence of the FLR event, denoted as LAG-A, and the second corresponding to times within the delay-time interval (delay-time ± 15 minutes), called LAG-B. The maximum correlation coefficients of each period were recorded. In this analysis, we found that 9 out of 90 (10%) FLRs show good correlation with solar wind proton density in an interval of 80 to 30 minutes prior the FLR occurrence, while good correlation inside the delay-time interval is found in less than 10% (7 out of 90 FLRs). We found similar results in all solar parameters and references to the individual percentages for the other solar parameters can be found in the result section. We inferred, then, that the successful rate of correlation of solar wind proton density and other solar parameters with FLR events detected with SuperDARN is very low. Therefore, we concluded that either a) Solar wind might drive FLRs in the magnetosphere in rare cases, or b) The correlation analysis is not a good method to establish coherence between solar wind and FLRs.

Second, we inspected the power spectra of the time series (section 5.1.2.), both for the FLRs and the solar parameters in a 4 hour interval surrounding the FLR occurrence. Prominent local maxima were found for the dynamic power of all solar parameters and were compared with their corresponding FLRs' power maxima. The time of prominent maxima on solar parameters, found prior the respective occurrences of FLRs were used in the fourth step. A case study of power spectra comparison between solar wind proton density and case of 4 FLRs occurring in the same time interval was presented. The results yielded that proton density local power maxima was found within the *delay time* prior the

events but most prominent proton density power maxima was found around 30 minutes prior the event, outside the *delay time interval* (*delay-time* ± 15 min). These results suggest that a) some specific magnetospheric configurations (such as uniform plasma distribution in the flux tubes or previous excitation of the magnetosphere at the driven frequency) might play an important role in driving the FLRs and/or b) additional mechanisms, other than ULF waves in the solar wind should be involved in driving the FLRs.

Third, we examined the band-pass and analytic signals for both ACE and SuperDARN at around the time of the event. (Section 5.1.3). This evaluation permitted the examination of wave packets in the solar wind of the same frequency as the natural frequency of the FLR, most specifically the time delay between them. For solar wind proton density, good correlation coefficients were found in 32% while excellent correlation coefficients were found in 38% of the cases. The reminding 29% showed poor correlation, which implies that the wave packets corresponding to the detected FLRs did not show good agreement with the wave packets found in the solar wind within the delay interval time, but rather with wave packets outside a physically possible time delay. Moreover, the proton density wave packets maximum values found between the two hours prior to the event agreed only in 2 occasions with the maximum values found in the delay time interval. Furthermore, for a majority of the events the maximum was found outside of the delay time interval: most of the events showed a maximum value corresponding for time intervals between proton density and radar maxima shorter than the delay time, while few showed time intervals longer than the delay time. These results agreed with the results found in the previous steps that additional mechanisms, such as wave packets ULF waves in the solar wind previous to the FLR occurrence, might be critical in setting specific magnetospheric configurations to allow the solar wind to drive the FLRs.

Fourth and lastly, we systematically calculated and assessed the cross-power and cross-phase of both series, a generalization of a technique introduced

and developed by *Fenrich and Waters* [2008] in a case study, to establish the level coherence (section 5.1.4). In this current study, we followed, step-by-step, the procedure detailed in *Fenrich and Waters* [2008], with the addition that the cross-power and cross-phase technique was systematically implemented using the time-lag defined in that study (Lag A) and also in two different time-lags (Lag B and Lag C), for comparison purposes. The majority of FLRs exhibited values of high cross-power and a low cross-phase variance compared to the red noise 5% confidence level, randomly generated, when solar parameter data was shifted by the delay time (Lag A) or the maximum found within 15-minute interval surrounding the delay-time interval (Lag b).

Results of good coherence percentages yielded from LAG C are slightly higher than those found with LAG B (and therefore significantly higher than those found for LAG A) with approximately only half of the cases having both lags to agree in the shifted time. However, since for a large number of events the times found in LAG C yielded a time shift less than the 15 minutes needed for propagation from the magnetopause to Earth. These results should be further examined in depth because they a) could point to an unforeseen bias in the technique that needs to be addressed or b) previous wave packets in the solar wind matching the natural frequency of the flux tube, are indeed essential in setting specific magnetospheric configurations to allow the solar wind to drive the FLRs. This could suggest that sudden increase in dynamic pressure [*Mthembu et al.*, 2009] and/or surface waves [*Southwood*, 1974; *Archer and Plaschke*, 2014] in the magnetopause are conditions necessary for the solar wind to directly drive FLRs in the magnetosphere.

Overall, this chapter presented a thorough, systematic evaluation of different techniques, applied to the large FLR database, for studying the coherence between solar wind and FLRs. The statistical results presented in this chapter are important considerations to be taken into account when applying an

individual techniques in case studies and introduce new ideas on the approach of the study of solar coherence for FLRs.

5.4 Conclusions

The new findings in this chapter include:

1) The correlation analysis was shown to be a poor method of establishing coherence between the solar wind fluctuations and FLRs.

2) The studies of power spectra and wave packets found by the band-passed analytic signal produced important results and were proven to be a good methodology to study coherence between solar wind and FLRs.

3) The cross-power and variance in cross-phase technique was demonstrated to be an inconclusive technique if applied in isolation.

4) Prior wave packets in the solar wind matching the natural frequency of the flux tube play an important role on setting specific magnetospheric configurations to allow the solar wind to drive the FLRs.

Chapter 6

Conclusions and future work

The main goal of this study was to statistically determine what percentage of Field Line Resonances (FLR) in Earth's Magnetic Field (Magnetosphere) between 0.5 mHz and 5 mHz had origin in the solar wind Ultra Low Frequency (ULF) waves. The second main goal of this thesis research was to systematically analyze the characteristics of FLRs and the statistics of their occurrences (such as frequency, latitude, local time, m-value, to name a few). To achieve those goals, it was important, as a secondary goal of this study, to produce an automated code to identify ULF waves using SuperDARN to create a large database of FLRs from which to study the coherence among FLRs and solar wind ULF waves and from which to determine FLR statistics on classification of their characteristics.

Many studies of FLRs have reported, in the past decades, the repetitiveness and discreteness nature of FLRs, in addition to their unresolved source of excitation. Recent work has indicated that discrete, continuous ULF waves in the solar wind are responsible to drive these FLRs. However, the existence, significance, and stability of the "magic frequencies" is disputed: many other studies, cited in this thesis, found no evidence of stable, recurring, discrete frequencies in the Pc5 range. This thesis work aimed to shed light on these issues. The premise of this study was that "magic frequencies" existed and the intent was to test the hypothesis that discrete ULF waves in the solar wind directly drove those FLRs.

Chapter 1 of this thesis provided useful background information and theory regarding FLRs and the SuperDARN radar network.

In chapter 2, the methodology for systematic detection of ULF wave, with SuperDARN, was explained in detailed. We successfully created a code to automatically detect ULF coherent waves over a large area within the field of view (FoV) of any SuperDARN radar station that could be later categorized as a "Field Line Resonance". The code was based on the "Cross-power-Cross-phase Technique" developed by *Fenrich and Waters* [2008] to find coherence between ULF solar wind waves and ULF waves detected by SuperDARN. The ULF detection code was designed to analyze multi-year data from multiple SuperDARN radars. The code analyzed data for the year 2003 for the 15 stations. The code output were 'flagged ULF candidates' that were later individually examined to past the established FLR characterization criteria. The major achievement of the development of this methodology was the systematic detection of ULF waves without using the cross-spectral techniques, utilized until now.

In chapter 3, the 161 ULF flags recorded using the methodology described in chapter 2 were examined using the cross-spectral and analytic signal the techniques explained in *Walker et al.* [1992] and *Fenrich et al.* [1995] for identification of FLRs using the SuperDARN Doppler velocity data. A total of 121 FLRs were identified during 2003 and their primary characteristics (frequency, propagation, phase variation with latitude, azimuthal wavenumber *m,* MLT, etc) were recorded and tabulated. A large database was created to analyze the characteristics of FLRs and to study the coherence of solar wind ULF waves with the FLRs to establish their wave sources. The efficiency of the methodology was: 66.50% of the ULF waves pre-selected were further characterized as FLRs and 91% of the ULF waves pre-selected were further characterized as FLRs when methodology was applied to only gates higher than 14.

In chapter 4, we described the processes of characterization of the FLRs in the database, as well as the statistical results on these properties. We also provided comparisons with previous characterization studies, presented in the introduction and at the beginning of that chapter.

Interesting aspects of the characteristics of the FLRs in the database included frequency distribution, latitude of occurrences, *m*-value, and magnetic local time, to name a few. The events in the database, presented in this study, showed some deviations for the characterizations proposed in *Fenrich et al.* [1995] in terms of the FLR phase variation vs. magnetic latitude, propagation (sundwards-antisunwards; eastwards-westwards) and location. A conclusion was drawn that the FLRs identified in this study were not able to be classified into the two distinct groups defined by *Fenrich et al.* [1995] and *Fenrich and Samson* [1997] based upon the size of the FLR azimuthal wavenumber *m*, but rather the classification involved many other variables.

In terms of frequency distribution, we asked ourselves if some frequency occurring more often than others. This was an important question, since the repetitive observation of "magic frequencies" was the premise assumed to find sources of both high-*m* and low-*m* in ULF waves in the solar wind.

For the 121 FLRs found in this study, 'magic frequencies' (1.3, 1.9, 2.6 and 3.4 mHz) were not particularly observed. The frequency with more occurrences in this study was the first in the array, 0.6±0.1 mHz. The observation of other frequencies showed a decreasing trend of observation of occurrences for increasing frequency. This result was compatible with the recent study by *Archer and Plaschke* [2014] on distribution of magnetopause surface waves observed throughout an entire solar cycle.

For FLRs with $m < 17$ we saw the decreasing trend for increasing frequency, which it was agreeable with ground magnetometer observations reported by *Murphy et al.* [2011]; however, the distribution for FLRs with azimuthal

wavenumbers $m \geq 17$ presented that maximum around the frequency 1.1±0.1 mHz FLR. These events should be the focus of future work, since a case-to-case study of the events in the database was beyond the scope of this thesis work.

With respect to their magnetic local time for their occurrence, we saw that all FLRs are evenly scattered in all MLT locations, with exception of the noon sector. For the FLRs presented in our database, there was not preference for events to be localized in a specific MLT sector depending on their azimuthal wavenumbers *m*. We also found that low-*m* events with low frequencies were localized in the night sector.

We also examined the classification of FLRs given their *m*-values and the phase variations as a function of latitude, since this was a topic of disagreements in the field. For the events in our database, results showed that all the events occurring in the magnetopause, as located using the simulations by *Pierrard and Stegen* [2008], exhibited '*reverse*' phase variation regardless of their azimuthal wavenumber *m*. We also saw that for events in the plasmatrough and beyond, two-thirds of the FLRs with "*reverse*" phase change had $m \geq 17$, while the rest exhibited "*standard*" phase change, most of them located between magnetic latitude 65 and 72 degrees; likewise, two-thirds of the FLRs with "*standard*" phase change had $m < 17$, while the rest exhibited *"reverse*" phase change, most of them located at lower magnetic latitude (62-66 degree).

We studied, as well, how often the same frequency was observed at different latitudes: in our results we found the same frequency extended throughout a wide range of latitudes. We found that variation of plasma density in the tubes, as well as MLT location of the events (due to dynamics in the plasmasphere and convection of field lines due to solar wind dynamic pressure) played an important role on finding the same frequency in different latitudes.

In terms of the propagation of the FLRs in our database, we found that half of the low-*m* FLRs propagated antisunwards; the other half propagated towards

the sun and most of those events exhibited a "*reverse*" phase variation. On the other hand, two-thirds of the high-*m* FLRs propagated westwards, with the high-*m* FLRs propagated eastwards mostly located in the night-to-dawn sector, a large number of those latest events displaying a "*standard*" phase variation. There were, however, numerous occurrences of westward propagating high-*m* FLRs that exhibited a "*standard*" phase variation as well, which it was puzzling.

There were several questions resulting from this study in terms of the characteristics of the FLRs that formed the large database. Previous studies have generalized certain characteristics of FLRs but results found in this study have raised questions on these generalizations. The discrepancies stress the importance of the individual study of the physics dynamics of each events, including studies on particle dynamics and substorm activity in the magnetosphere, which it was beyond the scope of this thesis research but will be the topic of future studies.

Finally, to close this research study, we presented in chapter 5 four different, complementary techniques as methodology to evaluate the coherence between ULF waves in the solar wind and FLRs. Solar wind properties were studied using measurements taken on board of the Advanced Composition Explorer (ACE). The methodology outlined in that chapter was systematically applied to the 120 events for which solar wind data was available. The rest of the events corresponded to periods of time where solar wind data was either bad or missing and data from other spacecraft should be used to analyze those FLRs. For the first technique, explained in section 5.1, additional requirements on number of valid data-points were needed; therefore, results for fewer than 116 events were available for each step of this technique. For time constrains, we only analyzed systematically the events for which ACE data was good. In future work, a deep and throughout study of each of the FLRs in the database would provide further insight in the particular physical characteristics of each of the events.

First, we evaluated the correlation of the times series. This technique was utilized by *Kepko et al.* [2002] to show high correlation between solar wind waves and magnetospheric ULF waves. The aim of systematically applying the technique to all solar parameters and all FLRs in the database was to find the lever for which this technique can be used in the study of coherence between solar wind and magnetospheric waves and to study the delay times among both. In this step, correlation coefficient were found for two different time intervals for comparison reasons. The first corresponded to the times between -80 and -30 minutes prior the occurrence of the FLR event, denoted as LAG-A, and the second corresponded to times within the delay-time interval (delay-time ± 15 minutes), called LAG-B. Good correlation was rarely found (10% of the times, 9 out of 90 cases) between solar wind proton density and SuperDARN in an interval denoted as LAG-A. Less than 10% (7 out of 90) FLRs showed good correlation with solar wind proton density for LAG-B. All solar parameters yielded similar results. These results infer that either a) Solar wind might be the driver of FLRs in the magnetosphere in rare cases, or b) The correlation analysis might not be a good method to establish coherence between solar wind and FLRs.

Second, we inspected the power spectra of the time series, in a 4 hour interval surrounding the FLR occurrence, both for the FLRs and the solar parameters. The results on the delay time between the maxima corresponding to the FLRs and the prominent maxima found on solar parameters prior the respective occurrences of FLRs were utilized in the fourth step. A case study of 4 FLRs occurring in the same time interval was presented and the time delay among the dynami power maxima for the most dominant FLR and few solar wind parameters was presented. The results in this step yielded that proton density local power maxima was found within the *delay time* prior the events but most prominent proton density power maxima was found around 30 minutes prior the event, outside the *delay time interval* (*delay-time* ± 15 min). Similar results were found for all other solar parameters. We concluded that a) some specific magnetospheric configurations might play an important role in allowing the field

lines to be driven, and/or b) additional mechanisms, other than ULF waves in the solar wind, should be the drivers of the FLRs.

Third, we examined the band-pass and analytic signals for both ACE and SuperDARN at around the time of the event in the search of wave packets in the solar wind with the same frequency as the natural frequency of the FLRs. Results demostrated that the wave packets corresponding to the detected FLRs did not show good agreement with the wave packets found in the solar wind within the interval time. Most of the events showed a maximum value between the solar parameters and radar maxima corresponding for time intervals shorter than the delay time, while few showed time intervals longer than the delay time. These results are in agreement with the results found in the previous steps and strengthen the idea that additional mechanisms and/or specific magnetospheric configurations are needed to allow the solar wind to drive the FLRs.

The fourth and last step was to systematically calculate and assessee the cross-power and cross-phase of both series, as presented by *Fenrich and Waters* [2008]. This was done to establish the level coherence. We applied the technique detailed in that study, with the addition that the cross-power and cross-phase technique for three different lags (Lag A, Lag B and Lag C, Lag A being the one established in *Fenrich and Waters* [2008]).

All lags yielded levels of high cross-power and a low cross-phase variance compared to the red noise 5% confidence level, randomly generated but results of good coherence percentages yielded from LAG C were slightly higher than those found with LAG B (and therefore significantly higher than those found for LAG A). Only half of the cases having both lags to agree in the shifted time. Moreover, the times found in LAG C yielded a time shift less than the 15 minutes needed for propagation from the magnetopause to Earth for a large number of events. These outcomes of this methodology should be further examined in depth because they a) might reveal an unforeseen bias in the technique or b) imply that previous wave packets in the solar wind matching the natural frequency of the flux tube

are indeed essential in setting specific magnetospheric configurations to allow other mechanisms to drive the FLRs.

Possible avenues in future studies include:

1) Refining the methodology for ULF systematic detection of FLR candidates presented in chapter 2. This methodology had a success rate of 66.50% for which ULF waves were later classified as FLRs. The unsuccessful flags corresponded to either FLRs for which a profile could not be successfully retrieved or ULF propagating waves that are not FLRs. A success rate of 91% was obtained if the detection technique was applied only to data corresponding to gates greater than 14 (above 900 km). Code improvement could include:

a) Pre-selecting data that includes good scatter for all beams and gates, to avoid detection of FLRs with no profile available, especially for lower gates.

b) Refining the threshold established to flag events: Instead of using a cross-power and variance in cross-phase calculated daily mean, the threshold could be established to be a 24-hour running mean cross-power and variance in cross-phase centered in the time of the event, with the addition of comparisons of those values with monthly and/or annual means for each radar and each beam-gate pair.

2) Developing an automated technique to characterize the FLRs by obtaining the profile from the analytic signal to eliminate eye-profiling, presented in chapter 3. The local maximum in analytic amplitude, with its corresponding phase difference and m, could be automatically found in the surrounding area to the beam-gate flag. Further studies would include what range of beam-gate pairs would maximize the success rate of FLR detection. The

database presented in this thesis could serve as a testing ground for this "profiling technique".

3) Analyzing in detail the reverse phase characterization of FLRs located in the plasmapause, as introduced in chapter 4. Collaboration with BISA has been established to produce simulations for times corresponding to high Kp activity. Information on the location of the plasmapause due to plumes in the plasmasphere will be used as time flags to search for FLRs that could produce statistics in terms of occurrences of FLRs with reverse phase in the plasmapause.

4) Extensively studying FLRs with azimuthal wavenumbers $m \geq 10$ in an effort to understand:

a) The distribution for maximum around the frequency 1.1 ±0.1 mHz for FLRs with azimuthal wavenumbers $m \geq 17$,

b) The significance of wave-particle interactions on both low-m and high-m events,

c) The occurrence of substorm-induced FLRs, simultaneous low-m and high-m events, to understand the dynamics of location and propagation of FLRs.

5) Examining in more depth FLR case studies where wave packets in the solar wind corresponding to the FLR frequency were present for time lags below the delay-time, as reported in chapter 5, to establish the significance of pre-existing configurations of the magnetosphere that are needed for the solar wind ULF waves to drive FLRs in the magnetosphere.

Overall, this thesis presented a thorough, systematic evaluation of different techniques both to detect FLRs at large scale, to characterize FLRs and to study

their wave sources in the solar wind. Most importantly, the statistical results gave important considerations to be taken into account when applying the individual techniques in case studies and introduced new ideas on the approach of the study of solar coherence for FLRs.

Bibliography

Allan, W., and E. M. Poulter, ***Damping of magnetospheric cavity modes: A discussion***, J. Geophys. Res., 9d, 11,843, 1989.

Allan, W., A.N. Wright, ***Large-m waves generated by small-m field line resonances via the nonlinear Kelvin-Helmholtz instability***, J. Geophys. Res., 102, 19927, 1997.

Archer, M. and Ferdinand Plaschke (2014), ***What are the frequencies of standing magnetopause surface waves?*** J. Geophys. Res. (accepted)

Baddeley, L. J., Yeoman, T. K, Wright, D. M., Trattner, K. J., Kellet, B. J. (2005) ***On the coupling between unstable magnetospheric particle populations and resonant high m ULF wave signatures in the ionosphere***, Annales Geophysicae, European Geosciences Union (EGU), 2005, 23 (2), pp.567-577

Baker, J. B., E. F. Donovan, and B. J. Jackel (2003), ***A comprehensive survey of auroral latitude Pc5 pulsation characteristics***, J. Geophys. Res., 108(A10), 1384, doi:10.1029/2002JA009801.

Baker, J. B., (2011), ***The Super Dual Auroral Radar Network (SuperDARN)***, PDF Tutorial available at: http://vt.superdarn.org/tiki-index.php?page=sd_tutorial.

Ballatore, P., J.P. Villain, N. Vilmer, M. Pick (2001), ***The influence of the interplanetary medium on SuperDARN radar scattering occurrence***, Ann. Geophysicae 18, 1576-1583

Baumjohann, W. and R. A. Treumann (1997), ***Basic Space Plasma Physics***; Publisher: World Scientific, ISBN: 1-86094-079-X

Berube, D., Moldwin, M. B., & Weygand, J. M. (2003), ***An automated method for the detection of field line resonance frequencies using ground magnetometer techniques***. Journal of Geophysical Research: Space Physics (1978–2012), 108(A9).

Bland, E.C., A. J. McDonald, F. W. Menk, and J. C. Devlin (2014), ***Multipoint visualization of ULF oscillations using the Super Dual Auroral Radar Network***. Geophys. Res. Lett. 41, 6314-6320, doi:10.1002/2014GL061371

Bracewell, R. N., ***The Fourier Transform and Its Applications***, 2nd ed., McGraw-Hill, New York, 1986.

Chen, F. F. (1974), ***Plasma Physics***. Plenum Press, NY.

Chen, L., and A. Hasegawa (1974), ***A theory of long-period magnetic pulsations: 1. Steady state excitations of field line resonance***, J. Geophys. Res., 79, 1024.

Chisham, G., M. Lester, S. E. Milan, M. P. Freeman, W. A. Bristow, A. Grocott, K. A. McWilliams, J. M. Ruohoniemi, T. K. Yeoman, P. L. Dyson, R. A. Greenwald, T. Kikuchi, M. Pinnock, J. P. S. Rash, N. Sato, G. J. Sofko, J.-P. Villain, A. D. M. Walker (2007). ***A decade of the Super Dual Auroral Radar Network (SuperDARN): scientific achievements, new techniques and future directions***. *Surveys in Geophysics* **28** (2007), doi:10.1007/s10712-007-9017-8.

Cummings, W. D., O'sullivan, R. J., & Coleman, P. J. (1969), ***Standing Alfvén waves in the magnetosphere***. Journal of Geophysical Research, 74(3), 778-793.

Dent, Zoë (2003), ***ULF Wave Remote Sensing of Magnetospheric Plasma Density***. Thesis (PhD). UNIVERSITY OF YORK (United Kindom)

Damiano, P. A., Wright, A. N., Sydora, R. D., & Samson, J. C., ***Energy dissipation via electron energization in standing shear Alfvén waves.*** Physics of Plasmas (1994-present) 14.6: 062904.

Danskin, Donald William (2003), ***HF auroral backscatter for the E and F regions***. Thesis (PhD). UNIVERSITY OF SASKATCHEWAN (CANADA), October 2003, 188 pages

Dungey, J. W. (1954), ***Electrodynamics of the outer atmosphere.*** The physics of the Ionosphere, p.229. Phys. Soc. London.

Dungey, J. W. (1954), ***The propagation of Alfvén waves through the ionosphere***. Sci. Rept. No. 57, Pennsylvania State Univ., Ionosphere Res. Lab.

Dungey, J.W. and D.J. Southwood (1970), ***Ultra low frequency waves in the magnetosphere***, Space Sci. Rev., 10, 672.

Elkington, Scot R., Mary K. Hudson, and Anthony A. Chan (1999), ***Acceleration of relativistic electrons via drift-resonant interaction with toroidal-mode Pc-5 ULF oscillations***. *Geophysical research letters* 26.21: 3273-3276.

Elkington, S. R., Hudson, M. K., & Chan, A. A. (2003), ***Resonant acceleration and diffusion of outer zone electrons in an asymmetric geomagnetic field.*** Journal of Geophysical Research: Space Physics (1978–2012), 108(A3).

Engebretson, M. J., Zanetti, L. J., Potemra, T. A., Baumjohann, W., Lühr, H., and Acuna, M.H. (1987), ***Simultaneous Observation of Pc3–4 Pulsations in the Solar Wind and in the Earth's Magnetosphere***, J. Geophys. Res., 92, 10053–10062.

Fenrich, F. R., J. C. Samson, G. Sofko, and R. A. Greenwald (1995), ***ULF High- and Low-m Field Line Resonances Observed With the Super Dual Auroral Radar Network***, J. Geophys. Res., 100(A11), 21, 535–21,547, doi:10.1029/95JA02024.

Fenrich, Frances Rose Erna (1997), ***The field line resonance: Observation and theory***. Thesis (PhD). UNIVERSITY OF ALBERTA (CANADA), Source DAI-B 58/09, p. 4892, Mar 1998, 119 pages.

Fenrich and Samson, (1997), ***Growth and decay of field line resonances***. Journal of Geophysical Research 102: doi: 10.1029/97JA01376

Fenrich, F. R., C. L. Waters, M. Connors, and C. Bredeson (2006), ***Ionospheric signatures of ULF waves: Passive radar techniques***, Magnetospheric Current Systems, edited by: Takahashi, K., Chi, P., Denton, R. E., and Lysak, R. L., Geophysical Monograph 169, pp. 259–272, American Geophysical Union, Washington, D.C..

Fenrich, F. R., and C. L. Waters (2008), ***Phase coherence analysis of a field line resonance and solar wind oscillation***, Geophys. Res. Lett., 35, L20102, doi:10.1029/2008GL035430.

Francia, P., and U. Villante (1997), ***Some evidence of ground power enhancements at frequencies of global magnetospheric modes at low latitude***, Ann. Geophys., 15, 17.

Francia, P., L. J. Lanzerotti, U. Villante, S. Lepidi, and D. Di Memmo (2005), ***A statistical analysis of low-frequency magnetic pulsations at cusp and cap latitudes in Antarctica***, J. Geophys. Res., 110, A02205, doi:10.1029/2004JA010680.

Glassmeier, K. H., Volpers, H., and Baumjohann, W. (1984). ***Ionospheric Joule dissipation as a damping mechanism for high latitude ULF pulsations: Observational evidence***. Planet. Space Sci., 32(11), 1463–1466.

Goldstein, M. L., and D. A. Roberts (1999), ***Magnetohydrodynamic turbulence in the solar wind***, Phys. Plasmas, 6, 4154

Grant, I. F., D. R. McDiarmid, and A. G. McNamara, ***A class of high-m pulsations and its auroral radar signature***, J. Geophys. Res., 97, 8439, 1992.

Greenwald, R. A., Weiss, W., Nielsen, E. and Thomson, N. P. (1978), ***Stare auroral radar observations of Pc 5 geomagnetic pulsations***, Radio Sci. 13, 1021.

Greenwald, R. A., K. B. Baker, R. A. Hutchins, and C. Hanuise (1985), ***An HF phased-array radar for studying small-scale structure in the high latitude ionosphere***, Radio Sci., 20, 63–79.

Greenwald, R. A., Baker, K. B., Dudeney, J. R., Pinnock, M., Jones, T. B., Thomas, E. C., Villain, J.-P.,Cerisier, J.-C., Senior, C., Hanuise, C., Hunsucker, R.D., Sofko, G., Koehler, J., Nielsen, E., Pellinen, R., Walker, A.D.M., Sato, N., Yamagishi, H. (1995), ***Darn/superdarn***. Space Science Reviews, 71(1-4), 761-796.

Hannah, Kevin (2004), ***Autocorrelation functions and Doppler spectra measured by the TIGER SuperDARN radar***. Thesis (Bachelor of Space Science with Honours). La Trobe University (Australia) November 2004, 60 pages.

Healey, Ryan (2005), ***Enhanced Beam Steering Capability for the TIGER SuperDARN radars***. Thesis (Bachelor of Space Science with Honours). La Trobe University (Australia) December 2005, 56 pages.

Hughes, J. H. (1994). ***Magnetospheric ULF waves: A tutorial with a historical perspective***. In M. J. Engebretson, K. Takahashi, and M. Scholer, editors, Geophysical Monograph 81: Solar Wind Sources of Magnetospheric Ultra-Low-Frequency Waves, pages 1–11. American Geophysical Union, Washington DC, USA.

Jacobs, J. A., Y. Kato, S. Matsushita, and V. A. Troitskaya (1964), ***Classification of geomagnetic micropulsations***, J. Geophys. Res., 69, 180-, 1964.

Kepko, L., H. E. Spence, and H. J. Singer (2002), ***ULF waves in the solar wind as direct drivers of magnetospheric pulsations***, Geophys. Res. Lett., 29(8), 1197, doi:10.1029/2001GL014405.

Kepko, L., and H. E. Spence (2003), ***Observations of discrete, global magnetospheric oscillations directly driven by solar wind density variations***, J. Geophys. Res., 108(A6), 1257, doi:10.1029/2002JA009676.

Kivelson and Russell (1995), ***Introduction to Space Physics***, Cambridge University Press.

Kivelson, M. G., and D. J. Southwood (1985), ***Resonant ULF waves: A new interpretation***, Geophys. Res. Lett., 12, 49– 52.

Lanza, R. and A. Meloni (2006). ***The Earth's Magnetism. An Introduction for Geologists***. Berlin, Heidelberg, New York: Springer-Verlag. ISBN13 978 3 540 27979 2

Lanzerotti, L. J., and C. G. Maclennan (1988), ***Hydromagnetic waves associated with possible flux transfer events***. Astrophysics and space science 144.1-2: 279-290.

Lanzerotti, L. J., and Chanchal Uberoi (1998), ***Earth's Magnetic Environment***, *Sky and Telescope*, Oct., 1998, pp. 360-362

Lester, Mark (2013), ***The Super Dual Auroral Radar Network (SuperDARN): An overview of its development and science***, Advances in Polar Science, March 2013 Vol. 24 No. 1: 1-11 doi: 10.3724/SP.J.1085.2013.00001

Lointier G., T. Dudok de Wit, C. Hanuise, X. Vallières, and J.-P. Villain (2008), ***A statistical approach for identifying the ionospheric footprint of magnetospheric boundaries from SuperDARN observations***. Ann. Geophys., 26, 305–314, 2008

Mager, P. N., D. Y. Klimushkin, and N. Ivchenko (2009), ***On the equatorward phase propagation of high-m ULF pulsations observed by radars***, J. Atmos. Sol. Terr. Phys., 71, 1677–1680, doi:10.1016/j. jastp.2008.09.001.

Mann, I. R. (1998), ***An MHD model for driven high m field line resonances***, Geophys. Res. Lett., 25(9), 1515–1518, doi:10.1029/98GL51092.

Mann, I. R., T. P. O'Brien, and D. K. Milling (2004), ***Correlations between ULF wave power, solar wind speed, and relativistic electron flux in the magnetosphere: solar cycle dependence***. Journal of atmospheric and solar-terrestrial physics 66.2: 187-198.

Mann, I. R., et al. (2008), ***The upgraded CARISMA magnetometer array in the THEMIS era***, Space Sci. Rev., 141, 413–451, doi:10.1007/s11214-008-9457-6.

Mathie, R. A., and I. R. Mann (2000), ***A correlation between extended intervals of Ulf wave power and storm-time geosynchronous relativistic electron flux enhancements***. *Geophysical research letters* 27.20: 3261-3264.

Mazzino, Laura; Cyamukungu, Mathias; Benck, Sylvie; Cabrera, Juan, (2008), ***Development of a statistical dynamic radiation belt model: Analysis of storm time particle flux variations***. ESA Ionizing Radiation Detection and Data Exploitation Workshop proceedings. January, 2008

McComas, D. J., Blame, S. J., Barker, P., Feldman, W. C., Phillips, J. L., Riley, P., and Griffee, J. W.: ***Solar Wind Electron Proton Alpha Monitor (SWEPAM) for the Advanced Composition Explorer***, Space Sci. Rev., 86, 563–612, 1998.

McIlwain, C. E. (1966), ***Magnetic Coordinates***, Space Science Reviews, Vol. 5, Issue 5, pp. 585-598.

Menk, F. W. (2011), ***Magnetospheric ULF waves: A review***, in The Dynamic Magnetosphere, IAGA Spec. Sopron Book Ser., vol. 3, edited by W. Liu and M. Fujimoto, pp. 223–256, Springer, Dordrecht, Netherlands.

Meyer-Vernet, N. ***Basics of the Solar Wind.*** 01/2007; Publisher: Cambridge University Press, ISBN: 10 0-521-81420-0

Mthembu, S. H., S. B. Malinga, A. D. M. Walker, and L. Magnus (2009), ***Characterization of ultra low frequency (ULF) pulsations and the investigation of their possible sources***, Ann. Geophys., 27, 3287–3296.

Murphy, KR; Mann, IR; Jonathan Rae, I; Milling, DK; (2011) ***Dependence of ground-based Pc5 ULF wave power on F10.7 solar radio flux and solar cycle phase***. Journal of Atmospheric and Solar-Terrestrial Physics , 73 (11-12) 1500 - 1510. 10.1016/j.jastp.2011.02.018.

Obayashi, T. and Jacobs, J. A. (1958). ***Geomagnetic pulsations in the earth's outer atmosphere***. Geophys. J. R. Astr. Soc., 1, 53–63.

Orr, D. and Hanson, H. W. (1981). ***Geomagnetic pulsation phase patterns over an extended latitudinal array***. J. Atmos. Terr. Phys., 43(9), 889–910.

Patel, V. L., & Cahill Jr, L. J. (1964), ***Evidence of hydromagnetic waves in the earth's magnetosphere and of their propagation to the earth's surface***. Physical Review Letters, 12(9), 213.

Parker, E. N. (1958) ***Dynamics of the Interplanetary Gas and Magnetic Fields***. Astrophysical Journal, vol. 128, p.664 11/1958, DOI: 10.1086/146579

Perraut, S., R. Gendrin, P. Robert, A. Roux, and C de Villedary (1978), ***ULF waves observed with magnetic and electric sensors of GEOS-1***. Space Sci. Rev. 22:347

Pierrard, V., and J. Lemaire (1996), ***Lorentzian ion exosphere model***, J. Geophys. Res., 101, 7923– 7934, doi:10.1029/95JA03802.

Pierrard, V., and J. Lemaire (1998), ***A collisional kinetic model of the polar wind***, J. Geophys. Res., 103(A6), 11,701 – 11,709, doi:10.1029/98JA00628.

Pierrard, V., and J. Lemaire (2001), ***Exospheric model of the plasmasphere***, J. Atmos. Sol. Terr. Phys., 63(11), 1261 – 1265, doi:10.1016/S1364-6826(00)00227-3.

Pierrard, V., and J. Lemaire (2004), ***Development of shoulders and plumes in the frame of the interchange instability mechanism for plasmapause formation***, Geophys. Res. Lett., 31(5), L05809, doi:10.1029/2003GL018919.

Pierrard V., and K. Stegen, ***A three dimensional dynamic kinetic model of the plasmasphere***, Journal Geophys. Res., 113, A10209, doi: 10.1029/2008ja013060, 2008.

Pierrard, V., and J. Cabrera (2005), ***Comparisons between EUV/IMAGE observations and numerical simulations of the plasmapause formation***, Ann. Geophys., 23(7), 2635– 2646, SRef-ID: 1432–0576/ag/2005–23–2635.

Pierrard, V., and J. Cabrera (2006), ***Dynamical simulations of plasmapause deformations***, Space Sci. Rev., 122(1–4), 119–126, doi:10.1007/s11214-006-5670-3.

Pierrard V., and K. Stegen (2008), ***A three dimensional dynamic kinetic model of the plasmasphere***, Journal Geophys. Res., 113, A10209, doi: 10.1029/2008ja013060.

Ponomarenko, P. V., Waters, C. L., Sciffer, M. D., Fraser, B. J., & Samson, J. C. (2001), ***Spatial structure of ULF waves: Comparison of magnetometer and Super Dual Auroral Radar Network data.*** Journal of Geophysical Research: Space Physics (1978–2012) 106.A6: 10509-10517.

Ponomarenko, P. V. (2003), ***Visualization of ULF waves in SuperDARN data***. Geophysical Research Letters 30, Issue 18. doi:10.1029/2003GL017757

Ponomarenko, P. V., Waters, C. L., and Menk, F. W. (2007), ***Factors determining spectral width of HF echoes from high latitudes***, Ann. Geophys., 25, 675-687, doi:10.5194/angeo-25-675-2007.

Poulter, E. M., Allan, W., Keys, J. G., and Nielsen, E. (1984). ***Plasmatrough ion mass densities determined from ULF pulsation eigenperiods***. Planet. Space Sci., 32(9), 1069–1078.

Provan, G. and T. K. Yeoman (1997), ***A Comparison of Field Line Resonances Observed at the Goose Bay and Wick Radars***, Ann. Geophysicae, 15, 231-235, 1997.

Rae, I. J., Donovan, E. F., Mann, I. R., Fenrich, F. R., Watt, C. E. J., Milling, D. K., Lester, M., Lavraud, B, Wild, J.A., Singer, H.J., Rème, H., Balogh, A. (2005) ***Evolution and characteristics of global Pc5 ULF waves during a high solar wind speed interval***. Journal of Geophysical Research: Space Physics (1978–2012) 110.A12.

Rae, I. J., Mann, I. R., Dent, Z. C., Milling, D. K., Donovan, E. F., & Spanswick, E. (2007), ***Multiple field line resonances: Optical, magnetic and absorption signatures***. *Planetary and Space Science* 55.6 (2007): 701-713.

Rae, I. J., Watt, C. E. J., Fenrich, F. R., Mann, I. R., Ozeke, L. G., & Kale, A. (2008, January). **Energy deposition in the ionosphere through a global field line resonance**. Annales Geophysicae. Vol. 25. No. 12. 2008.

Rae, I. J., I. R. Mann, K. R. Murphy, L. G. Ozeke, D. K. Milling, A. A. Chan, S. R. Elkington, and F. Honary (2012), ***Ground-based magnetometer***

determination of in situ Pc4–5 ULF electric field wave spectra as a function of solar wind speed, J. Geophys. Res., 117, A04221, doi:10.1029/2011JA017335.

Ramirez, R. W. (1985). ***The F.F.T.: The Fundamentals and Concepts***. Prentice- Hall, Englewood Cliffs, NJ, USA.

Ribeiro, A. J., J. M. Ruohoniemi, P. V. Ponomarenko, L. B. N. Clausen, J. B. H. Baker, R. A. Greenwald, K. Oksavik, and S. de Larquier, (2013), ***A comparison of SuperDARN ACF fitting methods***, RADIO SCIENCE, VOL. 48, 1–9, doi:10.1002/rds.20031

Richmond, A. D. (2010), ***On the ionospheric application of Poynting's theorem***. Journal of Geophysical Research: Space Physics (1978–2012) 115.A10.

Rostoker, G. and Samson, J.C. (1972). ***Pc micropulsations with discrete, latitude-dependent frequencies***. Journal of Geophysical Research 77: doi: 10.1029/JA077i031p06249. issn: 0148-0227.

Samson, J. C., J. A. Jacobs, and G. Rostoker (1971), ***Latitude-Dependent Characteristics of Long-Period Geomagnetic Micropulsations***, J. Geophys. Res., 76(16), 3675–3683, doi:10.1029/JA076i016p03675.

Samson, J.C. and Rostoker, G. (1972). ***Latitude-dependent characteristics of high-latitude Pc 4 and Pc 5 micropulsations***. Journal of Geophysical Research 77: doi: 10.1029/JA077i031p06133. issn: 0148-0227.

Samson, J. C., R. A. Greenwald, J. M. Ruohoniemi, T. J. Hughes, and D. D. Wallis (1991), ***Magnetometer and radar observations of magnetospheric cavity modes in the Earth's magnetosphere***, Can. J. Phys. , 69 , 929.

Schield, M. A., ***Pressure balance between solar wind and magnetosphere***, J. Geophys. Res., 74, 1275, 1969.

Schlegel, K. (1995) ***Coherent backscatter from ionospheric E-region plasma irregularities***, J. Geophys. Res., 58, Issues 8-9, Pages 933-941 doi:10.1016/0021-9169(95)00124-7.

Singer, H. J., D. J. Southwood, R. J. Walker, and M. G. Kivelson (1981), ***Alfven Wave Resonances in a Realistic Magnetospheric Magnetic Field Geometry***, J. Geophys. Res., 86(A6), 4589–4596, doi:10.1029/JA086iA06p04589.

Smith, C. W., Acuna, M. H., Burlaga, L. F., L'Heureux, J., Ness, N. F., and Scheifele, J. (1998), ***The ACE Magnetic Fields Experiment***, Space Sci. Rev., 86, 611–632, 1998.

Southwood, D. J. (1974), ***Some features of field line resonances in the magnetosphere***, Planet. Space Sci., 22, 483. doi:10.1016/0032-0633(74)90078-6

Stephenson, J. A. E., and A. D. M. Walker (2002), ***HF radar observations of Pc5 ULF pulsations driven by the solar wind***, Geophys. Res. Lett., 29(9), 1297, doi:10.1029/2001GL014291.

Stephenson, J. A. E. and Walker, A. D. M. (2010), ***Coherence between radar observations of magnetospheric field line resonances and discrete oscillations in the solar wind***, Ann. Geophys., 28, 47–59, doi:10.5194/angeo-28-47-2010, 2010.

B. Stewart (1861), ***On the great magnetic disturbance which extended from August 28 to September 7, 1859, as recorded by photography at the Kew Observatory***. Philosophical Transactions of the Royal Society of London, 151:423-430, 1861.

Stone, E. C., Frandsen, A. M., Mewaldt, R. A., Christian, E. R., Margolies, D., Ormes, J. F., and Snow, R: 1998a, ***The Advanced Composition Explorer***, Space Sci. Rev. 86, 1

Takahashi, K. and McPherron, R.L. (1982). ***Harmonic structure of Pc 3–4 pulsations***. Journal of Geophysical Research 87: doi: 10.1029/JA087iA03p01504. issn: 0148-0227.

Takahashi, K., McPherron, R. L., and Hughes, W. J. (1984). ***Multispacecraft observations of the harmonic structure of Pc 3–4 magnetic pulsations***. J. Geophys. Res., 89(A8), 6758–6774.

Tamao, T., ***Transmission and coupling resonance of hydro-magnetic disturbances in the non-uniform Earth's magnetosphere***, Sci. Rep. Tohoku Univ. Ser. S, 17, 43, 1966.

Taylor, J. P. H. and A.D.M. Walker [1987] , ***Theory of magnetospheric standing hydromagnetic waves with large azimuthal wave number: 2. Eigenmodes of the magnetosonic and Alfvén oscillations***, J. Geophys. Res., 92, 10046. DOI: 10.1029/JA092iA09p10046

Tian, M., T. K. Yeoman, M. Lester, and T. B. Jones (1991), ***Statistics of Pc 5 pulsation events observed by SABRE***, Planet. Space Sci., 39, 1239, 1991.

Thomson, D. J., L. J. Lanzerotti, F. L. Vernon III, M. R. Lessard, and L. T. P. Smith (2007), ***Solar modal structure of the engineering environment***, Proc. IEEE, 95, 1085– 1132.

Tsyganenko, N.A. (2002a), ***A model of the near magnetosphere with a dawn-dusk asymmetry: 1. Mathematical structure***, J. Geophys. Res., 107, 10.1029/2001JA000219, 2002.

Tsyganenko, N.A. (2002b), ***A model of the near magnetosphere with a dawn-dusk asymmetry: 2. Parameterization and fitting to observations***, J. Geophys. Res., 107, 10.1029/2001JA000220, 2002.

Vellante, M., and M. Forster (2005), ***Dependence of geomagnetic field line resonant frequencies on solar irradiance***. MEMORIE-SOCIETA ASTRONOMICA ITALIANA 76.4: 899.

Viall, N. M., L. Kepko, and H. E. Spence (2009), ***Relative occurrence rates and connection of discrete frequency oscillations in the solar wind density and dayside magnetosphere***, J. Geophys. Res., 114, A01201, doi:10.1029/2008JA013334.

Villain, J. P., R. A. Greenwald, K. B. Baker, J. M. Ruohoniemi (1987), ***HF radar observations of E region plasma irregularities produced by oblique electron streaming***, Volume 92, Issue A11, pages 12327–12342, 1 November 1987 DOI: 10.1029/JA092iA11p12327

Villante, U., P. Francia, and S. Lepidi (2001), ***Pc5 geomagnetic field fluctuations at discrete frequencies at a low latitude station***, Ann. Geophys., 19, 321– 325.

Waldock, J. A.; Jones, T. B.; Nielsen, E.; Southwood, D. J. (1983), ***First results of micropulsation activity observed by SABRE***. Planetary and Space Science (ISSN 0032-0633), vol. 31, May 1983, p. 573-575, 577, 578.

Walker, A. D. M., Greenwald, R. A., Stuart, W. F. and Green, C. A. (1979), ***STARE auroral radar observations of Pc5 geomagnetic pulsations***, J. geophys. Res. 84,3373.

Walker, A. D. M. (1980), ***Modelling of Pc5 pulsation structure in the magnetosphere*****,** Planet. Space Sci. 28,213.

Walker, A. D. M., J. M. Ruohoniemi, K. B. Baker, R. A. Greenwald, and J. C. Samson (1992), ***Spatial and temporal behavior of ULF pulsations observed by the Goose Bay HF radar***, J. Geophys. Res., 97, 12187.

Walker, A.D.M. (1987), ***Theory of magnetospheric standing Hydromagnetic waves with large azimuthal wave number, 1, Coupled magnetosonic and Alfvén waves***, J. Geophys. Res., 92, 10039. DOI: 10.1029/JA092iA09p10039.

Walker, A. D. M. (1995), ***Radar Studies of Magnetosphere Dynamics***, Astrophysics and Space Science, Volume 230, Issue 1-2, pp. 415-430

Walker, A.D.M. (1994), ***Theory of magnetospheric standing Hydromagnetic waves with large azimuthal wave number, 3, Particle resonance and instability***, J. Geophys. Res., 99, 11105.

Walker, A. D. M., H. Pekrides (1996), ***Theory of magnetospheric standing hydromagnetic waves with large azimuthal wavenumber, 4, Standing waves in the ring current region***, J. Geophys. Res., 101, 27133–27147.

Waters, C. L., F. W. Menk, and B. J. Fraser (1994), ***Low latitude geomagnetic field line resonance: Experiment and modeling***. Journal of Geophysical Research: Space Physics (1978–2012) 99.A9: 17547-17558.

Waters, C. L. (2000), ***ULF resonance structure in the magnetosphere***. Advances in Space Research 25.7: 1541-1558.

Weimer, D. R., D. M. Ober, N. C. Maynard, M. R. Collier, D. J. McComas, N. F. Ness, C. W. Smith, and J. Watermann (2003), ***Predicting interpla- netary magnetic field (IMF) propagation delay times using the minimum variance technique***, J. Geophys. Res., 108(A1), 1026, doi:10.1029/ 2002JA009405.

Wilcox, J. M., A. W. DeSilva, W. S. Cooper III (1961), Experiments on ***Alfvén-wave propagation***, Phys. Fluids, 4, 1506\u20131513.

Wright DM, Yeoman TK (1999) ***High-latitude HF Doppler observations of ULF waves: 2.Waves with small spatial scale sizes***. Ann Geophys 17:868–876

Wright, D. M., T. K. Yeoman, and T. B. Jones (1999), ***ULF wave occurrence statistics in a high-latitude HF Doppler sounder***, Ann. Geophysicae, 17, 749, 1999.

Wright, D. M., T. K. Yeoman, I. J. Rae, J. Storey, A. B. Stockton-Chalk, J. L. Roeder, and K. J. Trattner (2001), ***Ground-based and polar spacecraft observations of a giant (Pg) pulsation and its associated source mechanism***, J. Geophys. Res., 106, 10,837–10,852, doi:10.1029/2001JA900022.

Yeoman, T. K. and M. Lester (1990), ***Characteristics of MHD waves associated with storm sudden commencements observed by SABRE and ground magnetometers***, Planet. Space Sci., 38, 603 - 616.

Yeoman, T. K., M. Tian, M. Lester, and T. B. Jones (1992), ***A study of Pc 5 hydromagnetic waves with equatorward phase propagation***, Planet. Space Sci., 40, 797-810.

Yeoman T, Wright D, Chapman P, Stockton-Chalk A (2000) ***High-latitude observations of ULF waves with large azimuthal wavenumbers***. J Geophys Res 105:5453–5462

Yeoman, T. K., D. Yu. Klimushkin, and P. N. Mager, (2010) ***Intermediate-m ULF waves generated by substorm injection: a case study***, Ann. Geophys., 28, 1499\u20131509, http://dx.doi.org/10.5194/angeo-28-1499-2010

Yeoman, T. K., M. James, P. N. Mager, and D. Y. Klimushkin (2012), ***SuperDARN observations of high-m ULF waves with curved phase fronts and their interpretation in terms of transverse resonator theory***, J. Geophys. Res., 117, A06,231, doi:10.1029/2012JA017668.

Ziesolleck, C. W. S., Fenrich, F. R., Samson, J. C., & McDiarmid, D. R. (1998), ***Pc5 field line resonance frequencies and structure observed by SuperDARN and CANOPUS***. Journal of Geophysical Research: Space Physics (1978–2012) 103.A6: 11771-11785.

Zong, Q. G., Zhou, X. Z., Wang, Y. F., Li, X., Song, P., Baker, D. N., ... & Pedersen, A. (2009), ***Energetic electron response to ULF waves induced by interplanetary shocks in the outer radiation belt***. Journal of Geophysical Research: Space Physics (1978–2012) 114.A10.

Appendix A

Automated algorithm or code (IDL based)

```
;  pro identification_FLR_07
;  Written by  Laura Mazzino
;  Created on January 11th, 2010
;  Big modification: March, 2011
;  Modified on: October, 2011
;  Modified on: Nov, 2011
;  Modified on: Oct, 2012
;  Last Big modified on: Oct, 2014
;  This program loads data from SuperDARN files, for a desire date and
time, calls a procedure that loads the
;  data from fitac files and returns the crosspower, and find average in
crosspower organized in a daily basis.
;  This program, as the original writen by F. Fenrich, removes ground
scatter (v lt 30 or w lt 40).
;  Started the idea on August 6th, 2009 based on a program by Frances
Fenrich called read_fmt_wind11_an_p
;  Last version before major changes (generalization to any date, any
station) can be found in identification_FLR_05
;
;  The difference between FLR05 and FLR06 is that all problems in matrix
definitions, ground scatter, flags (both q and g), and no data, have been
all solved.
;  The difference between FLR06 and FLR07 is that additional conditions
have been imposed on adjacent gates to ensure identification of events is
efective...
;  Plot version of this code (plot on demand, in date, radar, beam, gate)
available at test_identificationFLR01.pro
;====================================================================
; WARNING! WARNING! WARNING! WARNING!WARNING! WARNING! WARNING! WARNING!
;====================================================================
; MAKE SURE YOU COMPILE STARTUP BEFORE RUNNING THIS PROGRAM
C:\IDL\startup by typing in console "@startup"
;====================================================================
@/local/home/mazzino/IDL/crosspowerphase03.pro
@/local/home/mazzino/IDL/save_jpg.pro
@/local/home/mazzino/IDL/converttime
pro identificationFLR07
for j= 1, 16  DO BEGIN ;Loop in 16 stations
   year  = 2003
     for i=1, 12 do begin
      month = i
  ;  ======Default ============
    if (i eq 1 or i eq 3 or i eq 5 or i eq 7 or i eq 8 or i eq 10 or i eq
12) then date1 = 31 else date1 =30
      if i eq 2 then date1=28
```

```
      if i eq 2 and year eq 1996 then date1=29
     dummy=identification_FLR07(j, date1, month, year)
     endcode:
   endfor
 endfor;

end

function identification_FLR07, station, date1, month, year
;====================================================================

main_directory    ='/local/home/mazzino/IDL/00_SuperDARN/'
station_ids = ['_','gbr', 'sch', 'kap', 'hal', 'sas', 'pgr', 'kod',
'sto', 'pyk', 'han', 'san', 'sys', $
                'sye', 'tig', 'ker', 'ksr']
                 ; --------- set  name of input file and load data -----
--------
 st_id = ['_','g', 's', 'k', 'h', 't', 'b', 'a', 'w', 'e', 'f', 'd', 'j',
'n', 'r', 'p', 'c']
 names_stations =['_', 'Goose Bay', 'Schefferville', 'Kapuskasing',
'Halley', 'Saskatoon', 'Prince George', $
                 'Kodiak','Stokkseyri', 'Pykkvibaer', 'Hankasalmi',
'Sanae', 'Syowa South',$
                 'Syowa East', 'Tiger',  $
                 'Kerguelen', 'King Salomon']

 j=station
 beginning_date=1
if (year eq 1996 and month eq 1) then beginning_date= 2 else
beginning_date=1

o=0L
ii=0L
for ii=beginning_date, date1 do begin ;loop in days
   ref_month = month
   ref_year  = year
   ref_day   = ii
   station=station

errorfile=main_directory+'Results/FLR/IDL_identification_errorfile_IFLR07
.txt'
get_lun, p
  openw, p, errorfile
   printf, p, 'station ', station, ' ', 'beginning_date ',
beginning_date, ' ',  'end date ', date1, ' ', $
   'date (month, m/y/d/, ii)', month, ' ', ref_month, ' ', ref_year, ' ',
ref_day, ii

o=o+1

close, p
free_lun, p

   ;account for gaps in database (SuperDARN data not available for those
days)
   ;create files with null data for dates with gaps in data
   if (year eq 2003 or year eq 2002  or  year eq 2001  or  year eq 2000
or  year eq 1996  or  year eq 1997  or  year eq 1998) $
```

```
    then begin
     if  $
     (year eq 1996 and ( $
     (station eq 1 and ((month eq 1  and (ii ge 27 and ii le 29)) or
(month eq 2  and (ii ge 10 and ii le 12)) $
      or (month eq 4  and (ii ge 27 and ii le 29)) or (month eq 5  and
(ii ge 29)) or (month eq 6  and (ii ge 16 and ii le 19)) )) or $
      (station eq 2) or (station eq 3 and (month eq 9  and (ii ge 25 and
ii le 30))) OR $
      (station eq 4 and (month eq 1  and (ii ge 2 and ii le 20)) )  $
      OR (station eq 5 and (month eq 3  and (ii ge 15 and ii le 18))) OR
(station eq 6)  $
      OR (station eq 7 ) OR (station eq 8 and ((month eq 2 and (ii le
11)) OR (month eq 3  and (ii ge 19 and ii le 22)) OR $
      (month eq 9  and (ii ge 6 and ii le 9)) ))  or $
      (station eq 11 OR station eq 12 OR station eq 13 OR station eq 14
OR station eq 15 OR station eq 16)  )) or  $

     (year eq 1997 and ($
     (station eq 1 and ((month eq 9  and (ii ge 6 and ii le 8 or ii ge 15
and ii le 17 or ii ge 27 and ii le 29)) $
      or (month eq 2  and (ii ge 12 )) or (month eq 3  ) or (month eq 4
and (ii ge 26 and ii le 28)) or $
       (month eq 7  and (ii ge 18 and ii le 21))  or $
       (month eq 11  and (ii ge 14 and ii le 28)))) or $
      ;or (month eq 2  and (ii ge 10 and ii le 12)) $
      (station eq 2) or $
      (station eq 3 and  ((month eq 4  and (ii ge 7 and ii le 12 or ii ge
17 and ii le 19 )) or  $
       (month eq 5  and (ii ge 9 and ii le 11)) or  $
       (month eq 6 and (ii ge 19 and ii le 21 or ii ge 23 and ii le 30
)))  ) or $
      (station eq 4 and  ((month eq 1  and (ii ge 25 and ii le 29)) or
(month eq 8  and (ii ge 2 and ii le 4)) ) ) or $
      (station eq 5 and ((month eq 1  and (ii ge 1 and ii le 2 or ii ge 8
and ii le 10)) or $
       (month eq 2  and (ii ge 2 and ii le 4)) ) ) OR $
      (station eq 6) OR  (station eq 7 ) OR $
      (station eq 8 and (month eq 3  and (ii ge 26 and ii le 28)) ) or  $
      (station eq 9 and ((month eq 4  and (ii ge 19 and ii le 21)) or
(month eq 6  and (ii ge 20 and ii le 23)))) OR $
      (station eq 10 and ((month eq 1  and (ii ge 12 and ii le 14))  or
(month eq 6  and (ii ge 22 and ii le 24))  or $
       (month eq 7  and (ii ge 31)) or (month eq 8 and (ii ge 1 and ii le
8))  )) OR $
      (station eq 11 and ((month eq 1 OR month eq 2 )) )  or $
      (station eq 14 OR station eq 15 OR station eq 16)  )) or  $

      (year eq 1998 and ( $
      (station eq 1 and ((month eq 1  and (ii le 10))  or $
       (month eq 2  and (ii ge 26 and ii le 28)) or $
       (month eq 3  and (ii le 2 or ii ge 15 and ii le 17 )) ) ) OR $
      (station eq 3 and (month eq 2  and (ii ge 7 and ii le 9))) OR $
      (station eq 4 and ((month eq 2  and (ii ge 22 and ii le 28))or $
       (month eq 3  and (ii eq 1)))) OR $
      (station eq 8 and (month eq 1  and (ii ge 13 and ii le 17 or ii ge
19 and ii le 21 ))) OR $
      (station eq 9 and (month eq 1  and (ii ge 2 and ii le 4))) )) or  $
```

```
     (year eq 2003 and ( $
     (station eq 1 and ((month eq 1  and (ii ge 6 and ii le 12 )) or
(month eq 2  and (ii ge 19 and ii le 28)) or $
                       (month eq 4  and (ii ge 3 and ii le 5)) or (month
eq 6  and (ii ge 22 and ii le 24)) or $
                       (month eq 9  and (ii ge 8 and ii le 15)) or (month
eq 10  and (ii ge 16 and ii le 28 or ii eq 31)) $
                        or (month eq 11  and (ii ge 1 and ii le 6 or ii
ge 10 and ii le 13 )) or (month eq 12) )) or $
     (station eq 2) or $
     (station eq 3 and ((month eq 1  and (ii ge 4 and ii le 6)) or (month
eq 3  and (ii ge 1 and ii le 1)))) or $;
     (station eq 4 and ((month eq 4  and (ii ge 13 and ii le 30)) or
(month eq 5  and (ii ge 1 and ii le 1)))) or $
     (station eq 6 and ((month eq 1  and (ii ge 22 and ii le 25)) or
(month eq 7  and (ii ge 11 and ii le 12)) or  $
                        (month eq 9  and (ii ge 22 and ii le 24)) or
(month eq 10  and ((ii ge 2 and ii le 7) or $
                        (ii ge 23 and ii le 24)) or (ii ge 20 and ii le
23)))) or $
     (station eq 7 and ((month eq 7 and ((ii ge 5 and ii le 9) or (ii ge
30 and ii le 31))) $
                       or (month eq 8 and (ii eq 1 and ii le 2)))) or $
     (station eq 8 and ((month eq 5  and (ii ge 8 and ii le 11)) )) or $
     (station eq 9 and ((month eq 2  and (ii ge 21 and ii le 28)) or
(month eq 8  and (ii ge 30 and ii le 31)) $
                        or (month eq 4  and (ii ge 25 and ii le 27)) or
(month eq 7  and (ii ge 6 and ii le 10 or ii ge 21 and ii le 23)) $
                        or (month eq 9  and (ii eq 1)) or (month eq 10
and (ii ge 12 and ii le 15)) )) or $
     (station eq 10 and (month eq 8  and (ii ge 2 and ii le 9)) ) or $
     (station eq 11 and ((month eq 3  and (ii ge 22 and ii le 24)) or
(month eq 4  and (ii ge 13 and ii le 30)) or $
        (month eq 5  and (ii ge 1 and ii le 1 or ii ge 23 and ii le 25))
or (month eq 9  and (ii ge 26 and ii le 28)) $
         or (month eq 10  and (ii eq 31)) or (month eq 11 and (ii ge 1
and ii le 2)) )) or $
     (station eq 12 and ((month eq 2  and (ii ge 19 and ii le 21))  or $
                        (month eq 4  and (ii ge 13 and ii le 30)) or
(month eq 5  and (ii ge 1 and ii le 1)) or $
                        (month eq 8  and (ii ge 12 and ii le 15 or ii ge
23 and ii le 31)) or $
                        (month eq 9  and (ii ge 1 and ii le 5 or ii ge 10
and ii le 18)) )) or $
     (station eq 13 and ((month eq 4  and (ii ge 13 and ii le 30)) or
(month eq 5  and (ii ge 1 and ii le 1)) or $
                        (month eq 6  and (ii ge 6 and ii le 8 or ii ge
11 and ii le 15 )) or $
                         (month eq 12  and (ii ge 11 and ii le 16)) ))
or $
     (station eq 14 and ( (month eq 4  and (ii ge 29 and ii le 30)) or
(month eq 5  and (ii ge 1 and ii le 5)) or  $
          (month eq 6  and (ii ge 2 and ii le 4 )) or (month eq 10  and
(ii ge 7 and ii le 13)) or $
           (month eq 11  and (ii ge 6 and ii ge 10 or ii le 16 and ii le
19)) or $
     (month eq 12  and (ii ge 21 and ii le 23 )) )) $
```

```
    or (station eq 15 and ((month eq 2  and (ii ge 17 and ii le 19)) or
(month eq 3  and (ii eq 31)) or $
              (month eq 4 or (ii ge 13 and ii le 30)) or (month eq 5  and
(ii ge 1 and ii le 1)) or (month eq 12  and (ii eq 31)) )) or $
     (station eq 16 and ((month eq 1  and (ii eq 1 or ii ge 7 and ii le 9
or ii ge 21 and ii le 27)) or (month eq 2  and (ii ge 4 and ii le 9 or $
                          ii ge 15 and ii le 17)) $
         or (month eq 3  and (ii ge 2 and ii le 4 or ii ge 7 and ii le
31)) $
         or (month eq 4  and (ii ge 19 and ii le 21  or ii ge 25 and ii
le 30)) or (month eq 5  and (ii ge 1 and ii le 5 or ii ge 10 and ii le 13
OR $
         ii ge 18 and ii le 28)) or (month eq 6  and (ii ge 7 and ii le
14 or ii ge 16 and ii le 24))  or (month eq 7  and (ii ge 24)) or $
       (month eq 8  and (ii ge 1 and ii le 13 or ii ge 15 and ii le 18 or
ii ge 22 and ii le 31)) $
            or (month eq 9  and (ii ge 3 and ii le 5 or ii ge 13)) or
(month eq 10  and (ii ge 1 and ii le 16)) $
       or (month eq 11  and (ii ge 6 )) or (month eq 12  and (ii eq 1 or
ii ge 28 and ii le 31)) )) )) $

;       or (year eq 2002 and ( $
;       (station eq 1 and  ((month eq 7 and (ii ge 3 and ii le 18 or ii
ge 28 )) or (month eq 8 and (ii ge 1 and ii le 12)) $
;       or (month eq 9 and (ii ge 25)) or (month eq 10)  or (month eq 11
and ii ge 14)  or (month eq 12 and (ii le 11 and ii ge 15 or ii le 18 $
;       or ii ge 21 )) )) or $
;       (station eq 2) or (station eq 3 and ((month eq 1 and (ii ge 12
and ii le 14)) or (month eq 9 and (ii ge 13)) or (month eq 10 or month eq
11) )) or $
;       (station eq 4 and ((month eq 1 and (ii ge 1 and ii le 1)) or
(month eq 2  and (ii ge 2 and ii le 4 or ii ge 10 and ii le 12 or ii ge
27)) or $
;       or (month eq 3 and (ii ge 1 and ii le 1)) ))or $
;       (station eq 5 and (month eq 1 and (ii ge 29 and ii le 31)) ) or $
;       (station eq 6 and (month eq 1 and (ii ge 4 and ii le 6 or ii ge
15 and ii le 17) )) or  $
;       (station eq 7 and ((month eq 1 and (ii ge 24)) or (month eq 2 and
(ii eq 1)) or (month eq 5 and (ii ge 25)) or $
;       (month eq 6 and (ii ge 1 and ii le 2)) or (month eq 12 and (ii ge
21)) )) or  $
;       (station eq 8 and ((month eq 1 and (ii ge 24 and ii le 26 )) or
(month eq 3 and (ii ge 24 and ii le 31)) or (month eq 4 and (ii ge 1 and
ii le 19)) )) or  $
;       (station eq 9 and (month eq 1 and (ii ge 2 and ii le 4  or ii ge
28 and ii le 30) )) or  $
;       (station eq 10  and ((month eq 1 and (ii ge   3 and ii le 5 or ii
ge 8  and ii le 10 or  $
;       ii ge 20  and ii le 22 )) or (month eq 7 and (ii ge 5 and ii le
7)))) or $
;        (station eq 11  and ((month eq 1 and (ii eq 1 or ii ge 10 and ii
le 17 )) or (month eq 9 and (ii ge 8 and ii le 11 )) $
;       or (month eq 2 and ((ii ge 12 and ii le 14) or (ii ge 20 and ii
le 22))) or (month eq 7 and (ii ge 1 and ii le 3)) $
;        or (month eq 10 and (ii ge 4 and ii le 7)) )) $
;       or (station eq 12  and ((month eq 1 and (ii eq 1)) or (month eq 2
and $
```

```
;        (ii ge 1 and ii le 3 or ii ge 9 and ii le 12 or ii ge 18 and ii
le 21 or ii ge 25 and ii le 27)) $
;       or (month eq 5 and (ii ge 11 and ii le 27 or ii eq 31)) or (month
eq 6 or month eq 7) )) $
;       or (station eq 13  and ((month eq 1 and (ii eq 1)) or (month eq 2
and (ii ge 7 and ii le 9 or ii ge 15 and ii le 17 or ii ge 23 and ii le
25))$
;       or (month eq 5 and (ii ge 26 and ii le 28)) )) $
;       or (station eq 14  and ((month eq 2 and (ii ge 8 and ii le 12 or
ii ge 26 and ii le 28)) or (month eq 5 and (ii ge 22 and ii le 29)) $
;       or (month eq 6 and (ii ge 8 and ii le 13)) or (month eq 8 and (ii
ge 12 and ii le 15))  or (month eq 9 and (ii ge 3 and ii le 5)) $
;        or (month eq 10 and (ii ge 19 and ii le 27)) or (month eq 11 and
(ii ge 10 and ii le 12)) )) $
;       or (station eq 15  and ((month eq 1 and (ii eq 1)) or (month eq 2
and (ii ge 5 and ii le 7 or ii ge 13 and ii le 15 or ii ge 21 and ii le
23)))) $
;        (station eq 16  and ((month eq 1 and (ii ge 1 and ii le 31)) or
(month eq 2) or (month eq 3 and (ii ge 4 and ii le 12)) $
;       or (month eq 4 and (ii ge 4 and ii le 8 or ii ge 16)) or (month
eq 5 and (ii ge 1 and ii le 18)) $
;       or (month eq 6 and (ii ge 9)) or (month eq 7 or month eq 8) or
(month ge 9 and month le 12) ))  )) $
;
       or (year eq 2001 and ( $
       (station eq 1 and ((month eq 2 and (ii ge 23)) or (month  eq 3 and
(ii le 4)) or $
       (month  eq 4 and (ii ge 24 and ii le 26)) or (month  eq 5 and (ii
ge 9 and ii le 11)) or (month  eq 6 and (ii ge 25 and ii le 27)) $
       or (month  eq 9 and (ii le 4))       )) or $
       (station eq 2) $
       or (station eq 3 and ((month eq 4 and (ii le 5 )) or (month  eq 7
and (ii ge 26 and ii le 28)) or (month  eq 9 and (ii eq 30)) $
       or  (month eq 10 and (ii le 2 )) )) $
      or  (station eq 4 and ((month eq 4 and (ii ge  7 and ii le 9))  or
$
      (month  eq 5 and (ii ge 22 and ii le 25)) or (month  eq 9 and (ii
ge 14 and ii le 19)) $
       or (month  eq 11 and (ii ge 30)) or (month  eq 12) ))  $
      or (station eq 5 and ((month eq 4 and (ii ge  23 and ii le 25))
)) or  $
       (station eq 6 and ((month eq 4 and (ii ge  14 and ii le 16)) or
(month  eq 7 and (ii ge 14 and ii le 16)) )) or  $
       (station eq 7 and ((month eq 3 and (ii ge 24 and ii le 26)) or
(month  eq 7 and (ii ge 2 and ii le 7)) )) or $
       (station eq 8 and (month eq 4 and (ii ge 25 and ii le 27)) ) $
      or  (station eq 9 and ((month eq 4 and (ii ge 25 and ii le 29))   $
       or (month  eq 5 and (ii ge 26 and ii le 28)) or (month  eq 12 and
(ii ge 24 and ii le 26))   )) $
       or (station  eq 10 and ((month  eq 1 and (ii le 6)) or  (month eq
2 and (ii ge 10 and ii le 13 )) or  (month eq 4 and (ii ge 3 and ii le 5
) or $
        (ii ge 28 ))   or (month  eq 5 and (ii eq 1)) or (month  eq 8
and (ii ge 17 and ii le 21)) or (month  eq 9 and (ii ge 12 and ii le 19))
$
         or (month  eq  10  and (ii ge 19 and ii le 21))  or (month  eq
11  and (ii ge 4 and ii le 6 or ii ge 21 and ii le 28))  )) $
```

```
       or  (station  eq 11 and ((month  eq 1 and (ii ge 7 and ii le 13
or ii eq 31)) or (month eq 2 and (ii le 2 ))or  $
        (month eq 3 and (ii ge 17 and ii le 23)) or (month  eq 6 and (ii
ge 24)) or (month  eq 7 and (ii ge 10 and ii le 12)) or  $
        (month  eq 9 and (ii ge 06 and ii le 11 or ii ge 21 and ii le
24))   or (month  eq  10  and (ii ge 28)) $
        or (month  eq  11  and (ii le 3 or ii ge 19 and ii le 25 or ii ge
30)) or (month  eq  12 )  )) $
       or (station eq 12 and ((month eq 4 and (ii ge 6 and ii le 10)) or
(month  eq  10  and (ii ge 26 and ii le 29)) $
         or (month  eq  11  and (ii ge 30))  or (month  eq  12 ) ))  $
        or (station eq 13 and ((month  eq  11  and (ii ge 30)) or (month
eq  12 ) ) )$
       or (station  eq 14 and ( (month  eq 1 and (ii le 4)) or  (month eq
2 and (ii ge 21 )) or  (month eq 3 and (ii le 14 or ii ge 21 )) $
        or  (month eq 4 and (ii le 11 or ii ge 25 and ii le 28))  or
(month  eq 7 and (ii ge 15 and ii le 17)) or $
         (month  eq 8 and (ii ge 16 and ii le 24)))) or (station eq 15)
or $
         (station eq 16  and ( (month eq 12 and (ii ge 17 )) )) $
;       or (month eq 4 and (ii ge 4 and ii le 8 or ii ge 16)) or (month
eq 5 and (ii ge 1 and ii le 18)) $
;       or (month eq 6 and (ii ge 9)) or (month eq 7 or month eq 8) or
(month ge 9 and month le 12) ))
         ))  $

        or (year eq 2000 and ( $
        (station eq 2) or  (station eq 3 and (month eq 8 and (ii le 2 or
ii ge 8 and ii le 17 or ii ge 26 and ii le 28))) or $
        (station eq 6 and ((month eq 12 and (ii ge  8 and ii le 11))))
or $
        (station eq 7 and ((month eq 9 and (ii ge  18 and ii le 20 or ii
ge  28))))   or (station eq 8 and ((month eq 10  and (ii ge 30)) or $
              (month eq 11  and (ii le 2 or ii ge 18 and ii le 24)) or
(month eq 12  and (ii ge 13 and ii le 18)) )) or $
        (station eq 9 and ((month eq 9  and (ii ge 10 and ii le 15 or ii
ge 24 and ii le 26 )))) or $
        (station eq 10 and ((month eq 9  and (ii ge 23 and ii le 25)) or
(month eq 10  and (ii ge 28 and ii le 30)) or $
                (month eq 11  and (ii ge 11 and ii le 18)) or (month eq
12  and (ii ge 11 and ii le 13 or ii ge 29)) )) or $
         (station eq 11 and ((month eq 8 and (ii ge 8 and ii le 12 or ii
ge 20 and ii le 22 or ii ge 24 and ii le 27)) or $
            (month eq 9  and (ii ge 13 and ii le 15)) or (month eq 10
and (ii ge 23 and ii le 25)))) or $
         (station eq 12 and ((month eq 9  and (ii ge 10 and ii le 12 or
ii ge 14 and ii le 16)) )) or $
         (station eq 14 and ((month eq 8 and (ii le 14 or ii ge 24 and ii
le 29)) or (month eq 12  and (ii ge 23)) ))  or $
         (station eq 15 and ((month eq 8 and ( ii ge 2 and ii le 6 or ii
ge 11 and ii le 13 or ii ge 18 and ii le 20)) or $
         (month eq 10  and (ii ge 25)) or (month eq 11  and (ii eq 1)) or
(month eq 12  and (ii ge 31)) )) or $
         (station eq 16 and (month eq 8 or month eq 9 or month eq 10 or
month eq 11 or month eq 12 ) ) ))  then begin
        print, 'no data this day ', names_stations[station], '      date
=> Year =', ref_year, ' month =',  ref_month , ' day= ', ref_day
        ref_day   = ii
```

```
        ref_year  = year
        ref_month_label=string(ref_month, format='(I02)')
        ref_year_label=string(ref_year, format='(I04)')

  ; Prepare directories to store results:
results_files=
main_directory+'Results/FLR/'+station_ids[station]+'/'+ref_year_label+'/'
+ref_month_label+'/'
   ;help, results_files
     picture_directory    = main_directory
+'Plots/'+station_ids[station]+'/'
     dummy=Label_Date(Date_format='%N %M %H:%I')
      ; ====================== ==================
     ; ====================== Define output files
      ;temp_file1: crosspower AND crossphase condition
     temp_file1= string(results_files,
station_ids[station],'_FLR_',ref_day,'_', $
                  ref_month,'_',ref_year, '_IFLR07.txt', $
                    format='(A61, A3, A5, I02,  A1, I02, A1, I4, A11)')
                    ;print, temp_file1
               get_lun, s
                  openw, s, temp_file1 ;both conditions
                   printf, s, 0.
          goto, end_days
      endif  else begin

      codebegin:
  ref_hour  = 0
  ref_hour1 = 23
  ref_month_label=string(ref_month, format='(I02)')
  ref_year_label=string(ref_year, format='(I04)')

   print, 'working on  station ', station, '  ', names_stations[station],
'  date => Year =', ref_year, ' month =',  ref_month , ' day= ', ref_day

 ; Prepare directories to store results:
results_files= main_directory
+'Results/FLR/'+station_ids[station]+'/'+ref_year_label+'/'+ref_month_lab
el+'/'
picture_directory    = main_directory +'Plots/'+station_ids[station]+'/'
 ; dummy=Label_Date(Date_format='%N %M %H:%I')
  ;temp_file1: crosspower AND crossphase condition
  temp_file1= string(results_files,
station_ids[station],'_FLR_',ref_day,'_', $
                  ref_month,'_',ref_year, '_IFLR07.txt', $
                    format='(A61, A3, A5, I02,  A1, I02, A1, I4, A11)')

                    ;print, temp_file1

;create an index for events
event_index=0
b=0
j=0
w=0
               get_lun, s
                  openw, s, temp_file1 ;both conditions
printf, s, ' '
lb   =    0 ; lower beam
```

```
hb   =   15 ; Higher beam
lg   =    0 ; lower gate
hg   =   60 ; higher gate
nb   = hb - lb+1
ng   = hg - lg+1
beam_names= STRARR(nb) ;create an array that holds names for all beams
gate_names= STRARR(ng) ;create an array that holds names for all beams
for i=0, nb-1 do begin
  beam_names[i]=string(i+lb , format='(I2)')
endfor

for i=0, ng-1 do begin
  gate_names[i]=string(i+lg , format='(I2)')
endfor

date=julday(ref_month, ref_day, ref_year, 00, 00, 00)
   input=crosspowerphase03(station, date, cpow_ephe, cpow, cpha, vcpha,
time_array, data, bmnum)
   ; => ephe is a matrix that returns ephemerides, including time and
beam, as a function of record number (i)
   ; => cpw1 is a 3D matrix that returns crosspower, frequency and time.
   ;  All above is a funtion of beam range and gate range
        data_file =
string('/local/home/mazzino/IDL/00_SuperDARN/Data/', ref_year, '/',
ref_month,'/',$
                 ref_year, ref_month, ref_day, '00', st_id[station],
'C.fit', $
               format='(A42, I04,  A1, I02, A1, I04, I02, I02, A2, A1,
A5)')
length=LON64ARR(24)
  if N_elements(cpow_ephe) le 1 then length[*]=0 else begin
   if (n_elements(cpow_ephe[*,1]) eq 0 or n_elements(cpow_ephe[*,1]) eq
1) then length[*]=0 else begin
       for i=0, 23 do begin
        hourly0=Julday(ref_month, ref_day, ref_year, i, 00, 00)
         hourly1=Julday(ref_month, ref_day, ref_year, i+1, 00, 00)
           dummy=where(cpow_ephe[*,1] ge hourly0 and cpow_ephe[*,1] lt
hourly1, lengthy)
            if lengthy eq 0 then length[i]=0 else begin
                 dummy2=where(Finite(cpow[dummy, *,*]) ne 0,
count_length)
                 dummy3=Where(Finite(vcpha[dummy, *,*]) ne 0,
count_length1)
                 ;print, count_length, count_length1
                 length[i]= count_length
            endelse
       endfor
     endelse
   endelse

j=0
;print number of events measured by Superdarn for the day
 printf, s, length
if n_elements(cpow_ephe) gt 1 then begin ;{
beam = reform(cpow_ephe[*,0])
time = reform(cpow_ephe[*,1])
;create the frequency array
        deltat=60
```

```
        freqarr = dindgen(30)
        deltaf = 1./(60.*deltat)
        freqarr=freqarr*deltaf
        ;print, freqarr
  ;create matrix to hold partial results and data of interest
Meancpow1    =fltarr(nb, ng, 19)
Meancpha     =fltarr(nb, ng, 19)
Meanvcpha    =fltarr(nb, ng, 19)
Variancecpow =fltarr(nb, ng, 19)
Variancecpha =fltarr(nb, ng, 19)
Variancevcpha=fltarr(nb, ng, 19)
Meancpow1[*, *, *]=  !VALUES.F_NAN
Meancpha[*, *, *]=   !VALUES.F_NAN
Meanvcpha[*, *, *]=  !VALUES.F_NAN
Variancecpow[*, *, *] =!VALUES.F_NAN
Variancecpha[*, *, *]=!VALUES.F_NAN
Variancevcpha[*, *, *]=!VALUES.F_NAN

;number of events can't be more than number of data points. Later on,
when events are identified, data_interest will be reformed and printed in
an output file with the data.
  for w = 2, 18 do begin   ; begin loop in frequency
    for j = 0, ng-1 do begin ;begin loop in gate
     for b = lb, hb-4 do begin ;begin loop in beam
       beam_index= where(beam eq b, bindex) ;select index for data in the
same beam
        if bindex le 1 then goto, nextbeam1
                    ; ------------- calculate mean crosspower ----------
result=0
result1=0
result2=0

         ; -------------- calculate crosspower ----------
              result=Moment(cpow[beam_index, j, w], /NaN)
               Meancpow1[b-lb, j, w]=result[0]
                 Variancecpow[b-lb, j, w]= result[1]
         ;         help, Mean_cpow,Variancecpow

             ; -------------- calculate crossphase ----------
                ;Meancpha[b-lb, j, w]=Mean(cpha[beam_index, j, w], /NaN)
                result1=Moment(cpha[beam_index, j, w], /NaN)
                 Variancecpha[b-lb, j, w]= result1[1]
                 Meancpha[b-lb, j, w]=result1[0]
         ;         help, Mean_cpha,Variancecpha
                 ;Meanvcpha[b-lb, j, w]=Mean(alog10(vcpha[beam_index, j,
w]), /NaN)
         ; -------------- calculate variance in crossphase ----------
               result2=Moment(alog10(vcpha[beam_index, j, w]), /NaN)
                Variancevcpha[b-lb, j, w]= result2[1]
               Meanvcpha[b-lb, j, w]=result2[0]

;                 print,'mean variance in crossphase',  mean_vcpha
;                 print, 'variance in crossphase', Variancevcpha
;                 print, 'threshold', Mean_vcpha-2*(Variancevcpha)^0.5
;=============================================================================
;=============================================================================
               nextbeam1:
            endfor ; end loop in beam
```

```
        endfor ;end loop in gate
    endfor ;end loop in frequency

 for w = 2, 18 do begin   ; begin loop in frequency
    for j = 2, ng-3 do begin ;begin loop in gate
     for b = lb, hb-4 do begin ;begin loop in beam
              beam_index= where(beam eq b, bindex) ;select index for data
in the same beam
              if bindex le 1 or finite(meancpow1[b-lb, j, w]) eq 0 or
finite(Meancpha[b, j, w]) eq 0 $
                   or  finite(Meanvcpha[b, j, w]) eq 0 then goto,
nextbeam

 ;   =============== determine data of interest ========
      for k=j-1, j+1 do begin
         if (meancpow1[b-lb, k, w] eq 0 or Meancpha[b-lb, k, w] eq 0 $
         or Meanvcpha[b-lb, k, w] eq 0) then begin
;print, 'no data of interest beam', beam[beam_index[0]], ' going to next
beam '
                  goto, nextbeam
                endif
             endfor
                   ;============================
                    ;find events with different criteria
                    vcphase
=dblarr(N_elements(alog10(vcpha[beam_index, j, w])), 5)
    crossvalue =dblarr(N_elements(cpow[beam_index, j, w]), 5)
    cphase     =dblarr(N_elements(cpow[beam_index, j, w]), 5)
             ;help, vcphase
                    for k=0, 4 do begin
                   vcphase[*, k]    = alog10(vcpha[beam_index,j-2+k , w])
                       crossvalue[*, k] = cpow[beam_index, j-2+k, w]
                        cphase[*, k]     = cpha[beam_index, j-2+k, w]
                    endfor
                    timevalue = time[beam_index]
                    frequencies= (round(freqarr[w]*100000.)*0.01)
                     gates = j+lg
                     l=0L
                    maxcrossvalue=dblarr(bindex-1)
                    crossphase_value=dblarr(bindex-1)
                    time_value=dblarr(bindex-1)
                    ;help, Meanvcpha[b-lb, j, w]
                     ;help, Variancevcpha[b-lb, j, w]
                      for h=0L, n_elements(crossvalue[*, 2])-1 do begin
                         if $
;(vcphase[h, 0] le abs(Meanvcpha[b-lb, j-2, w]-2*(Variancevcpha[b-lb, j-
2, w]^0.5))) and $
(vcphase[h, 1] le abs(Meanvcpha[b-lb, j-1, w]-2*(Variancevcpha[b-lb, j-1,
w]^0.5))) and $
(vcphase[h, 2] le abs(Meanvcpha[b-lb, j, w]-2*(Variancevcpha[b-lb, j,
w]^0.5))) and $
(vcphase[h, 3] le abs(Meanvcpha[b-lb, j+1, w]-2*(Variancevcpha[b-lb, j+1,
w]^0.5))) and $
 (abs(crossvalue[h, 1]-Meancpow1[b-lb, j-1, w]) ge 2*(variancecpow[b-lb,
j-1, w]^0.5)) and $
 (abs(crossvalue[h, 2]-Meancpow1[b-lb, j, w]) ge 2*(variancecpow[b-lb, j,
w]^0.5)) and $
```

```
(abs(crossvalue[h, 3]-Meancpow1[b-lb, j+1, w]) ge 2*(variancecpow[b-lb,
j+1, w]^0.5)) and $
           (crossvalue[h, 1] gt Meancpow1[b-lb, j-1, w]) and $
                 (crossvalue[h, 2] gt Meancpow1[b-lb, j, w])  and $
                 (crossvalue[h, 3] gt Meancpow1[b-lb, j+1, w]) $
                       then begin   ;and $

         caldat, timevalue[h], Month , Day , Year , Hour , Minute
                           crossvalue_data=crossvalue[h,2]
                           vcphase_data= vcphase[h,2]
                           Meancpow1_data=Meancpow1[b-lb, j, w]
                  cross_dif_data=(crossvalue[h,2]-Meancpow1[b-lb, j, w])
                         variance_data=02*(variancecpow[b-lb, j, w]^0.5)
                        abs_meanvariance_data=abs(Meanvcpha[b-lb, j, w])
   abs_meanvariancediff_data= abs(Meanvcpha[b-lb, j, w]-
2*(Variancevcpha[b-lb, j, w]^0.5))

 printf, s, Month , Day , Year , Hour , Minute, timevalue[h], b, gates,
frequencies, crossvalue_data, vcphase_data, Meancpow1_data,$
 cross_dif_data, variance_data, abs_meanvariance_data,
abs_meanvariancediff_data, $
  format='(I02, I4, I6, I4, I4, f14.5, I3, I3, f6.2, e12.5, f7.2 , e12.5,
e12.5, e12.5, f6.2, f7.2)'

       print, '==================    @@@@@@@@@@@@@@    ==============='
     print, '================  FLR Candidate found on:  ==============='
    print, '==================    @@@@@@@@@@@@@@    ==============='
print, Month , Day , Year , Hour , Minute, timevalue[h], $
  b, gates, frequencies, crossvalue[h,2], vcphase[h,2], Meancpow1[b-lb,
j, w], $
 abs(crossvalue[h,2]-Meancpow1[b-lb, j, w]),$
      2*(variancecpow[b-lb, j, w]^0.5), abs(Meanvcpha[b-lb, j, w]), $
        abs(Meanvcpha[b-lb, j, w]-2*(Variancevcpha[b-lb, j, w]^0.5)), $
   format='(I02, I4, I6, I4, I4, f14.5, I3, I3, f6.2, e12.5, f5.2 ,
e12.5, e12.5, e12.5, f6.2, f20.2)'
 print, '==================    @@@@@@@@@@@@@@    ==============='
                          endif
                      endfor
                  cphase=0
                  timevalue=0
                  crossvalue =0
                endcrops2:
             ;  endif
                 nextbeam:
           endfor ; end loop in beam
        endfor ;end loop in gate
    endfor ;end loop in frequency
    j=0
    w = 0
     b = 0
     h=0

 ;free memory
data_interest=0
cpow=0
cpow_ephe=0
cpha=0
vcpha=0
```

```
Meancpow1=0
Meancpha=0
Meanvcpha=0
Min_subscript=0
maxcrossvalue=0
maxcrossvalues=0
timevalue=0
crossphase_values=0
crossphase_value=0
timevalues=0
windownumber=0
 endif
 end_days:
close, s
 free_lun, s
 g=0
 u=0
 s=0

    endelse
  endif
 endfor

 print, '====================== end of code ======================='
end
```

~~~~~~~~~~~~~~~~~~~~~~~~~~~~~~~~~~~~

```
; crosspowerphase03.pro
; ==============
; Author: Laura Mazzino (July 2010, University of Alberta)
; Last modification: November 11, 2011
; For more details on the original procedure, see readfitacf01
; This program loads data from SuperDARN files and calculates and returns
crosspower
; Same as crosspowerphase, but runs for any station, any date.
@/local/home/mazzino/IDL/readfitacf09.pro
```

function crosspowerphase03, station, date, cpow_ephe, cpow, cpha, vcpha, time_array, data, bmnum

```
;---------  load SuperDarn Stations ---------
names_stations =['_', 'Goose Bay', 'Schefferville', 'Kapuskasing',
'Halley', 'Saskatoon', 'Prince George', $
'Kodiak','Stokkseyri', 'Pykkvibaer', 'Hankasalmi', 'Sanae', 'Syowa
South',$
               'Syowa East', 'Tiger',  $
     'Kerguelen', 'King Salomon']
station_ids = ['_','gbr', 'sch', 'kap', 'hal', 'sas', 'pgr', 'kod',
'sto', 'pyk', 'han', 'san', 'sys', $
                'sye', 'tig', 'ker', 'ksr']
     ; --------- set  name of input file and load data -------------
 st_id = ['_','g', 's', 'k', 'h', 't', 'b', 'a', 'w', 'e','f',  'd', 'j',
'n', 'r', 'p', 'c']
```

```
;---------  load directories ---------
      main_directory    ='/local/home/mazzino/IDL/00_SuperDARN/'
      data_files        = main_directory + '/Data/'
      results_files     = main_directory + 'Results/'
      picture_directory  = main_directory
+'Plots/'+station_ids[station]+'/'

caldat, date,  ref_month, ref_day, ref_year
;print, date,  ref_month, ref_day, ref_year

    ;read data from raw files
     print, 'Reading data from station: ',format='( A39)'
     print, names_stations[station], ' on ', ref_day , '/', ref_month,
'/',ref_year ,format='( A15, A6, I02, A1,I02, A1, I04)'


 if ref_day eq 1 then begin  ;account for previous month
   if ref_month eq 1 then begin ; account for January when previous month
is Dec previous year
    ref_year1  = ref_year-1
    ref_month1 = 12
    ref_day1   = 31
    ;print, 'here1'
   endif else begin
   if ref_month eq 3 then begin ;account for March, when previous month
is February
     ref_day1 = 28
     ref_year1= ref_year
     ref_month1= ref_month-1
     if ref_month eq 3 and ref_year eq 1996 then ref_day1 = 29
     ;print, 'here2'
   endif
    if (ref_month eq 5 or ref_month eq 7 or ref_month eq 10 or $
     ref_month eq 12)  then begin ;account for months which previous
months have 30 days
     ref_day1 = 30
     ref_year1= ref_year
     ref_month1= ref_month-1
     ;print, 'here3'
   endif
   if (ref_month eq 2 or ref_month eq 4 or ref_month eq 6 or ref_month eq
8 or $
     ref_month eq 9 or ref_month eq 11 )  then begin ;account for months
which previous months have 31 days
     ref_day1 = 31
     ref_year1= ref_year
     ref_month1= ref_month-1
     ;print, 'here4'
   endif
   endelse
  data_file =  string('/local/home/mazzino/IDL/00_SuperDARN/Data/',
ref_year1, '/', ref_month1,'/',$
        ref_year1, ref_month1, ref_day1, '00', st_id[station], 'C.fit', $
         format='(A42, I04, A1, I02, A1, I04, I02, I02, A2, A1, A5)')
 endif else begin
   data_file =  string('/local/home/mazzino/IDL/00_SuperDARN/Data/',
ref_year, '/', ref_month,'/',$
        ref_year, ref_month, ref_day-1, '00', st_id[station], 'C.fit', $
```

```
            format='(A42, I04, A1, I02, A1, I04, I02, I02, A2, A1, A5)')
endelse
   dummy=readfitacf09(data_file, param0,fitdata0)
 ;  dummy=readfitacf08(data_file, param0,fitdata0)
   help, param0,fitdata0

  data_file =  string('/local/home/mazzino/IDL/00_SuperDARN/Data/',
ref_year,  '/', ref_month,'/',$
        ref_year, ref_month, ref_day, '00', st_id[station], 'C.fit', $
         format='(A42, I04, A1, I02, A1, I04, I02, I02, A2, A1, A5)')
  ;read file
   dummy=readfitacf09(data_file, param1,fitdata1)
   ;help, param1,fitdata1
; account for end of month
if ((ref_day eq 28 and ref_month eq 2) or ((ref_month eq 4 or $
    ref_month eq 6 or ref_month eq 9 or ref_month eq 11) and  ref_day eq
30) or (ref_month eq 12 and ref_day eq 31)) then begin
 if (ref_month eq 2 and ref_day eq 28) or ((ref_month eq 4 or $
 ref_month eq 6 or ref_month eq 9 or ref_month eq 11) and ref_day eq 30)
then begin
data_file =  string('/local/home/mazzino/IDL/00_SuperDARN/Data/',
ref_year, '/', ref_month+1,'/',$
             ref_year, ref_month+1, 1, '00', st_id[station], 'C.fit', $
            format='(A42, I04,  A1, I02, A1, I04, I02, I02, A2, A1, A5)')
 endif

 if (ref_month eq 12 and ref_day eq 31) then begin ;account for December
   data_file =  string('/local/home/mazzino/IDL/00_SuperDARN/Data/',
ref_year+1, '/', 01,'/',$
                ref_year+1, 01, 1, '00', st_id[station], 'C.fit', $
        format='(A42, I04,  A1, I02, A1, I04, I02, I02, A2, A1, A5)')
 endif

 endif else begin
   data_file =  string('/local/home/mazzino/IDL/00_SuperDARN/Data/',
ref_year, '/', ref_month,'/',$
        ref_year, ref_month, ref_day+1, '00', st_id[station], 'C.fit', $
          format='(A42, I04,  A1, I02, A1, I04, I02, I02, A2, A1, A5)')
if ((ref_month eq 1 or ref_month eq 3 or ref_month eq 5 or ref_month eq
7 or $
 ref_month eq 8 or ref_month eq 10) and ref_day eq 31) then begin
;account for months that finish in 31 days
   data_file =  string('/local/home/mazzino/IDL/00_SuperDARN/Data/',
ref_year, '/', ref_month+1,'/',$
         ref_year, ref_month+1, 1, '00', st_id[station], 'C.fit', $
           format='(A42, I04,  A1, I02, A1, I04, I02, I02, A2, A1, A5)')
 endif
 endelse
  ;read file
   dummy=readfitacf09(data_file, param2, fitdata2)
   ;help, param2,fitdata2
   help, param0, param1, param2, fitdata0,fitdata1, fitdata2
 param   =[param0, param1, param2]
 fitdata =[fitdata0,fitdata1, fitdata2]

 cleaning = where (Finite(param[*, 0]) ne 0 and Finite(param[*, 1]) ne 0
and Finite(param[*, 2]) ne 0 and Finite(param[*, 3]) ne 0 and
Finite(param[*, 4]) ne 0 and $
```

```
Finite(param[*, 5]) ne 0 and Finite(param[*, 6]) ne 0 and Finite(param[*,
7]) ne 0 and Finite(param[*, 8]) ne 0, count)

;print, 'size of  data vector out', N_elements(param[cleaning, 8])
print, 'number of data points', count
if count lt 60 then begin
print, 'not enough points'
 goto, endcodeend
endif
;help, param[cleaning ,* ]
;help, fitdata[cleaning, *, *]
if N_elements(cleaning) gt 1 then begin
param   = reform(param[cleaning, *])
fitdata = reform(fitdata[cleaning, *, *])
endif
;print,  param, fitdata
;help, param , fitdata


    ;beam and gate range
smax =   700 ; spike maximum
lb   =     0 ; lower beam
hb   =    15; Higher beam
lg   =     0 ; lower gate
hg   =    60 ; higher gate
 nb     = 0
 ng     = 0

nb=hb-lb+1 ; number of beams
ng=hg-lg+1 ; number of gates
beam_names= STRARR(nb) ;create an array that holds names for all beams
gate_names= STRARR(ng) ;create an array that holds names for all beams
for i=0, nb-1 do begin
  beam_names[i]=string(i+lb , format='(I2)')
endfor

for i=0, ng-1 do begin
  gate_names[i]=string(i+lg , format='(I2)')
  ;print, 'gate name', gate_names[i]
endfor

  ;Prepare matrix that retrives data from file
 year  =    param[*, 0]
 month =    param[*, 1]
 day   =    param[*, 2]
 hour  =    param[*, 3]
 mn    =    param[*, 4]
 sec   =    param[*, 5]
 scan  =    param[*, 6]
 bmnum =    param[*, 7]
 intt  =    param[*, 8]
 v     =    reform(fitdata[*, 0, lg:hg])
 p     =    reform(fitdata[*, 1, lg:hg])
 w     =    reform(fitdata[*, 2, lg:hg])
 qflg  =    reform(fitdata[*, 3, lg:hg])
 gflg  =    reform(fitdata[*, 4, lg:hg])
help, v
```

```
date_label=string(names_stations[station], ref_year, ref_month, ref_day,
$
 format='(A15, I6, "/" , I02, "/", I02, "   ")')
print, 'working on ', date_label

;free some memory
param=0
fitdata=0

 tsize=N_elements(bmnum)
 data              = fltarr(tsize, ng)
 time_array        = dblarr(tsize)
 ;interpolated_data  = fltarr(tsize, ng)
 data[*,*]         = -1e10

;print, 'time array  ', tsize
;help, tsize, nb
;print, '*********************************************'

i=0L
for i=0L, tsize-1 do begin ;{
   ;convert time array into Julian Day
;=============================================================================
========================================
      time_array[i]=Julday(month[i], day[i],year[i], hour[i], mn[i],
sec[i])
;=============================================================================
========================================
        for j=0, ng-1 do begin ;{
                data[i, j] = float(v[i, j])
        endfor;}
     endloop:
 endfor
 ;help, v, data
;Despike data according to input spike max
 for j=0, ng-1 do begin
       spike=where(abs(data[*,j]) gt smax or (Finite(v[*, j]) eq 0),
county)
        if county gt 0 then begin
           data[spike, j]=-1e10
          ; x=x+1
        endif
      endfor
;interpolate (linear) data for gaps
for b= lb, hb do begin ;start loop in beams
  index_interp= where (bmnum eq b, beamcount)
      if beamcount le 0 then begin ;check if there is not data loaded
         ;print, 'beam', b, 'counts', beamcount
         ;print, 'no data in beam', b
         goto, endcrosp0
      endif
  for j=0,ng-1 do begin  ;start loop in gate
  interp_data = reform(data[index_interp, j])
  time_ar     = time_array[index_interp]
    if n_elements(interp_data) ne n_elements(time_array[index_interp])
then stop
    bad=where(interp_data[*] eq -1e10,bcount)
    if bcount gt 0 then begin
```

```
    ;if first or last point is bad, set them to zero
    if bad[0] eq 0 then interp_data[0]=0.0
     if bad[bcount-1] eq n_elements(interp_data)-1 then $
        interp_data[n_elements(interp_data)-1] = 0.0
      bad=where(interp_data eq -1e10, bcount)
       while bcount ne 0 do begin
          prev=bad[0]-1
           next=bad[0]+1
            while interp_data[next] eq -1e10 do begin
              next=next+1
            endwhile
          deltay=interp_data[next]-interp_data[prev]
          deltax=time_array[index_interp[next]]-
time_array[index_interp[prev]]
time_ar(prev))/deltax
         interp_data[prev:next]=$

interp_data[prev]+deltay*(time_array[index_interp[prev:next]]-
time_array[index_interp[prev]])/deltax
         bad=where(interp_data eq -1e10, bcount)
       endwhile
     endif
      data[index_interp, j] = interp_data
   endfor
   endcrosp0:
 endfor


 ;print, 'detrend low frequency noise'
 ;Detrend data to remove low frequency noise
 bm=0
 index_trend=0
 for bm= lb, hb do begin ;start loop in beams
   index_trend= where (bmnum eq bm, trendcount)
    ;print, 'index', beamcount
    ; print, 'data', data[index, *]
if trendcount le 0 then goto, endcrosp3 ;check if there is not data
loaded
            for j=0, ng-3 do begin  ;start loop in gate
             interp_data = data[index_trend, j]
             int_data_ave_noise=fltarr(trendcount)
             int_data_ave_noise[*]=!VALUES.F_NAN
              for r=0L, trendcount-1 do begin
  if r lt 15 or r gt trendcount-16 then
int_data_ave_noise[r]=interp_data[r] else begin
                 average=Mean(interp_data[r-15:r+15], /NaN)
                 int_data_ave_noise[r]=interp_data[r]-average
        ;         print, interp_data[r], average, int_data_ave_noise[r]
               endelse
             endfor
             data[index_trend, j]= int_data_ave_noise
    endfor
     endcrosp3:
  endfor
;~~~~~~~~~~~~~~~~~~~~~~~~~~~~~~~~~~~~~~~~~~~~~~~~~~~~~~~~~~~~~~~~~~~~~~~~~~~~
 ;print, '------------------------------------------------------------
 ;print, '                  Calculating Crosspower'
 ;print, '------------------------------------------------------------
```

```
 cpow      = dblarr(tsize, ng, 30)
 cpha      = dblarr(tsize, ng, 30)
 cpow_ephe = dblarr(tsize, 2)
 cpow[*,*,*]= !VALUES.F_NAN
cpha[*,*,*]= !VALUES.F_NAN
cpow_ephe[*,*] =  !VALUES.F_NAN
;begin windowing in one hour intervals
t=0L
        for i = 0, nb-5 do begin ;loop in beam
           bindex  = 0
           bindex4 = 0
              beam_index = Where(bmnum eq i+lb, bindex)
               beam_index4= Where(bmnum eq i+lb+4, bindex4)
                if bindex lt 1 or bindex4 lt 1 then goto, endcrossp
                   time_beam = time_array[beam_index]
                   time_beam4 = time_array[beam_index4]
                     for z=0, bindex-1 do begin
                        difference=abs(bindex-bindex4)
                            if difference gt 0 then begin
                           ; print, bindex, bindex4
                            minimumloop=Min(bindex, bindex4)
                           ; endloop=(minimumloop-difference-31)
                            endloop=(minimumloop-32)
                            print, 'end of loop ', endloop
          if bindex lt 1 or bindex4 lt 1 then goto, endcrossp
                          endif else endloop=(bindex-32)

        if (z lt 29 or z ge endloop) then begin
        cpow_ephe[beam_index[z],0]  = i+lb
          cpow_ephe[beam_index[z],1]  = time_array[beam_index[z]]
          cpow[beam_index[z], *, *]   = !VALUES.F_NAN
         cpha[beam_index[z], *, *]   = !VALUES.F_NAN
                               goto, endloop_bindex
                            endif else begin

difference_time=abs(hour[beam_index[z+30]]*3600+
mn[beam_index[z+30]]*60.+ sec[beam_index[z+30]] $
  - (hour[beam_index[z-29]]*3600+mn[beam_index[z-
29]]*60.+sec[beam_index[z-29]]))
 if (hour[beam_index[z-29]]) eq 23 then $

difference_time=abs((24+hour[beam_index[z+30]])*3600+
mn[beam_index[z+30]]*60.+ sec[beam_index[z+30]] $
- (hour[beam_index[z-29]]*3600+mn[beam_index[z-29]]*60.+sec[beam_index[z-
29]]))
   if (difference_time gt 3601 or difference_time lt 2000) then begin
             cpow_ephe[beam_index[z],0]  = i+lb
             cpow_ephe[beam_index[z],1]  = time_array[beam_index[z]]
            cpow[beam_index[z], *, *]   = !VALUES.F_NAN
            cpha[beam_index[z], *, *]   = !VALUES.F_NAN
                               goto, endloop_bindex
                               endif else begin
      cpow_ephe[beam_index[z],0]  =  i+lb
   cpow_ephe[beam_index[z],1]  =  time_array[beam_index[z]]
     for j = 0, ng-1 do begin ;begin loop in gate
        ;   print, 'HERE <=========='
```

```
       set=Finite(v[beam_index[z-29:z+30], j])
        set4=Finite(v[beam_index4[z-29:z+30], j])
         good_data=where(set[*] ne 0, count1)
           good_data4=where(set4[*] ne 0, count2)
      ;========== Begin editing =============
       if count1 eq 0 or count2 eq 0 then begin
         cpow[beam_index[z], j, *]   = !VALUES.F_NAN
        cpha[beam_index[z], j, *]   = !VALUES.F_NAN
          goto,  endcrossp1
          endif
 if (n_elements(set[good_data])) le 45 or (n_elements(set4[good_data4]))
le 45 then begin
         cpow[beam_index[z], j, *]   = !VALUES.F_NAN
         cpha[beam_index[z], j, *]   = !VALUES.F_NAN
            goto,  endcrossp1
               endif
;========== End of editing =============
    if (n_elements(set[good_data])) le 45 or
(n_elements(set4[good_data4])) le 45 then begin
     array_length=60
     data_ave_4 = fltarr(array_length, 1)
      data_ave_4[*, 0] = !VALUES.F_NAN

data_ave_4[*, 0]  =     $
Interpol(data[beam_index4[z-29:z+30], j], $
time_array[beam_index4[z-29:z+30]] , $
      time_array[beam_index[z-29:z+30]])


;=====================================================================
; ---------  Calculate Crosspower and Crossphase  -------------
;=====================================================================
             y_v = FFT(data(beam_index[z-29:z+30], j-lg), -1)
             yy_v = FFT(data_ave_4[*], -1)
     rcrosspec=float( y_v)*float(yy_v)+imaginary( y_v)*imaginary(yy_v)
     icrosspec=imaginary( y_v)*float(yy_v)-float( y_v)*imaginary(yy_v)
     crossp=(rcrosspec^2+icrosspec^2)^0.5
     crossph=(Atan(icrosspec , rcrosspec))*180/!PI
     cpow[beam_index[z], j, *] = crossp[0:29]
     cpha[beam_index[z], j, *] = crossph[0:29]
                               endcrossp1:
                                     endfor ; finalizes loop in gate
                                  t += 1
                               endelse
                            endelse
                  endloop_bindex:
                endfor      ;finalizes loop on tsize
              endcrossp:
             endfor    ; finalizes the loop in beam

;print, 'total records of crosspower/crossphase/variance in crosssphase
data points', t
if t eq 0 then begin
cpow_ephe=fltarr(1,1)
cpow_ephe[0,0] = 0
  cpow      = 0
  cpha      = 0
  vcpha     = 0
```

```
  goto, endcode
endif

vcpha=dblarr(tsize, ng, 30) ; define matrix to hold data dynamic variance
in cross phase
vcpha[*, *, *]= !VALUES.F_NAN
;print, ' ============================'
;=============================================================================
; -------  Correct for phase unwrapping in Crossphase at each frequency
;=============================================================================
bindex=0
for beamind = 0, nb-5 do begin ;loop in beam
       ;  print, 'beam => ', beamind+lb
          beam_index = Where(cpow_ephe[*,0] eq beamind+lb, bindex)
           for i=1, bindex-1 do begin
            for j=0, ng-1 do begin;loop in gate
              for q=0, 29 do begin ;loop in frequency
               dif= cpha[beam_index[i], j, q]-cpha[beam_index[i-1], j, q]
                if Finite(dif) ne 0 then begin
      if (dif lt -180.) then cpha[beam_index[i:bindex-1], j,
q]=cpha[beam_index[i:bindex-1], j, q]+360.
   if (dif gt  180.) then cpha[beam_index[i:bindex-1], j,
q]=cpha[beam_index[i:bindex-1], j, q]-360.
                endif
               endfor
             endfor
            endfor
endfor    ; finalizes the loop in beam

;=============================================================================
; -------  Calculate dynamice variance in cross phase  -------
;=============================================================================
            l=0L
            bindex1=0
            increment=30
                  for beamind = 0, nb-5 do begin ;loop in beam
                   ;   print, 'beam => ', beamind+lb
      beam_index1 = Where(cpow_ephe[*,0] eq beamind+lb, bindex1)
                        if bindex1 eq 0 then goto,  endcrossp8
       for c=0, bindex1-1 do begin
         for j=0, ng-1 do begin;loop in gate
          for q=0, 29 do begin ;loop in frequency
           if (c le 29 or c gt bindex1-31) then begin ; define end points
                           vcpha[beam_index1[c], j, q] = !Values.F_NAN
                                   endif else begin

dummy3=where(finite(cpha[beam_index1[c-increment:c+increment], j , q]) ne
0, condition_count3)
                         if condition_count3 le 50 then $
          vcpha[beam_index1[c], j, q]=!Values.F_NAN else begin

result=moment(cpha[beam_index1[c-increment:c+increment], j , q], /NaN)
           vcpha[beam_index1[c], j, q]=result(1)
          if result(1) le 0 then vcpha[beam_index1[c], j, q]=0.1^35.
                                                 endelse
                                    endelse
                                 endfor
                              endfor
```

```
                        endfor
                       endcrossp8:
                  endfor    ; finalizes the loop in beam


;print, '================== all data ======================='
;help, cpow_ephe
;help, cpow
;help, vcpha
;print, '============ here ==========='
;print, '============================='
;print, '================== Remove all data where original NaN data
======================'
    for beam=lb, hb-4 do begin
;    print, '====================================here============'
;    print, 'working on beam: ', beam
       beam_index=where(bmnum eq beam, count)
         beam_index4=where(bmnum eq beam+4, count4)
         if count le 0 or count4 le 30 then goto,  nextbeamloop
       condition=where(Finite(v[beam_index, j]) eq 0  or
Finite(v[beam_index4, j]) eq 0, condition_counter)
                        ;   help, condition_counter
     if condition_counter gt 0 then begin
    cpha[beam_index[condition], j, *]   =!Values.F_NAN
    cpow[beam_index[condition], j, *]   =!VALUES.F_NAN
    vcpha[beam_index[condition], j, *]  =!VALUES.F_NAN
                    endif
        if (count gt count4 and count-31 gt endingcount) then begin
          cpha[beam_index[endingcount:count-31], j, *]   =!Values.F_NAN
           cpow[beam_index[endingcount:count-31], j, *]   =!VALUES.F_NAN
           vcpha[beam_index[endingcount:count-31], j, *]  =!VALUES.F_NAN
                   endif
          if (count4 gt count and count-31 gt endingcount-32) then begin
                    ;print,'#############'
              ;  help, beam_index, endingcount, count-31, j, cpha
 cpha[beam_index[endingcount-32:count-31], j, *]   =!VALUES.F_NAN
cpow[beam_index[endingcount-32:count-31], j, *]   =!VALUES.F_NAN
        vcpha[beam_index[endingcount-32:count-31], j, *]  =!VALUES.F_NAN
                   endif
                     for c=30, endingcount-32 do begin
condition1=where(Finite(v[beam_index[c-30:c+29], j]) eq 0,
condition_count1)
condition2=where(Finite(v[beam_index4[c-30:c+29], j]) eq 0,
condition_count2)
                             if condition_count1 gt 15 or
condition_count2 gt 15  or intt[c] ne 3 then begin $
                   cpha[beam_index[c], j, *]   =!Values.F_NAN
                   cpow[beam_index[c], j, *]   =!VALUES.F_NAN
                   vcpha[beam_index[c], j, *]  =!VALUES.F_NAN
                            endif
                        endfor

          endfor
         nextbeamloop:
    endfor


caldat, cpow_ephe[0, 1], month, day, year, hour, min
```

```
;print, 'beginning', month, day, year, hour, min
caldat, cpow_ephe[N_elements(cpow_ephe[*,1])-1, 1], month, day, year,
hour, min
;print, 'end', month, day, year, hour, min
   dayshr = Julday(  ref_month, ref_day, ref_year,  0 , 0, 00 )
   dayehr = Julday(  ref_month, ref_day, ref_year, 23, 59, 59)
return_index= where(cpow_ephe[*,1] ge dayshr and cpow_ephe[*,1] le dayehr
, indi)
if indi eq 0 then begin
  cpow_ephe = 0
  cpow      = 0
  cpha      = 0
  vcpha     = 0
goto, endcode
endif
;print, 'selected data'
;help, cpow_ephe[return_index, *]
;help, cpow[return_index]
;help, vcpha[return_index]
;help, indi
if indi ne 0 then begin
  cpw_ephe = dblarr(indi, 2)
  cpw      = fltarr(indi, ng, 30)
  cpa      = fltarr(indi, ng, 30)
  vcpa     = fltarr(indi, ng, 30)
  cpw_ephe[0:indi-1, *]    = reform(cpow_ephe[return_index[0:indi-1], *])
    cpw[0:indi-1, *, *]      = reform(cpow[return_index[0:indi-1], *, *])
    cpa[0:indi-1, *, *]      = reform(cpha[return_index[0:indi-1], *, *])
   vcpa[0:indi-1, *, *]     = reform(vcpha[return_index[0:indi-1], *, *])

  cpow_ephe = 0
  cpow      = 0
  cpha      = 0
  vcpha     = 0

  cpow_ephe = dblarr(indi, 2)
  cpow      = fltarr(indi, ng, 30)
  cpha      = fltarr(indi, ng, 30)
  vcpha     = dblarr(indi, ng, 30)
  cpow_ephe = cpw_ephe
  cpow      = cpw
  cpha      = cpa
  vcpha     = vcpa

;print, 'returning crosspower data'
endcode:
;help, cpow_ephe
;help, cpow
;help, vcpha
  ;print, 'velocity vector'
  ;help, v
   dayshr = Julday(  ref_month, ref_day, ref_year,  0 , 0, 00 )
   dayehr = Julday(  ref_month, ref_day, ref_year, 23, 59, 00)
   keep= where(time_array ge dayshr and time_array le dayehr, keepers)

 return, cpow_ephe
 return, cpow
 return, cpha
```

```
 return, vcpha
 return, bmnum[keep]
 return, time_array[keep]
 return, data(keep, *)
endif

 ;free memory
cpow_ephe = 0
cpow = 0
cpha = 0
vcpha = 0
vpa=0
t=0
  cpw_ephe = 0
  cpw      = 0
  cpa      = 0
  vcpa     = 0
  data_file = 0
  bmnum[keep]= 0
  time_array[keep]= 0
  data(keep, *)= 0
  keep=0
   year  =    0
 month =     0
 day   =     0
 hour  =      0
 mn    =      0
 sec   =     0
 scan  =      0
 bmnum =      0
 intt  =      0
 v     =     0
 p     =      0
 w     =      0
 qflg  =      0
 gflg  =      0
  endcodeend:
end

pro trend,y,n

sumx=0.0
sumy=0.0
sumxx=0.0
sumyy=0.0
sumxy=0.0
for i=0,n-1 do begin
  sumx= sumx+float(i+1)
  sumy= sumy+y(i)
  sumxx=sumxx+float(i+1)*float(i+1)
  sumyy=sumyy+y(i)*y(i)
  sumxy=sumxy+float(i+1)*y(i)
endfor
del=float(n)*sumxx-sumx*sumx
a=(sumxx*sumy-sumx*sumxy)/del
b=(float(n)*sumxy-sumx*sumy)/del
;print, ' '
;print,'Best fit trend = ',a,' + ',b,'x'
```

```
;...  remove trend

for i=0,n-1 do begin
   y(i)=y(i)-a-b*float(i+1)
  endfor
end
```

~~~~~~~~~~~~~~~~~~~~~~~~~~~~~~~~~~~

```
; readfitacf09.pro
; ==============
; Author of original procedure (readfitacf.pro): R.J.Barnes
; Modified on:  Laura Mazzino (October 2011, University of Alberta)
; Last modified by: Laura Mazzino (June 2014, University of Alberta)
; This program reads  fitacf files, and prints data to file in .txt
format. Same as readfitacf07,
; but reads any file from any station for any date.
; This program is the same than readfitacf08 but also
; incorporates two other conditions: fit.qflg eq 1 and fit.gflg eq 0
;@/home/mmazzino/IDL/startup.pro
```

function readfitacf09, data_file1, param, fitdata

```
inp=0
s=0
prm=0
fit=0
param=0L
fitdata =0L
 counter=0L
param   = fltarr(90000, 9); 24 hours, 60 seconds in a min, 86400 data
points, rounded to 90000
     param[*,*]=!VALUES.F_NAN
     fitdata = fltarr(90000, 5, 61)
     fitdata[*,*,*]=!VALUES.F_NAN
      Print, 'opening file'
       inp=OldFitOpen(data_file1)
         print, 'reading',  data_file1
         while OldFitRead(inp, prm, fit) ne -1 do begin ;{
; Load data with hour ,minute ,sec ,beam number, scan, beamnumber,
integration time ,velocity ,power  ,width
if ((prm.scan[0] eq 1 or prm.scan[0] eq 0) and prm.intt.sc[0] eq 3) then
begin
              param[counter, 0] = prm.time.yr[0]  ;year
              param[counter, 1] = prm.time.mo[0]  ;month
              param[counter, 2] = prm.time.dy[0]  ;day
              param[counter, 3] = prm.time.hr[0]
              param[counter, 4] = prm.time.mt[0]
              param[counter, 5] = prm.time.sc[0]
              param[counter, 6] = prm.scan[0]
              param[counter, 7] = prm.bmnum[0]
              param[counter, 8] = prm.intt.sc[0]

                for i=0,60 do begin
;Remove ground scatter:  Ponomarenko 2007, Section 4.1 and calculate the
average Doppler velocity and (fit.gflg[i] eq 0)
```

```
                    Vmax=30
                    Wmax=90
 if ((fit.qflg[i] eq 1) ) and (abs(fit.v[i]) - Vmax * (1 -
abs(fit.w_l[i]/Wmax)) gt 0.0) then begin ;{
                                fitdata[counter, 0, i] = fit.v[i]
                                fitdata[counter, 1, i] = fit.p_l[i]
                                fitdata[counter, 2, i] = fit.w_l[i]
                                fitdata[counter, 3, i] = fit.qflg[i]
                                fitdata[counter, 4, i] = fit.gflg[i]
                     endif
              endfor

              counter += 1
        endif
        endwhile    ;
s=OldFitClose(inp)
 inp=0
 s=0
;remove unfilled lines:
cleaning = where(Finite(param[*, 0]) ne 0 and Finite(param[*, 1]) ne 0
and Finite(param[*, 2]) ne 0 and Finite(param[*, 3]) ne 0 and
Finite(param[*, 4]) ne 0 and $
Finite(param[*, 5]) ne 0 and Finite(param[*, 6]) ne 0 and Finite(param[*,
7]) ne 0 and Finite(param[*, 8]) ne 0, count)
print, 'size of  data vector out', N_elements(param[cleaning, 8])
if N_elements(cleaning) gt 1 then begin
param   = reform(param[cleaning, *])
fitdata = reform(fitdata[cleaning, *, *])
endif else begin
param   = param[cleaning, *]
fitdata = fitdata[cleaning, *, *]
endelse

return, param
return, fitdata
;print, param[*, 8]
;free some memory
counter=0
fitdata = 0
data_file1=0
param=0

s=0
u=0
end
```

APPENDIX A AUTOMATED ALGORITHM OR CODE (IDL BASED)

Appendix B

Maximum correlation coefficients of the time series corresponding to solar wind and SuperDARN

Internal ID number for Event
ST Station Number
M Month
D Day
H Hour
MI MInute
Freq Frequency

P Solar Parameter ID
Delay A Time difference between max. for Lag A
CC A Correlation Coefficient for Lag A
CDT Calculated Delay time
Delay B Time difference between max. for Lag B
CC B Correlation Coefficient for Lag B

#	ST	M	D	Year	H	Mi	Freq	P	Delay A	CC A	CDT	Delay B	CC B
1	7	1	3	2003	8	14	0.83	0	-61	0.23	53	-61	0.23
1	7	1	3	2003	8	14	0.83	1	-46	0.51	53	-68	0.39
1	7	1	3	2003	8	14	0.83	2	-61	0.35	53	-61	0.35
1	7	1	3	2003	8	14	0.83	3	-71	0.34	53	-71	0.34
1	7	1	3	2003	8	14	0.83	4	-73	0.22	53	-73	0.22
1	7	1	3	2003	8	14	0.83	5	-74	0.40	53	-74	0.40
1	7	1	3	2003	8	14	0.83	6	-74	0.34	53	-74	0.34
1	7	1	3	2003	8	14	0.83	7	-46	0.29	53	-83	0.09
1	7	1	3	2003	8	14	0.83	8	-61	0.39	53	-61	0.39
1	7	1	3	2003	8	14	0.83	9	-61	0.18	53	-83	0.21
2	7	1	3	2003	12	23	0.56	0	-65	0.22	48	-65	0.22
2	7	1	3	2003	12	23	0.56	1	-52	0.30	48	-52	0.30
2	7	1	3	2003	12	23	0.56	2	-37	0.25	48	-68	0.12
2	7	1	3	2003	12	23	0.56	3	-74	0.25	48	-74	0.25
2	7	1	3	2003	12	23	0.56	4	-66	0.27	48	-66	0.27
2	7	1	3	2003	12	23	0.56	5	-37	0.47	48	-61	0.22
2	7	1	3	2003	12	23	0.56	6	-50	0.19	48	-50	0.19
2	7	1	3	2003	12	23	0.56	7	-50	0.27	48	-50	0.27
2	7	1	3	2003	12	23	0.56	8	-45	0.29	48	-64	0.25
2	7	1	3	2003	12	23	0.56	9	-65	0.27	48	-65	0.27
3	7	1	3	2003	12	35	0.83	0	-45	0.22	48	-65	0.19
3	7	1	3	2003	12	35	0.83	1	-49	0.36	48	-49	0.36
3	7	1	3	2003	12	35	0.83	2	-68	0.29	48	-68	0.29
3	7	1	3	2003	12	35	0.83	3	-77	0.30	48	-77	0.30
3	7	1	3	2003	12	35	0.83	4	-67	0.33	48	-67	0.33
3	7	1	3	2003	12	35	0.83	5	-61	0.42	48	-61	0.42
3	7	1	3	2003	12	35	0.83	6	-50	0.25	48	-50	0.25
3	7	1	3	2003	12	35	0.83	7	-50	0.32	48	-50	0.32
3	7	1	3	2003	12	35	0.83	8	-45	0.27	48	-50	0.26
3	7	1	3	2003	12	35	0.83	9	-45	0.23	48	-48	0.19
4	7	1	3	2003	16	41	4.17	0	-58	0.22	46	-58	0.22

APPENDIX B MAXIMUM CORRELATION COEFFICIENTS OF THE TIME SERIES CORRESPONDING TO SOLAR WIND AND SUPERDARN

#	ST	M	D	Year	H	Mi	Freq	P	Delay A	CC A	CDT	Delay B	CC B
4	7	1	3	2003	16	41	4.17	1	-70	0.48	46	-70	0.48
4	7	1	3	2003	16	41	4.17	2	-63	0.32	46	-63	0.32
4	7	1	3	2003	16	41	4.17	3	-63	0.45	46	-63	0.45
4	7	1	3	2003	16	41	4.17	4	-52	0.38	46	-52	0.38
4	7	1	3	2003	16	41	4.17	5	-31	0.31	46	-67	0.24
4	7	1	3	2003	16	41	4.17	6	-30	0.33	46	-46	0.18
4	7	1	3	2003	16	41	4.17	7	-63	0.39	46	-63	0.39
4	7	1	3	2003	16	41	4.17	8	-42	0.25	46	-47	0.19
4	7	1	3	2003	16	41	4.17	9	-58	0.29	46	-58	0.29
5	7	1	3	2003	19	2	2.50	0	-34	0.39	46	-48	0.33
5	7	1	3	2003	19	2	2.50	1	-61	0.29	46	-61	0.29
5	7	1	3	2003	19	2	2.50	2	-51	0.44	46	-51	0.44
5	7	1	3	2003	19	2	2.50	3	-51	0.32	46	-51	0.32
5	7	1	3	2003	19	2	2.50	4	-60	0.32	46	-60	0.32
5	7	1	3	2003	19	2	2.50	5	-49	0.36	46	-49	0.36
5	7	1	3	2003	19	2	2.50	6	-52	0.45	46	-52	0.45
5	7	1	3	2003	19	2	2.50	7	-52	0.34	46	-52	0.34
5	7	1	3	2003	19	2	2.50	8	-49	0.32	46	-49	0.32
5	7	1	3	2003	19	2	2.50	9	-34	0.31	46	-48	0.30
6	7	1	3	2003	19	47	3.61	0	-61	0.28	46	-61	0.28
6	7	1	3	2003	19	47	3.61	1	-46	0.28	46	-46	0.28
6	7	1	3	2003	19	47	3.61	2	-52	0.23	46	-52	0.23
6	7	1	3	2003	19	47	3.61	3	-33	0.33	46	-52	0.18
6	7	1	3	2003	19	47	3.61	4	-80	0.26	46	-60	0.24
6	7	1	3	2003	19	47	3.61	5	-31	0.27	46	-46	0.09
6	7	1	3	2003	19	47	3.61	6	-52	0.44	46	-52	0.44
6	7	1	3	2003	19	47	3.61	7	-80	0.25	46	-52	0.21
6	7	1	3	2003	19	47	3.61	8	-61	0.26	46	-61	0.26
6	7	1	3	2003	19	47	3.61	9	-46	0.27	46	-46	0.27
7	7	1	3	2003	19	49	3.89	0	-65	0.25	46	-65	0.25
7	7	1	3	2003	19	49	3.89	1	-47	0.38	46	-47	0.38
7	7	1	3	2003	19	49	3.89	2	-53	0.34	46	-53	0.34
7	7	1	3	2003	19	49	3.89	3	-53	0.29	46	-53	0.29
7	7	1	3	2003	19	49	3.89	4	-46	0.41	46	-46	0.41
7	7	1	3	2003	19	49	3.89	5	-31	0.37	46	-48	0.13
7	7	1	3	2003	19	49	3.89	6	-53	0.44	46	-53	0.44
7	7	1	3	2003	19	49	3.89	7	-55	0.36	46	-55	0.36
7	7	1	3	2003	19	49	3.89	8	-46	0.32	46	-46	0.32
7	7	1	3	2003	19	49	3.89	9	-47	0.30	46	-47	0.30
8	7	1	3	2003	19	49	4.44	0	-69	0.28	46	-69	0.28
8	7	1	3	2003	19	49	4.44	1	-47	0.36	46	-47	0.36
8	7	1	3	2003	19	49	4.44	2	-53	0.34	46	-53	0.34
8	7	1	3	2003	19	49	4.44	3	-33	0.29	46	-53	0.23
8	7	1	3	2003	19	49	4.44	4	-46	0.29	46	-46	0.29
8	7	1	3	2003	19	49	4.44	5	-31	0.32	46	-48	0.16
8	7	1	3	2003	19	49	4.44	6	-53	0.44	46	-53	0.44
8	7	1	3	2003	19	49	4.44	7	-80	0.27	46	-55	0.20
8	7	1	3	2003	19	49	4.44	8	-38	0.28	46	-61	0.24
8	7	1	3	2003	19	49	4.44	9	-46	0.33	46	-46	0.33
9	10	1	7	2003	20	54	0.56	1	-61	0.46	72	-84	0.16
9	10	1	7	2003	20	54	0.56	2	-71	0.46	72	-72	0.44
9	10	1	7	2003	20	54	0.56	3	-61	0.32	72	-99	0.27
9	10	1	7	2003	20	54	0.56	4	-61	0.42	72	-92	0.09
9	10	1	7	2003	20	54	0.56	5	-76	0.35	72	-76	0.35
9	10	1	7	2003	20	54	0.56	6	-68	0.30	72	-73	0.19
9	10	1	7	2003	20	54	0.56	7	-34	0.27	72	-90	0.07

APPENDIX B MAXIMUM CORRELATION COEFFICIENTS OF THE TIME SERIES CORRESPONDING TO SOLAR WIND AND SUPERDARN

#	ST	M	D	Year	H	Mi	Freq	P	Delay A	CC A	CDT	Delay B	CC B
9	10	1	7	2003	20	54	0.56	8	-40	0.34	72	-97	0.21
10	10	1	7	2003	20	38	0.83	1	-55	0.51	72	-73	0.26
10	10	1	7	2003	20	38	0.83	2	-64	0.50	72	-87	0.17
10	10	1	7	2003	20	38	0.83	3	-75	0.41	72	-75	0.41
10	10	1	7	2003	20	38	0.83	4	-55	0.44	72	-72	0.25
10	10	1	7	2003	20	38	0.83	5	-64	0.48	72	-97	0.14
10	10	1	7	2003	20	38	0.83	6	-55	0.18	72	-89	0.15
10	10	1	7	2003	20	38	0.83	7	-38	0.18	72	-75	0.10
10	10	1	7	2003	20	38	0.83	8	-32	0.43	72	-102	0.19
11	10	1	7	2003	20	54	3.06	1	-34	0.36	72	-100	0.28
11	10	1	7	2003	20	54	3.06	2	-66	0.42	72	-88	0.42
11	10	1	7	2003	20	54	3.06	3	-77	0.33	72	-77	0.33
11	10	1	7	2003	20	54	3.06	4	-77	0.22	72	-77	0.22
11	10	1	7	2003	20	54	3.06	5	-64	0.33	72	-94	0.42
11	10	1	7	2003	20	54	3.06	6	-50	0.31	72	-83	0.27
11	10	1	7	2003	20	54	3.06	7	-31	0.19	72	-78	0.05
11	10	1	7	2003	20	54	3.06	8	-62	0.41	72	-77	0.36
12	10	1	7	2003	20	59	3.61	1	-79	0.35	72	-84	0.43
12	10	1	7	2003	20	59	3.61	2	-66	0.24	72	-94	0.24
12	10	1	7	2003	20	59	3.61	3	-78	0.37	72	-83	0.40
12	10	1	7	2003	20	59	3.61	4	-78	0.24	72	-86	0.35
12	10	1	7	2003	20	59	3.61	5	-66	0.33	72	-94	0.39
12	10	1	7	2003	20	59	3.61	6	-50	0.33	72	-94	0.07
12	10	1	7	2003	20	59	3.61	7	-80	0.28	72	-81	0.29
12	10	1	7	2003	20	59	3.61	8	-39	0.23	72	-88	0.24
13	9	1	7	2003	21	24	1.94	1	-50	0.29	75	-75	0.27
13	9	1	7	2003	21	24	1.94	2	-68	0.17	75	-81	0.23
13	9	1	7	2003	21	24	1.94	3	-54	0.28	75	-96	-0.01
13	9	1	7	2003	21	24	1.94	4	-76	0.35	75	-76	0.35
13	9	1	7	2003	21	24	1.94	5	-68	0.06	75	-86	0.24
13	9	1	7	2003	21	24	1.94	6	-60	0.05	75	-76	0.02
13	9	1	7	2003	21	24	1.94	7	-38	0.24	75	-76	0.23
13	9	1	7	2003	21	24	1.94	8	-39	0.27	75	-100	0.16
14	8	1	7	2003	23	7	1.11	1	-69	0.20	73	-94	0.15
14	8	1	7	2003	23	7	1.11	2	-38	0.22	73	-103	0.19
14	8	1	7	2003	23	7	1.11	3	-54	0.29	73	-74	0.09
14	8	1	7	2003	23	7	1.11	4	-42	0.30	73	-101	0.26
14	8	1	7	2003	23	7	1.11	5	-72	0.15	73	-73	0.13
14	8	1	7	2003	23	7	1.11	6	-69	0.56	73	-73	0.21
14	8	1	7	2003	23	7	1.11	7	-37	0.37	73	-103	0.11
14	8	1	7	2003	23	7	1.11	8	-36	0.35	73	-98	0.14
18	10	1	16	2003	20	59	1.67	1	-50	0.41	75	-101	0.29
18	10	1	16	2003	20	59	1.67	2	-64	0.45	75	-95	0.29
18	10	1	16	2003	20	59	1.67	3	-56	0.33	75	-95	0.30
18	10	1	16	2003	20	59	1.67	4	-56	0.31	75	-96	0.24
18	10	1	16	2003	20	59	1.67	5	-76	0.52	75	-76	0.52
18	10	1	16	2003	20	59	1.67	6	-64	0.48	75	-95	0.24
18	10	1	16	2003	20	59	1.67	7	-60	0.41	75	-95	0.43
18	10	1	16	2003	20	59	1.67	8	-55	0.38	75	-98	0.05
16	10	1	16	2003	23	24	0.83	1	-50	0.29	75	-78	0.29
16	10	1	16	2003	23	24	0.83	2	-43	0.33	75	-85	0.15
16	10	1	16	2003	23	24	0.83	3	-53	0.23	75	-90	0.15
16	10	1	16	2003	23	24	0.83	4	-63	0.40	75	-83	0.31
16	10	1	16	2003	23	24	0.83	5	-66	0.21	75	-85	0.24
16	10	1	16	2003	23	24	0.83	6	-63	0.36	75	-84	0.18
16	10	1	16	2003	23	24	0.83	7	-30	0.15	75	-99	0.07

APPENDIX B MAXIMUM CORRELATION COEFFICIENTS OF THE TIME SERIES CORRESPONDING TO SOLAR WIND AND SUPERDARN

#	ST	M	D	Year	H	Mi	Freq	P	Delay A	CC A	CDT	Delay B	CC B
16	10	1	16	2003	23	24	0.83	8	-63	0.30	75	-82	0.20
17	10	1	16	2003	23	20	1.39	1	-75	0.19	75	-89	0.34
17	10	1	16	2003	23	20	1.39	2	-61	0.50	75	-79	0.18
17	10	1	16	2003	23	20	1.39	3	-30	0.22	75	-103	0.32
17	10	1	16	2003	23	20	1.39	4	-77	0.61	75	-77	0.61
17	10	1	16	2003	23	20	1.39	5	-80	0.44	75	-81	0.45
17	10	1	16	2003	23	20	1.39	6	-61	0.46	75	-80	0.33
17	10	1	16	2003	23	20	1.39	7	-30	0.22	75	-97	0.27
17	10	1	16	2003	23	20	1.39	8	-60	0.40	75	-77	0.38
19	10	1	16	2003	23	18	2.78	1	-51	0.29	75	-89	0.17
19	10	1	16	2003	23	18	2.78	2	-59	0.30	75	-77	0.27
19	10	1	16	2003	23	18	2.78	3	-30	0.21	75	-84	0.07
19	10	1	16	2003	23	18	2.78	4	-76	0.36	75	-76	0.36
19	10	1	16	2003	23	18	2.78	5	-31	0.34	75	-96	0.18
19	10	1	16	2003	23	18	2.78	6	-78	0.29	75	-78	0.29
19	10	1	16	2003	23	18	2.78	7	-30	0.30	75	-89	-0.02
19	10	1	16	2003	23	18	2.78	8	-76	0.29	75	-76	0.29
20	8	1	19	2003	17	48	2.78	0	-50	0.27	43	-50	0.27
20	8	1	19	2003	17	48	2.78	1	-52	0.27	43	-52	0.27
20	8	1	19	2003	17	48	2.78	2	-44	0.38	43	-44	0.38
20	8	1	19	2003	17	48	2.78	3	-51	0.40	43	-51	0.40
20	8	1	19	2003	17	48	2.78	4	-54	0.31	43	-54	0.31
20	8	1	19	2003	17	48	2.78	5	-79	0.22	43	-61	0.07
20	8	1	19	2003	17	48	2.78	6	-54	0.25	43	-54	0.25
20	8	1	19	2003	17	48	2.78	7	-65	0.35	43	-65	0.35
20	8	1	19	2003	17	48	2.78	8	-39	0.34	43	-62	0.33
20	8	1	19	2003	17	48	2.78	9	-52	0.27	43	-52	0.27
21	14	1	21	2003	11	41	1.11	0	-66	0.36	37	-66	0.36
21	14	1	21	2003	11	41	1.11	1	-37	0.26	37	-37	0.26
21	14	1	21	2003	11	41	1.11	2	-30	0.32	37	-64	0.20
21	14	1	21	2003	11	41	1.11	3	-63	0.42	37	-63	0.42
21	14	1	21	2003	11	41	1.11	4	-50	0.33	37	-50	0.33
21	14	1	21	2003	11	41	1.11	5	-70	0.30	37	-67	0.15
21	14	1	21	2003	11	41	1.11	6	-37	0.23	37	-37	0.23
21	14	1	21	2003	11	41	1.11	7	-54	0.23	37	-54	0.23
21	14	1	21	2003	11	41	1.11	8	-42	0.43	37	-42	0.43
21	14	1	21	2003	11	41	1.11	9	-66	0.31	37	-66	0.31
22	13	1	26	2003	2	46	1.11	0	-70	0.29	35	-42	0.20
22	13	1	26	2003	2	46	1.11	1	-61	0.47	35	-61	0.47
22	13	1	26	2003	2	46	1.11	2	-55	0.39	35	-55	0.39
22	13	1	26	2003	2	46	1.11	3	-53	0.16	35	-53	0.16
22	13	1	26	2003	2	46	1.11	4	-32	0.43	35	-61	0.31
22	13	1	26	2003	2	46	1.11	5	-40	0.25	35	-40	0.25
22	13	1	26	2003	2	46	1.11	6	-63	0.50	35	-63	0.50
22	13	1	26	2003	2	46	1.11	7	-75	0.34	35	-35	0.34
22	13	1	26	2003	2	46	1.11	8	-75	0.43	35	-52	0.22
22	13	1	26	2003	2	46	1.11	9	-68	0.24	35	-48	0.21
23	3	1	29	2003	23	57	0.83	0	-38	0.33	58	-74	0.24
23	3	1	29	2003	23	57	0.83	1	-80	0.38	58	-80	0.38
23	3	1	29	2003	23	57	0.83	2	-31	0.25	58	-69	0.19
23	3	1	29	2003	23	57	0.83	3	-80	0.20	58	-87	0.26
23	3	1	29	2003	23	57	0.83	4	-40	0.29	58	-69	0.23
23	3	1	29	2003	23	57	0.83	5	-56	0.46	58	-58	0.25
23	3	1	29	2003	23	57	0.83	6	-30	0.28	58	-71	0.20
23	3	1	29	2003	23	57	0.83	7	-80	0.24	58	-80	0.24
23	3	1	29	2003	23	57	0.83	8	-30	0.31	58	-71	0.23

APPENDIX B MAXIMUM CORRELATION COEFFICIENTS OF THE TIME SERIES CORRESPONDING TO SOLAR WIND AND SUPERDARN

#	ST	M	D	Year	H	Mi	Freq	P	Delay A	CC A	CDT	Delay B	CC B
23	3	1	29	2003	23	57	0.83	9	-38	0.28	58	-74	0.23
24	3	1	29	2003	23	59	1.39	0	-41	0.36	58	-61	0.27
24	3	1	29	2003	23	59	1.39	1	-78	0.32	58	-78	0.32
24	3	1	29	2003	23	59	1.39	2	-67	0.15	58	-67	0.15
24	3	1	29	2003	23	59	1.39	3	-77	0.21	58	-77	0.21
24	3	1	29	2003	23	59	1.39	4	-34	0.21	58	-68	0.19
24	3	1	29	2003	23	59	1.39	5	-49	0.23	58	-79	0.08
24	3	1	29	2003	23	59	1.39	6	-34	0.15	58	-83	0.10
24	3	1	29	2003	23	59	1.39	7	-40	0.22	58	-81	0.23
24	3	1	29	2003	23	59	1.39	8	-74	0.22	58	-74	0.22
24	3	1	29	2003	23	59	1.39	9	-40	0.31	58	-63	0.25
28	13	2	7	2003	3	6	1.11	0	-37	0.33	48	-58	0.18
28	13	2	7	2003	3	6	1.11	1	-79	0.31	48	-48	0.30
28	13	2	7	2003	3	6	1.11	2	-32	0.26	48	-55	0.25
28	13	2	7	2003	3	6	1.11	3	-37	0.45	48	-56	0.28
28	13	2	7	2003	3	6	1.11	4	-37	0.47	48	-62	0.12
28	13	2	7	2003	3	6	1.11	5	-80	0.37	48	-65	0.33
28	13	2	7	2003	3	6	1.11	6	-33	0.35	48	-56	0.28
28	13	2	7	2003	3	6	1.11	7	-37	0.48	48	-57	0.17
28	13	2	7	2003	3	6	1.11	8	-36	0.44	48	-62	0.21
28	13	2	7	2003	3	6	1.11	9	-37	0.29	48	-58	0.19
31	13	2	19	2003	21	7	0.56	0	-65	0.52	45	-65	0.52
31	13	2	19	2003	21	7	0.56	1	-75	0.42	45	-75	0.42
31	13	2	19	2003	21	7	0.56	2	-55	0.66	45	-55	0.66
31	13	2	19	2003	21	7	0.56	3	-46	0.32	45	-46	0.32
31	13	2	19	2003	21	7	0.56	4	-44	0.41	45	-54	0.39
31	13	2	19	2003	21	7	0.56	5	-59	0.53	45	-59	0.53
31	13	2	19	2003	21	7	0.56	6	-73	0.33	45	-73	0.33
31	13	2	19	2003	21	7	0.56	7	-65	0.56	45	-65	0.56
31	13	2	19	2003	21	7	0.56	8	-34	0.64	45	-63	0.26
31	13	2	19	2003	21	7	0.56	9	-65	0.52	45	-65	0.52
32	13	2	19	2003	21	4	0.83	0	-76	0.29	45	-75	0.28
32	13	2	19	2003	21	4	0.83	1	-43	0.50	45	-56	0.40
32	13	2	19	2003	21	4	0.83	2	-71	0.37	45	-71	0.37
32	13	2	19	2003	21	4	0.83	3	-56	0.43	45	-56	0.43
32	13	2	19	2003	21	4	0.83	4	-58	0.43	45	-58	0.43
32	13	2	19	2003	21	4	0.83	5	-61	0.23	45	-61	0.23
32	13	2	19	2003	21	4	0.83	6	-39	0.49	45	-56	0.18
32	13	2	19	2003	21	4	0.83	7	-68	0.60	45	-68	0.60
32	13	2	19	2003	21	4	0.83	8	-70	0.50	45	-70	0.50
32	13	2	19	2003	21	4	0.83	9	-76	0.32	45	-75	0.27
33	13	2	19	2003	21	25	2.22	0	-63	0.31	45	-63	0.31
33	13	2	19	2003	21	25	2.22	1	-73	0.36	45	-73	0.36
33	13	2	19	2003	21	25	2.22	2	-33	0.25	45	-46	0.11
33	13	2	19	2003	21	25	2.22	3	-43	0.44	45	-54	0.39
33	13	2	19	2003	21	25	2.22	4	-54	0.44	45	-54	0.44
33	13	2	19	2003	21	25	2.22	5	-44	0.45	45	-50	0.44
33	13	2	19	2003	21	25	2.22	6	-65	0.33	45	-65	0.33
33	13	2	19	2003	21	25	2.22	7	-68	0.33	45	-68	0.33
33	13	2	19	2003	21	25	2.22	8	-33	0.33	45	-71	0.29
33	13	2	19	2003	21	25	2.22	9	-63	0.34	45	-63	0.34
34	13	2	19	2003	21	25	2.78	0	-64	0.54	45	-64	0.54
34	13	2	19	2003	21	25	2.78	1	-73	0.37	45	-73	0.37
34	13	2	19	2003	21	25	2.78	2	-55	0.66	45	-55	0.66
34	13	2	19	2003	21	25	2.78	3	-46	0.35	45	-46	0.35
34	13	2	19	2003	21	25	2.78	4	-45	0.38	45	-45	0.38

APPENDIX B MAXIMUM CORRELATION COEFFICIENTS OF THE TIME SERIES CORRESPONDING TO SOLAR WIND AND SUPERDARN

#	ST	M	D	Year	H	Mi	Freq	P	Delay A	CC A	CDT	Delay B	CC B
34	13	2	19	2003	21	25	2.78	5	-52	0.50	45	-52	0.50
34	13	2	19	2003	21	25	2.78	6	-72	0.32	45	-72	0.32
34	13	2	19	2003	21	25	2.78	7	-64	0.51	45	-64	0.51
34	13	2	19	2003	21	25	2.78	8	-33	0.60	45	-63	0.18
34	13	2	19	2003	21	25	2.78	9	-64	0.52	45	-64	0.52
47	13	3	3	2003	2	47	0.56	0	-77	0.44	68	-77	0.44
47	13	3	3	2003	2	47	0.56	1	-40	0.37	68	-68	0.12
47	13	3	3	2003	2	47	0.56	2	-31	0.22	68	-83	0.34
47	13	3	3	2003	2	47	0.56	3	-41	0.49	68	-72	0.43
47	13	3	3	2003	2	47	0.56	4	-60	0.23	68	-88	0.28
47	13	3	3	2003	2	47	0.56	5	-30	0.38	68	-87	0.66
47	13	3	3	2003	2	47	0.56	6	-32	0.45	68	-84	0.47
47	13	3	3	2003	2	47	0.56	7	-71	0.42	68	-71	0.42
47	13	3	3	2003	2	47	0.56	8	-32	0.34	68	-83	0.50
47	13	3	3	2003	2	47	0.56	9	-77	0.36	68	-77	0.36
50	5	3	6	2003	5	48	1.94	0	-49	0.64	47	-49	0.64
50	5	3	6	2003	5	48	1.94	1	-46	0.65	47	-47	0.61
50	5	3	6	2003	5	48	1.94	2	-65	0.43	47	-65	0.43
50	5	3	6	2003	5	48	1.94	3	-47	0.66	47	-47	0.66
50	5	3	6	2003	5	48	1.94	4	-56	0.57	47	-56	0.57
50	5	3	6	2003	5	48	1.94	5	-79	0.29	47	-76	0.29
50	5	3	6	2003	5	48	1.94	6	-65	0.41	47	-65	0.41
50	5	3	6	2003	5	48	1.94	7	-48	0.59	47	-48	0.59
50	5	3	6	2003	5	48	1.94	8	-31	0.29	47	-57	0.26
50	5	3	6	2003	5	48	1.94	9	-48	0.65	47	-48	0.65
52	9	3	8	2003	18	55	1.39	0	-71	0.24	57	-71	0.24
52	9	3	8	2003	18	55	1.39	1	-71	0.30	57	-71	0.30
52	9	3	8	2003	18	55	1.39	2	-53	0.06	57	-87	0.19
52	9	3	8	2003	18	55	1.39	3	-60	0.10	57	-60	0.10
52	9	3	8	2003	18	55	1.39	4	-37	0.19	57	-86	0.27
52	9	3	8	2003	18	55	1.39	5	-32	0.21	57	-69	0.18
52	9	3	8	2003	18	55	1.39	6	-49	0.08	57	-87	0.19
52	9	3	8	2003	18	55	1.39	7	-76	0.11	57	-76	0.11
52	9	3	8	2003	18	55	1.39	8	-66	0.18	57	-86	0.28
52	9	3	8	2003	18	55	1.39	9	-71	0.26	57	-71	0.26
53	9	3	10	2003	19	11	3.33	0	-77	0.52	62	-77	0.52
53	9	3	10	2003	19	11	3.33	1	-78	0.30	62	-78	0.30
53	9	3	10	2003	19	11	3.33	2	-56	0.39	62	-85	0.34
53	9	3	10	2003	19	11	3.33	3	-38	0.19	62	-77	0.16
53	9	3	10	2003	19	11	3.33	4	-51	0.34	62	-89	0.35
53	9	3	10	2003	19	11	3.33	5	-79	0.24	62	-92	0.31
53	9	3	10	2003	19	11	3.33	6	-51	0.41	62	-85	0.40
53	9	3	10	2003	19	11	3.33	7	-36	0.25	62	-76	0.17
53	9	3	10	2003	19	11	3.33	8	-52	0.46	62	-87	0.31
53	9	3	10	2003	19	11	3.33	9	-77	0.52	62	-77	0.52
54	13	3	12	2003	22	1	3.06	0	-73	0.29	54	-73	0.29
54	13	3	12	2003	22	1	3.06	1	-68	0.31	54	-68	0.31
54	13	3	12	2003	22	1	3.06	2	-45	0.23	54	-84	0.06
54	13	3	12	2003	22	1	3.06	3	-45	0.32	54	-80	0.28
54	13	3	12	2003	22	1	3.06	4	-59	0.15	54	-59	0.15
54	13	3	12	2003	22	1	3.06	5	-67	0.27	54	-67	0.27
54	13	3	12	2003	22	1	3.06	6	-64	0.31	54	-64	0.31
54	13	3	12	2003	22	1	3.06	7	-43	0.35	54	-83	0.16
54	13	3	12	2003	22	1	3.06	8	-46	0.38	54	-80	0.21
54	13	3	12	2003	22	1	3.06	9	-70	0.26	54	-70	0.26
55	13	3	12	2003	23	3	0.56	0	-70	0.22	52	-70	0.22

APPENDIX B MAXIMUM CORRELATION COEFFICIENTS OF THE TIME SERIES CORRESPONDING TO SOLAR WIND AND SUPERDARN

#	ST	M	D	Year	H	Mi	Freq	P	Delay A	CC A	CDT	Delay B	CC B
55	13	3	12	2003	23	3	0.56	1	-54	0.22	52	-54	0.22
55	13	3	12	2003	23	3	0.56	2	-76	0.26	52	-76	0.26
55	13	3	12	2003	23	3	0.56	3	-45	0.19	52	-78	0.17
55	13	3	12	2003	23	3	0.56	4	-59	0.17	52	-59	0.17
55	13	3	12	2003	23	3	0.56	5	-40	0.40	52	-67	0.11
55	13	3	12	2003	23	3	0.56	6	-72	0.26	52	-72	0.26
55	13	3	12	2003	23	3	0.56	7	-76	0.31	52	-76	0.31
55	13	3	12	2003	23	3	0.56	8	-43	0.31	52	-77	0.30
55	13	3	12	2003	23	3	0.56	9	-70	0.25	52	-70	0.25
57	14	3	15	2003	11	52	0.83	0	-49	0.45	40	-49	0.45
57	14	3	15	2003	11	52	0.83	1	-77	0.43	40	-40	0.37
57	14	3	15	2003	11	52	0.83	2	-46	0.23	40	-46	0.23
57	14	3	15	2003	11	52	0.83	3	-70	0.40	40	-70	0.40
57	14	3	15	2003	11	52	0.83	4	-49	0.31	40	-49	0.31
57	14	3	15	2003	11	52	0.83	5	-49	0.60	40	-49	0.60
57	14	3	15	2003	11	52	0.83	6	-79	0.55	40	-40	0.32
57	14	3	15	2003	11	52	0.83	7	-80	0.34	40	-56	0.30
57	14	3	15	2003	11	52	0.83	8	-38	0.18	40	-54	0.17
57	14	3	15	2003	11	52	0.83	9	-49	0.39	40	-49	0.39
58	13	3	17	2003	2	55	1.11	0	-71	0.52	35	-60	0.40
58	13	3	17	2003	2	55	1.11	1	-33	0.12	35	-44	0.03
58	13	3	17	2003	2	55	1.11	2	-80	0.55	35	-57	0.39
58	13	3	17	2003	2	55	1.11	3	-53	0.33	35	-53	0.33
58	13	3	17	2003	2	55	1.11	4	-57	0.49	35	-57	0.49
58	13	3	17	2003	2	55	1.11	5	-79	0.47	35	-53	0.23
58	13	3	17	2003	2	55	1.11	6	-33	0.34	35	-35	0.27
58	13	3	17	2003	2	55	1.11	7	-33	0.35	35	-35	0.18
58	13	3	17	2003	2	55	1.11	8	-33	0.16	35	-35	0.10
58	13	3	17	2003	2	55	1.11	9	-71	0.50	35	-60	0.39
61	9	3	29	2003	18	56	0.56	0	-55	0.30	60	-62	0.23
61	9	3	29	2003	18	56	0.56	1	-56	0.26	60	-80	0.20
61	9	3	29	2003	18	56	0.56	2	-48	0.24	60	-69	0.22
61	9	3	29	2003	18	56	0.56	3	-56	0.26	60	-80	0.11
61	9	3	29	2003	18	56	0.56	4	-67	0.26	60	-67	0.26
61	9	3	29	2003	18	56	0.56	5	-51	0.29	60	-72	0.23
61	9	3	29	2003	18	56	0.56	6	-48	0.31	60	-74	0.23
61	9	3	29	2003	18	56	0.56	7	-57	0.30	60	-80	0.21
61	9	3	29	2003	18	56	0.56	8	-48	0.28	60	-74	0.24
61	9	3	29	2003	18	56	0.56	9	-55	0.33	60	-62	0.21
62	8	3	29	2003	19	2	1.39	0	-75	0.46	62	-75	0.46
62	8	3	29	2003	19	2	1.39	1	-72	0.30	62	-72	0.30
62	8	3	29	2003	19	2	1.39	2	-62	0.22	62	-91	0.28
62	8	3	29	2003	19	2	1.39	3	-75	0.37	62	-75	0.37
62	8	3	29	2003	19	2	1.39	4	-58	0.28	62	-92	0.29
62	8	3	29	2003	19	2	1.39	5	-65	0.23	62	-65	0.23
62	8	3	29	2003	19	2	1.39	6	-65	0.29	62	-65	0.29
62	8	3	29	2003	19	2	1.39	7	-75	0.47	62	-75	0.47
62	8	3	29	2003	19	2	1.39	8	-63	0.40	62	-63	0.40
62	8	3	29	2003	19	2	1.39	9	-75	0.47	62	-75	0.47
63	8	3	29	2003	19	3	4.17	0	-78	0.24	62	-78	0.24
63	8	3	29	2003	19	3	4.17	1	-56	0.39	62	-62	0.23
63	8	3	29	2003	19	3	4.17	2	-39	0.14	62	-89	0.07
63	8	3	29	2003	19	3	4.17	3	-60	0.30	62	-62	0.23
63	8	3	29	2003	19	3	4.17	4	-30	0.17	62	-87	0.13
63	8	3	29	2003	19	3	4.17	5	-52	0.30	62	-69	0.26
63	8	3	29	2003	19	3	4.17	6	-38	0.36	62	-88	0.21

APPENDIX B MAXIMUM CORRELATION COEFFICIENTS OF THE TIME SERIES CORRESPONDING TO SOLAR WIND AND SUPERDARN

#	ST	M	D	Year	H	Mi	Freq	P	Delay A	CC A	CDT	Delay B	CC B
63	8	3	29	2003	19	3	4.17	7	-60	0.31	62	-62	0.20
63	8	3	29	2003	19	3	4.17	8	-40	0.21	62	-89	0.28
63	8	3	29	2003	19	3	4.17	9	-78	0.22	62	-78	0.22
66	6	4	1	2003	2	1	3.33	0	-37	0.15	48	-50	-0.05
66	6	4	1	2003	2	1	3.33	1	-56	0.34	48	-56	0.34
66	6	4	1	2003	2	1	3.33	2	-45	0.01	48	-54	-0.03
66	6	4	1	2003	2	1	3.33	3	-45	0.15	48	-66	0.06
66	6	4	1	2003	2	1	3.33	4	-37	0.09	48	-68	0.01
66	6	4	1	2003	2	1	3.33	5	-33	0.37	48	-63	0.27
66	6	4	1	2003	2	1	3.33	6	-45	0.09	48	-75	0.02
66	6	4	1	2003	2	1	3.33	7	-45	0.09	48	-75	-0.05
66	6	4	1	2003	2	1	3.33	8	-80	0.31	48	-55	0.20
66	6	4	1	2003	2	1	3.33	9	-40	0.21	48	-55	-0.03
68	6	4	8	2003	9	22	1.11	0	-53	0.33	57	-87	0.21
68	6	4	8	2003	9	22	1.11	1	-56	0.45	57	-57	0.44
68	6	4	8	2003	9	22	1.11	2	-30	0.23	57	-85	0.12
68	6	4	8	2003	9	22	1.11	3	-59	0.47	57	-59	0.47
68	6	4	8	2003	9	22	1.11	4	-74	0.26	57	-74	0.26
68	6	4	8	2003	9	22	1.11	5	-78	0.49	57	-78	0.49
68	6	4	8	2003	9	22	1.11	6	-39	0.36	57	-70	0.11
68	6	4	8	2003	9	22	1.11	7	-61	0.36	57	-87	0.53
68	6	4	8	2003	9	22	1.11	8	-77	0.16	57	-77	0.16
68	6	4	8	2003	9	22	1.11	9	-53	0.34	57	-87	0.19
77	8	4	26	2003	23	15	1.39	0	-64	0.27	58	-64	0.27
77	8	4	26	2003	23	15	1.39	1	-62	0.36	58	-62	0.36
77	8	4	26	2003	23	15	1.39	2	-68	0.22	58	-68	0.22
77	8	4	26	2003	23	15	1.39	3	-76	0.23	58	-86	0.23
77	8	4	26	2003	23	15	1.39	4	-54	0.48	58	-68	0.21
77	8	4	26	2003	23	15	1.39	5	-30	0.21	58	-83	0.27
77	8	4	26	2003	23	15	1.39	6	-68	0.23	58	-68	0.23
77	8	4	26	2003	23	15	1.39	7	-76	0.29	58	-76	0.29
77	8	4	26	2003	23	15	1.39	8	-54	0.45	58	-58	0.21
77	8	4	26	2003	23	15	1.39	9	-64	0.33	58	-64	0.33
82	13	5	6	2003	7	45	2.22	0	-69	0.27	37	-47	0.26
82	13	5	6	2003	7	45	2.22	1	-74	0.30	37	-53	0.26
82	13	5	6	2003	7	45	2.22	2	-64	0.27	37	-64	0.27
82	13	5	6	2003	7	45	2.22	3	-64	0.51	37	-64	0.51
82	13	5	6	2003	7	45	2.22	4	-45	0.34	37	-45	0.34
82	13	5	6	2003	7	45	2.22	5	-77	0.25	37	-64	0.12
82	13	5	6	2003	7	45	2.22	6	-53	0.30	37	-53	0.30
82	13	5	6	2003	7	45	2.22	7	-53	0.34	37	-53	0.34
82	13	5	6	2003	7	45	2.22	8	-37	0.23	37	-37	0.23
82	13	5	6	2003	7	45	2.22	9	-53	0.36	37	-53	0.36
83	13	5	6	2003	7	49	3.33	0	-47	0.17	37	-47	0.17
83	13	5	6	2003	7	49	3.33	1	-74	0.26	37	-53	0.20
83	13	5	6	2003	7	49	3.33	2	-64	0.27	37	-64	0.27
83	13	5	6	2003	7	49	3.33	3	-56	0.39	37	-56	0.39
83	13	5	6	2003	7	49	3.33	4	-45	0.30	37	-45	0.30
83	13	5	6	2003	7	49	3.33	5	-35	0.18	37	-37	0.17
83	13	5	6	2003	7	49	3.33	6	-53	0.40	37	-53	0.40
83	13	5	6	2003	7	49	3.33	7	-53	0.31	37	-53	0.31
83	13	5	6	2003	7	49	3.33	8	-37	0.29	37	-37	0.29
83	13	5	6	2003	7	49	3.33	9	-73	0.17	37	-47	0.15
85	13	5	6	2003	7	52	2.50	0	-47	0.19	37	-47	0.19
85	13	5	6	2003	7	52	2.50	1	-73	0.30	37	-53	0.25
85	13	5	6	2003	7	52	2.50	2	-64	0.24	37	-64	0.24

APPENDIX B MAXIMUM CORRELATION COEFFICIENTS OF THE TIME SERIES CORRESPONDING TO SOLAR WIND AND SUPERDARN

#	ST	M	D	Year	H	Mi	Freq	P	Delay A	CC A	CDT	Delay B	CC B
85	13	5	6	2003	7	52	2.50	3	-64	0.37	37	-64	0.37
85	13	5	6	2003	7	52	2.50	4	-45	0.29	37	-45	0.29
85	13	5	6	2003	7	52	2.50	5	-35	0.15	37	-38	0.15
85	13	5	6	2003	7	52	2.50	6	-53	0.30	37	-53	0.30
85	13	5	6	2003	7	52	2.50	7	-53	0.37	37	-53	0.37
85	13	5	6	2003	7	52	2.50	8	-37	0.21	37	-37	0.21
85	13	5	6	2003	7	52	2.50	9	-73	0.28	37	-47	0.21
86	13	5	6	2003	7	54	4.44	0	-47	0.20	37	-47	0.20
86	13	5	6	2003	7	54	4.44	1	-74	0.27	37	-53	0.23
86	13	5	6	2003	7	54	4.44	2	-56	0.31	37	-56	0.31
86	13	5	6	2003	7	54	4.44	3	-56	0.41	37	-56	0.41
86	13	5	6	2003	7	54	4.44	4	-45	0.29	37	-45	0.29
86	13	5	6	2003	7	54	4.44	5	-35	0.17	37	-38	0.14
86	13	5	6	2003	7	54	4.44	6	-53	0.40	37	-53	0.40
86	13	5	6	2003	7	54	4.44	7	-53	0.33	37	-53	0.33
86	13	5	6	2003	7	54	4.44	8	-37	0.20	37	-37	0.20
86	13	5	6	2003	7	54	4.44	9	-74	0.28	37	-47	0.19
101	7	5	31	2003	12	49	0.83	0	-70	0.18	36	-43	0.14
101	7	5	31	2003	12	49	0.83	1	-64	0.24	36	-64	0.24
101	7	5	31	2003	12	49	0.83	2	-70	0.32	36	-56	0.10
101	7	5	31	2003	12	49	0.83	3	-70	0.41	36	-53	0.07
101	7	5	31	2003	12	49	0.83	4	-79	0.20	36	-56	0.08
101	7	5	31	2003	12	49	0.83	5	-57	0.60	36	-57	0.60
101	7	5	31	2003	12	49	0.83	6	-65	0.29	36	-65	0.29
101	7	5	31	2003	12	49	0.83	7	-78	0.41	36	-59	0.34
101	7	5	31	2003	12	49	0.83	8	-45	0.19	36	-45	0.19
101	7	5	31	2003	12	49	0.83	9	-44	0.21	36	-44	0.21
105	9	6	3	2003	2	44	1.11	0	-73	0.23	31	-42	0.21
105	9	6	3	2003	2	44	1.11	1	-38	0.12	31	-38	0.12
105	9	6	3	2003	2	44	1.11	2	-65	0.33	31	-48	0.18
105	9	6	3	2003	2	44	1.11	3	-30	0.45	31	-31	0.22
105	9	6	3	2003	2	44	1.11	4	-50	0.32	31	-50	0.32
105	9	6	3	2003	2	44	1.11	5	-30	0.24	31	-31	0.17
105	9	6	3	2003	2	44	1.11	6	-58	0.11	31	-58	0.11
105	9	6	3	2003	2	44	1.11	7	-33	0.27	31	-33	0.27
105	9	6	3	2003	2	44	1.11	8	-80	0.17	31	-56	0.16
105	9	6	3	2003	2	44	1.11	9	-73	0.21	31	-42	0.19
106	6	6	8	2003	5	18	0.83	0	-72	0.15	32	-62	0.10
106	6	6	8	2003	5	18	0.83	1	-65	0.35	32	-62	0.25
106	6	6	8	2003	5	18	0.83	2	-54	0.40	32	-54	0.40
106	6	6	8	2003	5	18	0.83	3	-78	0.32	32	-35	0.22
106	6	6	8	2003	5	18	0.83	4	-66	0.37	32	-62	0.11
106	6	6	8	2003	5	18	0.83	5	-45	0.37	32	-45	0.37
106	6	6	8	2003	5	18	0.83	6	-64	0.33	32	-62	0.31
106	6	6	8	2003	5	18	0.83	7	-66	0.55	32	-47	0.32
106	6	6	8	2003	5	18	0.83	8	-78	0.32	32	-53	0.19
106	6	6	8	2003	5	18	0.83	9	-63	0.20	32	-62	0.19
107	8	6	8	2003	22	43	0.83	0	-77	0.40	34	-43	0.34
107	8	6	8	2003	22	43	0.83	1	-67	0.39	34	-43	0.34
107	8	6	8	2003	22	43	0.83	2	-75	0.44	34	-57	0.29
107	8	6	8	2003	22	43	0.83	3	-34	0.46	34	-34	0.46
107	8	6	8	2003	22	43	0.83	4	-30	0.34	34	-34	0.24
107	8	6	8	2003	22	43	0.83	5	-43	0.28	34	-43	0.28
107	8	6	8	2003	22	43	0.83	6	-66	0.46	34	-42	0.38
107	8	6	8	2003	22	43	0.83	7	-74	0.58	34	-41	0.24
107	8	6	8	2003	22	43	0.83	8	-55	0.44	34	-55	0.44

APPENDIX B MAXIMUM CORRELATION COEFFICIENTS OF THE TIME SERIES CORRESPONDING TO SOLAR WIND AND SUPERDARN

#	ST	M	D	Year	H	Mi	Freq	P	Delay A	CC A	CDT	Delay B	CC B
107	8	6	8	2003	22	43	0.83	9	-43	0.44	34	-43	0.44
108	8	6	8	2003	23	42	0.56	0	-66	0.16	36	-66	0.16
108	8	6	8	2003	23	42	0.56	1	-63	0.38	36	-63	0.38
108	8	6	8	2003	23	42	0.56	2	-76	0.57	36	-48	0.36
108	8	6	8	2003	23	42	0.56	3	-59	0.21	36	-59	0.21
108	8	6	8	2003	23	42	0.56	4	-74	0.40	36	-50	0.31
108	8	6	8	2003	23	42	0.56	5	-50	0.30	36	-50	0.30
108	8	6	8	2003	23	42	0.56	6	-36	0.18	36	-36	0.18
108	8	6	8	2003	23	42	0.56	7	-38	0.16	36	-38	0.16
108	8	6	8	2003	23	42	0.56	8	-60	0.48	36	-60	0.48
108	8	6	8	2003	23	42	0.56	9	-66	0.20	36	-66	0.20
109	8	6	15	2003	2	49	0.56	0	-34	0.36	45	-49	0.26
109	8	6	15	2003	2	49	0.56	1	-76	0.54	45	-75	0.53
109	8	6	15	2003	2	49	0.56	2	-61	0.55	45	-61	0.55
109	8	6	15	2003	2	49	0.56	3	-37	0.35	45	-75	0.27
109	8	6	15	2003	2	49	0.56	4	-79	0.24	45	-49	0.11
109	8	6	15	2003	2	49	0.56	5	-71	0.60	45	-71	0.60
109	8	6	15	2003	2	49	0.56	6	-61	0.62	45	-61	0.62
109	8	6	15	2003	2	49	0.56	7	-37	0.35	45	-75	0.18
109	8	6	15	2003	2	49	0.56	8	-39	0.21	45	-68	0.16
109	8	6	15	2003	2	49	0.56	9	-34	0.34	45	-46	0.34
110	5	6	15	2003	9	12	1.39	0	-77	0.42	47	-77	0.42
110	5	6	15	2003	9	12	1.39	1	-59	0.28	47	-59	0.28
110	5	6	15	2003	9	12	1.39	2	-48	0.33	47	-48	0.33
110	5	6	15	2003	9	12	1.39	3	-58	0.25	47	-58	0.25
110	5	6	15	2003	9	12	1.39	4	-60	0.33	47	-60	0.33
110	5	6	15	2003	9	12	1.39	5	-43	0.26	47	-55	0.18
110	5	6	15	2003	9	12	1.39	6	-48	0.27	47	-48	0.27
110	5	6	15	2003	9	12	1.39	7	-54	0.24	47	-54	0.24
110	5	6	15	2003	9	12	1.39	8	-60	0.20	47	-60	0.20
110	5	6	15	2003	9	12	1.39	9	-77	0.39	47	-77	0.39
112	13	6	16	2003	0	0	0.56	0	-36	0.36	41	-41	0.27
112	13	6	16	2003	0	0	0.56	1	-75	0.19	41	-54	0.19
112	13	6	16	2003	0	0	0.56	2	-39	0.09	41	-69	0.04
112	13	6	16	2003	0	0	0.56	3	-73	0.29	41	-69	0.25
112	13	6	16	2003	0	0	0.56	4	-73	0.31	41	-45	0.24
112	13	6	16	2003	0	0	0.56	5	-58	0.36	41	-58	0.36
112	13	6	16	2003	0	0	0.56	6	-54	0.60	41	-54	0.60
112	13	6	16	2003	0	0	0.56	7	-73	0.23	41	-68	0.18
112	13	6	16	2003	0	0	0.56	8	-73	0.24	41	-71	0.18
112	13	6	16	2003	0	0	0.56	9	-36	0.34	41	-43	0.27
118	8	7	1	2003	4	43	1.11	0	-46	0.42	37	-46	0.42
118	8	7	1	2003	4	43	1.11	1	-33	0.39	37	-65	0.35
118	8	7	1	2003	4	43	1.11	2	-41	0.44	37	-41	0.44
118	8	7	1	2003	4	43	1.11	3	-52	0.47	37	-52	0.47
118	8	7	1	2003	4	43	1.11	4	-52	0.58	37	-52	0.58
118	8	7	1	2003	4	43	1.11	5	-66	0.38	37	-66	0.38
118	8	7	1	2003	4	43	1.11	6	-33	0.37	37	-65	0.32
118	8	7	1	2003	4	43	1.11	7	-68	0.38	37	-67	0.26
118	8	7	1	2003	4	43	1.11	8	-62	0.33	37	-62	0.33
118	8	7	1	2003	4	43	1.11	9	-46	0.31	37	-46	0.31
121	6	7	9	2003	9	43	3.61	0	-33	0.28	60	-84	0.21
121	6	7	9	2003	9	43	3.61	1	-57	0.26	60	-60	0.21
121	6	7	9	2003	9	43	3.61	2	-42	0.07	60	-83	0.07
121	6	7	9	2003	9	43	3.61	3	-67	0.27	60	-67	0.27
121	6	7	9	2003	9	43	3.61	4	-30	0.21	60	-76	0.04

APPENDIX B MAXIMUM CORRELATION COEFFICIENTS OF THE TIME SERIES CORRESPONDING TO SOLAR WIND AND SUPERDARN

#	ST	M	D	Year	H	Mi	Freq	P	Delay A	CC A	CDT	Delay B	CC B
121	6	7	9	2003	9	43	3.61	5	-67	0.21	60	-67	0.21
121	6	7	9	2003	9	43	3.61	6	-36	0.22	60	-60	0.19
121	6	7	9	2003	9	43	3.61	7	-33	0.37	60	-75	0.24
121	6	7	9	2003	9	43	3.61	8	-59	0.25	60	-68	0.21
121	6	7	9	2003	9	43	3.61	9	-33	0.29	60	-84	0.17
122	13	7	26	2003	3	20	4.17	1	-67	0.47	75	-92	0.28
122	13	7	26	2003	3	20	4.17	2	-62	0.45	75	-79	0.41
122	13	7	26	2003	3	20	4.17	3	-67	0.17	75	-90	0.21
122	13	7	26	2003	3	20	4.17	4	-32	0.45	75	-90	0.19
122	13	7	26	2003	3	20	4.17	5	-46	0.40	75	-86	0.09
122	13	7	26	2003	3	20	4.17	6	-79	0.48	75	-79	0.48
122	13	7	26	2003	3	20	4.17	7	-66	0.30	75	-90	0.27
122	13	7	26	2003	3	20	4.17	8	-36	0.42	75	-90	0.30
123	8	7	26	2003	21	8	0.56	0	-42	0.28	50	-65	0.25
123	8	7	26	2003	21	8	0.56	1	-32	0.45	50	-59	0.26
123	8	7	26	2003	21	8	0.56	2	-37	0.16	50	-70	0.03
123	8	7	26	2003	21	8	0.56	3	-66	0.37	50	-66	0.37
123	8	7	26	2003	21	8	0.56	4	-53	0.36	50	-53	0.36
123	8	7	26	2003	21	8	0.56	5	-48	0.05	50	-77	0.02
123	8	7	26	2003	21	8	0.56	6	-55	0.46	50	-55	0.46
123	8	7	26	2003	21	8	0.56	7	-80	0.21	50	-80	0.21
123	8	7	26	2003	21	8	0.56	8	-63	0.32	50	-63	0.32
123	8	7	26	2003	21	8	0.56	9	-65	0.24	50	-65	0.24
126	6	7	31	2003	5	48	1.67	0	-33	0.32	31	-33	0.32
126	6	7	31	2003	5	48	1.67	1	-47	0.27	31	-47	0.27
126	6	7	31	2003	5	48	1.67	2	-65	0.40	31	-53	0.25
126	6	7	31	2003	5	48	1.67	3	-53	0.35	31	-53	0.35
126	6	7	31	2003	5	48	1.67	4	-56	0.32	31	-56	0.32
126	6	7	31	2003	5	48	1.67	5	-52	0.31	31	-52	0.31
126	6	7	31	2003	5	48	1.67	6	-42	0.22	31	-42	0.22
126	6	7	31	2003	5	48	1.67	7	-73	0.35	31	-33	0.24
126	6	7	31	2003	5	48	1.67	8	-79	0.36	31	-42	0.16
126	6	7	31	2003	5	48	1.67	9	-41	0.33	31	-41	0.33
130	6	8	8	2003	7	44	0.83	0	-39	0.30	38	-39	0.30
130	6	8	8	2003	7	44	0.83	1	-51	0.39	38	-51	0.39
130	6	8	8	2003	7	44	0.83	2	-60	0.34	38	-60	0.34
130	6	8	8	2003	7	44	0.83	3	-48	0.28	38	-48	0.28
130	6	8	8	2003	7	44	0.83	4	-58	0.37	38	-58	0.37
130	6	8	8	2003	7	44	0.83	5	-66	0.26	38	-66	0.26
130	6	8	8	2003	7	44	0.83	6	-60	0.40	38	-60	0.40
130	6	8	8	2003	7	44	0.83	7	-79	0.31	38	-40	0.29
130	6	8	8	2003	7	44	0.83	8	-56	0.37	38	-56	0.37
130	6	8	8	2003	7	44	0.83	9	-39	0.32	38	-39	0.32
133	8	8	8	2003	23	49	0.83	0	-43	0.35	34	-43	0.35
133	8	8	8	2003	23	49	0.83	1	-79	0.45	34	-50	0.28
133	8	8	8	2003	23	49	0.83	2	-71	0.52	34	-54	0.13
133	8	8	8	2003	23	49	0.83	3	-70	0.45	34	-45	0.25
133	8	8	8	2003	23	49	0.83	4	-30	0.39	34	-45	0.25
133	8	8	8	2003	23	49	0.83	5	-67	0.22	34	-40	0.18
133	8	8	8	2003	23	49	0.83	6	-67	0.33	34	-64	0.14
133	8	8	8	2003	23	49	0.83	7	-71	0.31	34	-55	0.22
133	8	8	8	2003	23	49	0.83	8	-30	0.43	34	-44	0.31
133	8	8	8	2003	23	49	0.83	9	-43	0.34	34	-43	0.34
136	8	8	22	2003	2	27	0.83	0	-33	0.34	32	-33	0.34
136	8	8	22	2003	2	27	0.83	1	-55	0.38	32	-55	0.38
136	8	8	22	2003	2	27	0.83	2	-46	0.20	32	-46	0.20

APPENDIX B MAXIMUM CORRELATION COEFFICIENTS OF THE TIME SERIES CORRESPONDING TO SOLAR WIND AND SUPERDARN

#	ST	M	D	Year	H	Mi	Freq	P	Delay A	CC A	CDT	Delay B	CC B
136	8	8	22	2003	2	27	0.83	3	-65	0.30	32	-41	0.26
136	8	8	22	2003	2	27	0.83	4	-79	0.20	32	-34	0.10
136	8	8	22	2003	2	27	0.83	5	-51	0.18	32	-51	0.18
136	8	8	22	2003	2	27	0.83	6	-55	0.34	32	-55	0.34
136	8	8	22	2003	2	27	0.83	7	-54	0.33	32	-54	0.33
136	8	8	22	2003	2	27	0.83	8	-66	0.25	32	-47	0.23
136	8	8	22	2003	2	27	0.83	9	-33	0.36	32	-33	0.36
145	13	9	16	2003	20	30	0.56	0	-73	0.65	54	-73	0.65
145	13	9	16	2003	20	30	0.56	1	-43	0.32	54	-81	0.26
145	13	9	16	2003	20	30	0.56	2	-61	0.29	54	-61	0.29
145	13	9	16	2003	20	30	0.56	3	-77	0.37	54	-77	0.37
145	13	9	16	2003	20	30	0.56	4	-31	0.47	54	-75	0.41
145	13	9	16	2003	20	30	0.56	5	-57	0.42	54	-57	0.42
145	13	9	16	2003	20	30	0.56	6	-56	0.39	54	-56	0.39
145	13	9	16	2003	20	30	0.56	7	-61	0.28	54	-61	0.28
145	13	9	16	2003	20	30	0.56	8	-55	0.48	54	-55	0.48
145	13	9	16	2003	20	30	0.56	9	-73	0.68	54	-73	0.68
146	14	9	21	2003	10	49	1.39	0	-74	0.40	42	-70	0.33
146	14	9	21	2003	10	49	1.39	1	-61	0.34	42	-61	0.34
146	14	9	21	2003	10	49	1.39	2	-46	0.35	42	-46	0.35
146	14	9	21	2003	10	49	1.39	3	-48	0.31	42	-48	0.31
146	14	9	21	2003	10	49	1.39	4	-50	0.26	42	-50	0.26
146	14	9	21	2003	10	49	1.39	5	-75	0.27	42	-72	0.19
146	14	9	21	2003	10	49	1.39	6	-61	0.17	42	-61	0.17
146	14	9	21	2003	10	49	1.39	7	-37	0.47	42	-44	0.28
146	14	9	21	2003	10	49	1.39	8	-76	0.10	42	-55	0.05
146	14	9	21	2003	10	49	1.39	9	-74	0.35	42	-70	0.24
151	13	9	29	2003	22	5	0.56	1	-80	0.13	85	-85	0.16
151	13	9	29	2003	22	5	0.56	2	-70	0.28	85	-113	0.11
151	13	9	29	2003	22	5	0.56	3	-43	0.34	85	-99	0.24
151	13	9	29	2003	22	5	0.56	4	-44	0.36	85	-107	0.16
151	13	9	29	2003	22	5	0.56	5	-37	0.18	85	-96	0.10
151	13	9	29	2003	22	5	0.56	6	-68	0.28	85	-113	0.18
151	13	9	29	2003	22	5	0.56	7	-63	0.22	85	-99	0.23
151	13	9	29	2003	22	5	0.56	8	-43	0.21	85	-104	0.29
152	13	9	29	2003	23	5	0.56	1	-75	0.20	84	-84	0.25
152	13	9	29	2003	23	5	0.56	2	-70	0.39	84	-99	0.21
152	13	9	29	2003	23	5	0.56	3	-36	0.30	84	-98	0.36
152	13	9	29	2003	23	5	0.56	4	-36	0.35	84	-96	0.20
152	13	9	29	2003	23	5	0.56	5	-30	0.20	84	-96	0.10
152	13	9	29	2003	23	5	0.56	6	-66	0.34	84	-98	0.19
152	13	9	29	2003	23	5	0.56	7	-66	0.46	84	-98	0.31
152	13	9	29	2003	23	5	0.56	8	-37	0.30	84	-98	0.38
154	7	10	8	2003	12	9	1.67	0	-30	0.29	43	-61	0.26
154	7	10	8	2003	12	9	1.67	1	-79	0.34	43	-59	0.28
154	7	10	8	2003	12	9	1.67	2	-52	0.42	43	-52	0.42
154	7	10	8	2003	12	9	1.67	3	-30	0.34	43	-71	0.31
154	7	10	8	2003	12	9	1.67	4	-61	0.35	43	-61	0.35
154	7	10	8	2003	12	9	1.67	5	-72	0.44	43	-72	0.44
154	7	10	8	2003	12	9	1.67	6	-52	0.42	43	-52	0.42
154	7	10	8	2003	12	9	1.67	7	-30	0.39	43	-52	0.37
154	7	10	8	2003	12	9	1.67	8	-31	0.28	43	-61	0.24
154	7	10	8	2003	12	9	1.67	9	-61	0.33	43	-61	0.33
161	5	10	13	2003	23	41	1.39	0	-42	0.36	51	-79	0.27
161	5	10	13	2003	23	41	1.39	1	-80	0.30	51	-80	0.30
161	5	10	13	2003	23	41	1.39	2	-32	0.17	51	-54	0.10

APPENDIX B MAXIMUM CORRELATION COEFFICIENTS OF THE TIME SERIES CORRESPONDING TO SOLAR WIND AND SUPERDARN

#	ST	M	D	Year	H	Mi	Freq	P	Delay A	CC A	CDT	Delay B	CC B
161	5	10	13	2003	23	41	1.39	3	-39	0.28	51	-71	0.20
161	5	10	13	2003	23	41	1.39	4	-52	0.25	51	-52	0.25
161	5	10	13	2003	23	41	1.39	5	-36	0.28	51	-73	0.17
161	5	10	13	2003	23	41	1.39	6	-80	0.20	51	-80	0.20
161	5	10	13	2003	23	41	1.39	7	-30	0.22	51	-52	0.21
161	5	10	13	2003	23	41	1.39	8	-78	0.21	51	-78	0.21
161	5	10	13	2003	23	41	1.39	9	-42	0.35	51	-79	0.31
162	5	10	13	2003	23	43	2.22	0	-42	0.37	51	-79	0.25
162	5	10	13	2003	23	43	2.22	1	-80	0.25	51	-80	0.25
162	5	10	13	2003	23	43	2.22	2	-54	0.27	51	-54	0.27
162	5	10	13	2003	23	43	2.22	3	-39	0.29	51	-51	0.16
162	5	10	13	2003	23	43	2.22	4	-50	0.19	51	-51	0.19
162	5	10	13	2003	23	43	2.22	5	-34	0.23	51	-58	0.14
162	5	10	13	2003	23	43	2.22	6	-31	0.11	51	-80	0.10
162	5	10	13	2003	23	43	2.22	7	-52	0.20	51	-52	0.20
162	5	10	13	2003	23	43	2.22	8	-71	0.20	51	-71	0.20
162	5	10	13	2003	23	43	2.22	9	-30	0.36	51	-79	0.26
163	7	10	13	2003	10	9	1.11	1	-58	0.27	73	-87	0.07
163	7	10	13	2003	10	9	1.11	2	-65	0.18	73	-73	0.09
163	7	10	13	2003	10	9	1.11	3	-33	0.23	73	-74	0.16
163	7	10	13	2003	10	9	1.11	4	-61	0.36	73	-75	0.16
163	7	10	13	2003	10	9	1.11	5	-31	0.18	73	-73	0.16
163	7	10	13	2003	10	9	1.11	6	-44	0.24	73	-86	0.15
163	7	10	13	2003	10	9	1.11	7	-43	0.12	73	-86	0.14
163	7	10	13	2003	10	9	1.11	8	-38	0.27	73	-98	0.21
164	5	10	14	2003	11	45	1.39	0	-57	0.37	53	-57	0.37
164	5	10	14	2003	11	45	1.39	1	-54	0.38	53	-54	0.38
164	5	10	14	2003	11	45	1.39	2	-36	0.31	53	-82	0.37
164	5	10	14	2003	11	45	1.39	3	-56	0.24	53	-56	0.24
164	5	10	14	2003	11	45	1.39	4	-56	0.29	53	-56	0.29
164	5	10	14	2003	11	45	1.39	5	-76	0.30	53	-76	0.30
164	5	10	14	2003	11	45	1.39	6	-44	0.36	53	-54	0.31
164	5	10	14	2003	11	45	1.39	7	-38	0.25	53	-80	0.24
164	5	10	14	2003	11	45	1.39	8	-38	0.30	53	-83	0.24
164	5	10	14	2003	11	45	1.39	9	-56	0.37	53	-56	0.37
165	5	10	14	2003	12	6	2.22	0	-56	0.30	53	-56	0.30
165	5	10	14	2003	12	6	2.22	1	-56	0.43	53	-56	0.43
165	5	10	14	2003	12	6	2.22	2	-36	0.39	53	-62	0.17
165	5	10	14	2003	12	6	2.22	3	-57	0.25	53	-57	0.25
165	5	10	14	2003	12	6	2.22	4	-57	0.27	53	-57	0.27
165	5	10	14	2003	12	6	2.22	5	-76	0.29	53	-76	0.29
165	5	10	14	2003	12	6	2.22	6	-56	0.46	53	-56	0.46
165	5	10	14	2003	12	6	2.22	7	-36	0.28	53	-78	0.12
165	5	10	14	2003	12	6	2.22	8	-40	0.35	53	-81	0.07
165	5	10	14	2003	12	6	2.22	9	-56	0.40	53	-56	0.40
166	5	10	16	2003	23	57	1.94	0	-52	0.26	42	-52	0.26
166	5	10	16	2003	23	57	1.94	1	-47	0.28	42	-47	0.28
166	5	10	16	2003	23	57	1.94	2	-35	0.29	42	-62	0.03
166	5	10	16	2003	23	57	1.94	3	-57	0.20	42	-57	0.20
166	5	10	16	2003	23	57	1.94	4	-45	0.17	42	-45	0.17
166	5	10	16	2003	23	57	1.94	5	-46	0.08	42	-46	0.08
166	5	10	16	2003	23	57	1.94	6	-47	0.28	42	-47	0.28
166	5	10	16	2003	23	57	1.94	7	-74	0.26	42	-69	0.17
166	5	10	16	2003	23	57	1.94	8	-78	0.36	42	-72	0.28
166	5	10	16	2003	23	57	1.94	9	-52	0.27	42	-52	0.27
167	5	10	16	2003	23	56	2.22	0	-30	0.22	42	-53	0.11

APPENDIX B MAXIMUM CORRELATION COEFFICIENTS OF THE TIME SERIES CORRESPONDING TO SOLAR WIND AND SUPERDARN

#	ST	M	D	Year	H	Mi	Freq	P	Delay A	CC A	CDT	Delay B	CC B
167	5	10	16	2003	23	56	2.22	1	-52	0.21	42	-52	0.21
167	5	10	16	2003	23	56	2.22	2	-47	0.32	42	-47	0.32
167	5	10	16	2003	23	56	2.22	3	-72	0.18	42	-72	0.18
167	5	10	16	2003	23	56	2.22	4	-30	0.49	42	-72	0.27
167	5	10	16	2003	23	56	2.22	5	-30	0.30	42	-43	0.06
167	5	10	16	2003	23	56	2.22	6	-52	0.19	42	-52	0.19
167	5	10	16	2003	23	56	2.22	7	-30	0.19	42	-52	0.05
167	5	10	16	2003	23	56	2.22	8	-76	0.18	42	-62	0.06
167	5	10	16	2003	23	56	2.22	9	-53	0.18	42	-53	0.18
174	7	10	27	2003	7	4	3.61	0	-43	0.42	53	-82	0.22
174	7	10	27	2003	7	4	3.61	1	-35	0.22	53	-70	0.20
174	7	10	27	2003	7	4	3.61	2	-50	0.24	53	-54	0.22
174	7	10	27	2003	7	4	3.61	3	-53	0.43	53	-53	0.43
174	7	10	27	2003	7	4	3.61	4	-69	0.31	53	-69	0.31
174	7	10	27	2003	7	4	3.61	5	-71	0.22	53	-71	0.22
174	7	10	27	2003	7	4	3.61	6	-73	0.32	53	-73	0.32
174	7	10	27	2003	7	4	3.61	7	-54	0.43	53	-54	0.43
174	7	10	27	2003	7	4	3.61	8	-46	0.21	53	-73	0.18
174	7	10	27	2003	7	4	3.61	9	-43	0.41	53	-82	0.23
176	6	11	7	2003	2	5	0.83	0	-32	0.32	44	-47	0.12
176	6	11	7	2003	2	5	0.83	1	-53	0.27	44	-53	0.27
176	6	11	7	2003	2	5	0.83	2	-64	0.40	44	-64	0.40
176	6	11	7	2003	2	5	0.83	3	-33	0.29	44	-53	0.12
176	6	11	7	2003	2	5	0.83	4	-77	0.39	44	-73	0.16
176	6	11	7	2003	2	5	0.83	5	-77	0.33	44	-73	0.25
176	6	11	7	2003	2	5	0.83	6	-64	0.28	44	-64	0.28
176	6	11	7	2003	2	5	0.83	7	-67	0.43	44	-67	0.43
176	6	11	7	2003	2	5	0.83	8	-77	0.29	44	-74	0.17
176	6	11	7	2003	2	5	0.83	9	-32	0.30	44	-47	0.16
177	6	11	7	2003	2	6	1.11	0	-35	0.29	44	-74	0.20
177	6	11	7	2003	2	6	1.11	1	-30	0.14	44	-44	0.09
177	6	11	7	2003	2	6	1.11	2	-67	0.51	44	-67	0.51
177	6	11	7	2003	2	6	1.11	3	-72	0.34	44	-72	0.34
177	6	11	7	2003	2	6	1.11	4	-79	0.42	44	-72	0.29
177	6	11	7	2003	2	6	1.11	5	-69	0.40	44	-69	0.40
177	6	11	7	2003	2	6	1.11	6	-68	0.41	44	-68	0.41
177	6	11	7	2003	2	6	1.11	7	-67	0.44	44	-67	0.44
177	6	11	7	2003	2	6	1.11	8	-76	0.34	44	-74	0.20
177	6	11	7	2003	2	6	1.11	9	-35	0.20	44	-74	0.14
178	6	11	7	2003	4	17	2.78	0	-70	0.52	44	-70	0.52
178	6	11	7	2003	4	17	2.78	1	-41	0.31	44	-68	0.28
178	6	11	7	2003	4	17	2.78	2	-63	0.41	44	-63	0.41
178	6	11	7	2003	4	17	2.78	3	-72	0.34	44	-72	0.34
178	6	11	7	2003	4	17	2.78	4	-35	0.23	44	-72	0.22
178	6	11	7	2003	4	17	2.78	5	-55	0.30	44	-55	0.30
178	6	11	7	2003	4	17	2.78	6	-64	0.27	44	-64	0.27
178	6	11	7	2003	4	17	2.78	7	-32	0.32	44	-45	0.24
178	6	11	7	2003	4	17	2.78	8	-71	0.32	44	-71	0.32
178	6	11	7	2003	4	17	2.78	9	-70	0.52	44	-70	0.52
179	10	11	7	2003	5	40	4.44	0	-58	0.21	45	-58	0.21
179	10	11	7	2003	5	40	4.44	1	-48	0.44	45	-48	0.44
179	10	11	7	2003	5	40	4.44	2	-58	0.36	45	-58	0.36
179	10	11	7	2003	5	40	4.44	3	-59	0.34	45	-59	0.34
179	10	11	7	2003	5	40	4.44	4	-39	0.22	45	-52	0.22
179	10	11	7	2003	5	40	4.44	5	-64	0.30	45	-64	0.30
179	10	11	7	2003	5	40	4.44	6	-79	0.25	45	-61	0.24

APPENDIX B MAXIMUM CORRELATION COEFFICIENTS OF THE TIME SERIES CORRESPONDING TO SOLAR WIND AND SUPERDARN

#	ST	M	D	Year	H	Mi	Freq	P	Delay A	CC A	CDT	Delay B	CC B
179	10	11	7	2003	5	40	4.44	7	-38	0.30	45	-60	0.28
179	10	11	7	2003	5	40	4.44	8	-48	0.23	45	-48	0.23
179	10	11	7	2003	5	40	4.44	9	-45	0.22	45	-45	0.22
180	13	11	7	2003	21	6	1.67	0	-52	0.37	56	-56	0.12
180	13	11	7	2003	21	6	1.67	1	-57	0.26	56	-57	0.26
180	13	11	7	2003	21	6	1.67	2	-52	0.15	56	-83	0.09
180	13	11	7	2003	21	6	1.67	3	-44	0.16	56	-86	0.14
180	13	11	7	2003	21	6	1.67	4	-64	0.32	56	-64	0.32
180	13	11	7	2003	21	6	1.67	5	-68	0.34	56	-68	0.34
180	13	11	7	2003	21	6	1.67	6	-38	0.18	56	-83	0.13
180	13	11	7	2003	21	6	1.67	7	-54	0.33	56	-83	0.22
180	13	11	7	2003	21	6	1.67	8	-53	0.20	56	-74	0.15
180	13	11	7	2003	21	6	1.67	9	-53	0.35	56	-56	0.18
181	13	11	8	2003	20	18	0.56	0	-75	0.37	56	-75	0.37
181	13	11	8	2003	20	18	0.56	1	-64	0.56	56	-64	0.56
181	13	11	8	2003	20	18	0.56	2	-74	0.21	56	-74	0.21
181	13	11	8	2003	20	18	0.56	3	-39	0.36	56	-56	0.09
181	13	11	8	2003	20	18	0.56	4	-48	0.35	56	-82	0.28
181	13	11	8	2003	20	18	0.56	5	-40	0.39	56	-65	0.28
181	13	11	8	2003	20	18	0.56	6	-60	0.43	56	-60	0.43
181	13	11	8	2003	20	18	0.56	7	-35	0.40	56	-82	0.17
181	13	11	8	2003	20	18	0.56	8	-60	0.35	56	-60	0.35
181	13	11	8	2003	20	18	0.56	9	-50	0.39	56	-75	0.34
182	5	11	20	2003	11	45	1.67	0	-76	0.26	35	-36	0.25
182	5	11	20	2003	11	45	1.67	1	-66	0.19	35	-65	0.17
182	5	11	20	2003	11	45	1.67	2	-48	0.24	35	-48	0.24
182	5	11	20	2003	11	45	1.67	3	-59	0.23	35	-59	0.23
182	5	11	20	2003	11	45	1.67	4	-63	0.24	35	-63	0.24
182	5	11	20	2003	11	45	1.67	5	-59	0.26	35	-59	0.26
182	5	11	20	2003	11	45	1.67	6	-60	0.28	35	-60	0.28
182	5	11	20	2003	11	45	1.67	7	-59	0.31	35	-59	0.31
182	5	11	20	2003	11	45	1.67	8	-35	0.24	35	-35	0.24
182	5	11	20	2003	11	45	1.67	9	-76	0.27	35	-36	0.24
183	5	11	20	2003	15	17	3.33	0	-30	0.30	39	-59	0.18
183	5	11	20	2003	15	17	3.33	1	-72	0.13	39	-66	0.13
183	5	11	20	2003	15	17	3.33	2	-55	0.21	39	-55	0.21
183	5	11	20	2003	15	17	3.33	3	-30	0.19	39	-60	0.17
183	5	11	20	2003	15	17	3.33	4	-42	0.21	39	-42	0.21
183	5	11	20	2003	15	17	3.33	5	-30	0.12	39	-46	0.08
183	5	11	20	2003	15	17	3.33	6	-66	0.21	39	-66	0.21
183	5	11	20	2003	15	17	3.33	7	-51	0.07	39	-51	0.07
183	5	11	20	2003	15	17	3.33	8	-33	0.07	39	-51	0.06
183	5	11	20	2003	15	17	3.33	9	-30	0.24	39	-59	0.18
185	9	12	4	2003	22	42	0.83	0	-65	0.21	70	-86	0.35
185	9	12	4	2003	22	42	0.83	1	-48	0.40	70	-86	0.38
185	9	12	4	2003	22	42	0.83	2	-72	0.55	70	-72	0.55
185	9	12	4	2003	22	42	0.83	3	-61	0.32	70	-86	0.16
185	9	12	4	2003	22	42	0.83	4	-44	0.37	70	-70	0.22
185	9	12	4	2003	22	42	0.83	5	-53	0.22	70	-96	0.22
185	9	12	4	2003	22	42	0.83	6	-72	0.48	70	-72	0.48
185	9	12	4	2003	22	42	0.83	7	-61	0.37	70	-100	0.15
185	9	12	4	2003	22	42	0.83	8	-35	0.24	70	-85	0.26
185	9	12	4	2003	22	42	0.83	9	-48	0.40	70	-86	0.40
186	9	12	4	2003	22	53	1.11	0	-59	0.30	70	-89	0.30
186	9	12	4	2003	22	53	1.11	1	-58	0.27	70	-87	0.47
186	9	12	4	2003	22	53	1.11	2	-74	0.43	70	-74	0.43

APPENDIX B MAXIMUM CORRELATION COEFFICIENTS OF THE TIME SERIES CORRESPONDING TO SOLAR WIND AND SUPERDARN

#	ST	M	D	Year	H	Mi	Freq	P	Delay A	CC A	CDT	Delay B	CC B
186	9	12	4	2003	22	53	1.11	3	-30	0.32	70	-86	0.22
186	9	12	4	2003	22	53	1.11	4	-45	0.38	70	-75	0.35
186	9	12	4	2003	22	53	1.11	5	-53	0.24	70	-96	0.05
186	9	12	4	2003	22	53	1.11	6	-74	0.34	70	-74	0.34
186	9	12	4	2003	22	53	1.11	7	-31	0.33	70	-98	0.24
186	9	12	4	2003	22	53	1.11	8	-75	0.29	70	-84	0.34
186	9	12	4	2003	22	53	1.11	9	-59	0.36	70	-88	0.29
187	5	12	5	2003	0	0	0.83	1	-58	0.11	70	-76	-0.07
187	5	12	5	2003	0	0	0.83	2	-74	0.36	70	-74	0.36
187	5	12	5	2003	0	0	0.83	3	-35	0.28	70	-76	0.23
187	5	12	5	2003	0	0	0.83	4	-33	0.26	70	-75	0.19
187	5	12	5	2003	0	0	0.83	5	-74	0.12	70	-74	0.12
187	5	12	5	2003	0	0	0.83	6	-74	0.38	70	-74	0.38
187	5	12	5	2003	0	0	0.83	7	-30	0.32	70	-76	0.19
187	5	12	5	2003	0	0	0.83	8	-33	0.29	70	-75	0.13
188	5	12	5	2003	11	17	2.78	0	-66	0.33	54	-66	0.33
188	5	12	5	2003	11	17	2.78	1	-47	0.33	54	-63	0.17
188	5	12	5	2003	11	17	2.78	2	-34	0.26	54	-66	0.20
188	5	12	5	2003	11	17	2.78	3	-57	0.25	54	-57	0.25
188	5	12	5	2003	11	17	2.78	4	-77	0.26	54	-77	0.26
188	5	12	5	2003	11	17	2.78	5	-34	0.12	54	-70	0.07
188	5	12	5	2003	11	17	2.78	6	-48	0.33	54	-61	0.09
188	5	12	5	2003	11	17	2.78	7	-39	0.21	54	-64	0.19
188	5	12	5	2003	11	17	2.78	8	-70	0.26	54	-70	0.26
188	5	12	5	2003	11	17	2.78	9	-55	0.22	54	-55	0.22
189	8	12	11	2003	21	17	0.56	0	-78	0.18	30	-54	0.16
189	8	12	11	2003	21	17	0.56	1	-33	0.45	30	-33	0.45
189	8	12	11	2003	21	17	0.56	2	-78	0.54	30	-51	0.35
189	8	12	11	2003	21	17	0.56	3	-51	0.53	30	-51	0.53
189	8	12	11	2003	21	17	0.56	4	-34	0.71	30	-34	0.71
189	8	12	11	2003	21	17	0.56	5	-33	0.25	30	-33	0.25
189	8	12	11	2003	21	17	0.56	6	-36	0.47	30	-36	0.47
189	8	12	11	2003	21	17	0.56	7	-71	0.46	30	-40	0.20
189	8	12	11	2003	21	17	0.56	8	-53	0.25	30	-53	0.25
189	8	12	11	2003	21	17	0.56	9	-32	0.30	30	-32	0.30
192	16	12	20	2003	18	46	1.67	0	-51	0.16	55	-69	0.11
192	16	12	20	2003	18	46	1.67	1	-70	0.48	55	-70	0.48
192	16	12	20	2003	18	46	1.67	2	-65	0.35	55	-65	0.35
192	16	12	20	2003	18	46	1.67	3	-56	0.14	55	-56	0.14
192	16	12	20	2003	18	46	1.67	4	-33	0.20	55	-56	0.19
192	16	12	20	2003	18	46	1.67	5	-52	0.20	55	-55	0.18
192	16	12	20	2003	18	46	1.67	6	-33	0.25	55	-65	0.18
192	16	12	20	2003	18	46	1.67	7	-58	0.11	55	-58	0.11
192	16	12	20	2003	18	46	1.67	8	-33	0.30	55	-58	0.17
192	16	12	20	2003	18	46	1.67	9	-69	0.19	55	-69	0.19
193	7	12	20	2003	18	56	1.11	0	-58	0.23	55	-58	0.23
193	7	12	20	2003	18	56	1.11	1	-76	0.47	55	-76	0.47
193	7	12	20	2003	18	56	1.11	2	-32	0.24	55	-84	0.38
193	7	12	20	2003	18	56	1.11	3	-31	0.44	55	-76	0.25
193	7	12	20	2003	18	56	1.11	4	-58	0.33	55	-58	0.33
193	7	12	20	2003	18	56	1.11	5	-40	0.28	55	-56	0.19
193	7	12	20	2003	18	56	1.11	6	-32	0.24	55	-83	0.37
193	7	12	20	2003	18	56	1.11	7	-31	0.41	55	-76	0.29
193	7	12	20	2003	18	56	1.11	8	-58	0.23	55	-58	0.23
193	7	12	20	2003	18	56	1.11	9	-43	0.34	55	-75	0.29
194	7	12	20	2003	19	56	2.78	0	-79	0.24	56	-83	0.25

APPENDIX B MAXIMUM CORRELATION COEFFICIENTS OF THE TIME SERIES CORRESPONDING TO SOLAR WIND AND SUPERDARN

#	ST	M	D	Year	H	Mi	Freq	P	Delay A	CC A	CDT	Delay B	CC B
194	7	12	20	2003	19	56	2.78	1	-52	0.19	56	-73	0.12
194	7	12	20	2003	19	56	2.78	2	-64	0.19	56	-64	0.19
194	7	12	20	2003	19	56	2.78	3	-62	0.12	56	-82	0.17
194	7	12	20	2003	19	56	2.78	4	-44	0.32	56	-70	0.16
194	7	12	20	2003	19	56	2.78	5	-66	0.24	56	-66	0.24
194	7	12	20	2003	19	56	2.78	6	-64	0.20	56	-64	0.20
194	7	12	20	2003	19	56	2.78	7	-71	0.20	56	-71	0.20
194	7	12	20	2003	19	56	2.78	8	-45	0.32	56	-62	0.17
194	7	12	20	2003	19	56	2.78	9	-41	0.33	56	-83	0.17
195	7	12	20	2003	20	5	1.67	0	-63	0.31	53	-63	0.31
195	7	12	20	2003	20	5	1.67	1	-53	0.31	53	-53	0.31
195	7	12	20	2003	20	5	1.67	2	-80	0.28	53	-81	0.29
195	7	12	20	2003	20	5	1.67	3	-76	0.19	53	-83	0.36
195	7	12	20	2003	20	5	1.67	4	-71	0.34	53	-71	0.34
195	7	12	20	2003	20	5	1.67	5	-60	0.23	53	-60	0.23
195	7	12	20	2003	20	5	1.67	6	-80	0.23	53	-80	0.23
195	7	12	20	2003	20	5	1.67	7	-71	0.28	53	-83	0.40
195	7	12	20	2003	20	5	1.67	8	-68	0.28	53	-68	0.28
195	7	12	20	2003	20	5	1.67	9	-50	0.38	53	-53	0.30
200	7	1	14	2003	15	51	2.22	0	-58	0.43	63	-63	0.14
200	7	1	14	2003	15	51	2.22	1	-33	0.35	63	-66	-0.14
200	7	1	14	2003	15	51	2.22	2	-72	0.26	63	-91	0.29
200	7	1	14	2003	15	51	2.22	3	-56	0.45	63	-63	0.24
200	7	1	14	2003	15	51	2.22	4	-76	0.42	63	-83	0.44
200	7	1	14	2003	15	51	2.22	5	-71	0.37	63	-87	0.37
200	7	1	14	2003	15	51	2.22	6	-71	0.31	63	-71	0.31
200	7	1	14	2003	15	51	2.22	7	-48	0.17	63	-82	0.18
200	7	1	14	2003	15	51	2.22	8	-80	0.31	63	-82	0.35
200	7	1	14	2003	15	51	2.22	9	-40	0.37	63	-63	0.08
201	7	1	14	2003	16	31	2.50	0	-59	0.26	63	-80	0.16
201	7	1	14	2003	16	31	2.50	1	-38	0.22	63	-79	0.04
201	7	1	14	2003	16	31	2.50	2	-76	0.22	63	-76	0.22
201	7	1	14	2003	16	31	2.50	3	-45	0.23	63	-82	0.26
201	7	1	14	2003	16	31	2.50	4	-69	0.23	63	-69	0.23
201	7	1	14	2003	16	31	2.50	5	-68	0.24	63	-87	0.24
201	7	1	14	2003	16	31	2.50	6	-70	0.43	63	-70	0.43
201	7	1	14	2003	16	31	2.50	7	-60	0.15	63	-82	0.36
201	7	1	14	2003	16	31	2.50	8	-79	0.27	63	-79	0.27
201	7	1	14	2003	16	31	2.50	9	-59	0.24	63	-80	0.13
202	11	1	17	2003	6	31	2.22	1	-57	0.44	76	-85	0.53
202	11	1	17	2003	6	31	2.22	2	-30	0.55	76	-94	0.34
202	11	1	17	2003	6	31	2.22	3	-57	0.44	76	-100	0.45
202	11	1	17	2003	6	31	2.22	4	-34	0.40	76	-76	0.35
202	11	1	17	2003	6	31	2.22	5	-64	0.35	76	-93	0.37
202	11	1	17	2003	6	31	2.22	6	-78	0.30	76	-78	0.30
202	11	1	17	2003	6	31	2.22	7	-76	0.45	76	-76	0.45
202	11	1	17	2003	6	31	2.22	8	-36	0.55	76	-76	0.36
203	7	1	21	2003	17	48	3.33	0	-39	0.25	37	-39	0.25
203	7	1	21	2003	17	48	3.33	1	-32	0.23	37	-62	0.13
203	7	1	21	2003	17	48	3.33	2	-39	0.14	37	-39	0.14
203	7	1	21	2003	17	48	3.33	3	-59	0.17	37	-59	0.17
203	7	1	21	2003	17	48	3.33	4	-32	0.25	37	-39	0.22
203	7	1	21	2003	17	48	3.33	5	-33	0.19	37	-44	0.14
203	7	1	21	2003	17	48	3.33	6	-32	0.27	37	-61	0.11
203	7	1	21	2003	17	48	3.33	7	-41	0.23	37	-41	0.23
203	7	1	21	2003	17	48	3.33	8	-37	0.23	37	-37	0.23

APPENDIX B MAXIMUM CORRELATION COEFFICIENTS OF THE TIME SERIES CORRESPONDING TO SOLAR WIND AND SUPERDARN

#	ST	M	D	Year	H	Mi	Freq	P	Delay A	CC A	CDT	Delay B	CC B
203	7	1	21	2003	17	48	3.33	9	-39	0.15	37	-39	0.15
204	14	2	19	2003	13	9	1.39	0	-61	0.32	48	-61	0.32
204	14	2	19	2003	13	9	1.39	1	-33	0.42	48	-72	0.23
204	14	2	19	2003	13	9	1.39	2	-38	0.21	48	-68	0.15
204	14	2	19	2003	13	9	1.39	3	-58	0.49	48	-58	0.49
204	14	2	19	2003	13	9	1.39	4	-58	0.47	48	-58	0.47
204	14	2	19	2003	13	9	1.39	5	-75	0.25	48	-75	0.25
204	14	2	19	2003	13	9	1.39	6	-59	0.40	48	-59	0.40
204	14	2	19	2003	13	9	1.39	7	-73	0.58	48	-73	0.58
204	14	2	19	2003	13	9	1.39	8	-61	0.42	48	-61	0.42
204	14	2	19	2003	13	9	1.39	9	-61	0.31	48	-61	0.31
205	11	2	23	2003	4	23	2.22	0	-76	0.27	41	-41	0.24
205	11	2	23	2003	4	23	2.22	1	-55	0.39	41	-55	0.39
205	11	2	23	2003	4	23	2.22	2	-71	0.40	41	-71	0.40
205	11	2	23	2003	4	23	2.22	3	-58	0.26	41	-58	0.26
205	11	2	23	2003	4	23	2.22	4	-52	0.23	41	-52	0.23
205	11	2	23	2003	4	23	2.22	5	-35	0.24	41	-71	0.20
205	11	2	23	2003	4	23	2.22	6	-56	0.34	41	-56	0.34
205	11	2	23	2003	4	23	2.22	7	-34	0.38	41	-70	0.24
205	11	2	23	2003	4	23	2.22	8	-70	0.45	41	-70	0.45
205	11	2	23	2003	4	23	2.22	9	-41	0.33	41	-41	0.33
206	13	3	3	2003	3	5	1.39	0	-75	0.52	66	-75	0.52
206	13	3	3	2003	3	5	1.39	1	-39	0.34	66	-86	0.14
206	13	3	3	2003	3	5	1.39	2	-79	0.62	66	-79	0.62
206	13	3	3	2003	3	5	1.39	3	-37	0.47	66	-67	0.40
206	13	3	3	2003	3	5	1.39	4	-80	0.54	66	-80	0.54
206	13	3	3	2003	3	5	1.39	5	-78	0.65	66	-78	0.65
206	13	3	3	2003	3	5	1.39	6	-79	0.80	66	-79	0.80
206	13	3	3	2003	3	5	1.39	7	-68	0.47	66	-68	0.47
206	13	3	3	2003	3	5	1.39	8	-79	0.70	66	-79	0.70
206	13	3	3	2003	3	5	1.39	9	-74	0.46	66	-74	0.46
207	5	3	6	2003	6	1	1.11	0	-66	0.12	49	-66	0.12
207	5	3	6	2003	6	1	1.11	1	-68	0.56	49	-68	0.56
207	5	3	6	2003	6	1	1.11	2	-58	0.37	49	-58	0.37
207	5	3	6	2003	6	1	1.11	3	-32	0.06	49	-78	0.00
207	5	3	6	2003	6	1	1.11	4	-38	0.15	49	-61	0.10
207	5	3	6	2003	6	1	1.11	5	-56	0.32	49	-56	0.32
207	5	3	6	2003	6	1	1.11	6	-58	0.37	49	-58	0.37
207	5	3	6	2003	6	1	1.11	7	-32	0.09	49	-74	-0.03
207	5	3	6	2003	6	1	1.11	8	-48	0.23	49	-75	0.22
207	5	3	6	2003	6	1	1.11	9	-66	0.33	49	-66	0.33
208	13	3	17	2003	2	44	0.83	0	-65	0.25	35	-65	0.25
208	13	3	17	2003	2	44	0.83	1	-77	0.58	35	-35	0.24
208	13	3	17	2003	2	44	0.83	2	-65	0.49	35	-65	0.49
208	13	3	17	2003	2	44	0.83	3	-74	0.61	35	-48	0.34
208	13	3	17	2003	2	44	0.83	4	-61	0.32	35	-61	0.32
208	13	3	17	2003	2	44	0.83	5	-50	0.43	35	-50	0.43
208	13	3	17	2003	2	44	0.83	6	-76	0.44	35	-35	0.36
208	13	3	17	2003	2	44	0.83	7	-35	0.46	35	-35	0.46
208	13	3	17	2003	2	44	0.83	8	-74	0.64	35	-49	0.41
208	13	3	17	2003	2	44	0.83	9	-42	0.18	35	-42	0.18
209	14	3	19	2003	12	12	0.56	0	-72	0.35	38	-38	0.31
209	14	3	19	2003	12	12	0.56	1	-45	0.33	38	-45	0.33
209	14	3	19	2003	12	12	0.56	2	-55	0.43	38	-55	0.43
209	14	3	19	2003	12	12	0.56	3	-42	0.19	38	-42	0.19
209	14	3	19	2003	12	12	0.56	4	-72	0.32	38	-46	0.19

APPENDIX B MAXIMUM CORRELATION COEFFICIENTS OF THE TIME SERIES CORRESPONDING TO SOLAR WIND AND SUPERDARN

#	ST	M	D	Year	H	Mi	Freq	P	Delay A	CC A	CDT	Delay B	CC B
209	14	3	19	2003	12	12	0.56	5	-54	0.30	38	-54	0.30
209	14	3	19	2003	12	12	0.56	6	-46	0.34	38	-46	0.34
209	14	3	19	2003	12	12	0.56	7	-64	0.33	38	-64	0.33
209	14	3	19	2003	12	12	0.56	8	-64	0.46	38	-64	0.46
209	14	3	19	2003	12	12	0.56	9	-72	0.36	38	-38	0.29
210	14	3	19	2003	12	6	1.11	0	-61	0.47	38	-61	0.47
210	14	3	19	2003	12	6	1.11	1	-46	0.42	38	-46	0.42
210	14	3	19	2003	12	6	1.11	2	-52	0.45	38	-52	0.45
210	14	3	19	2003	12	6	1.11	3	-39	0.48	38	-39	0.48
210	14	3	19	2003	12	6	1.11	4	-70	0.62	38	-68	0.44
210	14	3	19	2003	12	6	1.11	5	-53	0.66	38	-53	0.66
210	14	3	19	2003	12	6	1.11	6	-46	0.54	38	-46	0.54
210	14	3	19	2003	12	6	1.11	7	-52	0.54	38	-52	0.54
210	14	3	19	2003	12	6	1.11	8	-64	0.43	38	-64	0.43
210	14	3	19	2003	12	6	1.11	9	-61	0.51	38	-61	0.51
211	13	3	29	2003	22	47	0.56	0	-70	0.42	63	-70	0.42
211	13	3	29	2003	22	47	0.56	1	-59	0.39	63	-85	0.64
211	13	3	29	2003	22	47	0.56	2	-75	0.51	63	-75	0.51
211	13	3	29	2003	22	47	0.56	3	-43	0.33	63	-78	0.08
211	13	3	29	2003	22	47	0.56	4	-44	0.35	63	-71	0.32
211	13	3	29	2003	22	47	0.56	5	-78	-0.07	63	-78	-0.07
211	13	3	29	2003	22	47	0.56	6	-75	0.47	63	-75	0.47
211	13	3	29	2003	22	47	0.56	7	-44	0.23	63	-79	0.08
211	13	3	29	2003	22	47	0.56	8	-73	0.40	63	-73	0.40
211	13	3	29	2003	22	47	0.56	9	-70	0.34	63	-85	0.49
212	13	3	29	2003	22	20	0.83	0	-52	0.56	63	-91	0.34
212	13	3	29	2003	22	20	0.83	1	-66	0.67	63	-66	0.67
212	13	3	29	2003	22	20	0.83	2	-53	0.58	63	-79	0.13
212	13	3	29	2003	22	20	0.83	3	-49	0.12	63	-79	0.01
212	13	3	29	2003	22	20	0.83	4	-54	0.50	63	-74	0.09
212	13	3	29	2003	22	20	0.83	5	-43	0.10	63	-82	0.10
212	13	3	29	2003	22	20	0.83	6	-54	0.57	63	-79	0.25
212	13	3	29	2003	22	20	0.83	7	-54	0.25	63	-82	0.12
212	13	3	29	2003	22	20	0.83	8	-52	0.54	63	-79	0.15
212	13	3	29	2003	22	20	0.83	9	-67	0.48	63	-67	0.48
213	5	7	8	2003	6	20	1.11	0	-34	0.16	53	-82	0.18
213	5	7	8	2003	6	20	1.11	1	-50	0.16	53	-60	0.14
213	5	7	8	2003	6	20	1.11	2	-66	0.19	53	-66	0.19
213	5	7	8	2003	6	20	1.11	3	-31	0.29	53	-82	0.21
213	5	7	8	2003	6	20	1.11	4	-58	0.19	53	-58	0.19
213	5	7	8	2003	6	20	1.11	5	-35	0.27	53	-82	0.18
213	5	7	8	2003	6	20	1.11	6	-53	0.26	53	-53	0.26
213	5	7	8	2003	6	20	1.11	7	-70	0.23	53	-70	0.23
213	5	7	8	2003	6	20	1.11	8	-45	0.22	53	-69	0.11
213	5	7	8	2003	6	20	1.11	9	-31	0.17	53	-82	0.18

Appendix C

Results for the examination of the band-pass and analytic signals for both ACE and SuperDARN

Internal ID number for Event
ST Station Number
M Month
D Day
H Hour
MI MInute
Freq Frequency
P Solar Parameter ID
B Beam
G Gate
D Delay: Time difference between max.

#	ST	M	D	Year	H	Mi	Freq	P	B	G	Delay
1	7	1	3	2003	8	14	0.83	0	8	27	0.38
1	7	1	3	2003	8	14	0.83	1	8	27	0.38
1	7	1	3	2003	8	14	0.83	2	8	27	0.38
1	7	1	3	2003	8	14	0.83	3	8	27	32.38
1	7	1	3	2003	8	14	0.83	4	8	27	0.38
1	7	1	3	2003	8	14	0.83	9	8	27	0.38
2	7	1	3	2003	12	23	0.56	0	12	33	38.38
2	7	1	3	2003	12	23	0.56	1	12	33	59.72
2	7	1	3	2003	12	23	0.56	2	12	33	59.72
2	7	1	3	2003	12	23	0.56	3	12	33	22.38
2	7	1	3	2003	12	23	0.56	4	12	33	42.65
2	7	1	3	2003	12	23	0.56	9	12	33	31.98
3	7	1	3	2003	12	35	0.83	0	12	25	100.78
3	7	1	3	2003	12	35	0.83	1	12	25	100.78
3	7	1	3	2003	12	35	0.83	2	12	25	100.78
3	7	1	3	2003	12	35	0.83	3	12	25	100.78
3	7	1	3	2003	12	35	0.83	4	12	25	100.78
3	7	1	3	2003	12	35	0.83	9	12	25	100.78
4	7	1	3	2003	16	41	4.17	0	16	40	0.58
4	7	1	3	2003	16	41	4.17	1	16	40	3.78
4	7	1	3	2003	16	41	4.17	2	16	40	3.78
4	7	1	3	2003	16	41	4.17	3	16	40	10.18
4	7	1	3	2003	16	41	4.17	4	16	40	6.98
4	7	1	3	2003	16	41	4.17	9	16	40	72.05
5	7	1	3	2003	19	2	2.50	0	19	5	48.52
5	7	1	3	2003	19	2	2.50	1	19	5	48.52
5	7	1	3	2003	19	2	2.50	2	19	5	48.52
5	7	1	3	2003	19	2	2.50	3	19	5	57.05
5	7	1	3	2003	19	2	2.50	4	19	5	52.78
5	7	1	3	2003	19	2	2.50	9	19	5	16.52
6	7	1	3	2003	19	47	3.61	0	19	51	108.38
6	7	1	3	2003	19	47	3.61	1	19	51	0.65
6	7	1	3	2003	19	47	3.61	2	19	51	0.65
6	7	1	3	2003	19	47	3.61	3	19	51	93.45
6	7	1	3	2003	19	47	3.61	4	19	51	0.65
6	7	1	3	2003	19	47	3.61	9	19	51	28.38
7	7	1	3	2003	19	49	3.89	0	19	52	16.58
7	7	1	3	2003	19	49	3.89	1	19	52	0.58
7	7	1	3	2003	19	49	3.89	2	19	52	0.58
7	7	1	3	2003	19	49	3.89	3	19	52	89.12
7	7	1	3	2003	19	49	3.89	4	19	52	0.58
7	7	1	3	2003	19	49	3.89	9	19	52	27.25
8	7	1	3	2003	19	49	4.44	0	19	50	102.05
8	7	1	3	2003	19	49	4.44	1	19	50	90.32
8	7	1	3	2003	19	49	4.44	2	19	50	90.32
8	7	1	3	2003	19	49	4.44	3	19	50	66.85
8	7	1	3	2003	19	49	4.44	4	19	50	63.65
8	7	1	3	2003	19	49	4.44	9	19	50	9.25
20	8	1	19	2003	17	48	2.78	0	17	42	25.28
20	8	1	19	2003	17	48	2.78	1	17	42	23.15
20	8	1	19	2003	17	48	2.78	2	17	42	22.08
20	8	1	19	2003	17	48	2.78	3	17	42	30.62
20	8	1	19	2003	17	48	2.78	4	17	42	21.02
20	8	1	19	2003	17	48	2.78	9	17	42	25.28
21	14	1	21	2003	11	41	1.11	0	11	29	14.95
21	14	1	21	2003	11	41	1.11	1	11	29	0.02
21	14	1	21	2003	11	41	1.11	2	11	29	0.02
21	14	1	21	2003	11	41	1.11	3	11	29	17.08
21	14	1	21	2003	11	41	1.11	4	11	29	8.55
21	14	1	21	2003	11	41	1.11	9	11	29	11.75

APPENDIX C RESULTS FOR THE EXAMINATION OF THE BAND-PASS AND ANALYTIC SIGNALS FOR BOTH ACE AND SUPERDARN

#	ST	M	D	Year	H	Mi	Freq	P	B	G	Delay
22	13	1	26	2003	2	46	1.11	0	2	59	72.43
22	13	1	26	2003	2	46	1.11	1	2	59	61.77
22	13	1	26	2003	2	46	1.11	2	2	59	62.83
22	13	1	26	2003	2	46	1.11	3	2	59	106.57
22	13	1	26	2003	2	46	1.11	4	2	59	63.90
22	13	1	26	2003	2	46	1.11	9	2	59	67.10
23	3	1	29	2003	23	57	0.83	0	0	18	8.50
23	3	1	29	2003	23	57	0.83	1	0	18	17.03
23	3	1	29	2003	23	57	0.83	2	0	18	17.03
23	3	1	29	2003	23	57	0.83	3	0	18	10.63
23	3	1	29	2003	23	57	0.83	4	0	18	12.77
23	3	1	29	2003	23	57	0.83	9	0	18	1.03
24	3	1	29	2003	23	59	1.39	0	0	26	25.03
24	3	1	29	2003	23	59	1.39	1	0	26	25.03
24	3	1	29	2003	23	59	1.39	2	0	26	25.03
24	3	1	29	2003	23	59	1.39	3	0	26	13.30
24	3	1	29	2003	23	59	1.39	4	0	26	25.03
24	3	1	29	2003	23	59	1.39	9	0	26	25.03
28	13	2	7	2003	3	6	1.11	0	3	18	32.80
28	13	2	7	2003	3	6	1.11	1	3	18	9.33
28	13	2	7	2003	3	6	1.11	2	3	18	9.33
28	13	2	7	2003	3	6	1.11	3	3	18	15.73
28	13	2	7	2003	3	6	1.11	4	3	18	49.87
28	13	2	7	2003	3	6	1.11	9	3	18	28.53
30	10	2	19	2003	0	0	0.56	0	0	0	99.90
30	10	2	19	2003	0	0	0.56	1	0	0	99.90
30	10	2	19	2003	0	0	0.56	2	0	0	99.90
30	10	2	19	2003	0	0	0.56	3	0	0	99.90
30	10	2	19	2003	0	0	0.56	4	0	0	99.90
30	10	2	19	2003	0	0	0.56	5	0	0	99.90
30	10	2	19	2003	0	0	0.56	6	0	0	99.90
30	10	2	19	2003	0	0	0.56	7	0	0	99.90
30	10	2	19	2003	0	0	0.56	8	0	0	99.90
30	10	2	19	2003	0	0	0.56	9	0	0	99.90
31	13	2	19	2003	21	7	0.56	0	21	6	0.03
31	13	2	19	2003	21	7	0.56	1	21	6	0.03
31	13	2	19	2003	21	7	0.56	2	21	6	43.77
31	13	2	19	2003	21	7	0.56	3	21	6	0.03
31	13	2	19	2003	21	7	0.56	4	21	6	43.77
31	13	2	19	2003	21	7	0.56	9	21	6	0.03
32	13	2	19	2003	21	4	0.83	0	22	15	17.83
32	13	2	19	2003	21	4	0.83	1	22	15	25.30
32	13	2	19	2003	21	4	0.83	2	22	15	27.43
32	13	2	19	2003	21	4	0.83	3	22	15	44.50
32	13	2	19	2003	21	4	0.83	4	22	15	16.77
32	13	2	19	2003	21	4	0.83	9	22	15	21.03
33	13	2	19	2003	21	25	2.22	0	21	20	63.10
33	13	2	19	2003	21	25	2.22	1	21	20	48.17
33	13	2	19	2003	21	25	2.22	2	21	20	48.17
33	13	2	19	2003	21	25	2.22	3	21	20	68.43
33	13	2	19	2003	21	25	2.22	4	21	20	87.63
33	13	2	19	2003	21	25	2.22	9	21	20	87.63
34	13	2	19	2003	21	25	2.78	0	21	25	48.90
34	13	2	19	2003	21	25	2.78	1	21	25	63.83
34	13	2	19	2003	21	25	2.78	2	21	25	26.50
34	13	2	19	2003	21	25	2.78	3	21	25	63.83
34	13	2	19	2003	21	25	2.78	4	21	25	63.83
34	13	2	19	2003	21	25	2.78	9	21	25	47.83
35	13	2	20	2003	1	43	0.56	0	1	43	99.90
35	13	2	20	2003	1	43	0.56	1	1	43	99.90
35	13	2	20	2003	1	43	0.56	2	1	43	99.90
35	13	2	20	2003	1	43	0.56	3	1	43	99.90
35	13	2	20	2003	1	43	0.56	4	1	43	99.90
35	13	2	20	2003	1	43	0.56	5	1	43	99.90
35	13	2	20	2003	1	43	0.56	6	1	43	99.90
35	13	2	20	2003	1	43	0.56	7	1	43	99.90
35	13	2	20	2003	1	43	0.56	8	1	43	99.90
35	13	2	20	2003	1	43	0.56	9	1	43	99.90
43	11	2	23	2003	1	21	0.83	0	1	21	99.90
43	11	2	23	2003	1	21	0.83	1	1	21	99.90
43	11	2	23	2003	1	21	0.83	2	1	21	99.90
43	11	2	23	2003	1	21	0.83	3	1	21	99.90
43	11	2	23	2003	1	21	0.83	4	1	21	99.90
43	11	2	23	2003	1	21	0.83	5	1	21	99.90
43	11	2	23	2003	1	21	0.83	6	1	21	99.90
43	11	2	23	2003	1	21	0.83	7	1	21	99.90
43	11	2	23	2003	1	21	0.83	8	1	21	99.90
43	11	2	23	2003	1	21	0.83	9	1	21	99.90
46	13	3	3	2003	1	7	1.94	0	1	7	99.90
46	13	3	3	2003	1	7	1.94	1	1	7	99.90
46	13	3	3	2003	1	7	1.94	2	1	7	99.90
46	13	3	3	2003	1	7	1.94	3	1	7	99.90
46	13	3	3	2003	1	7	1.94	4	1	7	99.90
46	13	3	3	2003	1	7	1.94	5	1	7	99.90
46	13	3	3	2003	1	7	1.94	6	1	7	99.90
46	13	3	3	2003	1	7	1.94	7	1	7	99.90
46	13	3	3	2003	1	7	1.94	8	1	7	99.90
46	13	3	3	2003	1	7	1.94	9	1	7	99.90
47	13	3	3	2003	2	47	0.56	0	2	46	0.85
47	13	3	3	2003	2	47	0.56	1	2	46	117.12
47	13	3	3	2003	2	47	0.56	2	2	46	117.12
47	13	3	3	2003	2	47	0.56	3	2	46	7.25
47	13	3	3	2003	2	47	0.56	4	2	46	38.18
47	13	3	3	2003	2	47	0.56	9	2	46	0.85
50	5	3	6	2003	5	48	1.94	0	6	46	93.67
50	5	3	6	2003	5	48	1.94	1	6	46	85.13
50	5	3	6	2003	5	48	1.94	2	6	46	85.13
50	5	3	6	2003	5	48	1.94	3	6	46	85.13
50	5	3	6	2003	5	48	1.94	4	6	46	0.87
50	5	3	6	2003	5	48	1.94	5	6	46	101.13
50	5	3	6	2003	5	48	1.94	6	6	46	88.87
50	5	3	6	2003	5	48	1.94	7	6	46	43.53
50	5	3	6	2003	5	48	1.94	8	6	46	97.13
50	5	3	6	2003	5	48	1.94	9	6	46	94.73

APPENDIX C RESULTS FOR THE EXAMINATION OF THE BAND-PASS AND ANALYTIC SIGNALS FOR BOTH ACE AND SUPERDARN

#	ST	M	D	Year	H	Mi	Freq	P	B	G	Delay
51	9	3	8	2003	1	50	1.94	0	1	50	99.90
51	9	3	8	2003	1	50	1.94	1	1	50	99.90
51	9	3	8	2003	1	50	1.94	2	1	50	99.90
51	9	3	8	2003	1	50	1.94	3	1	50	99.90
51	9	3	8	2003	1	50	1.94	4	1	50	99.90
51	9	3	8	2003	1	50	1.94	5	1	50	99.90
51	9	3	8	2003	1	50	1.94	6	1	50	99.90
51	9	3	8	2003	1	50	1.94	7	1	50	99.90
51	9	3	8	2003	1	50	1.94	8	1	50	99.90
51	9	3	8	2003	1	50	1.94	9	1	50	99.90
52	9	3	8	2003	18	55	1.39	0	18	50	39.00
52	9	3	8	2003	18	55	1.39	1	18	50	39.00
52	9	3	8	2003	18	55	1.39	2	18	50	39.00
52	9	3	8	2003	18	55	1.39	3	18	50	77.40
52	9	3	8	2003	18	55	1.39	4	18	50	41.13
52	9	3	8	2003	18	55	1.39	9	18	50	39.00
53	9	3	10	2003	19	11	3.33	0	19	4	3.93
53	9	3	10	2003	19	11	3.33	1	19	4	10.33
53	9	3	10	2003	19	11	3.33	2	19	4	10.33
53	9	3	10	2003	19	11	3.33	3	19	4	42.33
53	9	3	10	2003	19	11	3.33	4	19	4	41.27
53	9	3	10	2003	19	11	3.33	9	19	4	5.00
56	9	3	15	2003	1	49	0.56	0	1	49	99.90
56	9	3	15	2003	1	49	0.56	1	1	49	99.90
56	9	3	15	2003	1	49	0.56	2	1	49	99.90
56	9	3	15	2003	1	49	0.56	3	1	49	99.90
56	9	3	15	2003	1	49	0.56	4	1	49	99.90
56	9	3	15	2003	1	49	0.56	5	1	49	99.90
56	9	3	15	2003	1	49	0.56	6	1	49	99.90
56	9	3	15	2003	1	49	0.56	7	1	49	99.90
56	9	3	15	2003	1	49	0.56	8	1	49	99.90
56	9	3	15	2003	1	49	0.56	9	1	49	99.90
57	14	3	15	2003	11	52	0.83	0	11	52	83.95
57	14	3	15	2003	11	52	0.83	1	11	52	86.08
57	14	3	15	2003	11	52	0.83	2	11	52	85.02
57	14	3	15	2003	11	52	0.83	3	11	52	65.82
57	14	3	15	2003	11	52	0.83	4	11	52	14.62
57	14	3	15	2003	11	52	0.83	9	11	52	86.08
58	13	3	17	2003	2	55	1.11	0	2	56	80.22
58	13	3	17	2003	2	55	1.11	1	2	56	80.22
58	13	3	17	2003	2	55	1.11	2	2	56	80.22
58	13	3	17	2003	2	55	1.11	3	2	56	80.22
58	13	3	17	2003	2	55	1.11	4	2	56	80.22
58	13	3	17	2003	2	55	1.11	9	2	56	80.22
59	13	3	24	2003	1	47	0.56	0	1	47	99.90
59	13	3	24	2003	1	47	0.56	1	1	47	99.90
59	13	3	24	2003	1	47	0.56	2	1	47	99.90
59	13	3	24	2003	1	47	0.56	3	1	47	99.90
59	13	3	24	2003	1	47	0.56	4	1	47	99.90
59	13	3	24	2003	1	47	0.56	5	1	47	99.90
59	13	3	24	2003	1	47	0.56	6	1	47	99.90
59	13	3	24	2003	1	47	0.56	7	1	47	99.90
59	13	3	24	2003	1	47	0.56	8	1	47	99.90
59	13	3	24	2003	1	47	0.56	9	1	47	99.90
66	6	4	1	2003	2	1	3.33	0	2	5	83.65
66	6	4	1	2003	2	1	3.33	1	2	5	83.65
66	6	4	1	2003	2	1	3.33	2	2	5	83.65
66	6	4	1	2003	2	1	3.33	3	2	5	83.65
66	6	4	1	2003	2	1	3.33	4	2	5	83.65
66	6	4	1	2003	2	1	3.33	5	2	5	28.98
66	6	4	1	2003	2	1	3.33	6	2	5	28.98
66	6	4	1	2003	2	1	3.33	7	2	5	28.98
66	6	4	1	2003	2	1	3.33	8	2	5	28.98
66	6	4	1	2003	2	1	3.33	9	2	5	83.65
68	6	4	8	2003	9	22	1.11	0	9	19	0.33
68	6	4	8	2003	9	22	1.11	1	9	19	0.33
68	6	4	8	2003	9	22	1.11	2	9	19	0.33
68	6	4	8	2003	9	22	1.11	3	9	19	0.33
68	6	4	8	2003	9	22	1.11	4	9	19	0.33
68	6	4	8	2003	9	22	1.11	9	9	19	0.33
77	8	4	26	2003	23	15	1.39	0	23	28	52.57
77	8	4	26	2003	23	15	1.39	1	23	28	52.57
77	8	4	26	2003	23	15	1.39	2	23	28	52.57
77	8	4	26	2003	23	15	1.39	3	23	28	52.57
77	8	4	26	2003	23	15	1.39	4	23	28	0.30
77	8	4	26	2003	23	15	1.39	9	23	28	49.37
82	13	5	6	2003	7	45	2.22	0	7	53	12.52
82	13	5	6	2003	7	45	2.22	1	7	53	49.85
82	13	5	6	2003	7	45	2.22	2	7	53	49.85
82	13	5	6	2003	7	45	2.22	3	7	53	26.38
82	13	5	6	2003	7	45	2.22	4	7	53	70.12
82	13	5	6	2003	7	45	2.22	9	7	53	11.45
83	13	5	6	2003	7	49	3.33	0	7	49	22.38
83	13	5	6	2003	7	49	3.33	1	7	49	61.85
83	13	5	6	2003	7	49	3.33	2	7	49	62.92
83	13	5	6	2003	7	49	3.33	3	7	49	84.25
83	13	5	6	2003	7	49	3.33	4	7	49	45.85
83	13	5	6	2003	7	49	3.33	9	7	49	84.25
85	13	5	6	2003	7	52	2.50	0	7	54	99.92
85	13	5	6	2003	7	52	2.50	1	7	54	33.78
85	13	5	6	2003	7	52	2.50	2	7	54	33.78
85	13	5	6	2003	7	52	2.50	3	7	54	27.38
85	13	5	6	2003	7	52	2.50	4	7	54	92.45
85	13	5	6	2003	7	52	2.50	9	7	54	95.65
86	13	5	6	2003	7	54	4.44	0	7	50	22.32
86	13	5	6	2003	7	54	4.44	1	7	50	36.18
86	13	5	6	2003	7	54	4.44	2	7	50	36.18
86	13	5	6	2003	7	54	4.44	3	7	50	28.72
86	13	5	6	2003	7	54	4.44	4	7	50	54.32
86	13	5	6	2003	7	54	4.44	9	7	50	22.32
101	7	5	31	2003	12	49	0.83	0	12	46	0.52
101	7	5	31	2003	12	49	0.83	1	12	46	0.52
101	7	5	31	2003	12	49	0.83	2	12	46	0.52
101	7	5	31	2003	12	49	0.83	3	12	46	47.45

APPENDIX C RESULTS FOR THE EXAMINATION OF THE BAND-PASS AND ANALYTIC SIGNALS FOR BOTH ACE AND SUPERDARN

#	ST	M	D	Year	H	Mi	Freq	P	B	G	Delay
101	7	5	31	2003	12	49	0.83	4	12	46	60.25
101	7	5	31	2003	12	49	0.83	9	12	46	0.52
105	9	6	3	2003	2	44	1.11	0	2	41	26.98
105	9	6	3	2003	2	44	1.11	1	2	41	117.65
105	9	6	3	2003	2	44	1.11	2	2	41	117.65
105	9	6	3	2003	2	44	1.11	3	2	41	71.78
105	9	6	3	2003	2	44	1.11	4	2	41	115.52
105	9	6	3	2003	2	44	1.11	9	2	41	26.98
106	6	6	8	2003	5	18	0.83	0	5	8	0.13
106	6	6	8	2003	5	18	0.83	1	5	8	52.40
106	6	6	8	2003	5	18	0.83	2	5	8	52.40
106	6	6	8	2003	5	18	0.83	3	5	8	50.27
106	6	6	8	2003	5	18	0.83	4	5	8	52.40
106	6	6	8	2003	5	18	0.83	5	5	8	8.93
106	6	6	8	2003	5	18	0.83	6	5	8	7.87
106	6	6	8	2003	5	18	0.83	7	5	8	35.33
106	6	6	8	2003	5	18	0.83	8	5	8	0.13
106	6	6	8	2003	5	18	0.83	9	5	8	0.13
107	8	6	8	2003	22	43	0.83	0	22	40	11.07
107	8	6	8	2003	22	43	0.83	1	22	40	0.40
107	8	6	8	2003	22	43	0.83	2	22	40	0.40
107	8	6	8	2003	22	43	0.83	3	22	40	0.40
107	8	6	8	2003	22	43	0.83	4	22	40	104.93
107	8	6	8	2003	22	43	0.83	9	22	40	18.53
108	8	6	8	2003	23	42	0.56	0	0	22	21.33
108	8	6	8	2003	23	42	0.56	1	0	22	14.93
108	8	6	8	2003	23	42	0.56	2	0	22	14.93
108	8	6	8	2003	23	42	0.56	3	0	22	21.33
108	8	6	8	2003	23	42	0.56	4	0	22	17.07
108	8	6	8	2003	23	42	0.56	9	0	22	21.33
109	8	6	15	2003	2	49	0.56	0	2	53	83.82
109	8	6	15	2003	2	49	0.56	1	2	53	82.75
109	8	6	15	2003	2	49	0.56	2	2	53	82.75
109	8	6	15	2003	2	49	0.56	3	2	53	80.62
109	8	6	15	2003	2	49	0.56	4	2	53	77.42
109	8	6	15	2003	2	49	0.56	9	2	53	87.02
110	5	6	15	2003	9	12	1.39	0	8	56	91.62
110	5	6	15	2003	9	12	1.39	1	8	56	15.88
110	5	6	15	2003	9	12	1.39	2	8	56	15.88
110	5	6	15	2003	9	12	1.39	3	8	56	48.95
110	5	6	15	2003	9	12	1.39	4	8	56	95.88
110	5	6	15	2003	9	12	1.39	9	8	56	95.88
112	13	6	16	2003	0	0	0.56	0	23	37	158.75
112	13	6	16	2003	0	0	0.56	1	23	37	158.75
112	13	6	16	2003	0	0	0.56	2	23	37	158.75
112	13	6	16	2003	0	0	0.56	3	23	37	158.75
112	13	6	16	2003	0	0	0.56	4	23	37	158.75
112	13	6	16	2003	0	0	0.56	9	23	37	158.75
118	8	7	1	2003	4	43	1.11	0	4	48	99.65
118	8	7	1	2003	4	43	1.11	1	4	48	33.52
118	8	7	1	2003	4	43	1.11	2	4	48	33.52
118	8	7	1	2003	4	43	1.11	3	4	48	33.52
118	8	7	1	2003	4	43	1.11	4	4	48	27.12
118	8	7	1	2003	4	43	1.11	5	4	48	49.52
118	8	7	1	2003	4	43	1.11	6	4	48	102.85
118	8	7	1	2003	4	43	1.11	7	4	48	95.92
118	8	7	1	2003	4	43	1.11	8	4	48	102.05
118	8	7	1	2003	4	43	1.11	9	4	48	96.45
121	6	7	9	2003	9	43	3.61	0	9	55	30.13
121	6	7	9	2003	9	43	3.61	1	9	55	51.47
121	6	7	9	2003	9	43	3.61	2	9	55	51.47
121	6	7	9	2003	9	43	3.61	3	9	55	47.20
121	6	7	9	2003	9	43	3.61	4	9	55	53.60
121	6	7	9	2003	9	43	3.61	9	9	55	30.13
122	13	7	26	2003	3	20	4.17	1	3	8	21.05
122	13	7	26	2003	3	20	4.17	2	3	8	22.12
122	13	7	26	2003	3	20	4.17	3	3	8	22.12
122	13	7	26	2003	3	20	4.17	4	3	8	7.18
122	13	7	26	2003	3	20	4.17	9	3	8	6.12
123	8	7	26	2003	21	8	0.56	0	21	9	39.65
123	8	7	26	2003	21	8	0.56	1	21	9	22.58
123	8	7	26	2003	21	8	0.56	2	21	9	18.32
123	8	7	26	2003	21	8	0.56	3	21	9	31.12
123	8	7	26	2003	21	8	0.56	4	21	9	0.18
123	8	7	26	2003	21	8	0.56	9	21	9	39.65
126	6	7	31	2003	5	48	1.67	0	5	55	0.32
126	6	7	31	2003	5	48	1.67	1	5	55	32.32
126	6	7	31	2003	5	48	1.67	2	5	55	32.32
126	6	7	31	2003	5	48	1.67	3	5	55	64.32
126	6	7	31	2003	5	48	1.67	4	5	55	109.12
126	6	7	31	2003	5	48	1.67	5	5	55	126.98
126	6	7	31	2003	5	48	1.67	6	5	55	66.45
126	6	7	31	2003	5	48	1.67	7	5	55	18.98
126	6	7	31	2003	5	48	1.67	8	5	55	38.45
126	6	7	31	2003	5	48	1.67	9	5	55	0.32
130	6	8	8	2003	7	44	0.83	0	7	55	128.87
130	6	8	8	2003	7	44	0.83	1	7	55	84.07
130	6	8	8	2003	7	44	0.83	2	7	55	84.07
130	6	8	8	2003	7	44	0.83	3	7	55	6.20
130	6	8	8	2003	7	44	0.83	4	7	55	63.80
130	6	8	8	2003	7	44	0.83	5	7	55	91.53
130	6	8	8	2003	7	44	0.83	6	7	55	92.07
130	6	8	8	2003	7	44	0.83	7	7	55	128.87
130	6	8	8	2003	7	44	0.83	8	7	55	99.00
130	6	8	8	2003	7	44	0.83	9	7	55	128.87
133	8	8	8	2003	23	49	0.83	0	0	5	0.20
133	8	8	8	2003	23	49	0.83	1	0	5	4.47
133	8	8	8	2003	23	49	0.83	2	0	5	4.47
133	8	8	8	2003	23	49	0.83	3	0	5	0.20
133	8	8	8	2003	23	49	0.83	4	0	5	4.47
133	8	8	8	2003	23	49	0.83	9	0	5	0.20
134	13	8	15	2003	0	43	0.56	0	0	43	99.90
134	13	8	15	2003	0	43	0.56	1	0	43	99.90
134	13	8	15	2003	0	43	0.56	2	0	43	99.90

APPENDIX C RESULTS FOR THE EXAMINATION OF THE BAND-PASS AND ANALYTIC SIGNALS FOR BOTH ACE AND SUPERDARN

#	ST	M	D	Year	H	Mi	Freq	P	B	G	Delay
134	13	8	15	2003	0	43	0.56	3	0	43	99.90
134	13	8	15	2003	0	43	0.56	4	0	43	99.90
134	13	8	15	2003	0	43	0.56	5	0	43	99.90
134	13	8	15	2003	0	43	0.56	6	0	43	99.90
134	13	8	15	2003	0	43	0.56	7	0	43	99.90
134	13	8	15	2003	0	43	0.56	8	0	43	99.90
134	13	8	15	2003	0	43	0.56	9	0	43	99.90
136	8	8	22	2003	2	27	0.83	0	2	16	53.38
136	8	8	22	2003	2	27	0.83	1	2	16	0.05
136	8	8	22	2003	2	27	0.83	2	2	16	0.05
136	8	8	22	2003	2	27	0.83	3	2	16	34.18
136	8	8	22	2003	2	27	0.83	4	2	16	52.32
136	8	8	22	2003	2	27	0.83	9	2	16	53.38
144	13	9	8	2003	0	50	1.39	0	0	50	99.90
144	13	9	8	2003	0	50	1.39	1	0	50	99.90
144	13	9	8	2003	0	50	1.39	2	0	50	99.90
144	13	9	8	2003	0	50	1.39	3	0	50	99.90
144	13	9	8	2003	0	50	1.39	4	0	50	99.90
144	13	9	8	2003	0	50	1.39	5	0	50	99.90
144	13	9	8	2003	0	50	1.39	6	0	50	99.90
144	13	9	8	2003	0	50	1.39	7	0	50	99.90
144	13	9	8	2003	0	50	1.39	8	0	50	99.90
144	13	9	8	2003	0	50	1.39	9	0	50	99.90
145	13	9	16	2003	20	30	0.56	0	20	44	0.90
145	13	9	16	2003	20	30	0.56	1	20	44	20.10
145	13	9	16	2003	20	30	0.56	2	20	44	16.90
145	13	9	16	2003	20	30	0.56	3	20	44	0.90
145	13	9	16	2003	20	30	0.56	4	20	44	96.90
145	13	9	16	2003	20	30	0.56	9	20	44	0.90
146	14	9	21	2003	10	49	1.39	0	10	36	0.92
146	14	9	21	2003	10	49	1.39	1	10	36	89.45
146	14	9	21	2003	10	49	1.39	2	10	36	89.45
146	14	9	21	2003	10	49	1.39	3	10	36	31.85
146	14	9	21	2003	10	49	1.39	4	10	36	99.05
146	14	9	21	2003	10	49	1.39	9	10	36	0.92
149	13	9	29	2003	1	14	1.11	0	1	14	99.90
149	13	9	29	2003	1	14	1.11	1	1	14	99.90
149	13	9	29	2003	1	14	1.11	2	1	14	99.90
149	13	9	29	2003	1	14	1.11	3	1	14	99.90
149	13	9	29	2003	1	14	1.11	4	1	14	99.90
149	13	9	29	2003	1	14	1.11	5	1	14	99.90
149	13	9	29	2003	1	14	1.11	6	1	14	99.90
149	13	9	29	2003	1	14	1.11	7	1	14	99.90
149	13	9	29	2003	1	14	1.11	8	1	14	99.90
149	13	9	29	2003	1	14	1.11	9	1	14	99.90
150	13	9	29	2003	1	39	2.50	0	1	39	99.90
150	13	9	29	2003	1	39	2.50	1	1	39	99.90
150	13	9	29	2003	1	39	2.50	2	1	39	99.90
150	13	9	29	2003	1	39	2.50	3	1	39	99.90
150	13	9	29	2003	1	39	2.50	4	1	39	99.90
150	13	9	29	2003	1	39	2.50	5	1	39	99.90
150	13	9	29	2003	1	39	2.50	6	1	39	99.90
150	13	9	29	2003	1	39	2.50	7	1	39	99.90
150	13	9	29	2003	1	39	2.50	8	1	39	99.90
150	13	9	29	2003	1	39	2.50	9	1	39	99.90
151	13	9	29	2003	22	5	0.56	1	23	46	34.67
151	13	9	29	2003	22	5	0.56	2	23	46	33.60
151	13	9	29	2003	22	5	0.56	3	23	46	50.67
151	13	9	29	2003	22	5	0.56	4	23	46	66.67
152	13	9	29	2003	23	5	0.56	1	23	3	0.20
152	13	9	29	2003	23	5	0.56	2	23	3	0.20
152	13	9	29	2003	23	5	0.56	3	23	3	7.67
152	13	9	29	2003	23	5	0.56	4	23	3	23.67
154	7	10	8	2003	12	9	1.67	0	12	17	0.62
154	7	10	8	2003	12	9	1.67	1	12	17	36.88
154	7	10	8	2003	12	9	1.67	2	12	17	33.68
154	7	10	8	2003	12	9	1.67	3	12	17	12.35
154	7	10	8	2003	12	9	1.67	4	12	17	21.95
154	7	10	8	2003	12	9	1.67	9	12	17	0.62
156	10	10	11	2003	0	53	0.56	0	0	53	99.90
156	10	10	11	2003	0	53	0.56	1	0	53	99.90
156	10	10	11	2003	0	53	0.56	2	0	53	99.90
156	10	10	11	2003	0	53	0.56	3	0	53	99.90
156	10	10	11	2003	0	53	0.56	4	0	53	99.90
156	10	10	11	2003	0	53	0.56	5	0	53	99.90
156	10	10	11	2003	0	53	0.56	6	0	53	99.90
156	10	10	11	2003	0	53	0.56	7	0	53	99.90
156	10	10	11	2003	0	53	0.56	8	0	53	99.90
156	10	10	11	2003	0	53	0.56	9	0	53	99.90
161	5	10	13	2003	23	41	1.39	0	23	44	61.50
161	5	10	13	2003	23	41	1.39	1	23	44	0.70
161	5	10	13	2003	23	41	1.39	2	23	44	0.70
161	5	10	13	2003	23	41	1.39	3	23	44	31.63
161	5	10	13	2003	23	41	1.39	4	23	44	0.70
161	5	10	13	2003	23	41	1.39	9	23	44	57.23
162	5	10	13	2003	23	43	2.22	0	23	47	4.77
162	5	10	13	2003	23	43	2.22	1	23	47	0.50
162	5	10	13	2003	23	43	2.22	2	23	47	0.50
162	5	10	13	2003	23	43	2.22	3	23	47	54.90
162	5	10	13	2003	23	43	2.22	4	23	47	0.50
162	5	10	13	2003	23	43	2.22	9	23	47	85.83
163	7	10	13	2003	10	9	1.11	1	10	12	49.50
163	7	10	13	2003	10	9	1.11	2	10	12	49.50
163	7	10	13	2003	10	9	1.11	3	10	12	49.50
163	7	10	13	2003	10	9	1.11	4	10	12	12.17
163	7	10	13	2003	10	9	1.11	9	10	12	49.50
164	5	10	14	2003	11	45	1.39	0	11	49	23.83
164	5	10	14	2003	11	45	1.39	1	11	49	93.17
164	5	10	14	2003	11	45	1.39	2	11	49	93.17
164	5	10	14	2003	11	45	1.39	3	11	49	73.97
164	5	10	14	2003	11	45	1.39	4	11	49	82.50
164	5	10	14	2003	11	45	1.39	9	11	49	86.77
165	5	10	14	2003	12	6	2.22	0	11	52	48.17
165	5	10	14	2003	12	6	2.22	1	11	52	96.17

APPENDIX C RESULTS FOR THE EXAMINATION OF THE BAND-PASS AND ANALYTIC SIGNALS FOR BOTH ACE AND SUPERDARN

#	ST	M	D	Year	H	Mi	Freq	P	B	G	Delay
165	5	10	14	2003	12	6	2.22	2	11	52	96.17
165	5	10	14	2003	12	6	2.22	3	11	52	73.77
165	5	10	14	2003	12	6	2.22	4	11	52	36.43
165	5	10	14	2003	12	6	2.22	9	11	52	43.90
166	5	10	16	2003	23	57	1.94	0	0	4	3.63
166	5	10	16	2003	23	57	1.94	1	0	4	3.63
166	5	10	16	2003	23	57	1.94	2	0	4	3.63
166	5	10	16	2003	23	57	1.94	3	0	4	3.63
166	5	10	16	2003	23	57	1.94	4	0	4	0.43
166	5	10	16	2003	23	57	1.94	9	0	4	3.63
167	5	10	16	2003	23	56	2.22	0	0	1	0.63
167	5	10	16	2003	23	56	2.22	1	0	1	0.63
167	5	10	16	2003	23	56	2.22	2	0	1	0.63
167	5	10	16	2003	23	56	2.22	3	0	1	0.63
167	5	10	16	2003	23	56	2.22	4	0	1	0.63
167	5	10	16	2003	23	56	2.22	9	0	1	0.63
174	7	10	27	2003	7	4	3.61	0	7	3	30.12
174	7	10	27	2003	7	4	3.61	1	7	3	13.05
174	7	10	27	2003	7	4	3.61	2	7	3	13.05
174	7	10	27	2003	7	4	3.61	3	7	3	5.58
174	7	10	27	2003	7	4	3.61	4	7	3	39.72
174	7	10	27	2003	7	4	3.61	9	7	3	0.25
176	6	11	7	2003	2	5	0.83	0	2	2	33.15
176	6	11	7	2003	2	5	0.83	1	2	2	29.95
176	6	11	7	2003	2	5	0.83	2	2	2	31.02
176	6	11	7	2003	2	5	0.83	3	2	2	52.35
176	6	11	7	2003	2	5	0.83	4	2	2	0.08
176	6	11	7	2003	2	5	0.83	9	2	2	37.42
177	6	11	7	2003	2	6	1.11	0	2	4	31.95
177	6	11	7	2003	2	6	1.11	1	2	4	26.62
177	6	11	7	2003	2	6	1.11	2	2	4	27.68
177	6	11	7	2003	2	6	1.11	3	2	4	30.88
177	6	11	7	2003	2	6	1.11	4	2	4	47.95
177	6	11	7	2003	2	6	1.11	9	2	4	35.15
178	6	11	7	2003	4	17	2.78	0	4	21	44.15
178	6	11	7	2003	4	17	2.78	1	4	21	8.95
178	6	11	7	2003	4	17	2.78	2	4	21	8.95
178	6	11	7	2003	4	17	2.78	3	4	21	23.88
178	6	11	7	2003	4	17	2.78	4	4	21	0.42
178	6	11	7	2003	4	17	2.78	5	4	21	18.02
178	6	11	7	2003	4	17	2.78	6	4	21	0.15
178	6	11	7	2003	4	17	2.78	7	4	21	42.02
178	6	11	7	2003	4	17	2.78	8	4	21	3.08
178	6	11	7	2003	4	17	2.78	9	4	21	15.35
179	10	11	7	2003	5	40	4.44	0	5	35	42.42
179	10	11	7	2003	5	40	4.44	1	5	35	100.02
179	10	11	7	2003	5	40	4.44	2	5	35	100.02
179	10	11	7	2003	5	40	4.44	3	5	35	43.48
179	10	11	7	2003	5	40	4.44	4	5	35	42.42
179	10	11	7	2003	5	40	4.44	5	5	35	48.82
179	10	11	7	2003	5	40	4.44	6	5	35	54.95
179	10	11	7	2003	5	40	4.44	7	5	35	14.15
179	10	11	7	2003	5	40	4.44	8	5	35	77.08
179	10	11	7	2003	5	40	4.44	9	5	35	42.42
180	13	11	7	2003	21	6	1.67	0	21	27	48.28
180	13	11	7	2003	21	6	1.67	1	21	27	47.22
180	13	11	7	2003	21	6	1.67	2	21	27	45.08
180	13	11	7	2003	21	6	1.67	3	21	27	48.28
180	13	11	7	2003	21	6	1.67	4	21	27	44.02
180	13	11	7	2003	21	6	1.67	9	21	27	10.95
181	13	11	8	2003	20	18	0.56	0	19	59	43.48
181	13	11	8	2003	20	18	0.56	1	19	59	0.82
181	13	11	8	2003	20	18	0.56	2	19	59	0.82
181	13	11	8	2003	20	18	0.56	3	19	59	0.82
181	13	11	8	2003	20	18	0.56	4	19	59	0.82
181	13	11	8	2003	20	18	0.56	9	19	59	40.28
182	5	11	20	2003	11	45	1.67	0	11	32	48.52
182	5	11	20	2003	11	45	1.67	1	11	32	0.52
182	5	11	20	2003	11	45	1.67	2	11	32	0.52
182	5	11	20	2003	11	45	1.67	3	11	32	0.52
182	5	11	20	2003	11	45	1.67	4	11	32	0.52
182	5	11	20	2003	11	45	1.67	9	11	32	47.45
183	5	11	20	2003	15	17	3.33	0	15	21	34.32
183	5	11	20	2003	15	17	3.33	1	15	21	37.52
183	5	11	20	2003	15	17	3.33	2	15	21	37.52
183	5	11	20	2003	15	17	3.33	3	15	21	33.25
183	5	11	20	2003	15	17	3.33	4	15	21	17.25
183	5	11	20	2003	15	17	3.33	9	15	21	34.32
185	9	12	4	2003	22	42	0.83	0	22	48	0.28
185	9	12	4	2003	22	42	0.83	1	22	48	15.22
185	9	12	4	2003	22	42	0.83	2	22	48	14.15
185	9	12	4	2003	22	42	0.83	3	22	48	0.28
185	9	12	4	2003	22	42	0.83	4	22	48	100.55
185	9	12	4	2003	22	42	0.83	9	22	48	0.28
186	9	12	4	2003	22	53	1.11	0	22	40	0.82
186	9	12	4	2003	22	53	1.11	1	22	40	98.95
186	9	12	4	2003	22	53	1.11	2	22	40	0.82
186	9	12	4	2003	22	53	1.11	3	22	40	0.82
186	9	12	4	2003	22	53	1.11	4	22	40	0.82
186	9	12	4	2003	22	53	1.11	9	22	40	0.82
187	5	12	5	2003	0	0	0.83	0	0	0	70.15
187	5	12	5	2003	0	0	0.83	1	0	0	85.08
187	5	12	5	2003	0	0	0.83	2	0	0	84.02
187	5	12	5	2003	0	0	0.83	3	0	0	60.55
187	5	12	5	2003	0	0	0.83	4	0	0	78.68
187	5	12	5	2003	0	0	0.83	9	0	0	70.15
188	5	12	5	2003	11	17	2.78	0	11	27	62.75
188	5	12	5	2003	11	17	2.78	1	11	27	56.35
188	5	12	5	2003	11	17	2.78	2	11	27	56.35
188	5	12	5	2003	11	17	2.78	3	11	27	57.42
188	5	12	5	2003	11	17	2.78	4	11	27	4.08
188	5	12	5	2003	11	17	2.78	9	11	27	62.75
189	8	12	11	2003	21	17	0.56	0	21	39	104.08
189	8	12	11	2003	21	17	0.56	1	21	39	0.62

APPENDIX C RESULTS FOR THE EXAMINATION OF THE BAND-PASS AND ANALYTIC SIGNALS FOR BOTH ACE AND SUPERDARN

#	ST	M	D	Year	H	Mi	Freq	P	B	G	Delay
189	8	12	11	2003	21	17	0.56	2	21	39	0.62
189	8	12	11	2003	21	17	0.56	3	21	39	0.62
189	8	12	11	2003	21	17	0.56	4	21	39	0.62
189	8	12	11	2003	21	17	0.56	9	21	39	53.95
192	16	12	20	2003	18	46	1.67	0	18	49	105.85
192	16	12	20	2003	18	46	1.67	1	18	49	106.92
192	16	12	20	2003	18	46	1.67	2	18	49	106.92
192	16	12	20	2003	18	46	1.67	3	18	49	111.18
192	16	12	20	2003	18	46	1.67	4	18	49	114.38
192	16	12	20	2003	18	46	1.67	9	18	49	105.85
200	7	1	14	2003	15	51	2.22	0	15	57	34.40
200	7	1	14	2003	15	51	2.22	1	15	57	89.87
200	7	1	14	2003	15	51	2.22	2	15	57	89.87
200	7	1	14	2003	15	51	2.22	3	15	57	96.27
200	7	1	14	2003	15	51	2.22	4	15	57	86.67
200	7	1	14	2003	15	51	2.22	9	15	57	32.27
201	7	1	14	2003	16	31	2.50	0	15	57	13.07
201	7	1	14	2003	16	31	2.50	1	15	57	0.27
201	7	1	14	2003	16	31	2.50	2	15	57	0.27
201	7	1	14	2003	16	31	2.50	3	15	57	90.93
201	7	1	14	2003	16	31	2.50	4	15	57	57.87
201	7	1	14	2003	16	31	2.50	9	15	57	14.13
202	11	1	17	2003	6	31	2.22	1	6	39	79.08
202	11	1	17	2003	6	31	2.22	2	6	39	79.08
202	11	1	17	2003	6	31	2.22	3	6	39	35.35
202	11	1	17	2003	6	31	2.22	4	6	39	70.55
202	11	1	17	2003	6	31	2.22	9	6	39	79.08
203	7	1	21	2003	17	48	3.33	0	17	49	83.48
203	7	1	21	2003	17	48	3.33	1	17	49	54.68
203	7	1	21	2003	17	48	3.33	2	17	49	54.68
203	7	1	21	2003	17	48	3.33	3	17	49	74.95
203	7	1	21	2003	17	48	3.33	4	17	49	48.28
203	7	1	21	2003	17	48	3.33	9	17	49	83.48
204	14	2	19	2003	13	9	1.39	0	13	3	33.30
204	14	2	19	2003	13	9	1.39	1	13	3	0.23
204	14	2	19	2003	13	9	1.39	2	13	3	0.23
204	14	2	19	2003	13	9	1.39	3	13	3	35.42
204	14	2	19	2003	13	9	1.39	4	13	3	35.42
204	14	2	19	2003	13	9	1.39	9	13	3	33.30
205	11	2	23	2003	4	23	2.22	0	4	23	85.03
205	11	2	23	2003	4	23	2.22	1	4	23	67.97
205	11	2	23	2003	4	23	2.22	2	4	23	66.90
205	11	2	23	2003	4	23	2.22	3	4	23	74.37
205	11	2	23	2003	4	23	2.22	4	4	23	1.83
205	11	2	23	2003	4	23	2.22	5	4	23	61.03
205	11	2	23	2003	4	23	2.22	6	4	23	100.23
205	11	2	23	2003	4	23	2.22	7	4	23	89.57
205	11	2	23	2003	4	23	2.22	8	4	23	92.77
205	11	2	23	2003	4	23	2.22	9	4	23	27.43
206	13	3	3	2003	3	5	1.39	0	3	14	45.92
206	13	3	3	2003	3	5	1.39	1	3	14	36.32
206	13	3	3	2003	3	5	1.39	2	3	14	37.38
206	13	3	3	2003	3	5	1.39	3	3	14	48.05
206	13	3	3	2003	3	5	1.39	4	3	14	33.12
206	13	3	3	2003	3	5	1.39	9	3	14	44.85
207	5	3	6	2003	6	1	1.11	0	6	0	79.67
207	5	3	6	2003	6	1	1.11	1	6	0	41.27
207	5	3	6	2003	6	1	1.11	2	6	0	40.20
207	5	3	6	2003	6	1	1.11	3	6	0	56.20
207	5	3	6	2003	6	1	1.11	4	6	0	42.33
207	5	3	6	2003	6	1	1.11	5	6	0	10.60
207	5	3	6	2003	6	1	1.11	6	6	0	25.27
207	5	3	6	2003	6	1	1.11	7	6	0	28.20
207	5	3	6	2003	6	1	1.11	8	6	0	65.00
207	5	3	6	2003	6	1	1.11	9	6	0	32.73
208	13	3	17	2003	2	44	0.83	0	2	42	70.48
208	13	3	17	2003	2	44	0.83	1	2	42	77.95
208	13	3	17	2003	2	44	0.83	2	2	42	77.95
208	13	3	17	2003	2	44	0.83	3	2	42	106.75
208	13	3	17	2003	2	44	0.83	4	2	42	90.75
208	13	3	17	2003	2	44	0.83	9	2	42	70.48
211	13	3	29	2003	22	47	0.56	0	23	28	0.25
211	13	3	29	2003	22	47	0.56	1	23	28	0.25
211	13	3	29	2003	22	47	0.56	2	23	28	19.45
211	13	3	29	2003	22	47	0.56	3	23	28	0.25
211	13	3	29	2003	22	47	0.56	4	23	28	0.25
211	13	3	29	2003	22	47	0.56	9	23	28	0.25
212	13	3	29	2003	22	20	0.83	0	22	19	50.72
212	13	3	29	2003	22	20	0.83	1	22	19	68.85
212	13	3	29	2003	22	20	0.83	2	22	19	68.85
212	13	3	29	2003	22	20	0.83	3	22	19	0.58
212	13	3	29	2003	22	20	0.83	4	22	19	83.78
212	13	3	29	2003	22	20	0.83	9	22	19	54.98
213	5	7	8	2003	6	20	1.11	0	6	29	60.93
213	5	7	8	2003	6	20	1.11	1	6	29	52.40
213	5	7	8	2003	6	20	1.11	2	6	29	53.47
213	5	7	8	2003	6	20	1.11	3	6	29	74.80
213	5	7	8	2003	6	20	1.11	4	6	29	56.67
213	5	7	8	2003	6	20	1.11	5	6	29	5.47
213	5	7	8	2003	6	20	1.11	6	6	29	28.67
213	5	7	8	2003	6	20	1.11	7	6	29	26.80
213	5	7	8	2003	6	20	1.11	8	6	29	63.87
213	5	7	8	2003	6	20	1.11	9	6	29	63.07
214	6	10	25	2003	1	54	2.22	0	1	54	99.90
214	6	10	25	2003	1	54	2.22	1	1	54	99.90
214	6	10	25	2003	1	54	2.22	2	1	54	99.90
214	6	10	25	2003	1	54	2.22	3	1	54	99.90
214	6	10	25	2003	1	54	2.22	4	1	54	99.90
214	6	10	25	2003	1	54	2.22	5	1	54	99.90
214	6	10	25	2003	1	54	2.22	6	1	54	99.90
214	6	10	25	2003	1	54	2.22	7	1	54	99.90
214	6	10	25	2003	1	54	2.22	8	1	54	99.90
214	6	10	25	2003	1	54	2.22	9	1	54	99.90